1999

Primary photoprocesses of light-activated antiviral and antitumor agents, hypericin and hypocrellin

Alexandre V. Smirnov
Iowa State University

INFORMATION TO USERS

This manuscript has been reproduced from the microfilm master. UMI films the text directly from the original or copy submitted. Thus, some thesis and dissertation copies are in typewriter face, while others may be from any type of computer printer.

The quality of this reproduction is dependent upon the quality of the copy submitted. Broken or indistinct print, colored or poor quality illustrations and photographs, print bleedthrough, substandard margins, and improper alignment can adversely affect reproduction.

In the unlikely event that the author did not send UMI a complete manuscript and there are missing pages, these will be noted. Also, if unauthorized copyright material had to be removed, a note will indicate the deletion.

Oversize materials (e.g., maps, drawings, charts) are reproduced by sectioning the original, beginning at the upper left-hand corner and continuing from left to right in equal sections with small overlaps. Each original is also photographed in one exposure and is included in reduced form at the back of the book.

Photographs included in the original manuscript have been reproduced xerographically in this copy. Higher quality 6" x 9" black and white photographic prints are available for any photographs or illustrations appearing in this copy for an additional charge. Contact UMI directly to order.

UMI

A Bell & Howell Information Company
300 North Zeeb Road, Ann Arbor MI 48106-1346 USA
313/761-4700 800/521-0600

Primary photoprocesses of light-activated antiviral and antitumor agents, hypericin and hypocrellin

by

Alexandre V. Smirnov

A dissertation submitted to the graduate faculty

in partial fulfillment of the requirements for the degree of

DOCTOR OF PHILOSOPHY

Major: Physical Chemistry

Major Professor: Jacob W. Petrich

Iowa State University

Ames, Iowa

1999

Graduate College
Iowa State University

This is to certify that the Doctoral dissertation of

Alexandre V. Smirnov

has met the dissertation requirements of Iowa State University

Signature was redacted for privacy.

Major Professor

Signature was redacted for privacy.

For the Major Program

Signature was redacted for privacy.

For the Graduate College

To my parents for their generous love, support and care.

TABLE OF CONTENTS

ABSTRACT vii

CHAPTER I. GENERAL INTRODUCTION 1

Overview 3

Hypericin 3

Hypocrellin A and Hypocrellin B 8

Intramolecular Proton Transfer in Polycyclic Quinones 15

Dissertation Organization 28

References 30

CHAPTER II. EXPERIMENTAL APPARATUS AND METHODS OF COMPUTATION 45

Fluorescence Upconversion Spectrometer 45

Computer Simulation of the Transient Absorbance and Anisotropy for the Hypocrellin A Excited-State Dynamics 68

References 74

CHAPTER III. EXCITED-STATE PROCESSES IN POLYCYCLIC QUINONES: THE LIGHT-INDUCED ANTIVIRAL AGENT, HYPOCRELLIN, AND A COMPARISON WITH HYPERICIN 77

Abstract 77

Introduction 78

Materials and Methods 80

Results 83

Discussion 85

Conclusions 88

Acknowledgements 91

References 91

CHAPTER IV. PICOSECOND LINEAR DICHROISM AND ABSORPTION ANISOTROPY OF HYPOCRELLIN: TOWARD A UNIFIED PICTURE OF THE PHOTOPHYSICS OF HYPERICIN AND HYPOCRELLIN 103

ABSTRACT 103

INTRODUCTION 104

EXPERIMENTAL 107

RESULTS 108

DISCUSSION 109

CONCLUDING REMARKS 117

ACKNOWLEDGEMENTS 118

REFERENCES 118

APPENDIX 137

CHAPTER V. EXPLORING GROUND-STATE HETEROGENEITY OF HYPERICIN AND HYPOCRELLIN A AND B: DYNAMIC AND 2D ROESY NMR STUDY 158

ABSTRACT 158

INTRODUCTION 159

EXPERIMENTAL 160

RESULTS AND DISCUSSION 161

CONCLUSIONS 173

ACKNOWLEDGEMENTS 176

REFERENCES 177

CHAPTER VI. PHOTOPHYSICS OF HYPERICIN AND HYPOCRELLIN A IN COMPLEX WITH SUBCELLULAR COMPONENTS: INTERACTIONS WITH HUMAN SERUM ALBUMIN 198

ABSTRACT 199

INTRODUCTION 199

MATERIALS AND METHODS 203

RESULTS 208

DISCUSSION AND CONCLUSIONS 217

ACKNOWLEDGEMENTS 221

REFERENCES 221

CHAPTER VII. EXCITED-STATE INTRAMOLECULAR H-ATOM TRANSFER OF HYPERICIN AND HYPOCRELLIN A INVESTIGATED BY FLUORESCENCE UPCONVERSION 245

ABSTRACT 245

INTRODUCTION 246

EXPERIMENTAL 247

RESULTS 249

DISCUSSION 250

CONCLUSIONS 257

ACKNOWLEDGEMENTS 259

REFERENCES 259

CHAPTER VIII. GENERAL CONCLUSIONS AND FUTURE WORK 277

GENERAL CONCLUSIONS 277

FUTURE WORK 280

REFERENCES 284

ACKNOWLEDGEMENTS 288

ABSTRACT

The dissertation focuses on the ultrafast primary photoprocesses of the title anti-viral and anti-cancer agents, whose activity depends on light which is also accompanied by photoacidification in vesicles and living cells.

By complementing the techniques of time-resolved absorption spectroscopy with those of fluorescence upconversion and applying them to hypericin, hypocrellin A and B, and their methylated analogs that are unable to execute proton transfer, it was demonstrated that intramolecular excited-state hydrogen atom transfer is a dominant primary nonradiative process.

For hypocrellin A in viscous solvents such as octanol and ethylene glycol, an absorption transient of ~10-ps duration, similar to the hypericin transient, can be detected together with another, much longer lived transient component (evident in only in pump/probe absorption spectroscopy). This long-lived 50-230 ps component exhibits a deuterium isotope effect and a strong solvent bulk viscosity dependence. Such behavior is rationalized by postulating that the excited-state tautomerization pathway, besides the proton stretch, involves at least one other reaction coordinate such as molecular skeletal motion or even conformational change. Temperature-dependant ^{1}H-NMR and 2D ROESY studies of hypericin and hypocrellins provide strong evidence that there is only one conformational isomer/tautomer for hypericin in the ground state. On the other hand, we found three significantly populated ground-state species for hypocrellin A. These species where identified and their relative energies and interconversion barriers were determined through dynamic NMR simulations. Hypocrellin B, like hypericin, was found to be essentially homogeneous in the ground state. This is attributed to the rigidity of its structure caused by the presence of a double bond in its seven-membered ring.

Time-resolved fluorescence and absorption measurements of hypericin complexed with human serum albumin (HSA) indicate that hypericin very rigidly binds to HSA by means of a specific hydrogen bonded interaction between its carbonyl oxygen and the N_1-H of the tryptophan residue in the II A subdomain of HSA.

Finally, the issue of absorption and emission "mirror-image" symmetry in the title polycyclic quinones, which was the key point of criticisms toward the very existence of excited-state proton transfer, is effectively addresses by appealing to the high symmetry of the aromatic core.

CHAPTER I. GENERAL INTRODUCTION

OVERVIEW

Since the very early stages of evolution, humans have faced a most important and inevitable problem: survival. Having limited supplies of food, fresh water and land resources and being poorly adapted to living on the ground man had to use the power of his intellect to overcome domination of other species, geographical boundaries and severe natural conditions and to expand his areas of habitation to the most far corners of the world. As human population on earth grew in number and the availability of natural resources diminished we could see how the fundamental urge to survive as species translated into the call for being independent as a group, culture, nation and race. These days we speak more and more often about preserving endangered species and wilderness. However, despite our great achievements in science and technology the very biological aspect of the survival of human kind should not be underestimated. It is often forgotten that more people lost their lives fighting a deadly strain of bacteria or virus than fighting in a battle or due to starvation [1,2]. For centuries healers, medicine men and practitioners of all walks of life tried their best to find protection or a cure for symptoms caused by these most simple forms of life. Unfortunately, lack of a rational approach often impeded their progress or even led them astray. These days the majority of the population turns their aspirations to scientists in hope for a happier future, which is free from fear of uncontrollable diseases and disorders. Despite the growing success in such fields as genetics, virology, bacteriology and biomolecular science man continues to be challenged by the age-old forms of microorganisms (e.g. influenza, tuberculosis [3]) as well as recently

discovered viruses (such as Ebola [4] and HIV [5]) and even proteins that cross interspecies barrier causing transmissible spongiform encephalophathies (TSE, or prion diseases) [6,7]. An increase in population density and mobility together with poorly controllable administration of such drugs as antibiotics [3], worsen the problem even further not to mention the widespread air and water pollution acting as an additional stress to immune system and leading to the whole variety of disorders associated with cancers, tumors and lupus.

As a result of tremendous efforts and dedication of a great number of chemists, biochemists, immunologists, biologists, medical doctors, etc. in the past few decades we see how traditional approaches to treating patients are replaced or complemented with novel alternative methods. Chemotherapy [8,9] and radiotherapy[10] are now standard approached for dealing with cancer and malignant tumors. Gene therapy is in its active development stage now [11,12]. And this list continues to grow.

Photodynamic therapy [13] utilizes the energy of light to be directly applied toward the target antigen, mutated or infected cell [14]. Its tremendous potential lies in the possibility to selectively disrupt the crucial steps in the life cycle of bacteria or virus in a way that can not be prevented by mutations. Of course, this approach requires a detailed understanding of exactly what happens once light is absorbed by a chromophore. With the recent progress in laser technology, especially in the visible portion of the electromagnetic spectrum, researchers were given an unprecedented range of tools to study molecular photophysics. Development of mode-locked pulsed lasers, such as the Ti: oscillator [15], enable us to investigate the very primary photophysical and photochemical processes *in vitro* and *in vivo* and to use that knowledge in a great variety of applications ranging from treating cancer [16] to holography [17]. Ultrafast laser spectroscopy enhances our understanding of events related to chemical bond dynamics [18], solvation dynamics [19-

22], proton [23-27] and electron [28-31] transfer as well as slower but not less important processes such as protein folding [32-34].

The work presented in this thesis is a continuation of our efforts [35-55] to investigate steady- and excited-state primary photophysics of several members of the polycyclic quinone family, namely, hypericin, hypocrellin A and hypocrellin B. These naturally occurring products were found to be active ingredients of folk medicines used in Europe, China and North America. Of even greater importance is their recently discovered light-dependent anti-viral [37,38,41,54,56-63] and anti-tumor [64-72] activity. The author of the following chapters believes that the unified picture of excited-state photophysics of hypericin and hypocrellin presented in the Chapter VII is another significant step to bring these naturally and synthetically available molecules as potent drugs for treating AIDS [73-76] and cancer patients [16,77-81]. Alternatively, this knowledge will enable researchers to design and synthesize novel drugs for photodynamic therapies, such as the "molecular flashlight" [45], with higher specificity, virucidal activity and smaller side effects.

HYPERICIN

The most well-known natural source of hypericin (Figure 1.1a) is St. John's Wort *(Hypericum perforatum* or other members of genus *Hypericum)* that freely grows in Europe [82], North America, China [83] and Central Asia (Armenia, Jordan) [84,85]. Extracts of its yellow flowering tops have a long history of use as a folk medicine for treating a wide range of ailments including headache, rheumatism, inflammation in wounds and diarrhea [86]. American Indians hinted at its current use as an over-the-counter antidepressant by chewing the fresh leaves for their sedative properties [87].

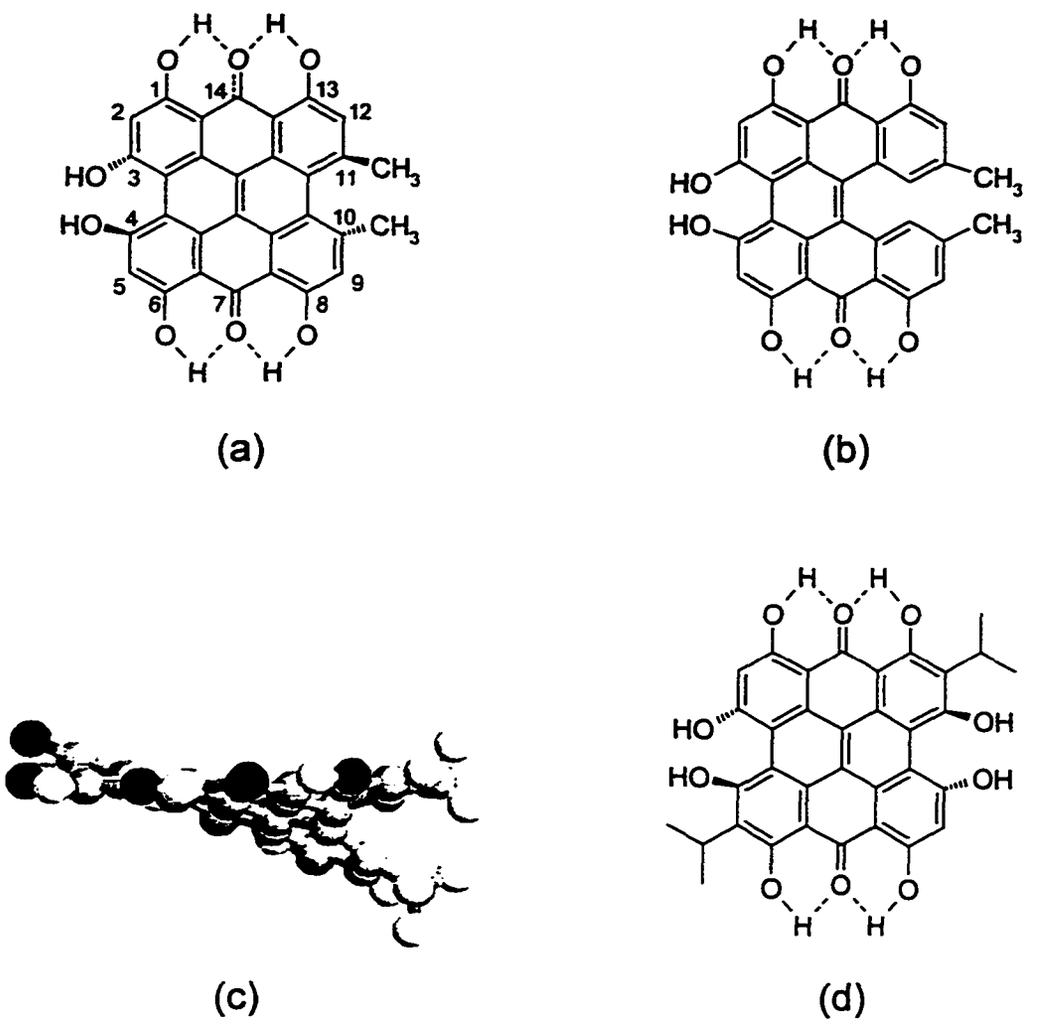

Figure 1.1 Structures of hypericin (a), protohypericin (b) and stentorin (d). Side-on view of hypericin showing twisted aromatic skeleton (c) is based on X-ray data from [88].

Just as in case of plants, hypericin was found to be a photodegradation product of the structurally similar protohypericin (Figure 1.1b) also isolated from fungus of genus *Dermocybe* growing in Australia [89] and South America as well as from various insects [90].

Hypericin is closely related, both structurally and spectrally, to the chromophore (Figure 1.1d) of membrane-bound protein stentorin in ciliates [91], *Stentor coerulus* [92,93] and *Blepharisma japonicum* [91,94,95], which is responsible for protozoan photophobic and phototactic response. Song and coworkers have discovered pH decrease of the surrounding solution upon illumination of stentorin embedded in protein and of the stentorin chromophore in vesicles [96]. Some ultrafast photochemical events of stentorin have been studied by Savikhin et al.[97] but their temporal and spectral capabilities did not allow for complete and unambiguous characterization of these processes. It has become clear, however, that understanding the photo-induced processes in this family of molecules is of primary biological relevance.

Historically, it was probably farmers who first discovered the photodynamic action of hypericin. It was noticed that after cattle graze on the herb with little yellow flowers they develop the condition subsequently called hypericinism [98], which could lead to animal death if the animal was not removed from the sunlight [98]. Consequently, the Russian name for the St. Johns' Wort is "Зверобой" (Zveroboy), literary "beast-killer". A systematic study of hypericin photophysics was not attempted until 1986, when Jardon and coworkers initiated a series of experiments on its triplet and singlet oxygen production [99]. Several years later it was discovered that the biological activity of hypericin, the most notable of which are inhibition of protein kinase C [66,70,71,100-103] and viruses [57,58,62,63,104-110,111], is triggered by light [73]. Many researchers suggested that such activity resulted merely from the ability of the hypericin excited-state to produce reactive

oxygen species (singlet oxygen, superoxide radical and anion [112-115]) [113,114,116-122]. A more detailed investigation by Fehr, Carpenter and Petrich at ISU revealed that hypericin retains its anti-retroviral activity even under hypoxic conditions [37]. The retention of toxicity in hypoxic conditions excludes the unique assignment of such activity to the trivial generation of singlet oxygen — even though hypericin does generate triplets in high yield [54] (however not as efficient as thought initially [99]). Recent results extended these observations to hypericin tumoricidal ability [65,68,70,71,81,100,123]. These experiments were encouraged by observation of light-induced acidification in vesicles [42,124] and living cells [67], just as it was found for stentorin [96]. While secondary oxygen dependence of hypericin biological activity should not be underestimated, it is evident that understanding a role of photogenerated protons is of primary relevance. This takes on additional significance in the context of the growing body of literature implicating a pH decrease with the above mentioned pharmacologically important functions [125]. Thus, it is imperative that a detailed picture of the primary photoprocesses of hypericin and other polycyclic quinones be established.

Prior to the series of experiments initiated in 1992 [35] under the direction of Professor Petrich at Iowa State University little was known about the primary events that occurred after hypericin absorbed a photon of light. Hypericin's fluorescence lifetime has been determined to be in the range of 5.5-6.5 ns depending on solvent [126]. Fluorescence quantum yield, quantum yield of intersystem crossing and singlet oxygen production in micelles and vesicles (see Table 1.1) were also measured by Jardon and coworkers, who have performed numerous studies on the hypericin triplet state [118,127-129]. A phosphorescence lifetime of 2.79 ms at 1.2 K in ethanol was measured by Angerhofer et al. [130]; and Malkin and Mazur reported triplet transient absorbance spectra characterized by single exponential decay of 4.3 μs at room temperature [131]. Their data suggest that in

Table 1.1 Basic photophysical properties of hypericin, HA and HB in benzene.

Compound	τ_f, ns	ϕ_f	ϕ_T	$\phi\,{}^1O_2$
Hypericin [126]	5.5	0.3	0.7	0.36
Hypocrellin A [136]	0.98	0.14	0.86	0.83
Hypocrellin B [136]	0.66	0.058	0.76	0.76

τ_f – fluorescence lifetime; ϕ_f – fluorescence quantum yield; ϕ_T – triplet quantum yield; $\phi\,{}^1O_2$ – siglet oxygen quantum yield

the absence of oxygen the hypericin triplet state can abstract a hydrogen atom, resulting in the formation of semiquinone species. These species were subject to a number of studies by ESR spectroscopy [121,132] and exhibited dramatic signal increase when hypericin was illuminated with light corresponding to its absorption spectrum [112,133-135].

The ground state of hypericin was subjected to absorbance [137], NMR [138] and surface-enhanced and resonance Raman spectroscopy (SERRS) studies [139-149]. X-ray crystallography data [88,150] confirmed results obtained through molecular mechanics and semi-empirical quantum mechanics computations that suggested a twisted (helical) arrangement of polycyclic skeleton (Figure 1.1c). More notable is the close proximity of four aromatic hydroxy and two keto-groups capable of intramolecular hydrogen bond formation. This arrangement is propitious for ground and/or excited-state tautomerization, which has been extensively studied in such models as malonaldehyde [151], methyl salicylate [152-154], 3-hydroxyflavone [25,155-160], etc. The other two (3-OH and 4-OH) hydroxyls are believed to sterically hinder to each other. Recent *ab initio* calculations performed in collaboration with Prof. Gordon at ISU [55] are the most reliable estimates to date of hypericin single and double tautomers energies (Figure 1.2). Existence of numerous species in hypericin ground state was subject to a controversy in literature

[49,150]. An extensive NMR study at various temperatures presented in the following chapters (supported by the above mentioned theoretical estimations) provide strong evidence that in non-ionizing and non-aqueous solutions the ground state of hypericin is homogeneous (at least on the time scale of NMR experiment).

In context of all this information it is surprising how little attention the singlet state received before 1993. Although Yamazaki et al. performed time-correlated single photon counting and steady-state measurements, they erroneously concluded that no proton transfer takes place [161]. It is now evident that the time scale they used was inadequately long. With the implementation of a transient absorbance spectrometer providing ~1 ps time resolution our group was the first to observe hypericin excited-state tautomerization in solution [35]. These and other recent results, together with the evolving picture of hypericin and hypocrellin primary photophysics, are summarized in the section on INTRAMOLECULAR PROTON TRANSFER IN POLYCYCLIC QUINONES (page 15).

HYPOCRELLIN A AND HYPOCRELLIN B

Hypocrellins are members of relatively small but growing family of biologically active perylenequinonoid (PQ) pigments obtainable from natural sources [162,163]. Its three forms, which are referred to as A, B and C, can be extracted in about equal proportions from stromatal tissues of Chinese medicinal fungus *Shiraia bambusicola*, which is parasitic on bamboo twigs [162]. Another fungus species, *Hypocrella bambusae*, is also a well-known source of both hypocrellin A (HA) and B (HB) [163]. Extracts from these fungi has been used as folk medicine for many years in the Peoples' Republic of China (PRC), particularly against skin lesions [163,164]. For that reason Hypocrellin A and B received considerable attention in a series of publications originating from the PRC.

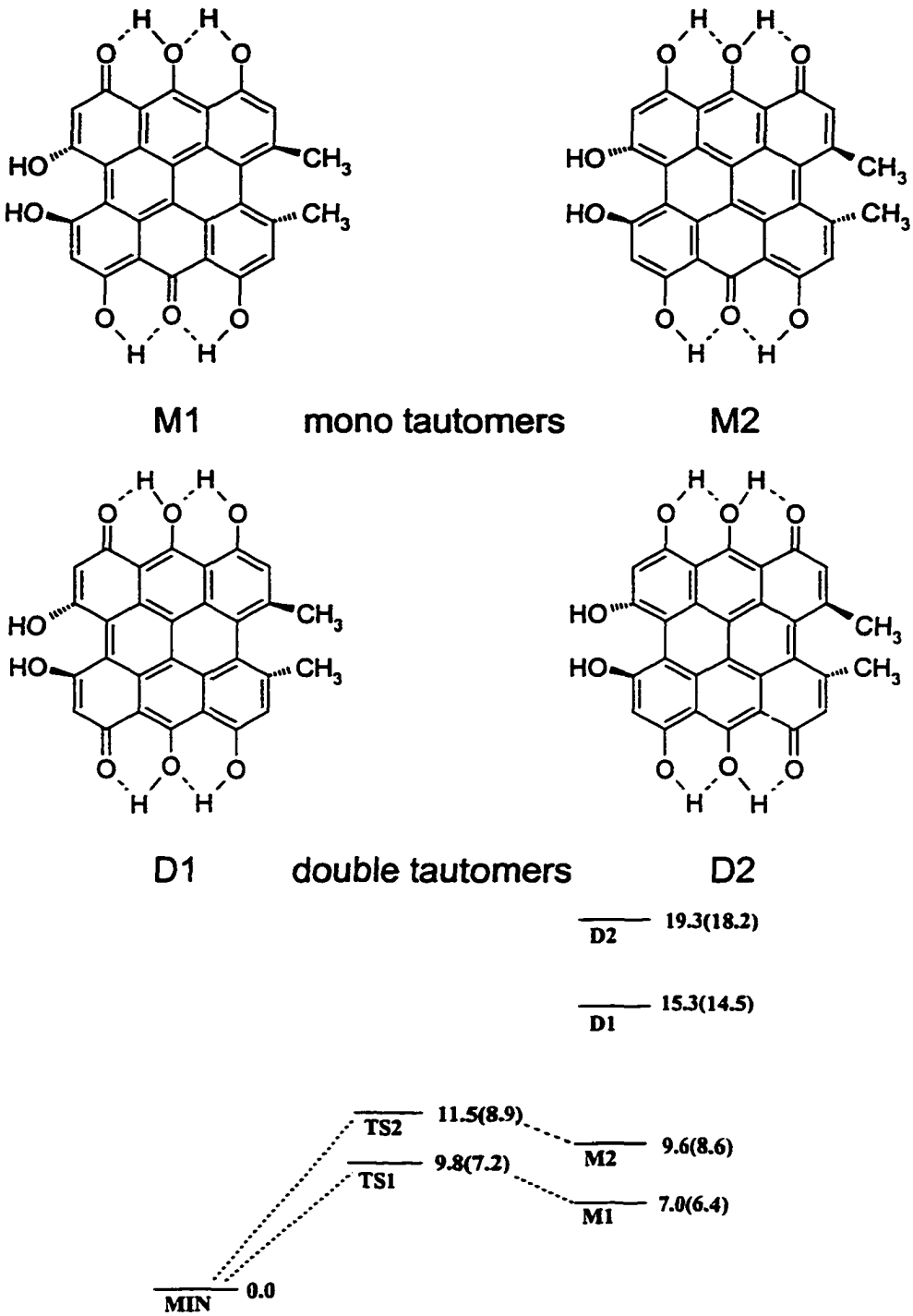

Figure 1.2 *Four of hypericin relevant tautomers and their ground-state ab initio energies* [55]in kcal/mol (values in parenthesis include zero-point corrections).

In fact, the kinase inhibition [165] and the anti-viral [56,60] and anti-tumor [79,163,166,167] activity of these and other perylenequinonoid photosensitizers were discovered earlier than that of hypericin and were also shown to be light and oxygen dependent. They have been successfully used in photodynamic therapy of cancers [72,136,166,168].

All hypocrellins can be viewed as derivatives of 4,9-dihydroxy-3,10-perylenequinone (Figure 1.3a). They have common unique structural feature: a seven-membered ring formed by carbon atoms in the "bay" region (positions C-1 and C-12, Figure 1.3b). Just as many other members of PQ family, hypocrellins form two intra-molecular hydrogen bonds which were studied both theoretically [169,170] and experimentally [171,172]. These bonds are believed to be essential in photoinduced biological activity as their methylation causes corresponding PQ to lose its valuable pharmacological properties [173].

The exact structure and naming convention for hypocrellins is subject to confusion and misunderstanding in the available literature. To be consistent with the majority of publications we refer to structure in Figure 1.3b and 1.4a as the "normal" form of HA. Although the majority of the other perylenequinones have a similar ("normal") arrangement of double and hydrogen bonds in the aromatic skeleton, the X-ray data [174] suggest that the HA double-tautomer (Figure 1.4b) is dominant, at least in the crystal form. For similar reasons the "normal" structure of HB is drawn as in Figure 1.3c. Recently isolated hypocrellin C (which is referred to as Hypocrellin B in the original publication [162]) appears to be just a diastereomer of HA and can be assigned the structure shown in Figure 1.3d that is also consistent with its higher tolerance to dehydration reaction of which HB is a product [162].

HA and HB, similar to hypericin, are soluble in both polar protic and aprotic

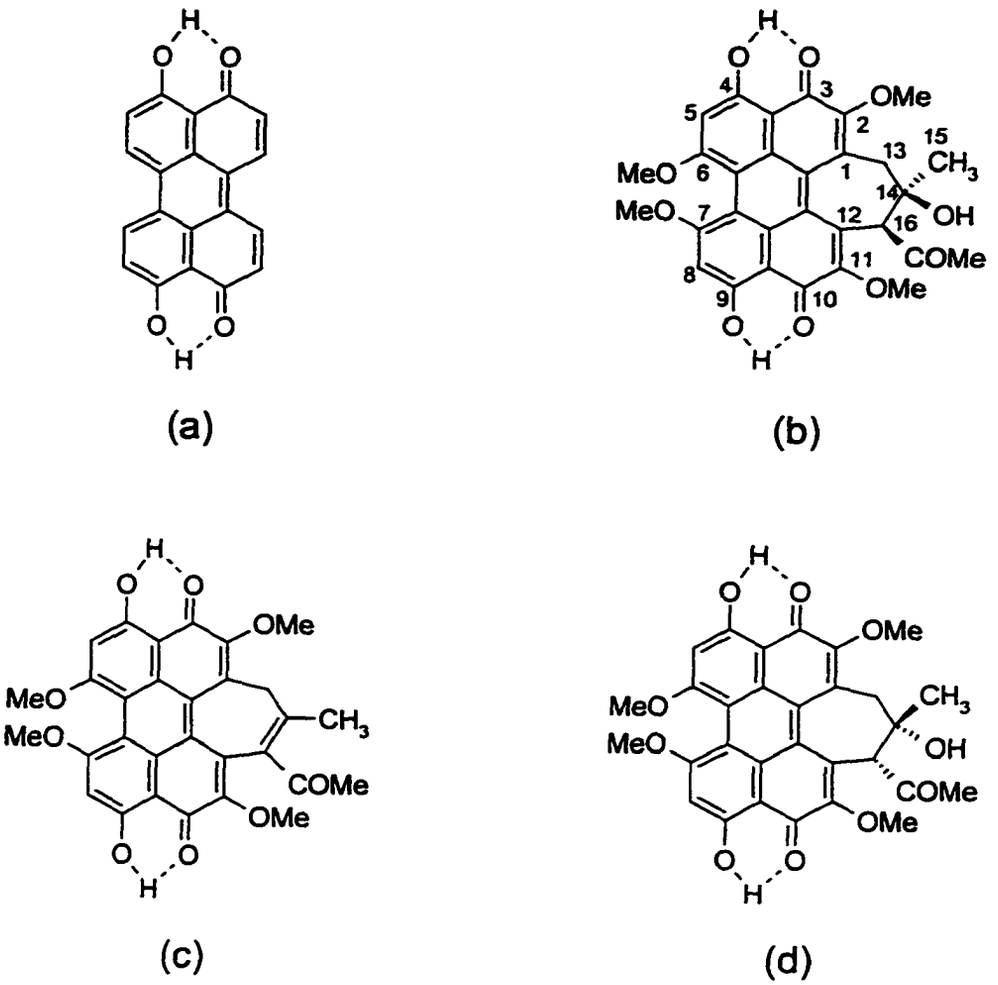

Figure 1.3 Structures of 4,9-dihydroxy-3,10-perylenequinone (a), hypocrellin A (b), hypocrellin B (c) and hypocrellin C (d).

solvents, but unlike hypericin they can also be dissolved in non-polar media such as cyclohexane and benzene [175]. Diwu et al. have measured most of the standard HA and HB photophysical properties in benzene which are summarized in Table 1.1. It appears that HB has a shorter fluorescence lifetime due to its higher intersystem crossing rate which, however, does not result in increase in triplet and singlet oxygen quantum yields, probably due to higher internal conversion rate [119,136]

Hu and co-workers report absorption spectrum of the HA triplet state in cyclohexane [176]. They observe that the triplet state of HA decays monoexponentially with a decay time constant of 4-6 μs at room temperature. It has also been reported that hypocrellins produce superoxide, hydroxy radicals and hydrogen peroxide upon illumination by light [166,177]. Their degradation decay pathways involve semiquinone radicals (extensively studied by ESR spectroscopy [177-183]) and anions in the presence of reducing species [179,182,184,185]. HA and HB are also capable of chelate complex formation with bivalent metals ions such as Mg^{2+} and Zn^{2+} in 1:1 ratio [186,187]. Fluorescence quenching by transition and rare earth ions in alchohols was also reported [188-190].

By the use of structural analogs Diwu et al. [175] suggested that intramolecular proton transfer plays an important role in the shape of HA fluorescence and absorbance spectra. A more detailed study of polarized fluorescence excitation spectra in a glass conducted in our lab [52] revealed two closely separated excited states with orthogonal transition dipole moments which is also the case for hypericin. It was also necessary to invoke the concept of ground-state heterogeneity in this class of polycyclic quinones to interpret peculiar details of their room temperature data. The most evident source of such heterogeneity is the phenol-quinone tautomerism found in majority of 4,9-dihydroxy-3,10-perylenequinone derivatives [171]. A total of four different tautomers should be expected

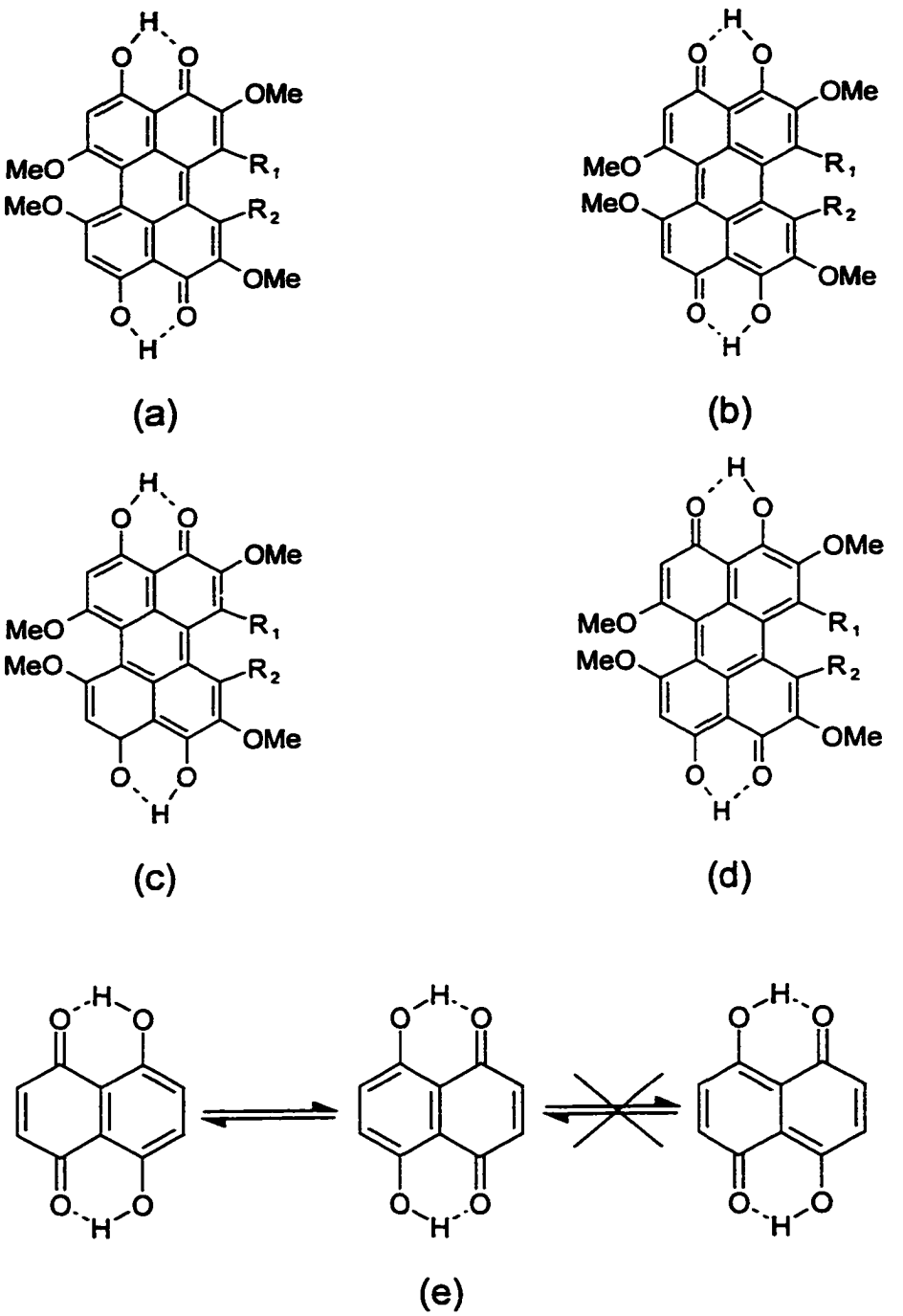

Figure 1.4 Four possible tautomers of hypocrellins A, B and C (a-d) and ground-state tautomerization of naphthazarin (e).

from hypocrellin asymmetric structure (Figure 1.4a-d). Based on solid state NMR data [171] and semiempirical AM1 calculations [191] it is argued that only "normal" and "double" tautomeric forms (a) and (b) are significantly populated in the ground state whereas single tautomers (c) and (d) are expected to have lower energy in the first excited state. These conclusions are in qualitative agreement with experimental studies and *ab initio* calculations (see refs. in [171]) of naphthazarin in the ground state (Figure 1.4e), which provides slightly oversimplified model to study phenol-keto equilibria in our case.

Finally, although it has been shown that the antiviral and antitumor activities of policyclic quinones can be dependent on oxygen [41,54,184,192,193], comparative studies of nine perylenequinones, including HA, HB, and hypericin, provide evidence that the quantum yield of singlet oxygen formation is not sufficient to explain the reported relative level of antiviral activities of these molecules, and that other structural features of perylenequinones are involved [56] (see also [194] regarding DNA damage ability). Of special relevance to the role of labile protons for this light-induced biological activity is the observation that hypericin and hypocrellin acidify their surroundings upon light absorption [42,64,67,124]. It is remarkable that, although no detectable acidification was observed for the DPPC vesicle interior in the presence of HA [41], this same agent caused pH decrease at a higher rate compared to the living cells [64].

It is yet to be revealed whether inter- or intra-molecular proton or hydrogen atom transfer is a key to understanding hypericin and hypocrellin photodynamic function. In any event elucidation of primary photoprocesses in both families of polycyclic quinones is of fundamental and urgent practical importance.

INTRAMOLECULAR PROTON TRANSFER IN POLYCYCLIC QUINONES

Proton and hydrogen atom transfer reactions, like electron transfer reactions, are of fundamental importance in both the physical and biological sciences. Proton and hydrogen atom transfer lies at the heart of acid-base chemistry and of a wide range of catalytic reactions in biological systems. Much progress has been made in understanding electron transfer reactions through the combination of experimental and theoretical work. Theoretical treatments for both nonadiabatic and adiabatic proton transfer [195-208] bear some similarities to those for electron transfer [209,210]. But many aspects of excited-state proton transfer reactions are poorly understood, in particular, the way in which the solvent or the intramolecular modes of the solute couple to the reaction.

Ground-state proton transfer has been one of the most important topics in chemistry for many years [211,212]. Only recently, however, has the study of excited-state proton transfer become popular both experimentally and theoretically. Huppert [213] and Arnaut and Formosiho [211,212] reviewed excited-state proton transfer reactions. These reviews include experimental results concerning inter- and intramolecular proton transfers in both the ground and the excited states. Two examples of molecules that exhibit excited-state proton transfer behavior are methyl salicylate, described by Weller [214], and 3-hydroxyflavone, described by Sengupta and Kasha [215]. Before fast laser sources were available, the methods employed to study excited-state proton transfer were mainly steady-state approaches. For example, the Förster cycle [216,217] is used to determine the pKa change between ground state and excited state from the steady-state absorption and fluorescence spectra. Also, dual emission is taken as an indication of tautomerization in the excited-state. However, in the last decades, with the advent of fast pulsed laser light sources, kinetic data with ultrafast time resolution has become available for excited-state proton transfer processes. Many very interesting and important phenomena occurring on

the femtosecond timescales have been observed. Theoretical approaches have emerged to permit one to cope with the quantum character of the proton at a molecular dynamics simulation level. Those include diabatic curve-crossing approaches [196,218], adiabatic quantum simulation techniques [197,219,220] and possible nonadiabatic extensions, path-integral formulations [221-223] and semiclassical tunneling algorithms [224,225]. Computational studies using these methods have helped us a great deal to understand many features of proton-transfer reactions in solution [196,218,221] and in biological systems [220]. For example, Hynes et al. [226] have developed a dynamic theory for the proton transfer rate constant both in the nonadiabatic, weak coupling regime and in the adiabatic limit. The overall rate constant is expressed as resulting from an incoherent superposition of proton tunneling events in a distribution of inhomogeneous solvent environments. The classical Arrhenius behavior is determined by the solvent molecules orientation and the vibrational factors. Three coordinates have been shown to play an important role: the proton coordinate; the intramolecular separation of the two "heavy" atoms (oxygens for example) between which the proton is transferred; and the collective solvent coordinate. In Hynes' work, electrons were treated adiabatically, but the proton transfer was considered either nonadiabatically or adiabatically depending on the separation of the two heavy atoms. The threshold between the adiabatic and nonadiabatic regions is determined by the O–O distance which was found to be 2.7 Å. When proton transfer is in the adiabatic region, small isotope effect is expected. Otherwise tunneling is considered to be important and a large isotope effect should be observed[226].

The following summary puts together the recent advances in understanding excited-state proton transfer in hypocrellin and hypericin which is often compared against its analogs (Figure 1.5). Our evolving interpretation of the observed phenomena is presented in the context of the theory developed by Hynes and coworkers [195,197-199,208]. We

have used the naturally occurring polycyclic aromatic quinones hypericin and hypocrellins to test this theory.

Summary of Results

The most significant accomplishments *prior* to this work are summarized below.

1. Time-resolved absorption (stimulated emission) spectra and kinetics [35,39,40] indicate that the hypericin emission spectrum grows in on a 6-12-ps time scale in all the solvents investigated. Based on the model compounds, the rise time for the appearance of the hypericin emission is taken as evidence for an excited-state proton transfer. In sulfuric acid, where all the carbonyl groups are expected to be protonated, the excited-state transient appears instantaneously. On the other hand, in a solvent such as DMSO, the transient appears with a finite rise time.

3. Although no deuterium isotope effect for proton transfer is observed for hypericin, an isotope effect of 1.4 is observed in the excited-state transients of hypocrellin [46]. This unambiguously identifies the process as a proton transfer event.

4. The proton transfer rate in hypericin does not depend on viscosity and depends only very weakly on solvent [35,39,40]. Hence, little charge separation is expected in the excited state.

5. The proton transfer rate in hypocrellin has a strong dependence on the bulk viscosity and is very well correlated with polarity for solvents of a certain kind, for example alcohols [47]. The time constant for proton transfer in hypocrellin ranges from 50 to 230 ps in the solvents we have studied. The viscosity dependence is remarkable not only because it is absent in hypericin, but also because it appears to be exceedingly well described by a bulk property and does not require specific consideration of the structural aspects of the solvents, which vary considerably. It

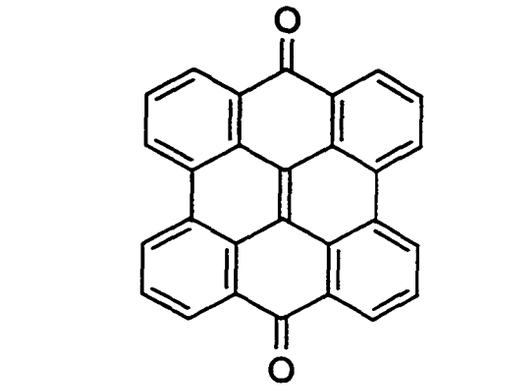

(a)

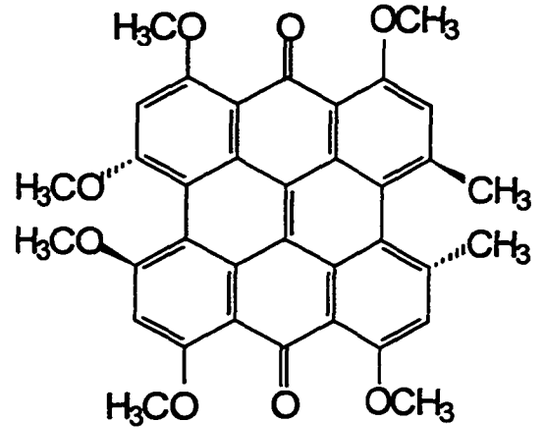

(b)

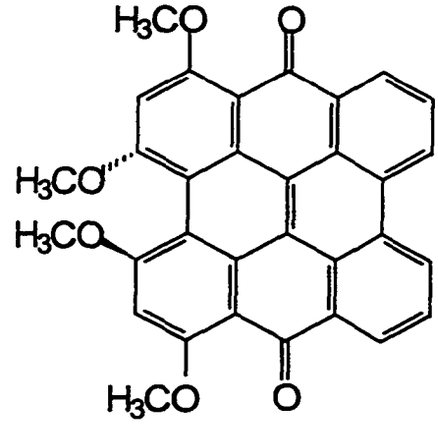

(c)

Figure 1.5 Structures of hypericin analogs: (a) mesonaphthobianthrone, (b) "hexamethoxyhypericin", (c) "tetramethoxyhypericin".

is often the case that trends are only followed for solvents of a given kind: alkane or alcohol; primary alcohol or higher degree alcohol; hydrogen bonding or nonhydrogen bonding, etc. Das et al. [47] suggested that the viscosity dependence on the excited-state transfer process is a consequence of the coupling of the H-transfer to a conformational change between twisted configurations about the long molecular axis. It is important to note, however, that similar twisted configurations exist in hypericin, which exhibits no viscosity dependence. This suggests that the hypocrellin seven-member ring plays an important role in such a process.

6. The transient absorbance kinetics of hypericin differs with excitation and probe wavelengths [49]. This along with "mirror-image" symmetry of absorbance and emission spectra (Figure 1.6) suggested that hypericin is heterogeneous in the ground state. In the light of a more detailed investigation presented in the following chapters it was found that peculiar structural features of this molecule allow for different interpretation which is also consistent with temperature-dependent NMR data (see for example [150] and Chapter V) and the results of *ab initio* calculations [55].

7. In order to gain additional information on hypericin and hypocrellin excited-state proton transfer reactions, our group studied them as a function of temperature in 1:1 ethanol/methanol mixtures (Figure 1.7a from ref. [227]). The activation energy for the hypericin reaction was 0.044 ± 0.008 kcal/mol; for the hypocrellin reaction, 2.12 ± 0.07 kcal/mol. (In a previous study the estimated activation energy for the hypericin reaction was determined over a very limited temperature range [39].)

8. Because the hypocrellin reaction exhibits a viscosity dependence and because viscosity is temperature dependent, the activation energy reported in point 7 above cannot be totally indicative of the intrinsic barrier in the conformational coordinate.

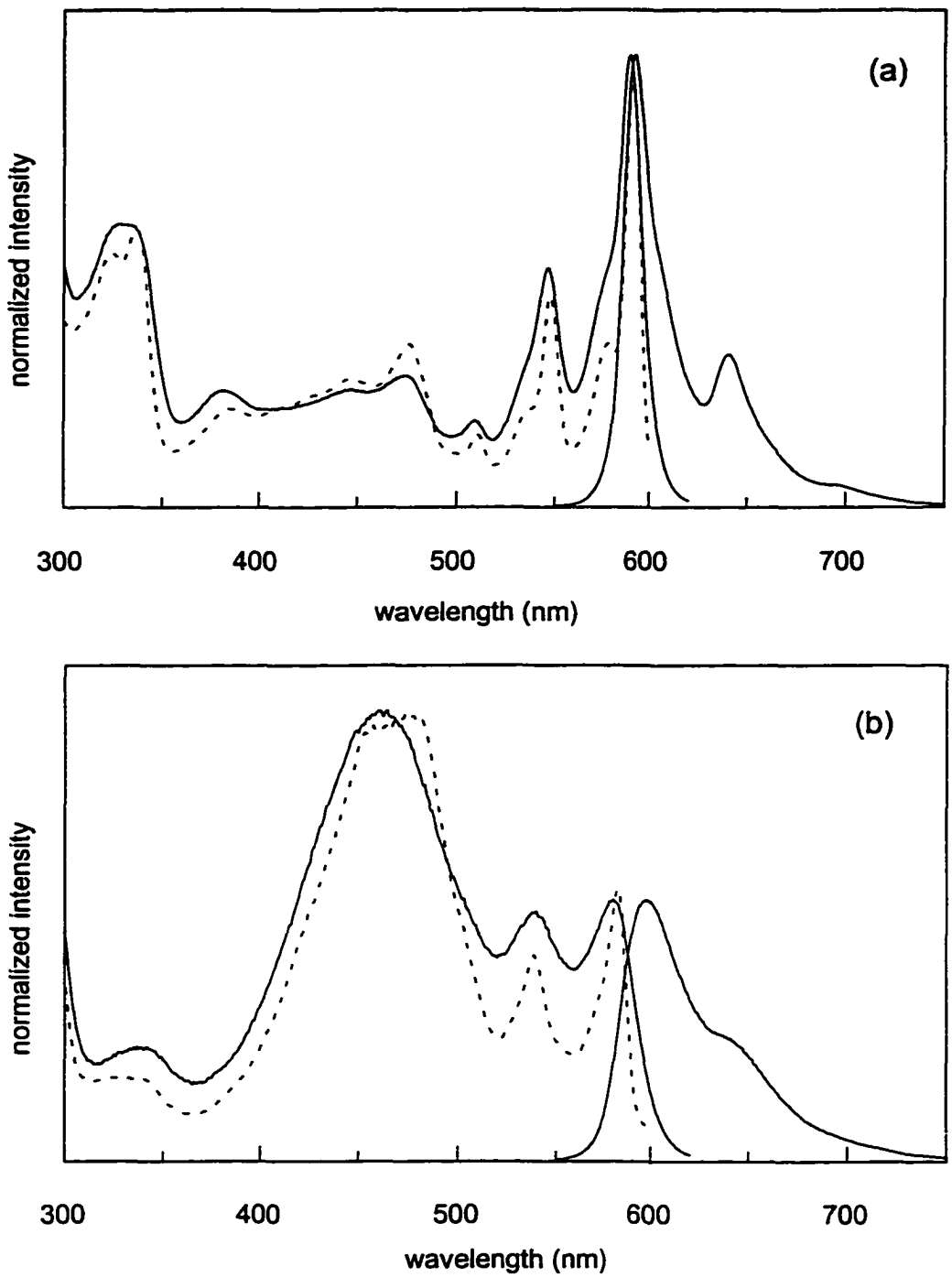

Figure 1.6 Comparison of the fluorescence excitation and emission spectra of hypericin (a) and hypocrellin (b) in a 1:1 ethanol/methanol mixture at room temperature. The excitation spectra were measured at 295 K (solid line) and at 77 K (dashed line). The excitation spectra were monitored at 650 nm at 295 K and at 620 nm at 77 K [52].

In order to separate the contribution of solvent viscosity from the internal barrier, isoviscosity plots were constructed in which the temperature dependence of the rate could be examined at constant viscosity (Figure 1.7b). These plots indicate that the intrinsic barrier is indeed considerably higher than that in hypericin: 0.41 ± 0.09 kcal/mol [227].

Origins (and Lack of) an Isotope Effect

In the early work on primary photophysics of hypericin, Feng Gai and co-workers assigned transients in the stimulated emission signal to proton transfer. This was based on the observation that protonation of the carbonyl group in the 7 or 14 positions renders the rise in the stimulated emission instantaneous and causes the "stripped-down" hypericin analog (normally non-fluorescing), mesonaphthobianthrone (Figure 1.5a), to produce hypericin-like fluorescence. Even with this evidence the idea of intramolecular excited-state proton was not readily accepted. Lack of change in risetime upon deuterium substitution and the presence of "mirror-image" symmetry in steady-state spectra were the key counterarguments against the proposed excited-state photochemisty.

The absence of an isotope effect and whether proton or atom transfer is a significant nonradiative decay process in hypericin may be responded to in the context of work by Hynes, Borgis, and coworkers [195,197-199,208]. These workers discuss proton transfer of a linear system OH•••O in the nonadiabatic and adiabatic limits. The limiting cases are determined by the extent to which the reactant and product species are separated by a barrier in the proton coordinate that is large with respect to the thermal energy, kT. When the barrier is large, the ground-state vibrational levels of the reactants and products lie well below the barrier, and the reactants and products are consequently localized, the transfer event can be described by a tunneling process, in which case very large isotope effects can

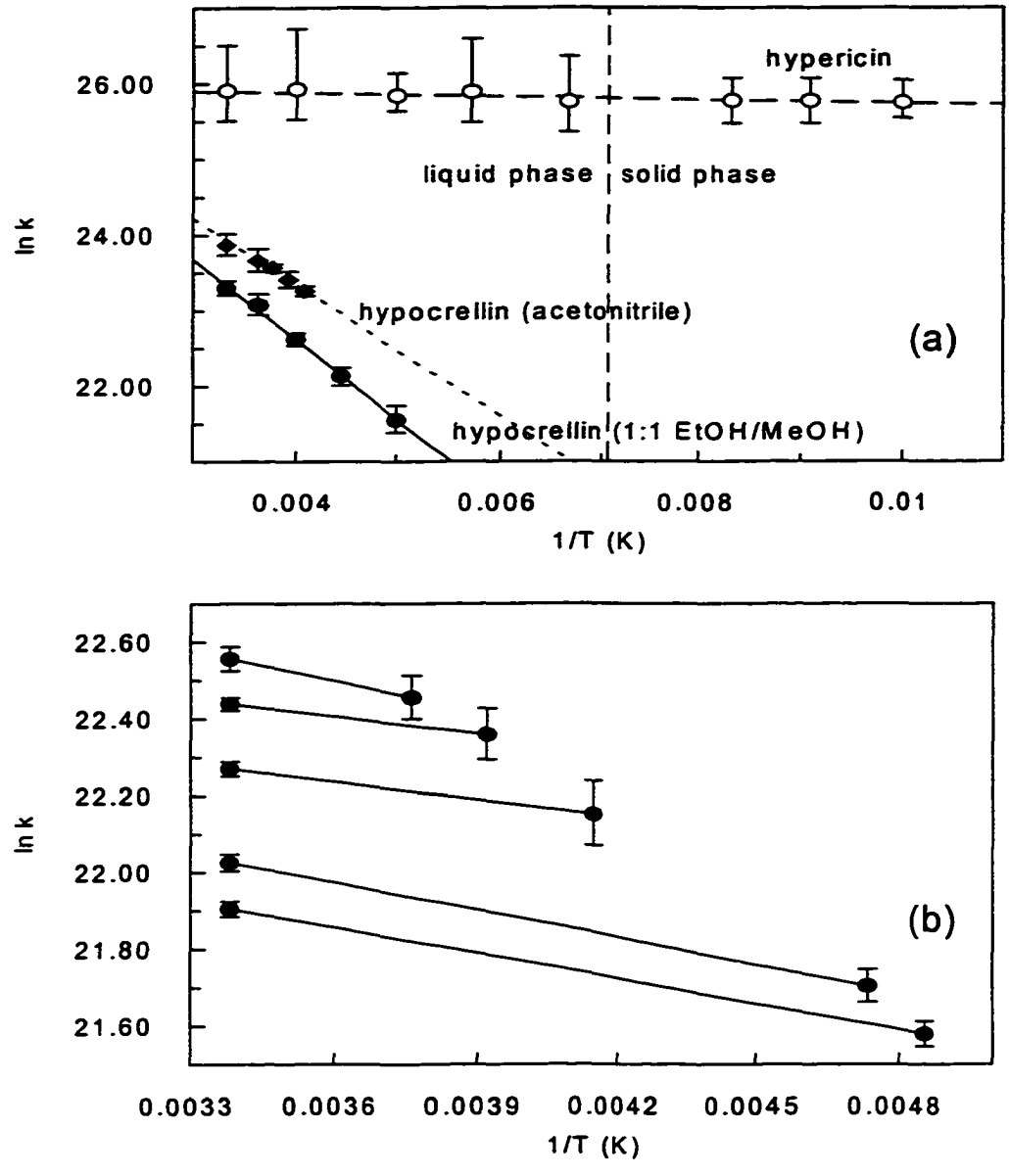

Figure 1.7 (a) Arrhenius plots for hypericin and hypocrellin in a 1:1 methanol:ethanol mixture [227]. Each point represents the average of at least five experiments. The error bars indicate one standard deviation from the mean. The Arrhenius prefactors and activation energies obtained from these plots are: hypericin, $A = 1.89 \pm 0.06 \times 10^{11}$ s^{-1} and $E_a = 0.044 \pm 0.008$ kcal/mol; hypocrellin, $A = 4.65 \pm 0.62 \times 10^{11}$ s^{-1} and $E_a = 2.12 \pm 0.07$ kcal/mol. For plot in acetonitrile $A = 4.54 \pm 1.11 \times 10^{11}$ s^{-1} and $E_a = 1.75 \pm 0.14$ kcal/mol.

(b) Five sets of isoviscosity plots for hypocrellin A. The solvents are (from top to bottom, first point of each line): cyclohexanone, butanol, pentanol, nonanol and decyl alcohol at room temperature. The corresponding viscosities of ethanol, at different temperatures are plotted as the end points. The viscosity independent Arrhenius energy of activation is 0.41 ± 0.09 kcal/mol.

be expected. This nonadiabatic limit is expected to hold for weak or intermediate strength hydrogen bonded systems that are characterized by heavy atom (O-O) distances of 2.6-2.7 Å. This O-O distance strongly modulates the magnitude of the matrix element that couples the reactant and product states and thus determines the size of the barrier separating them.

When the heavy atom distance is less than 2.6 Å, the adiabatic limit is obtained (Figure 1.8a). Here, because the vibrational energy levels of the proton stretch mode lie above a small barrier in the proton coordinate separating the reactant and product species, an isotope effect will not be observed as a result of proton transfer. One can argue that hypericin falls into the adiabatic limit because its relevant oxygen-oxygen distance is 2.5 Å [55, 88, 150]. In hypocrellin, this distance is only slightly higher [174]. The present work addresses the excited-state photophysics of hypocrellin in the light of what is known concerning hypericin and in terms of the theory of proton transfer referred to above.

In the modern treatment of proton transfer, a Born-Oppenheimer separation is used to distinguish the fast proton motion (~2500 cm^{-1}) from the slow heavy-atom motion (e.g., the O-O vibration) and from the even slower solvent motions (~100 cm^{-1}). The proton can thus adjust immediately to any instantaneous nuclear configuration of these slow degrees of freedom. The proton wavefunction depends on the proton coordinate, q; and it depends parametrically on the heavy-atom coordinates, Q, and the solvent coordinates, S.

Figure 1.8a presents schematic potential energy surfaces as a function of the proton stretch coordinate for a system in the adiabatic limit. Whether the system is in the reactant or product configuration or in an intermediate configuration depends on the stabilization imparted by the Q and S. In the theory, this stabilization is discussed mostly in terms of the solvent. Most reference to the heavy-atom coordinate is made in terms of the O-O vibration (i.e., the heavy atoms between which the proton is transferred) because it usually

has the most pronounced effect on the coupling between the reactant and product states. Because this distance is so short in hypocrellin and hypericin, we suggest that the proton transfer should always be considered to be in the adiabatic limit. More important heavy atom motions for hypocrellin and hypericin are likely to involve the twisting motion of the aromatic skeleton and the rearrangement of double bonds in the aromatic skeleton subsequent to or during transfer.

In the adiabatic limit, because the vibrational energy levels of the proton stretch mode lie above a small barrier, an isotope effect will not be observed as a result of proton transfer. Staib et al. [199], however, suggest the intriguing possibility that deuterium substitution may lower the ground vibrational energy below the top of the barrier in the proton coordinate. Such a lowering of the ground state energy level would induce an isotope effect because now the proton could tunnel through the barrier or undergo an activated crossing of it. We propose that the isotope effect observed in hypocrellin has its origins in such an explanation. That the isotope effect is relatively small suggests that the vibrational ground state is not significantly lowered below the barrier, and that the proton transfer is an activated process. Temperature studies and theory will permit us to confirm this hypothesis.

Temperature Dependence of the Proton Transfer Rates in Hypericin and Hypocrellin

The most striking features of the Arrhenius plots (Figure 1.7a) are i) the difference between the activation energies, ii) the essentially zero activation energy of hypericin, iii) and that the liquid-glass transition of the solvent does not have an effect on the hypericin plot; but, as this transition is approached, there is a dramatic effect on the hypocrellin kinetics. The first two of these features are consistent with the lack of an isotope effect in

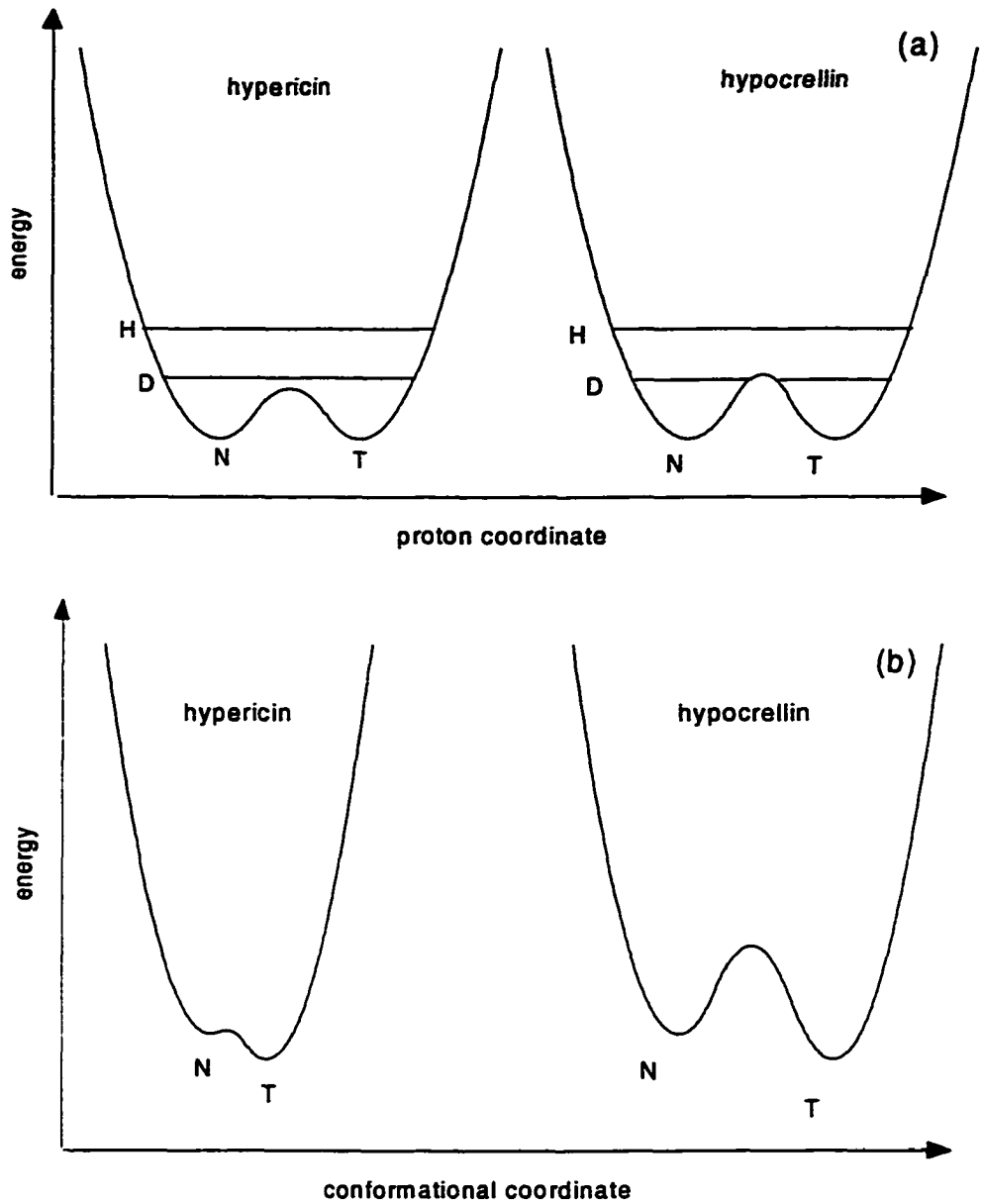

Figure 1.8 (a) Schematic illustrations of the potential energy surfaces of hypericin and hypocrellin in the proton and "conformational" coordinates. Our justification for the placement of the zero-point level slightly below the barrier for deuterated hypocrellin is explained in detail elsewhere [227]. It provides an elegant means, suggested by Staib et al. [199], to introduce an isotope effect in a situation where there is an adiabatic proton transfer and where the zero-point vibrational level for the protiated species lies above the barrier.

(b) Fluctuations of the polarization of the solvent and the solute are responsible for trapping the molecule in either a "normal" form (left side of well) or "tautomer" form (right side of the well). The potential energy curves at the top of the figure (in the proton coordinate) indicate a configuration of the solvent and solute polarization at which the normal and tautomer forms are isoenergetic. Note that the potential energy surfaces drawn against the proton coordinate are simplified in that they depict a symmetric hydrogen bonding interaction.

hypericin and the small isotope effect in hypocrellin. In particular, the near-zero activation energy in hypericin is consistent with our previous proposal that the proton transfer reaction is adiabatic in the proton coordinate and that the zero-point vibrational energy lies above the barrier in this coordinate (Figure 1.8a).

If the zero-point energy lies above the barrier in the proton coordinate, the proton (or hydrogen atom) is effectively delocalized between the two oxygen atoms until a change in another coordinate can trap the system in the tautomerized form (Figure 1.8b). We propose that this latter conformational change is the rate determining step for the observed proton transfer time.

In the model system for excited-state proton transfer, 3-hydroxyflavone [25,155-158], the reaction occurs in ~100 fs in dry non-hydrogen bonding solvents [25]. In hydrogen bonding solvents such as alcohols, the observed proton transfer time in 3-hydroxyflavone reflects the timescale for the displacement of the solvent molecule, hydrogen-bonded to the enol proton of the solute, thus stabilizing the proton-transfer product. Specific hydrogen bonding interactions between hypericin and hypocrellin with solvent cannot explain the relatively slow proton transfer times (~10 ps) because the hypericin reaction is insensitive to solvent [35,39,40] and because the hypocrellin reaction, while sensitive to solvent, is only well correlated to the bulk viscosity of different solvents and not to solvents of a given "type" [47]. The insensitivity of the hypericin reaction to solvent is most likely a result of the strong association of the proton with the oxygens of both the peri hydroxyl and the carbonyl groups.

Since the oxygen-oxygen distance (in the ground state) is essentially the same in both hypericin and hypocrellin (2.5 Å), a different origin for the solvent dependence of the hypocrellin reaction must be found. The 2.12 ± 0.07 kcal/mol activation energy for hypocrellin, in addition to the strong dependence of its proton transfer reaction on

viscosity [47], indicate that, unlike hypericin, its conformational change must be rather large in amplitude and may involve torsion of the aromatic skeleton or displacements of its 7-membered ring. Consistent with the idea of a large-amplitude transition occurring in hypocrellin is that the form of the kinetic traces changes drastically as the liquid-glass transition is approached.

The negligible activation energy for hypericin is consistent with previous suggestions that the proton-transfer reaction is adiabatic [35,39,40,46,47,49-51] which requires that displacement in at least one other coordinate be taken into account in order to describe the reaction dynamics. The negligible activation energy for hypericin also indicates that the displacement in the "conformational" coordinate is very low-amplitude (Figure 1.8*b*). The proton transfer for hypocrellin is also considered to occur in the adiabatic regime, but the activation energy for the process is significant (2.12 ± 0.07 kcal/mol), consistent with the strong correlation for the proton transfer reaction on bulk viscosity [47], and suggesting that a larger amplitude motion than for the case of hypericin comprises part of the reaction coordinate [227]. The conformational changes that are coupled to the proton transfer reaction in hypocrellin is a subject of the Chapter V of this thesis. Hypericin skeletal motions are much more subtle to observe and are currently under investigation.

Toward a Unified Picture of the Hypericin and Hypocrellin Photophysics

Based on the above points, we are constructing a unified picture of the excited state proton transfer phenomena in these molecules. At first glance, the similarity of the structures and the spectra (Figure 1.6) of hypericin and hypocrellin would lead one to believe that they exhibit, at least superficially, similar excited-state photophysics. This is not the case. The time constant for excited-state proton transfer in hypericin is ~10 ps and

essentially independent of solvent [35,39,40] whereas for hypocrellin it ranges from 50-250 ps in the solvents we have investigated [47]. Also, the proton transfer reaction in hypericin exhibits no isotope effect, whereas in hypocrellin a small isotope effect of 1.4 is observed [46]. This further suggests substantial difference in origin of the primary excited-state reaction coordinate.

As more and more experimental data become available we gain confidence in putting together different pieces of the photophysical puzzle. It is now clear that the "picture" of primary photoprocesses in hypericin and hypocrellins is not "plane" but rather involves a set of vibrational, conformational and possibly solvent coordinates. The challenge of building theoretically solid and consistent model that is also charged with considerable predictive power is complicated by inherently nonequilibrium nature of the processes under consideration. Indeed, in less than 300 fs after excitation the system is undergoing internal vibrational relaxation and solvent is reorganizing to adjust for the changes in electrical dipole moment and geometry of the excited state. Both vibrational energy redistribution (vibronic cooling) and solvent reorganization may affect the measured properties of the excited state. Nevertheless, we do not cease our efforts in constructing meaningful potential energy surfaces to explain excited-state photophysics of polycyclic quinones.

DISSERTATION ORGANIZATION

Comprehensive description of fluorescence upconversion apparatus constructed by the candidate is presented in Chapter II. It also includes a detailed account on the computer simulations of the transient absorbance and anisotropy decay in pump/probe type experiment, which we use to support self-consistence of the model for hypocrellin A excited-state photophysics.

Chapters III-VII are based on the articles already published or in preparation for publication in scientific research journals.

Our initial accounts on fundamentals of excited-state processes in hypocrellin A and a comparison with hypericin form Chapter III. Just as with about any other project conducted in our lab this study involved joint effort of several individuals with about equal contribution to the results presented. Being one of the keystones of the whole project inclusion of this paper was recommended by the Chair of the Program of Study Committee as a vital part of this thesis, strongly contributing to its integrity.

The results of a more detailed study of hypocrellin A are shown to be consistent with the evolving picture of its photophysics by the computer simulations of the kinetic model developed in Chapters IV with details provided in Chapter II. An essential part of this work related to modeling the results of pump/probe absorbance experiment was performed and discussed by the candidate. The code for computer simulations is included as an appendix to Chapter IV.

A long-needed investigation into the structural features and dynamics of hypericin, hypocrellin A and hypocrellin B ground-state, done by a combination of dynamic and 2D ROESY NMR techniques, can be found in Chapter V.

Chapter VI demonstrates the use of time-correlated single photon counting and fluorescence upconversion as complimentary methods to study transient fluorescence of hypericin and hypocrellin, in this case, in complexes with subcellular components of pharmacological importance. This is our first publication to include description of fluorescence upconversion spectrometer presented in Chapter II in detail. Candidate also performed steady-state absorption and emission as well as conventional fluorescence lifetime measurements of the title compounds.

In Chapter VII our latest results and ideas help bring together the whole body of

information collected in the past few years, as well as recent fluorescence upconversion results, to build what we believe is a unified picture of the hypericin and hypocrellin excited-state primary photophysics.

General conclusions are summarized in Chapter VIII. Figures and lists of references can be found in the end of each chapter. Numbering for figures, tables and equations shows also the corresponding chapter number.

REFERENCES

1. Oldstone, M. B. A. *Viruses, Plagues, and History*; Oxford University Press: New York, 1998.
2. Diamond, J. M. *Guns, germs, and steel : the fates of human societies*; 1st ed.; W.W. Norton & Co.: New York, 1997.
3. Kling, J. *Modern Drug Discovery* **1999**, *2*, 32-45.
4. Bowen, E. T.; Lloyd, G.; Harris, W. J.; Platt, G. S.; Baskerville, S. A.; Vella, E. E. *Lancet* **1977**, *1*, 571.
5. Coffin, J. M. *Fundamental Virology*; Fields, B. N. and Knipe, D. N., Ed.; Raven Press: New York, 1991, pp 645-708.
6. Gadjusek, D. C. *Science* **1977**, *197*, 193.
7. Bolton, C.; McKinley, M. P.; Prusinek, S. B. *Biochemistry* **1984**, *23*, 5898.
8. Kuemmerle, H. P. *Clinical chemotherapy*; G. Thieme Verlag, Thieme-Stratton: Stuttgart, New York, 1983.
9. Pratt, W. B. *Fundamentals of chemotherapy*; Oxford University Press: New York,, 1973.
10. Fletcher, G. H. *Textbook of radiotherapy*; 3d ed.; Lea & Febiger: Philadelphia, 1980.
11. Buchschacher, G. L. *JAMA* **1993**, *269*, 2880.

12. Seeley, T. *Detection of loss of the wild-type huBUB1 gene in the diagnosis and treatment of cancers*: PCT Int. Appl., 1998.

13. Moan, J. B. K. *Photochem. Photobiol.* **1992**, *55*, 931-948.

14. Henderson, B. W.; Dougherty, T. J. *Photochem. Photobiol.* **1992**, *55*, 145-157.

15. Spence, D. E.; Kean, P. N.; Sibbett, W. *Opt. Lett.* **1991**, *16*, 42-44.

16. Koren, H.; Schenk, G. M.; Jindra, R. H.; Alth, G.; Ebermann, R.; Kubin, A.; Koderhold, G.; Kreitner, M. *J. Photochem. Photobiol., B* **1996**, *36*, 113-119.

17. Minassian, A.; Crofts, G. J.; Damzen, M. J. *Opt. Lett.* **1997**, *22*, 697-699.

18. Lambert, W. R.; Felker, P. M.; Zewail, A. H. *J. Chem. Phys.* **1981**, *75*, 6958.

19. Castner, E. W., Jr.; Bagchi, B.; Maroncelli, M.; Webb, S. P.; Ruggiero, A. J.; Fleming, G. R. *Ber. Bunsen-Ges. Phys. Chem.* **1988**, *92*, 363-372.

20. Gardecki, J.; Horng, M. L.; Papazyan, A.; Maroncelli, M. *J. Mol. Liq.* **1995**, *65/66*, 49-57.

21. Jarzeba, W.; Kahlow, M.; Barbara, P. F. *J. Imaging Sci.* **1989**, *33*, 53-57.

22. Maroncelli, M.; Castner, E. W., Jr.; Webb, S. P.; Fleming, G. R. *Springer Ser. Chem. Phys.* **1986**, *46*, 303-307.

23. Strandjord, A. J. G.; Courtney, S. H.; Fnedrich, O. M.; Barbara, P. F. *J. Chem. Phys.* **1983**, *87*, 1125.

24. Kim, Y. R.; Yardley, J. T.; Hochstrasser, R. M. *Chem. Phys.* **1989**, *136*, 311-319.

25. Schwartz, B. J.; Peteanu, L. A.; Harris, C. B. *J. Phys. Chem.* **1992**, *96*, 3591-3598.

26. Barbara, P. F.; Walker, G. C.; Smith, T. P. *Science* **1992**, *256*, 975.

27. Kosover, E. M.; Huppert, D. *Ann. Rev. Phys. Chem.* **1986**, *37*, 127.

28. Heitele, H. *Angew. Chem.Int. Ed. Engl.* **1993**, *32*, 359.

29. Johnson, A. E.; Levinger, N. E.; Jarzeba, W.; Schlief, R. E.; Kliner, A. B.; Barbara, P. F. *Chem. Phys.* **1993**, *176*, 555.

30. Kang, T. J.; Jarzeba, W.; Barbara, P. F.; Fonesca, T. *Chem.Phys.* **1990**, *149*, 81.

31. Kosower, E. M.; Huppert, D. *Chem. Phys. Lett.* **1983**, *96*, 433.

32. Wen, Y.-X.; Chen, E.; Lewis, J.-W. *Review of Scientific Instruments* **1996**, *67*, 3010-3016.

33. Ratner, V.; Haas, E. *Review of Scientific Instruments* **1998**, *69*, 2147-2154.

34. Kellermayer, M.-S. Z.; Smith, S.-B.; Granzier, H.-L. *Science* 1112, *276*, 1112-1116.

35. Gai, F.; Fehr, M. J.; Petrich, J. W. *J. Am. Chem. Soc.* **1993**, *115*, 3384-3385.

36. Carpenter, S.; Fehr, M. J.; Kraus, G. A.; Petrich, J. W. *Proc. Natl. Acad. Sci. U. S. A.* **1994**, *91*, 12273-12277.

37. Fehr, M. J.; Carpenter, S. L.; Petrich, J. W. *Bioorg. Med. Chem. Lett.* 1994, *4*, 1339-1344.

38. Fehr, M. J.; Gai, F.; Petrich, J. W. *Springer Ser. Chem. Phys.* 1994, *60*, 462-465.

39. Gai, F.; Fehr, M. J.; Petrich, J. W. *J. Phys. Chem.* 1994, *98*, 8352-8358.

40. Gai, F.; Fehr, M. J.; Petrich, J. W. *J. Phys. Chem.* **1994**, *98*, 5784-5795.

41. Fehr, M. J.; Carpenter, S. L.; Wannemuehler, Y.; Petrich, J. W. *Biochemistry* 1995, *34*, 15845-15848.

42. Fehr, M. J.; McCloskey, M. A.; Petrich, J. W. *J. Am. Chem. Soc.* 1995, *117*, 1833-1836.

43. Petrich, J. W. *Excited-state proton transfer in hypericin and other polycyclic quinones.*; American Chemical Society: Chicago, IL, August 20-24, 1995, pp PHYS-085.

44. Das, K.; English, D. S.; Fehr, M. J.; Smirnov, A. V.; Petrich, J. W. *J. Phys. Chem.* 1996, *100*, 18275-18281.

45. Kraus, G. A.; Zhang, W.; Fehr, M. J.; Petrich, J. W.; Wannemuehler, Y.; Carpenter, S. *Chem. Rev.* 1996, *96*, 523-535.

46. Das, K.; English, D. S.; Petrich, J. W. *J. Phys. Chem. A* 1997, *101*, 3241-3245.

47. Das, K.; English, D. S.; Petrich, J. W. *J. Am. Chem. Soc.* **1997**, *119*, 2763-2764.

48. English, D. S.; Das, K.; Petrich, J. W. *Hypericin, hypocrellin and model compounds: Primary photoprocesses of light-induced antiviral agents.*; American Chemical Society, Washington, D. C., 1997, pp PHYS-405.

49. English, D. S.; Das, K.; Ashby, K. D.; Park, J.; Petrich, J. W.; Castner, E. W. J. *J. Am. Chem. Soc.* **1997**, *119*, 11585-11590.

50. English, D. S.; Das, K.; Zenner, J. M.; Zhang, W.; Kraus, G. A.; Larock, R. C.; Petrich, J. W. *J. Phys. Chem. A* **1997**, *101*, 3235-3240.

51. English, D. S.; Zhang, W.; Kraus, G. A.; Petrich, J. W. *J. Am. Chem. Soc.* **1997**, *119*, 2980-2986.

52. Das, K.; Dertz, E.; Paterson, J.; Zhang, W.; Kraus, G. A.; Petrich, J. W. *J. Phys. Chem. B* **1998**, *102*, 1479-1484.

53. Kraus, G. A.; Carpenter, S. L.; Petrich, J. W. *Photoactivated antiviral and antitumor compositions using a photosensitizing chemical and an energy donating chemical, optionally linked by a chemical tether*: U.S., 1998.

54. Park, J.; English, D. S.; Wannemuehler, Y.; Carpenter, S.; Petrich, J. W. *Photochem. Photobiol.* **1998**, *68*, 593-597.

55. Petrich, J. W.; Gordon, M. S.; Cagle, M. *J. Phys. Chem. A* **1998**, *102*, 1647-1651.

56. Hudson, J. B.; Imperial, V.; Haugland, R. P.; Diwu, Z. *Photochem. Photobiol.* **1997**, *65*, 352-354.

57. Tobin, G. J.; Ennis, W. H.; Clanton, D. J.; Gonda, M. A. *Antiviral Res.* **1996**, *33*, 21-31.

58. Cohen, P. A.; Hudson, J. B.; Toweres, G. H. N. *Experientia* **1996**, *52*, 180-183.

59. Miskovsky, P.; Sureau, F.; Chinsky, L.; Wheeler, G. V.; Turpin, P. Y. *Studies of the photophysical mechanisms involved in the antiviral activity of hypericin at the cellular level.*; Merlin, J. C. T., Sylvia; Huvenne, Jean Pierre, Ed.; Kluwer, Dordrecht, Neth, 1995, pp 539-540.

60. Hudson, J. B.; Zhou, J.; Chen, J.; Harris, L.; Yip, L.; Towers, G. H. N. *Photochem. Photobiol.* **1994**, *60*, 253-255.

61. Weber N. D., M., B. K., North, J. A. Wood, S. G. *Anti. Chem. Chemotherapy* **1994**, *5*, 83-90.

62. Tang. J, C. J. M. L. S. H. S. W. *Antiviral Res.* **1990**, *13*, 313-326.

63. Stevenson, N. R.; Lenard, J. *Antiviral Res* **1993**, *21*, 119-127.

64. Chaloupka, R.; Sureau, F.; Kocisova, E.; Petrich, J. W. *Photochem. Photobiol.* **1998**, *68*, 44-50.

65. Vandenbogaerde, A. L.; de Witte, P. A. *Phytother. Res.* **1996**, *10*, S150-S152.

66. Kil, K.-S.; Yum, Y.-N.; Seo, S.-H.; Lee, K.-T. *Arch. Pharmacal Res.* **1996**, *19*, 490-496.

67. Sureau, F.; Miskovsky, P.; Chinsky, L.; Turpin, P. Y. *J. Am. Chem. Soc.* **1996**, *118*, 9484-9487.

68. Vandenbogaerde, A. L.; Geboes, K. R.; Cuveele, J. F.; Agostinis, P. M.; Merlevede, W. J.; De Witte, P. A. *Anticancer Res.* **1996**, *16*, 1619-1626.

69. Zhang, W.; Anker, L.; Law, R. E.; Hinton, D. R.; Gopalakrishna, R.; Pu, Q.; Gundimeda, U.; Weiss, M. H.; Couldwell, W. T. *Clin. Cancer Res.* **1996**, *2*, 843-846.

70. Weller, M.; Trepel, M.; Grimmel, C.; Schabet, M.; Bremen, D.; Krajewski, S.; Reed, J. C. *Neurol. Res.* **1997**, *19*, 459-470.

71. Zhang, W.; Law, R. E.; Hinton, D. R.; Couldwell, W. T. *Cancer Lett. (Shannon, Irel.)* **1997**, *120*, 31-38.

72. Zhang, J.; Cao, E.-H.; Li, J.-F.; Zhang, T.-C.; Ma, W.-J. *J. Photochem. Photobiol., B* **1998**, *43*, 106-111.

73. Carpenter, S.; Kraus, G. A. *Photochem. Photobiol.* **1991**, *53*, 169-174.

74. *AIDS Treatment News* **1991**, 4-6.

75. *Science* **1991**, *254*, 522.

76. *AIDS Treatment News* **1992**, 1-4.

77. Dets, S. M.; Joffe, A. Y.; Buryi, A. N.; Denisov, N. A.; Melnik, I. S.; Ravicz, A. H. *Proc. SPIE-Int. Soc. Opt. Eng.* **1997**, *2972*, 173-178.

78. Diwu, Z. *Photochem. Photobiol.* **1995**, *61*, 529-539.

79. Estey, E. P.; Brown, K.; Diwu, Z.; Liu, J.; Lown, J. W.; Miller, G. G.; Moore, R. B.; Tulip, J.; McPhee, M. S. *Cancer Chemother. Pharmacol.* **1996**, *37*, 343-350.

80. Melnik, I. S.; Dets, S. M.; Rusina, T. V.; Denisov, N. A.; Braun, E. M.; Kikot, V. O.; Chornyi, V. y. A. *Proc. SPIE-Int. Soc. Opt. Eng.* **1996**, *2675*, 67-74.

81. VanderWerf, Q. M.; Saxton, R. E.; Chang, A.; Horton, D.; Paiva, M. B.; Anderson, J.; Foote, C.; Soudant, J.; Mathey, A.; Castro, D. J. *Laryngoscope* **1996**, *106*, 479-483.

82. Bueter, B.; Orlacchio, C.; Soldati, A.; Berger, K. *Planta Med.* **1998**, *64*, 431-437.

83. Bremness, L. *Herbs*; Dorling Kindersley: New York, 1994.

84. Al-Khalil, S. *Acta Technol. Legis Med.* **1997**, *8*, 97-104.

85. Melikian, E.; Boroyan, R.; Karaguezian, A.; Charchoglian, A.; Gabrielian, E.; Panossian, A. *Pharm. Pharmacol. Lett.* **1998**, *8*, 101-102.

86. Kreitmair, H. *Pharmazie* **1950**, *5*, 556-557.

87. Winterhoff, H.; Butterweck, V.; Nahrstedt, A.; Gumbinger, H. G.; Schulz, V.; Erping, S.; Bosshammer, F.; Wieligmann, A. *Pharmacological study of the antidepressive effect of Hypericum perforatum L*; Loew, D. R., Norbert, Ed.; Steinkopff, Darmstadt, Germany, 1995, pp 39-56.

88. Freeman, D.; Frolow, F.; Kapinus, E.; Lavie, D.; Lavie, G.; Meruelo, D.; Mazur, Y. *J. Chem. Chem. Soc., Chem. Commun.* **1994**, 891-892.

89. Gill, m.; Gimenez, a.; McKenzie *j. nat. prod.* **1988**, *51*, 1251-1256.

90. Banks, H. J.; Cameron, D. W.; Raverty, W. D. *Aust. J. Chem.* **1976**, *29*, 1509.

91. Song, P. S. *Kagaku to Kogyo (Tokyo)* **1995**, *48*, 1222-1225.

92. Tao, N.; Orlando, M.; Hyon, J. S.; Gross, M.; Song, P. S. *J. Am. Chem. Soc.* **1993**, *115*, 2526-2528.

93. Yang, K. C.; Prusti, R. K.; Walker, E. B.; Song, P. S.; Watanabe, M.; Furuya, M. *Photochem. Photobiol.* **1986**, *43*, 305-310.

94. Cubbedu, R.; Ghetti, F.; Lenci, F.; Ramponi, R.; Taroni, P. *Photochem. Photobiol.* **1990**, *52*, 567.

95. Sevenants, M. R. *J. Protozool* **1965**, *12*, 240-245.

96. Song, P. S.; Walker, E. B.; Auerbach, R. A.; Robinson, G. W. *Biophys. J.* **1981**, *35*, 551-555.

97. Savikhin, S.; Tao, N.; Song, P. S.; Struve, W. S. *J. Phys. Chem.* **1993**, *97*, 12379-12386.

98. Giese, A. C. *Hypericism*; Smith, K. C., Ed.; Plenum: New York, 1980; Vol. 5, pp 229.

99. Racinet, H.; Jardon, P.; Gautron, R. *J. Chim. Phys. Phys.-Chim. Biol.* **1988**, *85*, 971-977.

100. Vandenbogaerde, A. L.; Delaey, E. M.; Vantieghem, A. M.; Himpens, B. E.; Merlevede, W. J.; De Witte, P. A. *Photochem. Photobiol.* **1998**, *67*, 119-125.

101. Agostinis, P.; Donella-Deana, A.; Cuveele, J.; Vandenbogaerde, A.; Sarno, S.; Merlevede, W.; de Witte, P. *Biochem. Biophys. Res. Commun.* **1996**, *220*, 613-617.

102. Utsumi, T.; Okuma, M.; Utsumi, T.; Kanno, T.; Takehara, Y.; Kobuchi, H.; Yoshioka, T.; Horton, A. A.; Yasuda, T.; Utsumi, K. *Arch. Biochem. Biophys.* **1995**, *323*, 355-342.

103. Takahashi, I. N. S.; Kobayashi, E.; Nakano, H.; Suziki, K.; Tamaoki, T. *Biochem. Biophys. Res. Commun* **1989**, *165*, 1207-1212.

104. Kraus, G. A. P. D. T. J. C. S. *Biochem. Biophys. Res. Corn.* **1990**, *172*, 149-153.

105. Farnet, C. M.; Wang, B.; Hansen, M.; Lipford, J. R.; Zalkow, L.; Robinson, W. E., Jr.; Siegel, J.; Bushman, F. *Antimicrob. Agents Chemother.* **1998**, *42*, 2245-2253.

106. Meruelo, D.; Lavie, G. *Method of treating papilloma virus infection using hypericin*: U.S., 1996.

107. Zepp, C. M.; Heefner, D. L. *Method for inactivating non-enveloped viruses using a virucide-potentiating agent*: PCT Int. Appl., 1996.

108. Degar, S.; Prince, A. M.; Pascual, D.; Lavie, G.; Levin, B.; Mazur, Y.; Lavie, D.; Ehrlich, L. S.; Carter, C.; Meruelo *AIDS Res. Hum. Retroviruses* 1992, *8*, 1929-1936.

109. Mazur, Y.; Lavie, G.; Prince, A. M.; Pascual, D.; Liebes, L.; Levin, B.; Meruelo, D. *Transfusion* 1995, *35*, 392-400.

110. Makovetska, E. J.; Bojko, I. I.; Usachova, M. M.; Kovaljova, T. V.; Kapinus, E. I.; Lebeda, A. F. *Farm. Zh. (Kiev)* 1997, 93-97.

111. Makovetskaya, E. Y.; Boiko, I. I.; Kapinus, E. I.; Lebeda, A. P. *Farm. Zh. (Kiev)* 1997, 49-52.

112. Weiner, L.; Mazur, Y. *J. Chem. Soc. Perkin Trans* 1992, *2*, 1439-1442.

113. Hadjur, C.; Jeunet, A.; Jardon, P. *J. Photochem. Photobiol., B* 1994, *26*, 67-74.

114. Hadjur, C.; Jardon, P. *J. Photochem. Photobiol., B* 1995, *29*, 147-156.

115. Hadjur, C.; Jeunet, A. *EPR evidence of generation of superoxide anion radicals ($O_2^{\cdot -}$) by irradiation of a PDT photosensitizer: Hypericin*; Favier, A. E., Ed.; Birkhaeuser, Basel, Switz, 1995, pp 119-126.

116. Jardon, P.; Lazortchak, N.; Gautron, R. *J. Chim. Phys. Phys.-Chim. Biol.* 1987, *84*, 1141-1145.

117. Thomas, C.; Pardini, R. S. *Photochem. Photobiol* 1993, *55*, 831-837.

118. Bouirig, H.; Eloy, D.; Jardon, P. *J. Chim. Phys. Phys.-Chim. Biol.* 1992, *89*, 1391-1411.

119. Darmanyan, A. P.; Burel, L.; Eloy, D.; Jardon, P. *J. Chim. Phys. Phys.-Chim. Biol.* 1994, *91*, 1774-1785.

120. Anderson, J. L. *Singlet oxygen production from and photophysical studies on chlorine dioxide, hypericin, and buckminsterfullerene derivatives*, 1996, pp 111.

121. Zhao, H.; Zhang, H.; Zhang, Z.; Li, M. *Fushe Yanjiu Yu Fushe Gongyi Xuebao* 1997, *15*, 149-154.

122. Ehrenberg, B.; Anderson, J. L.; Foote, C. S. *Photochem. Photobiol.* 1998, *68*, 135-140.

123. Vandenbogaerde, A. L.; Cuveele, J. F.; Proot, P.; Himpens, B. E.; Merlevede, W. J.; de Witte, P. A. *J. Photochem. Photobiol., B* 1997, *38*, 136-142.

124. Eloy, D.; Le Pellec, A.; Jardon, P. *J. Chim. Phys. Phys.-Chim. Biol.* 1996, *93*, 442-457.

125. Newell, K. J.; Tannock, I. F. *Cancer Res.* 1989, *49*, 4447-4482.

126. Jardon, P.; Lazorchak, N.; Gautron, R. *J. Chim. Phys. Phys.-Chim. Biol.* 1986, *83*, 311-315.

127. Arabei, S. M.; Galaup, J. P.; Jardon, P. *Chem. Phys. Lett.* 1997, *270*, 31-36.

128. Bouirig, H.; Eloy, D.; Jardon, P. *J. Chim. Phys. Phys.-Chim. Biol.* 1993, *90*, 2021-2038.

129. Jardon, P.; Gautron, R. *J. Chim. Phys. Phys.-Chim. Biol.* 1989, *86*, 2173-2190.

130. Angerhofer, A.; Falk, H.; Meyer, J.; Schoppel, G. *J. Photochem. Photobiol., B* 1993, *20*, 133-137.

131. Malkin, J.; Mazur, Y. *Photochem. Photobiol.* 1993, *57*, 929-933.

132. Gerson, F.; Gescheidt, G.; Haering, P.; Mazur, Y.; Freeman, D.; Spreitzer, H.; Daub, J. *J. Am. Chem. Soc.* 1995, *117*, 11861-11866.

133. Wells, T. A.; Losi, A.; Dai, R.; Scott, P.; Park, S. M.; Golbeck, J.; Song, P. S. *J. Phys. Chem.* 1997, *101*, 366-372.

134. Diwu, Z.; Lowen, J. W. *Free Rad. Biol. Med* 1993, *14*, 209-215.

135. Wells, T. A.; Losi, A.; Dai, R.; Scott, P.; Park, S.-M.; Golbeck, J.; Song, P.-S. *J. Phys. Chem. A* 1997, *101*, 366-372.

136. Diwu, Z.; Lown, J. W. *J. Photochem. Photobiol., A* **1992**, *64*, 273-287.

137. Etzlstorfer, C.; Falk, H.; Mueller, N.; Tran, T. N. H. *Monatsh. Chem.* **1996**, *127*, 659-668.

138. Falk, H.; Tran, T. N. H. *Monatsh. Chem.* **1996**, *127*, 717-723.

139. Jancura, D.; Sanchez-Cortes, S.; Kocisova, E.; Tinti, A.; Miskovsky, P.; Bertoluzza, A. *Biospectroscopy* **1995**, *1*, 265-273.

140. Jancura, D.; Sanchez-Cortes, S.; Miskovsky, P.; Garcia-Ramos, J. V. *Surface-enhanced Raman spectroscopy study of hypericin-albumin interaction*; Carmona, P. N., Raquel; Hernanz, Antonio, Ed.; Kluwer, Dordrecht, Neth, 1997, pp 367-368.

141. Jancura, D.; Sanchez-Cortes, S.; Miskovsky, P.; Rivas, L.; Stanicova, J.; Garcia-Ramos, J. V. *Spectrochim. Acta, Part A* **1998**, *54A*, 1519-1526.

142. Sanchez-Cortes, S.; Jancura, D.; Kocisova, E.; Tinti, A.; Miskovsky, P.; Bertoluzza, A. *Surface-enhanced resonance Raman spectroscopy of hypericin and emodin*; Merlin, J. C. T., Sylvia; Huvenne, Jean Pierre, Ed.; Kluwer, Dordrecht, Neth, 1995, pp 573-574.

143. Sanchez-Cortes, S.; Miskovsky, P.; Jancura, D.; Bertoluzza, A. *J. Phys. Chem.* **1996**, *100*, 1938-1944.

144. Yoon, W.-S.; Im, J.-H.; Kim, J.-H. *Anal. Sci. Technol.* **1995**, *8*, 699-705.

145. Miskovsky, P.; Chinsky, L.; Wheeler, G. V.; Turpin, P.-Y. *J. Biomol. Struct. Dyn.* **1995**, *13*, 547-552.

146. Kocisova, E.; Chinsky, L.; Miskovsky, P. *J. Biomol. Struct. Dyn.* **1998**, *15*, 1147-1154.

147. Miskovsky, P.; Jancura, D.; Sanchez-Cortes, S.; Kocisova, E.; Chinsky, L. *J. Am. Chem. Soc.* **1998**, *120*, 6374-6379.

148. Mylrajan, M.; Hildebrandt, P.; Mazur, Y. *J. Mol. Struct.* **1997**, *407*, 5-10.

149. Raser, L. N.; Kolaczkowski, S. V.; Cotton, T. M. *Photochem. Photobiol.* **1992**, *56*, 157-162.

150. Etzlstorfer, C.; Falk, H.; Mueller, N.; Schmitzberger, W.; Wagner, U. G. *Monatsh. Chem.* **1993**, *124*, 751-761.

151. Carrington, T. J.; Miller, W. H. *J. Phys. Chem.* **1986**, *84*, 4364.

152. Goodman, J.; Brus, L. E. *J. Am. Chem. Soc.* **1978**, *100*, 7472-7474.

153. Herek, J. L.; Pedersen, S.; Banares, L.; Zewail, A. H. *J. Chem. Phys.* **1992**, *97*, 9046-9061.

154. Nishiya, T.; Yamauchi, S.; Hirota, N.; Baba, M.; Hanasaki, I. *J. Phys.Chem.* **1986**, *90*, 5730-5735.

155. Brucker, G. A.; Swinney, T. C.; Kelley, D. F. *J. Phys. Chem.* **1991**, *95*, 3190-3195.

156. Strandjord, A. J. G.; Barbara, P. F. *J. Phys. Chem.* **1985**, *89*, 2355-2361.

157. McMorrow, D.; Kasha, M. *Hydrogen-bonding solvent perturbations. J. Phys. Chem.* **1984**, *88*, 2235-2243.

158. Brucker, G. A.; Kelley, D. F. *J. Phys. Chem.* **1987**, *91*, 2856-2861.

159. Chattoraj, M.; King, B.; Boxer, S. G. *Investigating the solvent dependence of proton and deuterium transfer in 3-hydroxy flavone using femtosecond fluorescence upconversion.*; American Chemical Society: Chicago, IL, August 20-24, 1995, pp PHYS-108.

160. Swinney, T. C.; Kelley, D. F. *J. Phys. Chem.* **1991**, *95*, 10369-10373.

161. Yamazaki, T.; Ohta, N.; Yamazaki, I.; Song, P.-S. *J. Phys. Chem.* **1993**, *97*, 7870-7875.

162. Kishi, T.; Tahara, S.; Taniguchi, N.; Tsuda, M.; Tanaka, C.; Takahashi, S. *Planta Med.* **1991**, *57*, 376-379.

163. Diwu, Z.; Lown, J. W. *Photochem. Photobiol.* **1990**, *52*, 609-616.

164. Lin, S. *Skin tonic cream containing hypocrellin*: Faming Zhuanli Shenqing Gongkai Shuomingshu, 1986.

165. Diwu, Z.; Zimmermann, J.; Meyer, T.; Lown, J. W. *Biochem. Pharmacol.* **1994**, *47*, 373-385.

166. Diwu, Z.; Lown, J. W. *J. Photochem. Photobiol., B* **1993**, *18*, 145-154.

167. Dong, C.; Jia, H.; Zhang, L.; Ma, C. *Shengwu Huaxue Zazhi* **1987**, *3*, 468-472.

168. Diwu, Z.; Lown, J. W. *J. Photochem. Photobiol., A* **1992**, *69*, 191-199.

169. Zhang, H.; Zhang, Z. *Sci. China, Ser. B: Chem.* **1998**, *41*, 85-90.

170. Zhang, H.; Zhang, Z. *Sci. China, Ser. B: Chem.* **1997**, *40*, 428-433.

171. Arnone, A.; Merlini, L.; Mondelli, R.; Nasini, G.; Ragg, E.; Scaglioni, L.; Weiss, U. *J. Chem. Soc., Perkin Trans. 2* **1993**, 1447-1454.

172. Mazzini, S.; Merlini, L.; Mondelli, R.; Nasini, G.; Ragg, E.; Scalioni, L. *J. Chem. Soc., Perkin Trans. 2* **1997**, 2013-2021.

173. Diwu, Z.; Lown, J. W. *J. Photochem. Photobiol., B* **1993**, *18*, 131.

174. Chen, W. S.; Chen, Y. T.; Wan, X. Y.; Friedrichs, E.; Puff, H.; Breitmaier, E. *Liebigs Ann. Chem.* **1981**, 1880-1885.

175. Diwu, Z.; Jiang, L.; Zhang, M. *Chin. Sci. Bull.* **1989**, *34*, 258.

176. Hu, Y.-Z.; An, J.-Y.; Qin, L.; Jiang, L.-J. *J. Photochem. Photobiol., A* **1994**, *78*, 247-251.

177. Hu, Y.-z.; Chiang, L.-j. J. *J. Photochem. Photobiol., A* **1996**, *94*, 37-41.

178. Wang, Z.; Zhang, M.; Jiang, L. *Huaxue Xuebao* **1992**, *50*, 186-192.

179. Wang, N.; An, J.; Jiang, L. *Huaxue Xuebao* **1992**, *50*, 702-707.

180. An, J.; Zhao, K.; Jiang, L. *Sci. China, Ser. B* **1991**, *34*, 1281-1289.

181. Wang, Z.; Ma, L.; Zhang, M.; Jiang, L.; Chen, D. *Chin. Sci. Bull.* **1992**, *37*, 1007-1011.

182. Hu, Y.-Z.; An, J.-Y.; Jiang, L.-J.; Chen, D.-W. *J. Photochem. Photobiol., A* **1995**, *89*, 45-51.

183. Weng, M.; Zhang, M.-H.; Shen, T. *J. Photochem. Photobiol., A* **1997**, *111*, 105-109.

184. Zang, L.; Misra, B. R.; Misra, H. P. *Photochem. Photobiol.* **1992**, *56*, 453-462.

185. Wang, N.; An, J.; Jiang, L. *Huaxue Xuebao* **1992**, *50*, 905-909.

186. An, J.; Tian, F.; Hu, Y.; Jiang, L. *Chin. J. Chem.* **1993**, *11*, 532-539.

187. Sun, J.; Zhang, L.; Zhang, Z. *Fushe Yanjiu Yu Fushe Gongyi Xuebao* **1991**, *9*, 108-112.

188. Jiang, X.-P.; He, H.-Z.; Wang, D.-Y. *Sci. China, Ser. B* **1992**, *35*, 776-782.

189. Wang, D.; He, H. *Zhongguo Xitu Xuebao* **1988**, *6*, 1-5.

190. Nafis, M.; Jardon, P. *J. Chim. Phys. Phys.-Chim. Biol.* **1994**, *91*, 99-112.

191. Dewar, M. J.; E.F., Z.; Healey, E. F.; Stewart, J. J. *J. Am. Chem. Soc.* **1985**, *107*, 3902.

192. Chen, B.; An, J. Y.; Zhang, M.; Wang, B. *Ganguang Kexue Yu Guang Huaxue* **1998**, *16*, 105-110.

193. Zang, L. Y.; Zhang, Z.; Misra, H. P. *Photochem. Photobiol.* **1990**, *52*, 677-683.

194. Zou, W.; An, J.-y.; Jiang, L.-j. *J. Photochem. Photobiol., B* **1996**, *33*, 73-78.

195. Azzouz, H.; Borgis, D. *J. Chem. Phys.* **1993**, *98*, 7361-7374.

196. Borgis, D.; Hynes, J. T. *J. Chem. Phys.* **1991**, *94*, 3619-3628.

197. Borgis, D.; Tarjus, G.; Azzouz, H. *J. Phys. Chem.* **1992**, *96*, 3188-3191.

198. Borgis, D.; Hynes, J. T. *J. Chem. Phys.* **1996**, *100*, 1118-1128.

199. Staib, A.; Borgis, D.; Hynes, J. T. *J. Phys. Chem.* **1995**, *102*, 2487-2505.

200. Hammes-Schiffer, S.; Tully, J. C. *J. Chem. Phys.* **1994**, *101*, 4657-4667.

201. Hammes-Schiffer, S.; Tully, J. C. *J. Phys. Chem.* **1995**, *99*, 5793-5797.

202. Cukier, R. I.; Morillo, M. *J. Chem. Phys.* **1989**, *91*, 857-863.

203. Li, D.; Voth, G. A. *J. Phys. Chem.* **1991**, *95*, 10425-10431.

204. Scheiner, S. *Acc. Chem. Res* **1985**, *18*, 174-180.

205. Warshel, A. *Computer Modeling of Chemical Reactions in Enzymes and Solutions*; Wiley: New York,, 1991.

206. Tuckerman, M.; Laasonen, K.; Sprik, M.; Parinello, M. *J. Chem. Phys.* **1995**, *103*, 150-161.

207. Laasonen, K.; Klein, M. L. *J. Am. Chem. Soc* **1994**, *116*, 11620-11621.

208. Ando, K.; Hynes, J. T. *Ionization of acids in water*; Cramer, C. J. and Truhlar, D. G., Ed.; American Chemical Society: Washington D. C., 1994, pp 143-153.

209. Ulstrup, J. *Charge Transfer Processes in Condensed Media*; Springer: Berlin, 1979.

210. DeVault, D. *Quantum Mechanical Tunnelling in Biological Systems*; 2 ed.; Cambridge University Press: Cambridge, 1984.

211. Arnaut, L. G. F., S. J. *J. Photochem. Photobiol. A: Chem* **1993**, *75*, 21.

212. Arnaut, L. G. F., S. J. *J. Photochem. Photobiol. A: Chem* **1993**, *75*, 1.

213. Kosower, E. M. H., D. *Ann. Rev. Phys. Chem.* **1986**, *37*, 127.

214. Weller, A. *Naturwissenschaften* **1955**, *42*, 175.

215. Sengupta, P. K.; Kasha, M. *Chem. Phys. Lett.* **1979**, *68*, 382.

216. Forster, T. *Naturwiss.* **1949**, *36*, 186.

217. Forster, T. *Z. Elektrochem.* **1950**, *54*, 43.

218. Borgis, D.; Lee, S.; Hynes, J. T. *Chem. Phys. Left.* **1989**, *162*, 19.

219. Truong, T. N.; McCammon, J. A.; Kouri, D. J.; Hoffman, D. K. *J. Chem. Phys.* **1992**, *96*, 8136.

220. Haug, K.; Wahnstrom, G.; Metiu, H. *J. Chem. Phys.* **1990**, *92*, 2083.

221. Warshel, A.; Chu, Z. T. *J. Chem. Phys.* **1990**, *93*, 4003.

222. Hwang, J. K.; Chu, Z. T.; Yadav, A.; Warshel, A. *J. Phys. Chem.* **1991**, *95*, 8445.

223. Gillan, M. *Phys Rev. Lett.* **1987**, *58*, 563.

224. Makri, N.; Miller, W. H. *J. Chem. Phys.* **1987**, *87*, 5781.

225. Bosch, E.; Moreno, M.; Lluch, J. M. *Chem. Phys.* **1992**, *159*, 99.

226. Borgis, D.; Hynes, J. T. *Chem. Phys* **1993**, *170*, 315.

227. Das, K.; Ashby, K.; Wen, J.; Petrich, J. W. *J. Phys. Chem.*, In press.

CHAPTER II. EXPERIMENTAL APPARATUS AND METHODS OF COMPUTATION

FLUORESCENCE UPCONVERSION SPECTROMETER

Introduction

Among the major steps in the new exciting developments of applied laser spectroscopy was the discovery by Sibbett et al. of a laser oscillator based on titanium-doped sapphire crystal to operate in the self mode-locked regime [1]. This meant relatively cheap, readily available near-infrared pulses of sub-picosecond duration which can be frequency- doubled, amplified and "mixed" with other light of various wavelengths to produce excitation sources of up to petawatt peak powers [2]. Currently Ti:sapphire based systems, besides being heavily employed by ultra-fast spectroscopists, are used in a spectacularly diverse range of applications: from pulsed X-ray generation [3,4] to microscopic imaging [5].

In the present work we combine the Ti:sapphire oscillator ~50 fs pulse train and recent successes in non-linear crystal technology to obtain second-harmonic generation (~400 nm), which serves as a polarized excitation light source to prepare and to observe evolution of molecular fluorescence (and its anisotropy) on a femtosecond to nanosecond time scale. The key point of this set up is that time-resolution is only limited by the fundamental pulse width and optics and not by jitter noise in detector or electronic components as in conventional time-correlated single photon counting technique (TCSPC) [6]. Disadvantages include low sensitivity (typical sample conc. is 10^{-4} M, or 100 times more than in TCSPC), mandatory sample translation or circulation (due to power densities

as high as $3x10^3$ W/cm^{-3}) and susceptibility to long-term drift in sample concentration, oscillator and pump source power. The fluorescence upconversion apparatus can be a challenge to construct but once set up and aligned it requires minimum tuning and maintenance especially if the pump laser has good, reproducible pointing stability and non-linear crystals are coated for moisture protection.

Besides the quality of the pump source (intracavity-doubled diode-pumped solid state lasers such as SpectraPhysics Millenia V are strongly recommended) the critical components include a high-reflective curved mirror or an anti-reflection coated microscope objective for efficient fluorescence collection, an efficient and properly cut non-linear crystal for sum-frequency generation (β-barium borate, BBO, is recommended), and a high-resolution stepper-motor driven translation stage for which excellent flatness over the entire usable range is a requirement. Spectral bandwidth is mostly determined by the acceptance angle of the upconversion crystal (~5 nm for BBO) but a monochromator with an appropriately blazed grating is still needed for wavelength calibration and to ensure acceptable signal/background ratio. A low or zero dark-count photomultiplier tube or microchannel plate with a UV-pass filter or, preferably a solar-blind device, is a good choice for the detector. Unfortunately, recently introduced avalanche photodiodes, known for their high sensitivity, cannot be utilized for visible fluorescence upconversion because of unresponsiveness to UV-light. On the other hand they may show their potential if difference frequency generation is used for time discrimination.

Originally, the ultrafast fluorescence upconversion experiment was performed by Kopainsky and Kaiser in 1978 [7]. Initially picosecond tunable dye lasers were employed to study such molecules as tryptophan in water [8,9]. These systems are quite difficult to optimize and maintain, use complex mixtures of laser dyes which are subject to degradation and also require additional amplification stages [8]. When solid-state lasers,

Ti:sapphire in particular, came into play the applicability of technique expanded to studies of light harvesting complexes [10,11], β-carotene isomerization [12], green fluorescent protein [13], water mobility in reversed micelles [14] and excited-state proton transfer events [15-17]. One of the most exciting extensions of fluorescence upconversion would be coupling the detection system with output of a new generation optical parametric amplifier (OPA) which enables continuous tuning of the excitation wavelength from 475 to 785 nm with sub-200 fs pulsewidth [18,19]. Such a system effectively bridges the gap between the fundamental and the second harmonic of Ti:sapphire laser and is currently under construction in our laboratory.

Frequency Doubled Ti:Sapphire Oscillator

Introduction

The broad gain bandwidth of Ti:sapphire makes it an excellent solid-state material both for a femtosecond oscillator and amplifier. Its gain bandwidth extends approximately from 670 to 1100 nm, providing a large tuning range and the ability to produce ultrashort pulses. Various mode-locking schemes have been employed in Ti:sapphire lasers whereby sub-100-fs pulses can be generated, one of them is the, so called, self-mode-locking [20,21]. Using passively mode-locked mechanisms, the shortest pulse which can be generated scales inversely with the gain bandwidth multiplied by the square root of the saturable absorption. Theoretically it is suggested that pulses as short as ~3 fs may be generated from Ti:sapphire lasers [22]. Although the self-mode-locking mechanism is not fully understood, in the first approximation it is decribed through the non-linear phenomenon known as the Kerr lens effect [23]. The Kerr lensing occurs when when an intense pulse of light with a varying spatial profile propagates through material and causes intensity dependent change of refractive index. The Gaussian profile of a typical laser pulse causes

the index of refraction to increase more at the center of the beam than on its periphery. This results in a formation of a transient positive focal length lens that brings about "self-focusing" or "self-narrowing" of the light pulse in the active medium. Here it should be noted that the Ti:sapphire oscillator will also readily operate in spectrally narrow continuous-wave (CW) mode which is characterized by a certain minimum beam waist. Therefore by optimizing the laser components to favor the Kerr lens effect it is possible to preferentially select the self-modelocked set of modes over the CW modes. The most important factor in such an optimization is ight focusing of the pump source onto the sapphire crystal by a combination of a beam expanding 3x to 5x telescope and a 15-20 cm focusing lens. This is most efficient with monochromatic pump lasers (such as intracavity-doubled Nd^{3+}:YAG or Nd^{3+}:YVO_4) but also works well with Ar-ion gas lasers which contain a set of lines in their spectrum. Another technique which is most useful during the initial setup and alignment is to use the intracavity pair of prisms as a slit to filter CW which is dominant at shorter wavelengths. The main purpose for the pair of quartz prisms is, of course, compensation for the group velocity dispersion (GVD) in the the laser crystal itself as well as in the output coupler to produce the shortest possible pulses [1]

Laser setup and operation

In our lab we have built two oscillators based on the design by Murnane and coworkers [24]. Pulses as short as 17-fs have been generated by such systems. The primary difference between the two is the laser rod length. The crystal of the oscillator discussed here is a 4.75 mm long Ti:sapphire rod, 0.015% doped. It is about twice shorter than in our first setup used for chirped-pulse amplification [25]. The shorter crystals are believed to produce shorter pulses at the expense of the maximum output power. (The main reason for choosing the smaller crystal was our initial plans to employ the oscillator for impulsive Raman experiment demanding the best available time resolution.) Initially we used 4.5-5.0

W of Spectra Physics 2060 Beamloc argon-ion laser as pump sourse. The typical mode-locked output power was 400-600 mW. Later the gas laser was replaced by intra-cavity doubled diode-pumped Spectra Physics Millenia V, a solid state laser based on Nd^{3+}-doped yttrium vanadate (YVO_4) crystal which provides unprecedented power stability and ease of maintenance but was found to be sensitive to slight touch or vibrations. Despite the higher price, in the long run this solution for the pump source is a much cheaper alternative to plasma and flash-lamp pumped lasers as diodes have relatively long lifetime, cooling water is provided by a simple bath circulator and electrical power requirements are no more than of a cooking stove.

A detailed description of the complete setup and alignment procedures for the Ti:sapphire oscillator has been addressed in the recent dissertations published by the members of our research group [25,26]. Here only factors of crucial importance are reiterated and additional information is provided regarding changes in system components or when non-standard procedures are to be followed.

After expansion by 3x telescope (L1, L2), 2.3 - 5.3 W of 532 nm horizontally polarized CW light (pump) is focused by a 12.5 cm focal length lens (L3) through 10 cm spherical dichroic mirror (M2) into the Ti:sapphire crystal. It is essential to have the green light passing through the centers of curved high-reflectors (M2 and M3) and to select a good spot on the crystal (C1) that produce minimal scatter. One should be able to see a sharp "needle" of light passing through the bulk of the crystal. It was suggested that the side of the crystal is better because of more efficient heat dissipation but I found that in my setup focusing in about the center axis produces even more mode-locked power (>1 W when pumped with 4.5-5.0 W of green). To avoid multiple pulses travelling in the cavity one has to reduce the amount of incoming energy to about 2.4 W which still afford enough power (400-600 mW). Also if oscillator is slightly mistuned to allow for both CW and

mode-locked output it was noticed that further increase in pump power will only suppress pulsed operation, increase relative amount of CW, and ultimately reduce the amount of second harmonic light that can be produced from the fundamental.

To reduce its footprint on the table the oscillator cavity is folded by high-reflector M4 which is aligned only at the initial setup. A pair of fused silica prisms (P1, P2) manufactured at a Brewster 63° angle are used to minimize the third-order dispersion in the laser cavity. Two 10-cm radius of curvature concave IR-coated mirrors (M2, M3) are employed to focus the reflected fluorescence back inside the crystal. An output coupler (M4) dumps 10% of the cavity energy out. The configuration of the oscillator is schematically shown in Figure 2.1. The total cavity length and the length on either arm of the laser are not critical, and they can be varied considerably. However, the separation between the prisms is somewhat critical in order to get the shortest pulse duration. Also, the sapphire rod position and the separation between the two curved mirrors M2 and M3 are very critical. Before any alignment is attempted each spherical mirror should be verified to be within distance of 100.0 ± 0.5 mm from the center of the Ti:sapphire crystal.

The Ti:sapphire laser is self-modelocking but not self-starting. One needs a considerable amount of time and patience to get it lasing and mode-locked and to ensure that only a single pulse is in the cavity. Laser needs a warm up time of about 20 -30 min with full (regular) power applied. The crystal must be cooled with tap water for stable operation while in use. To achieve lasing conditions faster, I found it useful to maximize intensity of IR-light leaking through the high-reflector (M1) by monitoring it with a large-area unamplified photodiode connected to a voltmeter. The output coupler side can also be used but with great caution as sudden lasing can damage the detector. Another hint is that the double spot on the output coupler can be quite misleading in that the *brighter* part as viewed with the IR-card is actually *not* the relevant one.

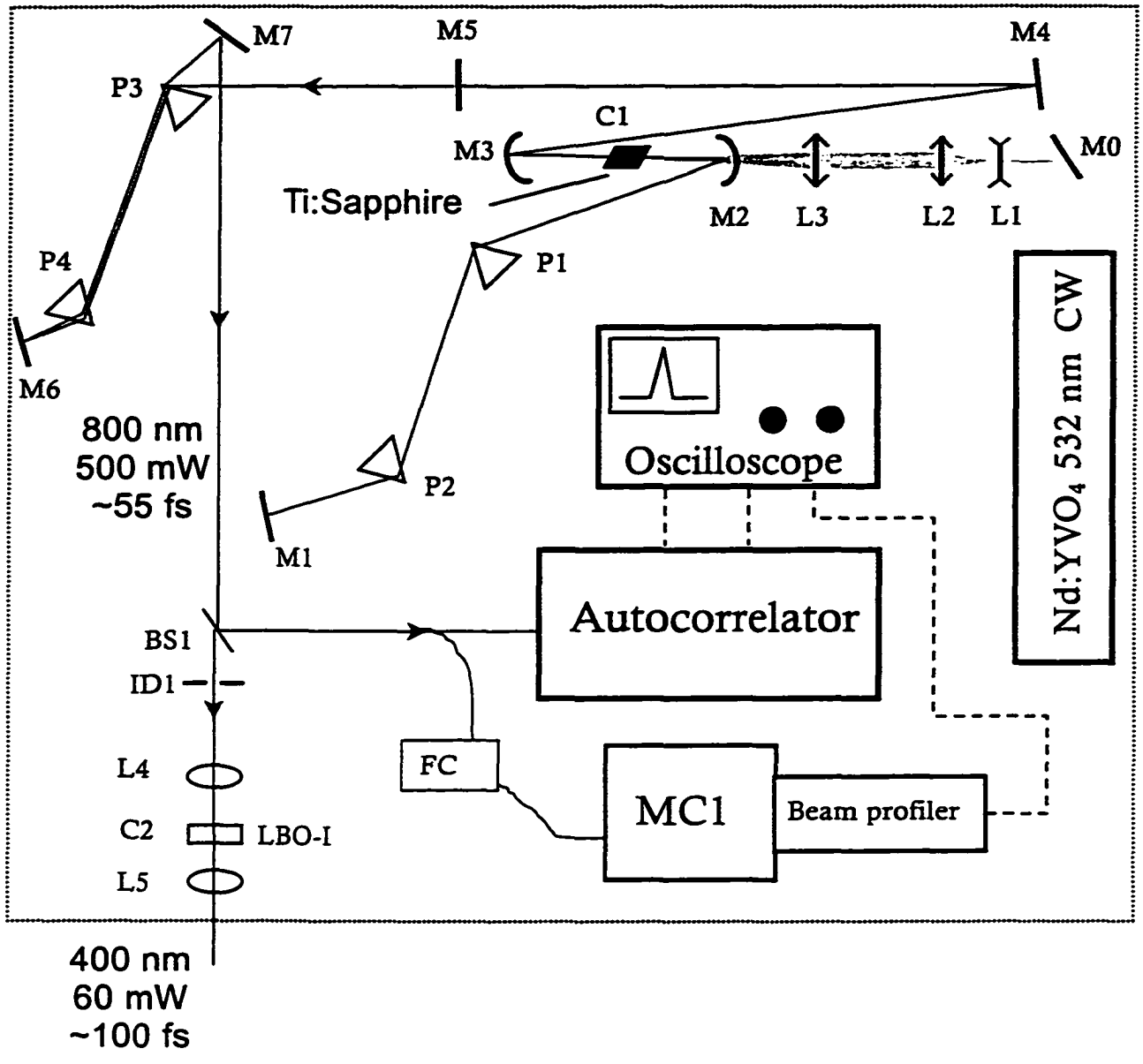

Figure 2.1 Schematic diagram of Ti:sapphire oscillator with GVD precompensator and frequency doubler. Legend: BS - beam splitter, C - crystal, FC - fiber optics cable, ID - iris diaphragm, L - lens, M-mirror or output coupler, MC - monochromator, P - prism.

The detailed instructions on mode-locking have been already described elsewhere [25,26] but I should note that it is often a matter of luck when one wishes to get the results quickly. If the output power or pulse quality happens to be somewhat close to that desired, it is better to move on to the next alignment step rather than search for absolute perfection. If the system is slightly optimized on a daily basis, one usually obtains increasingly better results. On the other hand after about a week or two of down-time it is not uncommon to lose mode-locked state and even lasing. Generally for good mode-locking, a stable, almost Gaussian spectral profile with 30-40 nm fwhm (the wider the better) should be obtained. The maximum can be centered from 790 to 830 nm, but with our doubling crystal it is better to keep it close to 810 nm. Special care must be taken to avoid touching or vibrating any of the pump laser parts and metal post with polarization flipping mirrors (M0). Telescope lenses (M1-M3) and the above mentioned mirrors should be protected from dust as much as possible and cleaned only when necessary. Even when using soft tissue slight misalignment can hardly be avoided and may cause the oscillator to lose mode-locking.

When mode-locked operation is achieved and the power is optimized, the laser spot should have a symmetric Gaussian profile as viewed by eye on white paper with mat finish. It is common to have a slightly diverging beam that approaches a diameter of *ca.* 5 mm by the time it reaches the focusing lens for second harmonic generation (SHG). To achieve maximum efficiency in SHG, this is even desirable since the smaller spot size w_o can be produced with the larger incident Gaussian beam of radius w, as it follows from

$$w_o = \frac{\lambda f}{\pi w} \tag{2.1}$$

where f is the lens focal length and λ is the light wavelength [27].

At the same time having maximum possible power of SHG is critical for system performance. Because the amount of SHG is proportional to the square of the incident

power, the power of frequency-doubled light can be an indication of fundamental pulsewidth . This is especially handy when one realizes that the first focusing lens inevitably contributes to pulse broadening but that the autocorrelation function often only can be measured before or after the "doubler". Thus the usefulness of the autocorrelator is limited to an *estimation* of the temporal profile of the pulse but it is still essential to monitor the number of pulses in the cavity. To compensate for GVD in the focusing lens and the residual GVD within the laser cavity, a second pair of prisms (P3, P4) cut at Brewster's angle and gold mirror (M6) . This second pair of prisms was chosen to be made from a higher refractive index glass (cut at 60.9° from SF10 glass, not widely available) because it provides better dispersion and hence able to fit within limited space on the laser table. One should be very careful to position both prisms at the angle of "minimum deviation" and parallel to the laser beam as translation of one of them while monitoring the pulsewidth or SHG power should not result in beam deviation causing misleading observations. The prisms and the gold mirror should be inserted sequentially only after each previous element has been completely aligned. At this time it is useful to position the second prism on a rail so that later it can moved later should the initial distance (*ca.* 45 cm) happen to be too long or too short for proper dispersion.

In our setup a small portion of light is reflected to the autocorrelator by a thin microscope cover slide (BS1) just before entering the frequency doubler. When aligning the autocorrelator it is crucial to keep in mind that the beam polarization of the Ti:sapphire oscillator is parallel to the laser table (otherwise utilization of Brewster's prisms could be problematic). Thus for successful type II autocorrelation function generation the stationary and delayed beams should travel one above the other and not in the horizontal plane, as for a typical dye laser. It is also imperative to filter out the fundamental efficiently and let SHG be detected by PMT. Most conventional UV-pass filters are not

suitable as they generally also transmit close to 50% of IR radiation. An interference filter centered about 400 or 410 nm works quite well despite their higher reflectivity. With the gold plated retroreflectors and the points mentioned above in mind the autocorrelation can be set up in less than an hour. With the Ar^+ laser as a pump source the shortest measured fwhm of autocorrelation function was 64 fs corresponding to ~43 fs Gaussian pulsewidth (a value of ~60 fs was measured before second pair of prisms was inserted).

Another important characteristic of any laser radiation is its frequency spectrum. A method adopted in our lab uses a single-mode fiber (F) to direct suitable reflection of fundamental or "blue" light into the entrance slit of an ISA H-10 monochromator (MC1) equipped with beam profiler. The dispersed spectrum can be observed on the screen of oscilloscope. The monochromatanor calibration is easily done with a conventional He-Ne or diode laser and was found to satisfy the factory specifications. With our setup, near-transform-limited pulses were produced with a typical spectrum of 30-35 nm fwhm which corresponds to the temporal pulsewidth of 20-30 fs.

Second harmonic generation

Second harmonic generation was produced by type I phase matching in an oven-protected lithium triborate (LBO) crystal (1 mm thick) specially cut (Super Optronics) to be used at about 800 nm fundamental wavelength. The crystal (C2) was mounted in a mirror holder with 3 micrometers for fine adjustments in both angle and distance to the first focusing lens. For the success of further alignment, it is desirable to have the beam after the "doubler" be parallel to the table. For that, one must *then* insert the focusing (L4) and collimating (L5) optics in the beam path. Having an IR card with a aperture in the middle is very useful when trying center the lens. If everything is done carefully enough, there is a chance that a portion of incident light and SHG is reflected during optimization directly back to the laser, which can cause sudden loss of mode-locking. Possible solutions for this

problem include inserting a pinhole in front of the "doubler", changing one of the crystal angles, and finally finding a different fundamental center wavelength if nothing else works. The crystal optical axis has to be adjusted for maximum blue power. Typically 60-120 mW of SHG was produced corresponding to about 15-20% conversion efficiency. One has to be careful using short-pass filters when measuring the amount of second harmonic generated. Many filters are not designed to block IR radiation efficiently. The amount of power registered by our meter seems to have a noticable dependance on the spot size and hence on the distance from the source. The most practical way to check for the second harmonic component is to place a power meter just in front of the second prism (P6) for blue light GVD precompensation (see Figure 2.2 in the following subsection). With this arrangement IR component is greatly reduced by the dichroic mirror and directed away from the sensitive portion of the meter by dispersion with the first prism (P5). The approximate crystal position can be found simply by hand, then optimized when mounted. For maximum conversion, one of precompensation prisms (usually the first) needs to be translated in a certain direction. This also helps obtain the shortest possible pulse. Finally, the doubling crystal may need further small corrections, which are also needed each time the laser is remode-locked.

Pumped with 532 nm of CW mode of a solid state laser, our frequency-doubled Ti:sapphire oscillator produces 60-120 mW of 400-415 nm vertically polarized femtosecond pulses collinear with 200-400 mW of residual fundamental in horizontal polarization.

Time-correlated Detection of Fluorescence Signal by Sum-frequency Generation

Introduction

Detection of fluorescence intensity by mixing with intense laser light of a different wavelength can be quite a challenge. The major problem here is to achieve above-threshold

conditions for power density in the non-linear crystal. Optical components with high numerical aperture are needed. Then the GVD of both the excitation soucre (especially if SHG or THG is used) and the fluorescence itself need to be addressed to avoid "smearing" information in time as light pulses travel toward the mixing crystal. All-reflective optics can be used for demanding applications but they are very expensive and difficult to align. For example our attempts to use an elliptical reflector for one-step focusing of fluorescence were unsuccessful apparently because it was sightly bent in the machine shop and because it had so many degrees of freedom to adjust before upconverted light could be found. However, it was not difficult to obtain THG and generate cross-correlation function with the SHG excitation light. Since our research objective called for time-resolution of no better that 100 fs reflective part was replaces with a fused silica microscope objective which is the major time-broadening element in the whole system. Another challenge is to find an appropriate position for the sum-frequency mixing crystal relative to the incident fluorescence and residual fundamental (gate) pulse train which has to be controlled within ±0.1 degree. Less important difficulties include high background level arising from fundamental self-doubling and self-tripling when detecting fluorescence close to the red (700 nm) and the blue (450 nm) edges respectively of the spectral window of the apparatus. Due to the generally low efficiency of non-linear processes especially at the threshold the power density, the upconverted signal has to be well separated from all other light sources and detected by means of single-photon counting technique.

Theory of measurement

The instantaneous power of the radiation generated at the sum frequency in a nonlinear optical mixing experiment is proportional to the product of the instantaneous power of the two input waves. In an optically sampled fluorescence measurement, a high power gate pulse is mixed with a low power fluorescence signal. For a fixed gate pulse

power, the temporal shape of the fluorescence decay can be mapped out by delaying the gate pulse with respect to the fluorescence excitation pulse and measuring the upconverted power as a function of the optical delay. Since radiation at the sum frequency can only be generated when both waves are in the crystal simultaneously, the crystal acts as an optical sampling gate that is only open for the duration of the gate pulse. The observed signal $S(t')$ at the sum frequency (v_f+ v) as a function of delay time t' is given by [28]

$$S(t') = \int_{-\infty}^{t'} I_{vf}(t) P_v(t-t')\mathrm{d}t \tag{2.2}$$

where $P_v(t)$ is the pulse shape of the dye laser fundamental at frequency v, and $I_{vf}(t)$ is the sample fluorescence intensity at time t and frequency v_f. The experimentally measured fluorescence intensity is related to the true fluorescence decay function, $i_{vf}(t)$, that would result with delta function excitation by the convolution operation

$$I_{vf}(t) = \int_{-\infty}^{t'} i_{vf}(t') P_{2v}(t-t')\mathrm{d}t' \tag{2.3}$$

where $P_{2v}(t)$ is the second harmonic excitation pulse shape. Combining equations (2.2) and (2.3) gives

$$S(t') = \int_{-\infty}^{t'} i_{vf}(t) C_{3v}(t-t')\mathrm{d}t \tag{2.4}$$

where $C_{3v}(t)$ is the measured cross-correlation function for the fundamental gate pulse and second harmonic excitation pulse given by

$$C_{3v}(t') = \int_{-\infty}^{t'} P_{2v}(t) P_v(t-t')\mathrm{d}t \tag{2.5}$$

The cross correlation is measured by generation of the third harmonic of the dye laser in the same crystal and through the same optics used for upconversion of the sample fluorescence. It is the appropriate instrument response function for deconvolution of the optically gated fluorescence data and requires no assumptions about the laser pulse shape.

in order to determine the fluorescence anisotropy decay, the sum frequency correlation functions for the polarization components of the emission polarized parallel, $I_{par}(t)$, and perpendicular, $I_{per}(t)$, to the excitation polarization are measured as well as the cross-correlation function for the gate and excitation pulses. The observed polarized emission curves are related to the impulse response decay functions, $i_{par}(t)$ and $i_{per}(t)$ by convolution with the cross-correlation function as shown previously. The excited state population decay law, $K(t)$, and the anisotropy decay law, $r(t)$, are related to the deconvoluted emission curves by [29]

$$K(t) = i_{par}(t) + 2i_{per}(t) \tag{2.6}$$

$$r(t) = \frac{i_{par}(t) - i_{per}(t)}{i_{par}(t) + 2i_{per}(t)} \tag{2.7}$$

Setup, alignment and maintenance

The schematic diagram for the fluorescence upconversion spectrometer is presented in Figure 2.2. It features a minimum number of reflective surfaces, pump GVD precompensation for better time resolution, and a collinear geometry for type I precompensation for better time resolution, and a collinear geometry for type I sum-frequency generation (upconversion). The latter greatly simplifies the alignment procedure by eliminating another degree of freedom and speeding the process of emission wavelength tuning. This is, of course, done at the expense of somewhat greater background level which is not a significant problem for upconverted wavelengths in the range from 295 to 365 nm. Both Fleming et al. [8] and Maroncelli [30] used a combination of a fused silica prism and a manually translating lens to reduce contributions from SHG and fundamental, but this also introduced a number of additional reflective surfaces that attenuate the already weak (~300 counts per second) signal.

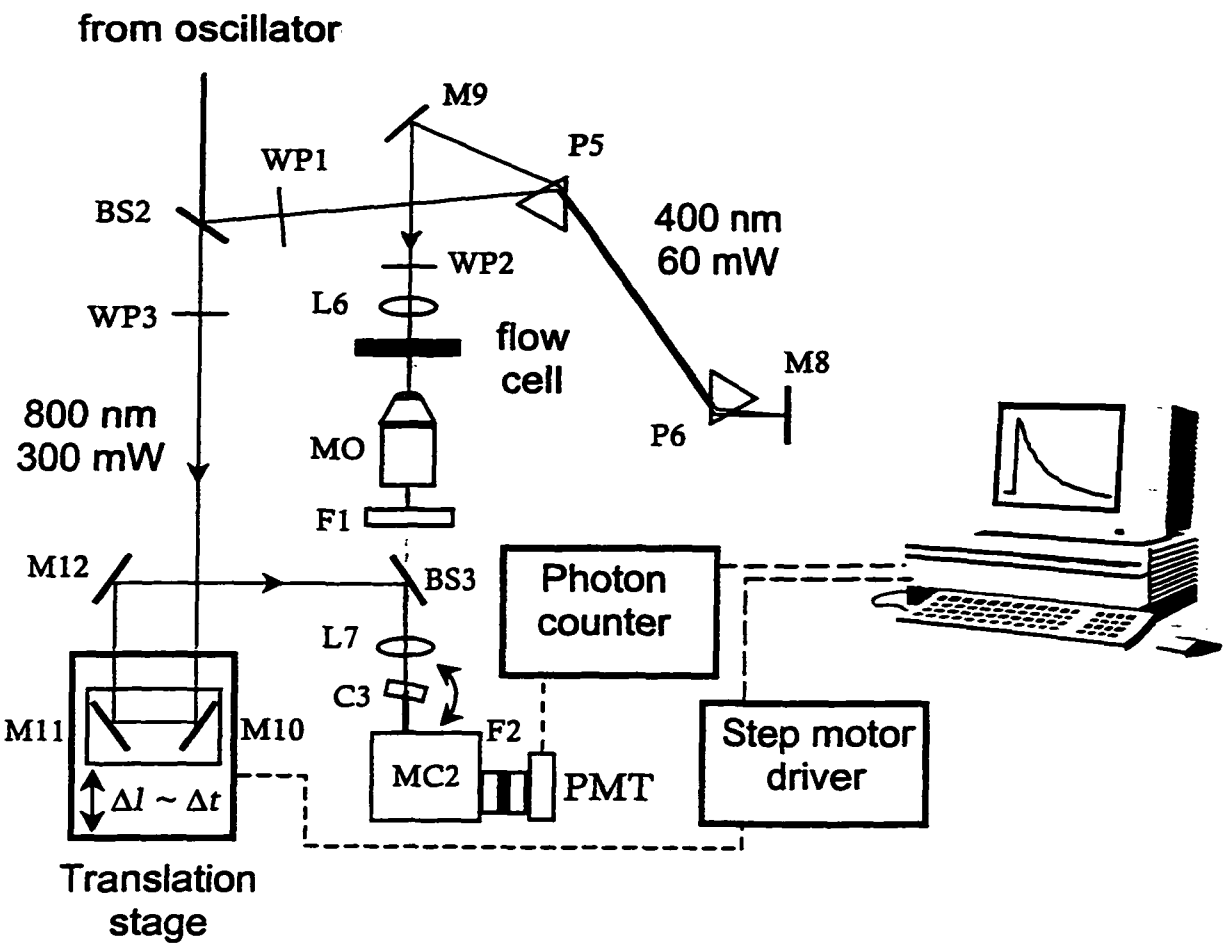

Figure 2.2 Schematic diagram of fluorescence upconversion spectrometer with GVD precompensator for excitation pulse. Legend: BS - beam splitter, C - crystal, F - filter, L - lens, M - mirror, MC - monochromator, P - prism

The frequency-doubled excitation light for our experiment, typically centered about 414 nm, is separated from the fundamental by a 400-nm dielectric mirror BS2 (CVI Optics). To precompensate for group velocity dispersion a third pair of prisms (P5, P6) made of fused silica specially cut and oriented at Brewster's angle (63°) is used before focusing into the sample with 15 cm convex lens (L6) with anti-reflection coating for 400 nm. In order to reduce energy losses during precompensation, a 400-nm zero-order quartz half-waveplate (W1) is used to minimize reflections at air-prism interfaces. The polarization orientation of the excitation light is then adjusted to the desired angle by another similar half-waveplate (W2). The excitation light is removed from fluorescence by a 450-nm long-pass filter (F1). This is not necessary for time scales shorter than 30 ps since 400 nm light is considerably delayed by microscope objective relative to fluorescence. The residual fundamental pulses are used as the time gate during upconversion of fluorescence, which is collected with an LMH-10x microscope objective (MO) from OFR Precision Optical Products coated for near infrared transmission. After being combined by the fused silica dichroic mirror (BS3) coated for 800 nm, both the fundamental and the collimated fluorescence are focused by a 15-cm quartz lens (L7) onto a type I 0.4-mm BBO crystal (cut at 31° and mounted by Quantum Technology, Inc.). The crystal (C3) is protected with MgF_2 coating and does not require desiccation overnight. It is desirable to keep it in dry place when not used for a long time. The polarization of both excitation and gate beams is controlled with a set of zero-order half-wave plates manufactured for 400 (W2) and 800 nm (W3) respectively. The upconverted signal is sent directly into H-10 (8 nm/mm) monochromator (Instruments S.A., Jobin Yvon/Spex Group) coupled to a Hamamatsu R760 photomultiplier equipped with UG11 UV-pass filter (F2) and operated at maximum sensitivity. Spectral resolution was limited by the bandwidth (more specifically, acceptance angle) of the upconversion crystal (BBO) and was estimated to be ca. 5 nm

[31]. The photomultiplier output is amplified with two stages (a total factor of 25) by a Stanford Research Systems SR-445 DC-300 MHz amplifier with input terminated at 500 Ω and carefully calibrated (zeroed) after a long (1-2 hours) warm-up. Photon arrival events are registered with SR400 gated photon counter operated in CW mode with threshold level of 100-120 mV. A translation stage (Klinger Scientific) with a resolution of 1 step/μm or 10 microsteps/μm is used to delay gate pulses and is controlled by a computer via an IEEE interface and Klinger Scientific CD-4 motor driver. The cross correlation function is obtained by combining the non-absorbed second harmonic (excitation) and the fundamental (with the long-pass filter removed): the resulting third harmonic intensity is plotted against delay time. Cross correlation functions typically have a fwhm of 280-300 fs and for time scales greater 20 ps are safely assumed to be delta-function like. All curves were fit and deconvoluted from the instrument response function using an iterative convolute-and-compare nonlinear least-squares algorithm.

The key alignment steps include:

1. Ensure that fundamental is exactly parallel to the translation stage. In the previous section it was already made parallel to the laser table so only minimum adjustment of mirror M7 may be needed. The horizontal component should be controlled by slight rotation of the stage itself around the vertical axis. If a cornercube is employed, care should be taken to avoid the beam hitting the mirror junction lines. For a pair of mirrors, the second mirror (M11) must provide a beam that is not shifted upon stage translation. Deviations must only be corrected after the incoming beam is made exactly parallel to the stage !
2. Next pump beam alignment can be attempted. First, the third pair of prisms (P5, P6) is inserted just as described in the section on the oscillator. Then, the beam is made to propagate parallel to the table in the desired direction. Next the

fundamental is combined with the SHG by a dichroic mirror (BS3) and is directed collinearly towards a monochromator (MC2). At this point one should be able to see each component coming out the MC2 exit slit when set for the appropriate wavelength. Then the sample cell, microscope objective (MO), pump focusing lens (L6) and fluorescence focusing lens (L7) are sequentially introduced so that blue and red light is still going through the MC after each step. The frequency-mixing crystal (C3) is mounted at the last step with the initial orientation ~30° to the incident radiation. At this point it is beneficial to fill the sample cell with fluorescent dye and adjust the microscope objective for symmetric collimated fluorescence that is also collinear with the fundamental. The crystal is then moved to a spot where fluorescence is focused. The fundamental may have a smaller spot size whereas the SHG (pump) will appear loosely focused, which is just enough. All this is to ensure minimum adjustment when real fluorescence upconversion is attempted after time-zero and THG signal are found. Before the next step one needs to have the SHG and fundamental overlapped in the crystal, both going well through the MC. The PMT with UV-pass filter must be mounted and optimized for photon counting mode of detection. Another short-pass filter just after the objective (in place of F1) may be useful to facilitate spot overlap.

3. Now it is time to look for time-zero by monitoring THG intensity with photon counter. The following conditions must be used:

   a) MC should be set for the expected wavelength, calculated from the wavelength of maximum intensity of SHG;

   b) polarization of both incoming beams should be set vertical with the corresponding half-waveplates (W2 and W3) to within 0.5° and the optical axis of the upconversion crystal (marked by a line on its holder) must be set at about

45° to the beams polarization;

c) both MC slits should be removed and ambient room light should be minimized. With both beams blocked 3-4 counts per second (cps) is acceptable. Total background should be definitely less than 300 cps.

d) PMT is set for maximum sensitivity;

e) photon counter is set for continuous operation with 0.3 s period time and minimum wait time. Typical discrimination level is -100 mV but sometimes it can be lowered to -80 mV without too much dark count increase;

f) translation stage is set to operate in microstepping mode with minimum speed and acceleration.

By scanning the stage within the estimated range of time-zero position and carefully observing photon counter readout it is usually a matter of minutes to register a spike of THG. Once found, upconversion crystal and overlap should be optimized for maximum intensity.

When looking for fluorescence upconversion a dye with high quantum yield and not very short fluorescence lifetime (1-5 ns) should be used. Zinc tetraphenylporphyrin (Zn TPP) in alchohols was found to be a good choice. It has absorption maximum close to second harmonic and exhibits ultrafast rising component at emission maximum. Setting the translation stage 100 ps past time zero, and the monochromator to the calculated sum-frequency of the peak in fluorescence spectrum and slowly scanning the BBO angle (C3) with rotary stage micrometer along the vertical axis while continuously monitoring the count rate (count period 3 s) should allow one to find signal fairly easily. Attempts to do so "by hand" are most often unsuccessful as the proper angle within <1° has to be maintained for at least 3 seconds before appreciable number of photons above background can be detected with photon counter.

When using a cutoff filter to block SHG, one should bear in mind that the microscope objective delays shorter wavelengths more than longer ones, so that a cross-correlation function maximum occurs about 5 ps after the apparent instantaneous rise in fluorescence signal (with all other necessary optical elements in the path). A filter will add another 5 ps of delay to the fluorescence.

As it is follows from the previous discussion the signal detected is proportional to the 3rd power of fundamental *and* to the chromophore concentration. A digital power meter with response time of <0.3 s should provide resonable indication of laser stability when used to monitor SHG. Fluctuations should be in the last decimal place. Fleming et al. [8] had to use special precautions to minimize noise in signal but with such Millenia V as a fairly stable pump source such experiment complication is not imperative but may be required with the OPA pumped by a chirped-pulse amplifier as excitation source.

Robust Data Acquisition and Instrument Communication Techniques:

Visual Basic Program "AquiSys" for Data Collection and Instrument Control

This experiment requires timely coordination of data flow produced by photon counter, movement of translation stage and real-time plotting for monitoring purposes. An original data acquisition program, "AquiSys", with modular design, was written in MS Visual Basic 4.0 (16 bit) environment by the author of this dissertation. The choice of programming language was determined by short learning curve and development time and also availability of a variety of custom controls and more importantly "Visual Test Extension" software from Keithley Metrabyte which provides a useful and efficient set of modules for data collection, separation, analysis and plotting in Visual Basic.

The program is has standard *Windows* interface, easy to use, modify and expand when new equipment is available. All communications with instruments are currently

handled through one of the computer standard COM ports. Hardware with IEEE-488 interface is daisy-chained to RS232-IEEE converter "500-SERIAL" from Keithley Metrabyte so that several device can be handled with just a single serial port. Currently supported devices include Klinger Scientific CD-4 and Compumotor for stepping motor drivers and Stanford Research SR400 photon counter and SR830 digital lock-in amplifier for signal source.

Sensitive detection systems and data communication lines are always subject to electromagnetic noise in the research lab environment. A fluorescence upconversion experiment often lasts several hours and is not be possible to complete without data protection mechanisms. These mechanisms including digital garbage rejection, spike elimination and drift detection are all built into the program and allow for easy real-time tuning. Signal fluctuations due to dust particles in the air, sample inhomogeneity, air bubbles in solution, sudden vibrations or change in lighting conditions in the room can be easily handled.

At each delay step, the signal is obtained by averaging 3-5 count periods (samples) normally lasting for 1 s each. To eliminate noise due to the factors mentioned above data are resampled if significant (user defined) relative standard deviation or relative drift is detected. Then translation stage is moved one step further and the process repeated. A typical scan consists of 100 steps and normally averaging 5-10 scans provided acceptable signal to noise ratio.

Another highly recommended feature of this original data acquisition system is real-time signal monitoring complemented with easy to read digital and bar-graph displays. Plotting capabilities include accumulated average display, automatic rescaling and intuitive zooming along the intensity axis.

A limitation exists for the maximum number of steps imposed by the VTX graph

module which should be less than 8000. Practically more than 500 steps for each scan may slowdown data collection process, especially with an old computer, as the majority of the time will be spent on replotting the data. Another point where care should be exercised is when the total number of steps or microsteps in one full scan exceeds (2^{16}-1) or about 65500. Such a big number is outside the limit of motor driver internal step counter and may cause unexpected behavior especially in the "manual" mode. A fairly successful attempt was made to automatically handle this problem but not all the glitches were eliminated.

The complete program code cannot be included as an appendix for practical reasons but is freely available from the author upon request along with a set of all the necessary modules.

Sample Preparation

Typically 1 mg of dye such as hypericin or hypocrellin is enough for one or two days of experimenting depending on solvent and the excitation power.

A sample of a total volume of ~10 ml was constantly pumped through a 1-mm quartz flow cell by a dye circulator or pulsating pump with voltage-controlled rotation speed. A conical flask with specially positioned inlet and outlet was desinged to eliminate bubble trapping during sample circulation. Tygon® tubing with the Teflon® lining was used to avoid destruction by solvents. A septum in place of a glass stopcock with a thin short needle for pressure equilibration helped slow down solvent evaporation dramatically. All experiments, excluding sample preparation, were performed in an unlit room.

Sample degradation can be noticed by decoloration of solution. Absorption and emision spectra need to be registered before and after each experiment for each new solvent used. DMSO was found to be most destructive for hypocrellin A and alchohols

were poorly tolerated by hypericin. Solvent deoxygenation for about 30 minutes helped slow down the process but could not impede it completely.

Low-temperature Control with the Joule-Thompson Refrigerator

Several experiments were attempted by means of MMR Technologies Joule-Thompson refrigerator. This device uses temperature drop arising from adiabatic expansion of nitrogen or argon gas from regulated high (500 psig) to atmospheric pressure. Degassed sample in sealed in 1 mm cuvette is mounted within 10x4x2 cm vacuum sealed aluminum container with quartz optical window on each side. Sample mounting point is equipped with thermocouple and flat resistor which allow for accurate (±0.05 K) temperature control and monitor via microcomputer based communication device.

When preparing sample one should use a little more volume than desired as solvent does evaporate during the freeze-pump-thaw cycles. Usually during the 3rd cycle no bubbling is observed while thawing and sample can be frozen again in liquid nitrogen and quickly sealed off with acetylene-oxygen burner. Sharp melting point transition is also an indication of good degassing.

During the experiment sample in its vacuum chamber was horizontally translated at a frequency of 5-7 Hz. This was necessary to avoid thermal blooming and sample local heating. When approaching melting point of pure solvents it may take 5-10 min before all the heat gradients and flows are settled. Often it is exceedingly hard to distinguish between very viscous solvent at reduced temperature and true glass formation. One factor to periodically check on is solvent volume which drops noticeably upon liquid to solid transition. Hypocrellin A in 50/50 methanol/ethanol glass behaved very well and was not loosing its transparency even at liquid N_2 temperatures.

The common difficulty working with this apparatus is apparent clogging in the gas

line which often appear within a hour of operation. This leads to interruptions is gas flow and instability in temperature of even its uncontrollable rise. The only remedies are either to keep increasing the pressure until the maximum allowed is reached or, without lowering the pressure, make the sample warm up above freezing point of water, or wait for the gas flow to normalize and allow it cool back down again.

COMPUTER SIMULATIONS OF THE TRANSIENT ABSORBANCE AND ANISOTROPY FOR HYPOCRELLIN A EXCITED-STATE DYNAMICS

Introduction

This section is devoted to the description of theory behind simulations of hypocrellin A excited-state dynamics thoroughly discussed in Chapter IV. The proposed model, illustrated in Figure 2.3, includes two species in the ground state and three species in the first excited-state which undergo H-atom transfer, capable of excited-state absorption, stimulated emission, intersystem crossing to form triplet and decay to the ground state. Isotropic rotational diffusion is accounted for every state except the triplet since its contribution to the signal becomes significant only at times much longer than the anisotropy lifetime. The values of the intersystem crossing, internal conversion and radiative decay rates were calculated from the known fluorescence lifetime and the quantum yields for fluorescence, triplet and singlet oxygen production reported in [32]

The discussion below follows in part the treatment of internal conversion between low-lying ^1L_a and ^1L_b states of tryptophan presented by Fleming and coworkers in reference [8].

Theory of Isotropic Rotational Diffusion: Application for Pump/Probe Anisotropy Experiment

Simulations of hypocrellin A time-resolved absorbance and its anisotropy including the effects of excited-state proton transfer were based on the treatment of fluorescence depolarization given by Cross *et al.*[33]. A more general treatment by Szabo [34] gave identical results for this problem. In the algorithm of Cross *et al.*, it is assumed that the excited-state dynamics can be described by first-order rate processes that are independent of

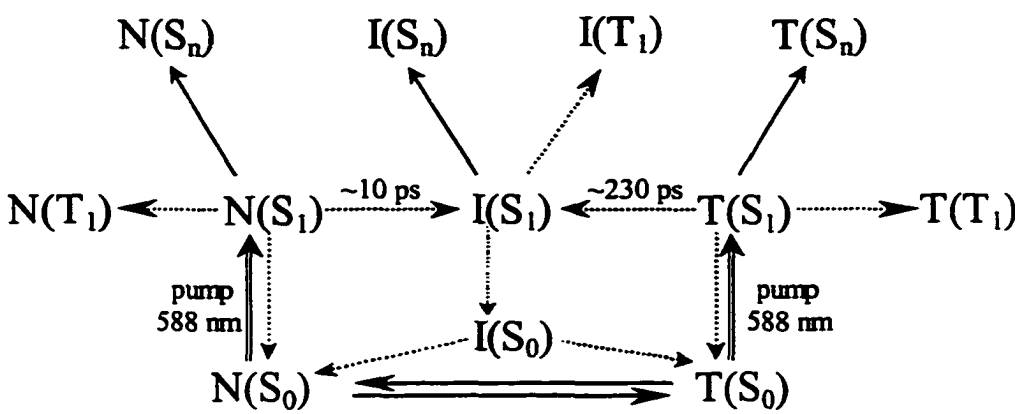

Figure 2.3 Schematic diagram for the simulated model of hypocrellin A excited-state photophysics.

the overall orientation of the molecules and that molecular reorientation occurs by anisotropic rotational diffusion. To simplify the problem, it is assumed that the rotational diffusion tensor is state independent. The ground- and excited-state populations are then given by

$$\frac{d}{dt}K^{(i)}(t) = \sum_{j=0}^{n-1} k_{ij}K^{(j)}(t) \qquad (2.8)$$

i = 0,1 , ..., n-1

where $K^{(i)}(t)$ is the number density of molecules in state (i), and is k_{ij} is a matrix of first-order rate constants in the n-level system. The normalized orientational probability distribution for each level (state) is defined such that the probability of finding a molecule in a state with an orientation between Ω and $\Omega+d\Omega$ is proportional to $f^{(i)}(\Omega, t)\, d\Omega$, and

$$K^{(i)}(t) = \int d\Omega\, f^{(i)}(\Omega, t) \tag{2.9}$$

where $\Omega \equiv (\alpha, \beta, \gamma)$ are the Euler angles that specify the orientation of the molecular axis with respect to the laboratory fixed axis system, and the integration is over the limits $0 \le \alpha \le 2\pi$, $0 \le \beta \le \pi$, $0 \le \gamma \le 2\pi$. Assuming that the orientation of the molecule does not change during a state-to-state transition, the set of coupled partial differential equations that describes the time solution of the system can be written as [33,35]

$$\frac{d}{dt} f^{(i)}(\Omega, t) = -\sum_{\alpha=0}^{3} D_{\alpha}^{(i)} L_{\alpha}^{2} f^{(i)}(\Omega, t) + \sum_{j=0}^{n-1} k_{ij} f^{(i)}(\Omega, t) \tag{2.10}$$

$i = 0,1, \ldots, n\text{-}1$

where $D_{\alpha}^{(i)}$ ($\alpha = 1, 2, 3$) are the diagonal elements of the diffusion tensor in the molecular coordinate system for state (i), and L_{α} are the orbital angular momentum operators with respect to the molecular coordinate system. This set of equations can be solved by expanding the probability function for each state in terms of asymmetric rotor wave functions [36]. The time evolution of the system can then be separated out and described in terms of the expansion coefficients. The general result can be expressed as

$$f^{(i)}(\Omega, t) \equiv f^{(i)}(\theta, \phi, t) = \frac{1}{4\pi}\left[1 + 2\, c_{2,0}^{(i)}(t) P_2(\cos\theta)\right] \tag{2.11}$$

where $c_{2,0}^{(i)}(t)$ is the only non-unity (due to certain boundary conditions) time-dependent coefficient in the Green's function $G^{(i)}(\Omega_{\circ} \mid \Omega, t)$ expansion with spherical harmonics. Green's function is obviously defined as [35]:

$$f^{(i)}(\Omega,t) = \int_{\Omega_0} G^{(i)}(\Omega_0 \mid \Omega,t) f^{(i)}(\Omega_0) d\Omega_0 \tag{2.12}$$

where $f^{(i)}(\Omega_0) \equiv f^{(i)}(\theta_0) = \frac{1}{4\pi}[1 + 2P_2(\cos\theta_0)]$ is a normalized anglular distribution of transition dipoles relative to pulse polarization just after the excitation at time t=0 and $P_2(\cos\theta_0)$ is a second-order Legendre polymonial with respect to $\cos\theta_0$.

A detailed account of the methods used in solving this set of equations can be found in ref. [33-35] and references therein.

In our experiment the signal measured at each polarization, $I_{\|}(t)$ and $I_{\perp}(t)$ is sum of contributions, which are proportional to the instantaneous population $K^{(i)}(t)$ of species (i) and the square of the scalar product of its transition dipole vector in its current orientation $\vec{\mu}^{(i)}(\Omega,t)$ and the probe pulse polarizarion direction $\vec{\mu}_{probe}$, averaged over all possible Ω :

$$I_{\|}(t) = \sum_{i=0}^{n-1} I_{\|}^{(i)}(t) = \sum_{i=0}^{n-1} \frac{1}{4\pi} \int_{\Omega} K^{(i)}(t) \left| \vec{\mu}_{probe}^{\|} \cdot \vec{\mu}^{(i)}(\Omega,t) \right|^2 f^{(i)}(\Omega,t) d\Omega \tag{2.13a}$$

$$I_{\perp}(t) = \sum_{i=0}^{n-1} I_{\perp}^{(i)}(t) = \sum_{i=0}^{n-1} \frac{1}{4\pi} \int_{\Omega} K^{(i)}(t) \left| \vec{\mu}_{probe}^{\perp} \cdot \vec{\mu}^{(i)}(\Omega,t) \right|^2 f^{(i)}(\Omega,t) d\Omega \tag{2.13b}$$

Since the absorption and (stimulated) emission transition dipoles are body fixed vectors in the molecular axis system, an effective excited-state absorbance or stimulated emission intensity for each state (i) can be defined with respect to an arbitrary ground-state absorption transition dipole (j), forming an angle $\theta^{(i,j)}$ with transition dipole for such absorption (emission). After substitution of $f^{(i)}(\Omega,t)$ in the expressions found above and evaluating the surface-average one obtains:

$$I_{\|}^{(i)}(t) = \left[\frac{1}{3} + \frac{4}{15} c_{2,0}^{(i)}(t) P_2(\cos\theta^{(i)}) \right] K^{(i)}(t) \left| \vec{\mu}^{(i)} \right|^2 \tag{2.14a}$$

$$I_{\perp}^{(i)}(t) = \left[\frac{1}{3} - \frac{2}{15} c_{2,0}^{(i)}(t) P_2(\cos\theta^{(i)}) \right] K^{(i)}(t) \left| \vec{\mu}^{(i)} \right|^2 \tag{2.14b}$$

Since the overall molecular tumbling behavior of hypocrellin A in alchohols as measured by fluorescence depolarization is well described by a monoexponential decay

[37] with time constant τ_r, it can be reasonably approximated as a spherical diffuser with a state-independent diffusion coefficient $D=1/(6\tau_r)$ over the time scale of interest in these initial simulations. This then leaves as parameters only the angles between the ground-state absorption and stimulated emission (or excited state absorbance) transition dipoles in each state and corresponding probability coefficients, which we shall refer to as $\left|\varepsilon^{(i)}\right| = \left|\vec{\mu}^{(i)}\right|$.

For generality we shall think of $\varepsilon^{(i)}$ as signed property with negative values corresponding to processes associated with photon emission, such as fluorescence and stimulated emission. Of course, sample fluorescence is not relevant to our case as it is not detected in pump/probe experiment.

Hence, after expansion of Legendre polynomial, for each radiative transition that species *(i)* can afford we have:

$$I_{\parallel}^{(i)}(t) = \varepsilon^{(i)}\left[\frac{1}{9} + \frac{2}{45}\exp(-6Dt)(3\cos^2\theta^{(i)} - 1)\right]K^{(i)}(t) \tag{2.15a}$$

$$I_{\perp}^{(i)}(t) = \varepsilon^{(i)}\left[\frac{1}{9} - \frac{1}{45}\exp(-6Dt)(3\cos^2\theta^{(i)} - 1)\right]K^{(i)}(t) \tag{2.15b}$$

Finally the total observed time-dependent change in absorbance $\Delta A(t)$ is a sum of contributions form photobleach, excited-state absorbance and stimulated emission (negligible for triplet state) [38]:

$$\Delta A(t) = \frac{1}{3}\left(\Delta A_{\parallel}(t) + 2\Delta A_{\perp}(t)\right) = I_{PB}(t) + I_{EA}(t) + I_{SE}(t) \tag{2.16a}$$

$$\Delta A_{\parallel}(t) = I_{\parallel,PB}(t) + I_{\parallel,EA}(t) + I_{\parallel,SE}(t) \tag{2.16b}$$

$$\Delta A_{\perp}(t) = I_{\perp,PB}(t) + I_{\perp,EA}(t) + I_{\perp,SE}(t) \tag{2.16c}$$

The anisotropy decay can then be easily extracted as

$$r(t) = \frac{\Delta A_{\parallel}(t) - \Delta A_{\perp}(t)}{\Delta A_{\parallel}(t) + 2\Delta A_{\perp}(t)} \tag{2.17}$$

To minimize the number of degrees of freedom we postulate that excited-state absorption transition dipole ($S_1 \rightarrow S_n$) for each species is orthogonal to its ground-state

counterpart ($S_0 \rightarrow S_1$) because of molecule near C_{2v} symmetry. Further, since decay to the triplet and the ground state occurs on time scales at least one order of magnitude longer than the depolarization time, it is assumed that decay to any of these states also induce a complete depolarization. Other simplifications of the model include equivalence of all decay rates to triplet state, equivalence of all the triplet state absorption coefficients, and also equivalence of normal (N, N*) and tautomeric (T, T*) species light absorption (emission) properties with the exception of excited-state "intermediate" (I*). It is also assumed that N, N* and T, T* have identical orientations of all transition dipole moment with respect to molecular frame but at some angle ϕ relative to those of I*. The sum of radiative and nonradiative rate constants as well as the intersystem crossing rate were set equal to the experimental values found in [32].

After all these simplifications, the fitted parameters of the model are the absorption coefficients $\varepsilon^{(i)}$ of each of the excited states (including triplet), stimulated emission coefficient for N*, T* and I* and the angle ϕ. In this context the physical meaning of $\varepsilon^{(i)}$ is simply the probability for specific type of species to absorb (for EA) or emit (for SE) photon relative to the ground state (PB). To bind all these model parameters to the experimental data in the most direct way we first performed simulations-fitting with MathCAD software for isotropic averages of these variables and then used that information to simulate and fit the experimental anisotropy profiles so that ϕ can be extracted and SE can be separated from EA components. Our very first step, of course, was the solution of coupled differential equations that describe model kinetics. We found that Maple V was the easiest way to accomplish this with symbolic expression as an output (see Appendix for Chapter IV).

REFERENCES

1. Spence, D. E.; Sibbett, W. *J. Opt. Soc. Am. B: Opt. Phys.* **1991**, *8*, 2053-2060.

2. Backus, S. D., Charles G., III; Murnane, Margaret M *Review-of-Scientific-Instruments.* **1998**, *69*, 1207-1223.

3. Chang, Z.; Rundquist, A.; Wang, H.; Murnane, M. M.; Kapteyn, H. C. *Phys. Rev. Lett.* **1997**, *79*, 2967-2970.

4. Rundquist, A.; Durfee, C.; Chang, Z.; Taft, G.; Zeek, E.; Backus, S.; Murnane, M. M.; Kapteyn, H. C.; Christov, I.; Stoev, V. *Appl. Phys. B: Lasers Opt.* **1997**, *B65*, 161-174.

5. Lindek, S. P., Rainer; Stelzer, Ernst H. K *Review of Scientific Instruments.* **1994**, *65*, 3367-3372.

6. O'Connor, D. V. *Time-correlated single photon counting.*; Academic Press: Orlando, Fla., 1984.

7. Kopainsky, B.; Kaiser, W. *Opt. Commun.* **1978**, *26*, 219-224.

8. Ruggiero, A. J.; Todd, D. C.; Fleming, G. R. *J. Am. Chem. Soc.* **1990**, *112*, 1003-1014.

9. Hansen, J. E.; Rosenthal, S. J.; Fleming, G. R. *J.Phys. Chem.* **1992**, *96*, 3034-3040.

10. Jimenez, R.; Fleming, G. R. *Adv. Photosynth.* **1996**, *3*, 63-73.

11. Krueger, B. P.; Scholes, G. D.; Yu, J.-Y.; Fleming, G. R. *Acta Phys. Pol., A* **1999**, *95*, 63-83.

12. Macpherson, A. N.; Gillbro, T. *J. Phys. Chem. A* **1998**, *102*, 5049-5058.

13. Chattoraj, M.; King, B. A.; Bublitz, G. U.; Boxer, S. G. *Proc. Natl. Acad. Sci. U. S. A.* **1996**, *93*, 8362-8367.

14. Riter, R. E.; Willard, D. M.; Levinger, N. E. *J. Phys. Chem. B* **1998**, *102*, 2705-2714.

15. Marks, D.; Prosposito, P.; Zhang, H.; Glasbeek, M. *Chem. Phys. Lett.* **1998**, *289*, 535-540.

16. Chattoraj, M.; King, B.; Boxer, S. G. *Investigating the solvent dependence of proton and deuterium transfer in 3-hydroxy flavone using femtosecond fluorescence upconversion.*; American Chemical Society: Chicago, IL, August 20-24, 1995, pp PHYS-108.

17. Smith, T. P.; Zaklika, K. A. *J.Phys.Chem.* **1991**, *95*, 10465-10475.

18. Greenfield, S. R.; Wasielewski, M. R. *Opt. Lett.* **1995**, *20*, 1394-1396.

19. Greenfield, S. R.; Wasielewski, M. R. *Appl* **1995**, *34*, 2688-2691.

20. Krausz, F. F., M. E.; Brabec, T.; Curley, P. F.; Hofer, M.; Ober, M. H.; Spielmann, C.; Wintner, E.;Schmidt, A. J. *IEEE J. Quantum Electron.* **1992**, *28*, 2097.

21. Martinez, O. E. C., J. L. A. *Opt. Lett.* **1992**, *17*, 1210.

22. Zhou, J.; Taft, G.; Huang, C.-P.; Christov, I. P.; Kapteyn, H. C.; Murnane, M. M. *Springer Ser. Chem. Phys.* **1994**, *60*, 39-40.

23. Christov, I. P.; Stoev, V. D.; Murnane, M. M.; Kapteyn, H. C. *J. Opt. Soc. Am. B* **1998**, *15*, 2631-2633.

24. Huang, C. P.; Asaki, M. T.; Backus, S.; Murnane, M. M.; Kapteyn, H. C. *Opt. Lett.* **1992**, *17*, 1289-1291.

25. English, D. S. *Elucidation of the primary photophysical processes in the light-activated antiviral agents, hypericin and hypocrellin.*; Iowa State University: Ames, 1998, pp 118.

26. Gai, F. *Photophysics of a novel optical probe, 7-azaindole, and an antiviral agent, hypericin*; Iowa State University: Ames, 1994, pp 193.

27. Siegman, A. E. *Lasers*; University Science Books: Mill Valley, CA, 1986.

28. Beddard, G. S.; Doust, T.; Windsor, M. W. *Springer Ser. Chem. Phys.* **1980**, *14*, 167-170.

29. Cross, A. J.; Fleming, G. R. *Biophys. J.* **1984**, *46*, 45-56.

30. Gardecki, J.; Horng, M. L.; Papazyan, A.; Maroncelli, M. *J. Mol. Liq.* **1995**, *65/66*, 49-57.

31. Adhav, R. S.; Adhav, S. R.; Pelaprat, J. M. *Laser-Focus* **1987**, *23*, 88.

32. Diwu, Z.; Lown, J. W. *J. Photochem. Photobiol., A* **1992**, *64*, 273-287.

33. Cross, A. J.; Waldeck, D. H.; Fleming, G. R. *J. Chem. Phys.* **1983**, *78*, 6455-6467.

34. Szabo, A. *J. Chem. Phys.* **1984**, *81*, 150-167.

35. Chuang, T. J.; Eisenthal, K. B. *J. Chem. Phys.* **1972**, *57*, 5094-5097.

36. Tao, T. *Biopolymers* **1969**, *8*, 609-632.

37. Das, K.; Dertz, E.; Paterson, J.; Zhang, W.; Kraus, G. A.; Petrich, J. W. *J. Phys. Chem. B* **1998**, *102*, 1479-1484.

38. Savikhin, S.; Tao, N.; Song, P. S.; Struve, W. S. *J. Phys. Chem.* **1993**, *97*, 12379-12386.

CHAPTER III. EXCITED-STATE PROCESSES IN POLYCYCLIC QUINONES: THE LIGHT-INDUCED ANTIVIRAL AGENT, HYPOCRELLIN, AND A COMPARISON WITH HYPERICIN

A paper published in the Journal of Physical Chemistry[1]

K. Das, D. S. English, M. J. Fehr, A. V. Smirnov, and J. W. Petrich[2]

ABSTRACT

Hypocrellin is a naturally occurring perylene quinone that possesses light-induced antiviral activity, most notably against the human immunodeficiency virus (HIV), as does the related molecule, hypericin. White-light continuum is employed to examine the excited-state processes in hypocrellin from the picosecond to the nanosecond time scales. These processes are assigned to intramolecular proton transfer, intersystem crossing, and interconversion between different conformations of hypocrellin, which is constrained to be nonplanar in its ground state owing to its bulky side chains. The ground state of hypocrellin is suggested to be heterogeneous and to be comprised of an equilibrium between at least two tautomeric forms. The results are discussed in terms of the properties of hypericin, which bears marked similarities and differences with respect to hypocrellin, both in terms of its excited-state properties as well as its mode of induced antiviral activity.

---

[1] Reprinted with permission from Journal of Physical Chemistry, 1996, *100*, 18275-18281.

[2] To whom correspondence should be addressed.

INTRODUCTION

Hypocrellin and hypericin (Figure 3.1) are naturally occurring polycyclic quinones that have been used for centuries as folk medicines in the orient [1] and the occident [2,3], respectively. Hypericin is the pigment found in the common plant, St. John's wort. Hypocrellin is obtained from the mold, *Hypocrella bambusae*. Our motivation for the study of hypocrellin is that, owing to its similarities with respect to hypericin, which are at least superficial, it may provide a means of better understanding hypericin and hypericin-like molecules.

Our laboratory's interest in hypericin was stimulated by the report that it possesses antiviral activity against the human immunodeficiency virus (HIV) [4-7] and by the discovery of Kraus and Carpenter that toxicity against the class of enveloped lentiviruses, of which HIV is a member, absolutely depends on light [8,9]. Hypericin is in fact currently being used in clinical trials for HIV [10-13]; and extracts from St. John's wort can be purchased in health food stores and are taken orally by individuals infected with HIV [14,15]. Results from our group [16] as well as from others [17] indicate that hypocrellin also exhibits antiviral activity that absolutely depends on light. The enormous potential of such quinone species in photodynamic therapies against viruses and tumors [18,19] prompted our investigations into the role of light in virucidal activity and into the nature of the excited-state species that are responsible for such activity [20-26].

The proximity of the enol and keto groups in organic molecules provides an environment that is propitious for excited-state intramolecular proton transfer or hydrogen atom transfer (in this article, we use the two terms interchangeably). Malonaldehyde [27], salicylic acid [28], 3-hydroxyflavone [29], benzothiazole [30], and tropolone [31] are but a few of the examples of a litany of species that execute intramolecular excited-state proton transfer. The disposition and the number of enol and keto groups in hypericin is

immediately suggestive of the possibility of excited-state intramolecular proton transfer, and we have interpreted our picosecond spectroscopic studies of this molecule in these terms [20-22]. Of special relevance to the role of labile protons for light-induced antiviral activity is the observation that hypericin retains its toxicity in the absence of oxygen and that it acidifies its surroundings upon light absorption [23,24]. The retention of toxicity in the absence of oxygen excludes unique assignment of antiviral activity to the trivial generation of singlet oxygen--even though hypericin does generate triplets in high yield [38-40].

In parallel with our investigations into the origin of the light-induced antiviral activity of hypericin, we have begun a program devoted to the specific targeting and triggering of its activity by the chemiluminescent generation of light in virus-infected cells [25]. Preliminary results with dog cells *in vitro* indicate that chemiluminescence can be specifically induced by the presence of the infecting virus [25,26]. We have focused our attention on the development of this type of a gene therapy [26] because it can in principle reduce the appearance of drug-resistant mutants, which typically emerge and block the efficiency of current treatments [32,33].

The structural similarities of hypocrellin and hypericin would seem to suggest that hypocrellin exhibits excited-state and antiviral behavior similar to, if not identical with, that of hypericin. But this is not the case. Hypocrellin absolutely requires oxygen for antiviral activity whereas hypericin does not. Also, hypocrellin does not provide a light-induced pH drop of its surrounding, as a result of *intermolecular* proton transfer, under conditions in which hypericin does exhibit such an effect [16]. Clearly the superficial resemblance between hypocrellin and hypericin belies more profound differences that demarcate their activities. In this article, the excited-state photophysics of hypocrellin are investigated. White-light continuum is employed to examine the excited-state processes in

hypocrellin from the picosecond to the nanosecond time scales. These processes are assigned to intramolecular proton transfer, intersystem crossing, and interconversion between different conformations of hypocrellin, which is constrained to be nonplanar in its ground state owing to its bulky side chains. The ground state of hypocrellin is suggested to be heterogeneous and to be comprised of an equilibrium between at least two tautomeric forms. In the Conclusions section, these processes are summarized in a kinetic scheme and comparisons are made with hypericin.

MATERIALS AND METHODS

Hypocrellin A (to which we refer as hypocrellin) was obtained from Molecular Probes Inc. and was used as received. Solvents were obtained from Aldrich. Methylcyclohexane and 2,2,2-trifluorethanol, which were used in fluorescence lifetime measurements, were carefully distilled under nitrogen and over calcium sulfate. Octanol was dried by stirring overnight with magnesium sulfate. The solvents were subsequently used in transient absorption experiments after which a drop of water was added and the experiments repeated. This was done to assure that the transients were not a result of residual water in the solvents.

All experiments were performed at ambient temperatures (22 °C). Fluorescence spectra were measured with a Spex Fluoromax with emission and excitation bandpass of 4 nm. The time correlated single photon counting experiments are performed with an apparatus described elsewhere [34]. The instrument response function had a full width at half maximum of 70 ps.

Pump-probe experiments with white-light continuum were performed with the apparatus described elsewhere [21,34]. The time and spectral resolution are 1-2 ps and ±4 nm respectively. Transient absorption spectra were obtained with a liquid nitrogen cooled

charge-coupled device (CCD) (Princeton Instruments LN/CCD-1152UV) mounted on an HR 320 (Instruments SA, Inc.) monochromator with a grating (1200 grooves/mm) blazed at 5000 Å. The following protocol was employed. The CCD pixels were binned such as to allow simultaneous collection of both the probe and the reference beams, I and I_0 respectively, of the transient absorption spectrometer. The signal was integrated for 5 s. Four five second acquisitions were averaged to give a single spectrum. Absorption spectra were constructed from -log(I/ I_0). These spectra were corrected by subtraction of back ground spectra obtained by delaying pump pulse to arrive after the probe and reference. The horizontal array of the CCD consists of 1152 pixels. In our optical arrangment, there were 19 pixels/nm, giving a full scale spectral range of 60 nm.

Transient spectra are presented in Figures 3 and 4. Although the two panels could, in principle, be displayed as one, covering the whole 120 nm range of our experiment, we chose not to splice the data together in this way for three reasons. First, such a presentation without the aid of colored graphics is very congested and makes it very difficult to follow a single trace through the entire region. Secondly, due to slight difference in laser intensity and spatial overlap of pump and probe beams from experiment to experiment it was not always possible to ensure an exact match up at the blue edge of one experiment to the red edge of the other experiment that would be required in order to splice the spectra together correctly. Lastly, the region around 588 nm is contaminated by leakage from the pump laser pulse. Distortions from the pump source are still detectable in the deviations of the flat negative time signal from zero (Figure 3.4).

Sample concentrations for Hypocrellin were $4x10^{-5}$ M for steady state and time correlated single photon counting experiments and $5x10^{-4}$ M for transient absorption measurements.

For transient absorption measurements care was taken to prevent destruction of the sample and introduction of artifacts from high pulse powers. Typical peak pump intensities were 2.5 GW/cm^2. At very high intensities, artifacts arise, perhaps from triplet-triplet annihilation, since hypocrellin has a substantial triplet yield [35].

Kinetic traces acquired at various wavelengths were fit using a global fitting procedure found in Spectra Solve ^{TM}. The global parameters in our case were time constants and local parameters were amplitudes or preexponential factors. The time constants are specified and each curve is fit iteratively varying only the local parameters, that is the amplitudes. A local χ^2 is calculated for each local fit. After all curves are fit (typically 4 to 8), a global χ^2 is calculated as shown below. The global parameters are varied and the whole process is repeated to calculate a new global χ^2. This process is repeated until a minimum is reached for χ^2, which is defined as:

$$\chi^2 = \frac{\sum_{i=1}^{n} \frac{\chi^2_{local,i}}{\chi^2_{best,i}}}{n}$$

where $\chi^2_{best,i}$ is obtained for each curve letting all parameters local and global (that is amplitudes and time constants) vary; and n is the number of curves. The quality of the fit was determined by visual inspection of the fit and its residuals.

Four contributions are considered when fitting the pump-probe data. These are: 1) a rising component in the induced absorbance; 2) an instantaneous component corresonding to appearance of signal within the pump pulse; 3) a long lived component (assigned to a time constant of infinity for experiments on time scales up to 200 ps) corresponding to the triplet state; and 4) a decaying component in the stimulated emission. The time constants obtained in this manner are reproducible to within ± 10%.

The absorbance data are fit to the following form:

$$\Delta A(t) = a_1 [1-\exp(-t/\tau_1)] + a_2 \exp(-t/\tau_2) + a_3 \exp(-t/\infty)$$

The stimulated emission pump probe data were fit to the form:

$$\Delta A(t) = -a_1 \exp(-t/\tau_1) - a_2 \exp(-t/\infty)$$

RESULTS

Figure 3.2a presents the steady-state absorption and emission spectra of hypocrellin in ethanol. These spectra differ significantly from those of hypericin (Figure 3.2b), which exhibit a remarkable mirror image symmetry and whose emission has no Stokes shift. For comparison, we present the spectra of the analog, mesonaphthobianthrone [21] in H_2SO_4 (Figure 3.2c). In aprotic solvents this analog has no visible absorption and no detectable emission. In strong acid, however, its spectra resemble those of hypericin and especially of hypocrellin.

Figures 3.3 and 3.4 present the time-resolved spectra of hypocrellin in ethanol and octanol, respectively. The salient features of the transient spectra are the following:

1. Both stimulated emission and induced absorption are present at zero time.
2. The stimulated emission *decays* with time.
3. In addition to the component of transient absorption that is present at zero time, there is also transient absorption that *grows* in with time. Transients appearing on the picosecond and the nanosecond time scales are resolved. At some probe wavelengths, the transient absorption appears very rapidly and does not decay on the time scale of the experiment (~2 ns).

The evolution of the above spectra and the relationship between the species giving rise to them can best be studied by monitoring kinetics at individual probe wavelengths.

These data are presented in Figures 5 and 7 for ethanol. Stimulated emission and transient absorption are observed.

Absorption transients are present at zero time and are also seen to grow in with time. The amount of transient absorbance appearing instantaneously depends on the probe wavelength. Consequently, it *may* appear that the measured time constants depend on the probe wavelength. *A global analysis of the data, however, indicates that the noninstantaneous rise time of the transient at all probe wavelengths matches, within experimental error, the decay time of the stimulated emission.* This time constant is 80 ps in ethanol and 100 ps in octanol. Because of the presence of multiple components of transient absorption and their dependence on probe wavelength, it can be misleading to use a single transient absorption trace as a measure of the intramolecular proton transfer time (see below) unless care is taken in the data analysis. The decay of stimulated emission provides a much more direct and uncomplicated measure of the proton transfer time.

In octanol, both stimulated emission and transient absorption are also observed (Figure 3.6). As for ethanol, *both an instantaneous and a slow component of transient absorption are observed.* In addition to these, however, is the appearance of transient absorption that grows in on an intermediate time scale, i.e., with a time constant of ~10 ps. A 10-ps component is also observed for hypocrellin in the even more viscous solvent, ethylene glycol (Figure 3.8).

DISCUSSION

Excited-State Processes: Intramolecular Proton Transfer, Intersystem Crossing, and Conformational Relaxation

A. Proton Transfer

We assign the decay of stimulated emission and the concomitant rise in induced absorbance to excited-state intramolecular proton transfer. This assignment is based on the huge precedent established in other aromatic molecules [27-31], including hypericin [20-22]. It is supported by the kinetic relatedness of the stimulated emission to the induced absorbance, and by the observation, discussed immediately below, that the decay time of the stimulated emission is comparable to the fluorescence decay of hypocrellin in H_2SO_4.

Hypocrellin in H_2SO_4 is weakly fluorescent. As is indicated in Figure 3.9, in H_2SO_4 its fluorescence decay comprises a 200-ps component that represents ~60 % of the intensity. The fluorescence quantum yield of hypocrellin in H_2SO_4 is 0.02. The fluorescence decay of hypocrellin in all the other solvents we investigated is single exponential and ranges from 1.3-1.6 ns. The fluorescence quantum yield in, for example, benzene [35], is 0.14.

We are unable to observe a rapid component in the fluorescence decay of hypocrellin in any nonacidic solvent. That we cannot observe, for example, a 80-ps component in the fluorescence decay of hypocrellin in ethanol (fluorescence lifetime of 1.3 ns) is surprising given the appearance of the 80-ps component in the stimulated emission (Figure 3.5). The point is discussed below and in the Conclusions section. We rationalize this result by postulating that hypocrellin exists in the ground state in a tautomerized form (Figures 1b or 1c) and that this species is as weakly fluorescent as hypocrellin in H_2SO_4.

In the excited state, this tautomeric species undergoes a "back transfer" reaction to

produce the normal form (Figure 3.1a): this reaction occurs in 80 ps in ethanol (Figure 3.5). We propose that it is the normal form of hypocrellin that is strongly fluorescent and that gives rise to the ~1.5-ns fluorescence decay referred to above. We further propose that the fluorescence spectrum of the normal form overlaps with that of the tautomer substantially. Owing to this spectral overlap, as the normal form is produced, the rise in its emission roughly cancels out the decay of the emission of the tautomer, at least within the spectral resolution of our experiment (16 nm). See Figure 3.10 for more details.

B. Intersystem Crossing

Above we have discussed the absorbance transients in terms of the appearance of a back transfer reaction occurring on a time scale of 80-100 ps to produce the normal form of the hypocrellin molecule. Examination of the transient spectra and of the kinetic traces indicates that very long lived species are also produced. We assign these transients to the production of triplet species. The triplet yield of hypocrellin in benzene is 0.83 [35].

The generation of triplet is most clearly manifested in Figures 3 and 4 and in Figure 3.7 where the transient absorbance *appears on a nanosecond time scale* at 600 nm. The time scale for these rise times is in very good agreement with the fluorescence decay time of the singlet state of hypocrellin. (Note that we have identified the long-lived fluorescent state of hypocrellin with the untautomerized or normal species, Figure 3.1a. See above.)

Of additional interest is the transient in ethanol in the region from 500-570 nm. This transient appears with both an instantaneous and a 80-ps component (Figures 5). *But examination on a 2-ns time scale (Figure 3.7) indicates that it does not decay.* Clearly, a contribution to the transient absorption at this wavelength must also be due to triplet-triplet absorbance. We propose that the triplet species whose formation is revealed in these kinetics arises from the decay of the hypocrellin tautomer (Figure 3.1b or 1c). See Figure

3.10 for a detailed kinetic scheme.

We are obliged to conclude that the transient absorbance in the region of 570 nm for hypocrellin in ethanol arises from:

1. singlet-singlet absorption of the normal form of hypocrellin that is produced immediately upon optical excitation;

2. the singlet-singlet absorption of the normal form of hypocrellin that is formed by excited-state back proton transfer;

3. the absorption of triplets produced from the tautomerized and the untautomerized species.

Similar assignments of the absorbing transients are made for hypocrellin in octanol.

C. Conformational Relaxation

In ethanol the subnanosecond transients at all probe wavelengths can be described by a global analysis employing instantaneous and ~80-ps molecular responses. The kinetics for hypocrellin in octanol are more complicated in that the absorption kinetics reveal a 10-ps component (Figure 3.6) in addition to the longer 100-ps component, which corresponds to the decay of stimulated emission (and consequently to the proton transfer time).

We interpret this 10-ps component as a slow conformational change of the excited-state normal form (Figure 3.1a) of hypocrellin that is produced upon optical excitation. This component is not observed in solvents of low viscosity, but it is observed in high-viscosity solvents such as ethylene glycol (Figure 3.8).

The x-ray structure of hypocrellin indicates that it is not a planar molecule [36]. (Similar conclusions can be drawn from semiempirical calculations or, more simply, from molecular models. Hypericin is also a twisted molecule [37].) The large side chains

protruding from the perylene quinone skeleton repel each other and prevent the molecule from acquiring a planar conformation. We propose that upon optical excitation hypocrellin converts from one twisted conformation to another. This process is too rapid to be observed with our time resolution in ethanol, but is proposed to occur in 10 ps in octanol. That a time constant of ~10 ps is also observed in the much more viscous solvent, ethylene glycol, suggests that this process is already saturated with respect to viscosity in this solvent.

CONCLUSIONS

Based on the above results, we present the following kinetic scheme for hypocrellin (Figure 3.10). Both untautomerized (N) and tautomerized hypocrellin exist in the ground state. They are excited in roughly equal proportions. The 80-100 ps decays of stimulated emission correspond to an excited-state back proton transfer to form the "untautomerized" or "normal" species.

Absorption transients are seen to appear on a nanosecond time scale (Figures 3, 4, and 7). They are also seen to appear in ≤ 100-ps and not to decay on a nanosecond time scale. These transients are attributed to triplet-triplet absorption. The former are formed from the fluorescent species of hypocrellin, the untautomerized form N, that has a ~1.3-ns lifetime. The latter is formed from the excited-state tautomer of hypocrellin, which is characterized by a 80-ps decay in ethanol and a 100-ps decay in octanol.

Finally, a component of ~10 ps is resolved in the rise time of transient absorbance in octanol and ethylene glycol. This transient is tentatively attributed to a conformational change between twisted forms of the aromatic ring that occurs in the excited state.

These results and conclusions provide an interesting point of comparison with those for the antiviral agent, hypericin (Figure 3.1d) [21,22]. Hypericin is strongly

fluorescent in H_2SO_4, whereas hypocrellin is not (Figure 3.9).

As noted in the Introduction and as can be seen from Figure 3.2, hypericin has a mirror image symmetry between its absorption and emission spectra. Elsewhere we rationalized this mirror image relationship in terms of the presence of ground-state tautomerized hypericin [21,22]. The time-resolved data for hypocrellin are very suggestive of ground-state heterogeneity. For example, on a subnanosecond time scale, the transient absorbance appears with two time constants. There is a component that appears instantaneously, that is, within the excitation pulse width. And there is another component with time constants of 80 ps and 100 ps in ethanol and octanol, respectively.

In the context of what is known concerning hypericin and hypocrellin, the analog mesonaphthobianthrone (Figures 1e and 2c) is of considerable interest. In aprotic solvents such as DMSO, it has no visible absorbance and no detectable fluorescence. In H_2SO_4, however, it acquires absorption and emission spectra in the visible. In large part because of this observation, indicating that protonated carbonyl groups are responsible for the fluorescent species, *rise times* in the stimulated emission of hypericin were attributed to intramolecular proton transfer in this molecule.

Although the two-dimensional aromatic skeleton of hypericin is essentially identical to that of mesonaphthobianthrone the absorption and emission spectra of the latter in H_2SO_4 are much more similar to those of hypocrellin than of hypericin. It is not clear how to interpret this similarity. Also, while hypericin is strongly fluorescent in H_2SO_4 [21,22], hypocrellin is not (Figure 3.9).

Because protonated hypocrellin is weakly fluorescent, the 80-100-ps transients cited here are attributed to *back intramolecular proton transfer*, which forms the longer-lived nanosecond fluorescent species.

The stimulated emission observed in hypericin is more complicated than that in hypocrellin. This is not surprising since there are twice as many hydroxyl hydrogens that may transfer to the carbonyl oxygen. In hypericin, the time of stimulated emission, attributed to intramolecular proton transfer, is essentially independent of solvent and occurs in 6-12 ps. There is also a 1-2-ps *decay* of stimulated emission, whose origin is less certain [21,22].

That the proton transfer time in hypericin is almost negligibly dependent on solvent is of considerable interest. For example, in one of the best studied excited-state proton transfer systems, 3-hydroxy flavone [29], the transfer time is on the order of 100 fs in aprotic solvents. In a hydrogen bonding solvent such as an alcohol, however, the proton transfer time is determined by hydrogen-bonding interactions between the solvent and solute. In other words, in a hydrogen-bonding solvent, the proton transfer reaction is strongly coupled to the solvent coordinate. *The independence of solvent on the proton transfer rate in hypericin suggests that the reaction is coupled to intramolecular conformational changes.* This conclusion is very likely appropriate for hypocrellin as well. But at this point, it is unclear why the proton transfer times in ethanol and octanol are almost an order of magnitude longer than those in hypericin.

In conclusion, the superficial structural similarities between hypericin and hypocrellin are belied by their different modes of antiviral activity (for example, hypericin does not require oxygen; and hypocrellin does not acidify a solution in the presence of light) and by their different behaviors in the excited state. Further clarification of these excited-state photophysics will be of importance not only to the development of light-induced antiviral and antitumor therapies, but also to the development of molecules that provide light-induced pH drops. Most importantly, understanding these differences will prove fundamental to an understanding of excited-state intra- and intermolecular proton

transfer reactions.

ACKNOWLEDGMENTS

D. S. E was supported by a fellowship from Amoco. Part of this work was supported by NSF grant BIR9413969.

REFERENCES

1. Diwu, Z. *Photochem. Photobiol.* 1995, **61**, 529-539.

2. Durán, N.; Song, P.-S. *Photochem. Photobiol.* 1986, **43**, 677-680.

3. Kreitmair, H. *Pharmazie* 1950, **5**, 556-557.

4. Meruelo, D.; Lavie, G.; Lavie, D. *Proc. Natl. Acad. Sci. USA* 1988, **85**, 5230-5234.

5. Degar, S.; Prince, A. M.; Pascual, D.; Lavie, G.; Levin, B.; Mazur, Y.; Lavie, D.; Ehrlich, L. S.; Carter, C.; Meruelo, D. *AIDS Res. Hum. Retroviruses* 1992, **8**, 1929-1936.

6. Lenard, J.; Rabson, A.; Vanderoef, R. *Proc. Natl. Acad. Sci. USA* 1993, **90**, 158-162.

7. Meruelo, D., Degar, S., Nuria, A., Mazur, Y., Lavie, D., Levin B., and Lavie, G. (1992) in *Natural Products as Antiviral Agents* (C. K. Chu and H. G. Cutler, Eds.) pp. 91-119 (and references therein). Plenum Press, New York.

8. Kraus, G. A.; Pratt, D.; Tossberg, J.; Carpenter, S. L. *Biochem. Biophys. Res. Commun.* 1990, **172**, 149-153.

9. Carpenter, S.; Kraus, G. A. *Photochem. Photobiol.* 1991, **53**, 169-174.

10. *Treating AIDS with Worts, Science,* 1991 **254**, 522.

11. Steinbeck-Klose, A.; Wernet, P. Int. Conf. AIDS. 1993 June 6-11; 9(1):470 (abstract no. PO-B26-2012). Successful long term treatment over 40 months of HIV patients with intravenous hypericin.

12. Valentine, F. T.; Itri, V.; Kudler, N.; Georgescu, R. Int. Conf AIDS. 1991 June 16-21; 7(2):97 (abstract no. W.A.1022). Synthetic hypericin enters blood lymphocytes and monocytes in vitro and decreases culturable HIV in blood obtained from infected individuals.

13. Cooper, W.C.; James, J. Int. Conf. AIDS. 1990 June 20-23; 6(2):369 (abstract no. 2063). An observational study of the efficacy of hypericin in HIV+ subjects.

14. *AIDS Treatment News*, 1991 April 19, number 125. pp. 4-6. Hypericin update.

15. *AIDS Treatment News*, 1992 March 6, number 146. pp. 1-4. Hypericin, February 1992. The current clinical trial.

16. Fehr, M. J.; Carpenter, S. L.; Wannemuehler, Y.; Petrich, J. W. *Biochemistry* 1995, 34, 15845-15848.

17. Hudson, J. B.; Zhou, J; Chen, J.; Harris, L.; Yip, L.; Towers, G. H. N. *Photochem. Photobiol.* 1994, 60, 253-255.

18. Dahl, T. *Photochem. Photobiol.* 1993, 57, 248-254

19. Thomas, C.; Pardini, R. *Photochem. Photobiol.* 1993, 55, 831-837.

20. Gai, F.; Fehr, M. J.; Petrich, J. W. *J. Am. Chem. Soc.* 1993, 115, 3384-3385.

21. Gai, F.; Fehr, M. J.; Petrich, J. W. *J. Phys. Chem.* 1994, 98, 5784-5795.

22. Gai, F.; Fehr, M. J.; Petrich, J. W. *J. Phys. Chem.* 1994, 98, 8352-8358.

23. Fehr, M. J.; Carpenter, S. L.; Petrich, J. W. *Bioorg. Med. Chem. Lett.* 1994, 4, 1339-1344.

24. Fehr, M. J.; McCloskey, M. A.; Petrich, J. W. *J. Am. Chem. Soc.* 1995, 117, 1833-1836.

25. Carpenter, S.; Fehr, M. J.; Kraus, G. A.; Petrich, J. W. *Proc. Natl. Acad. Sci. USA* 1994, 91, 12273-12277.

26. Kraus, G. A.; Zhang, W.; Fehr, M. J.; Petrich, J. W.; Wannemuehler, Y.; Carpenter, S. *Chem. Rev.* **1996, 96**, 523-535.

27. Carrington, T. Jr.; Miller, W. H. *J. Phys. Chem.* **1986, 84**, 4364.

28. Barbara, P. F.; Walsh, P. K.; Brus, L. E. *J. Phys. Chem.* 1989, **93**, 29-34.

29. a) Brucker, G. A.; Swinney, T. C.; Kelley, D. F. *J. Phys. Chem.* 1991, **95**, 3190-3195.

b) Strandjord, A. J. G.; Barbara, P. F. *J. Phys. Chem.* 1985, **89**, 2355-2361.

c) McMorrow, D.; Kasha, M. *J. Phys. Chem.* 1984, **88**, 2235-2243. d) Brucker, G. A.; Kelley, D. F. *J. Phys. Chem.* 1987, **91**, 2856-2861. e) Schwartz, B. J.; Peteanu, L. A.; Harris, C. B. *J. Phys. Chem.* 1992, **96**, 3591-3598.

30. a) Frey, W.; Laermer, F.; Elsaesser, T. *J. Phys. Chem.* 1991, **95**, 10391-10395.

b) Laermer, F.; Elsaesser, T.; Kaiser, W. *Chem. Phys. Lett.* 1988, **148**, 119-124.

31. Ensminger, F. A.; Plassard, J.; Zwier, T. S.; Hardinger, S. *J. Chem. Phys.* 1993, **99**, 8341-8344.

32. Buchschacher, G. L. *JAMA* 1993, **269**, 2880-2886.

33. Johnston, M. I.; Hoth, D. F. *Science* 1993, **260**, 1286-1293

34. Gai, F.; Rich, R. L.; Petrich, J. W. *J. Am. Chem. Soc.* 1994, **116**, 735.

35. Diwu, Z.; Lowen, J. W. *J. Photochem. Photobiol. A:Chem.* 1992, **64**, 273-287.

36. Wei-shin, C.; Yuan-teng, C.; Xiang-yi, W.; Friedrichs, E.; Puff, H.; Breitmaier, E. *Liebigs Ann. Chem.* 1981, 1880-1885.

37. a) Etzlstorfer, C.; Falk, H.; Müller, N.; Schmitzberger, W.; Wagner, U. G. *Monatsh. Chem.* 1993, **124**, 751-761. b) Falk, H. Personal communication. c) Freeman, D.; Frolow, F.; Kapinus, E.; Lavie, D.; Lavie, G.; Meruelo, D.; Mazur, Y. *J. Chem. Soc. Chem. Commun.* 1994, 891-892.

38. Racinet, H.; Jardon, P.; Gautron, R. *J. Chim. Phys.* 1988, **85**, 971-977.

39. Diwu, Z.; Lowen, J. W. *Free Radical Biology and Medicine* 1993, **14**, 209-215.

40. Malkin, J.; Mazur, Y. *Photochem. Photobiol.* 1993, 57, 929-933.

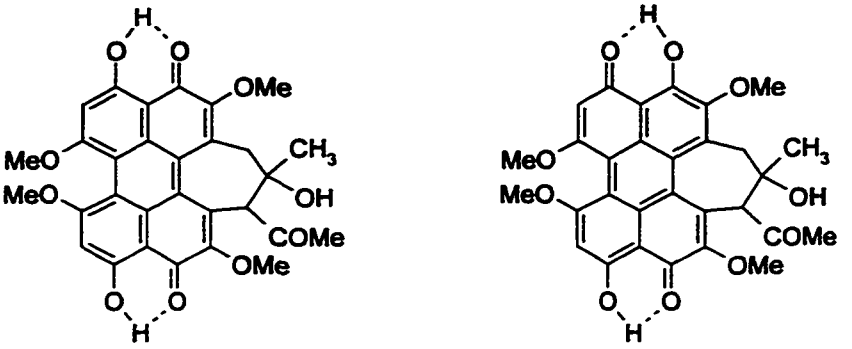

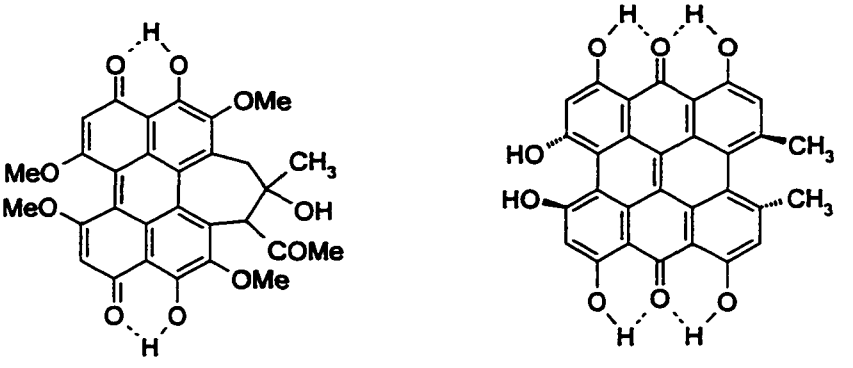

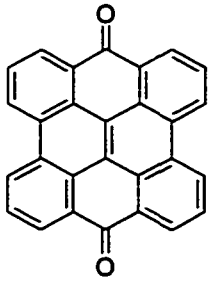

Figure 3.1 Two-dimensional structures of (a) the normal, that is untautomerized, form of hypocrellin A; (b) a partially tauotmerized form of hypocrellin; (c) the completely tautomerized form of hypocrellin A; (d) the normal form of hypericin; and (e) the hypericin analog, mesonaphthobianthrone. It is important to note that these Figures are very misleading in that hypericin and hypocrellin are not planar molecules: interactions of the substituents on the aromatic skeleton twist these molecules out of planarity [37]. This twisting is particularly acute for hypocrellin [36].

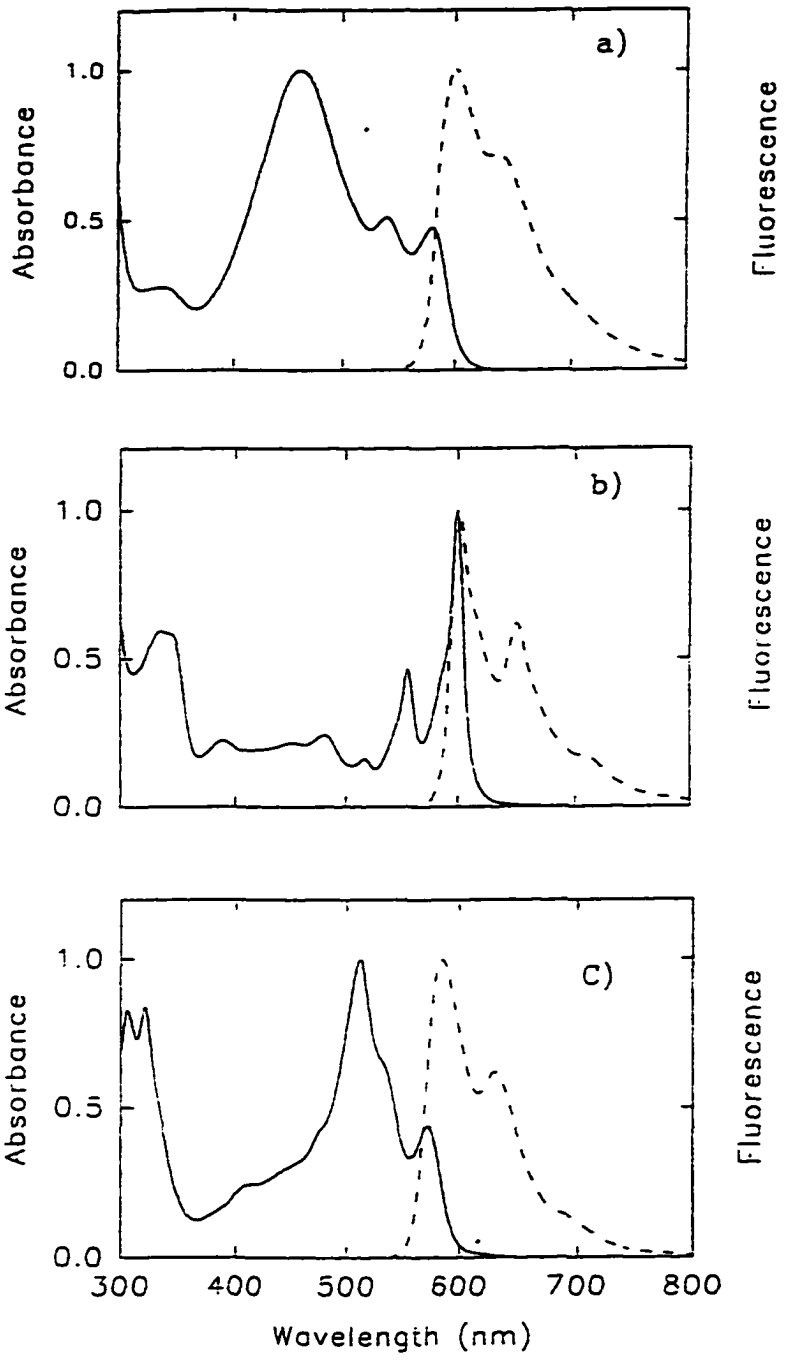

Figure 3.2 Steady state absorption (solid lines) and emission (dashed lines, $\lambda_{ex} = 588$ nm) spectra of (a) hypocrellin in ethanol; (b) hypericin in DMSO; and (c) mesonaphthobianthrone in H_2SO_4. Emission spectra are arbitrary normalized to the maximum of the visible absorption band.

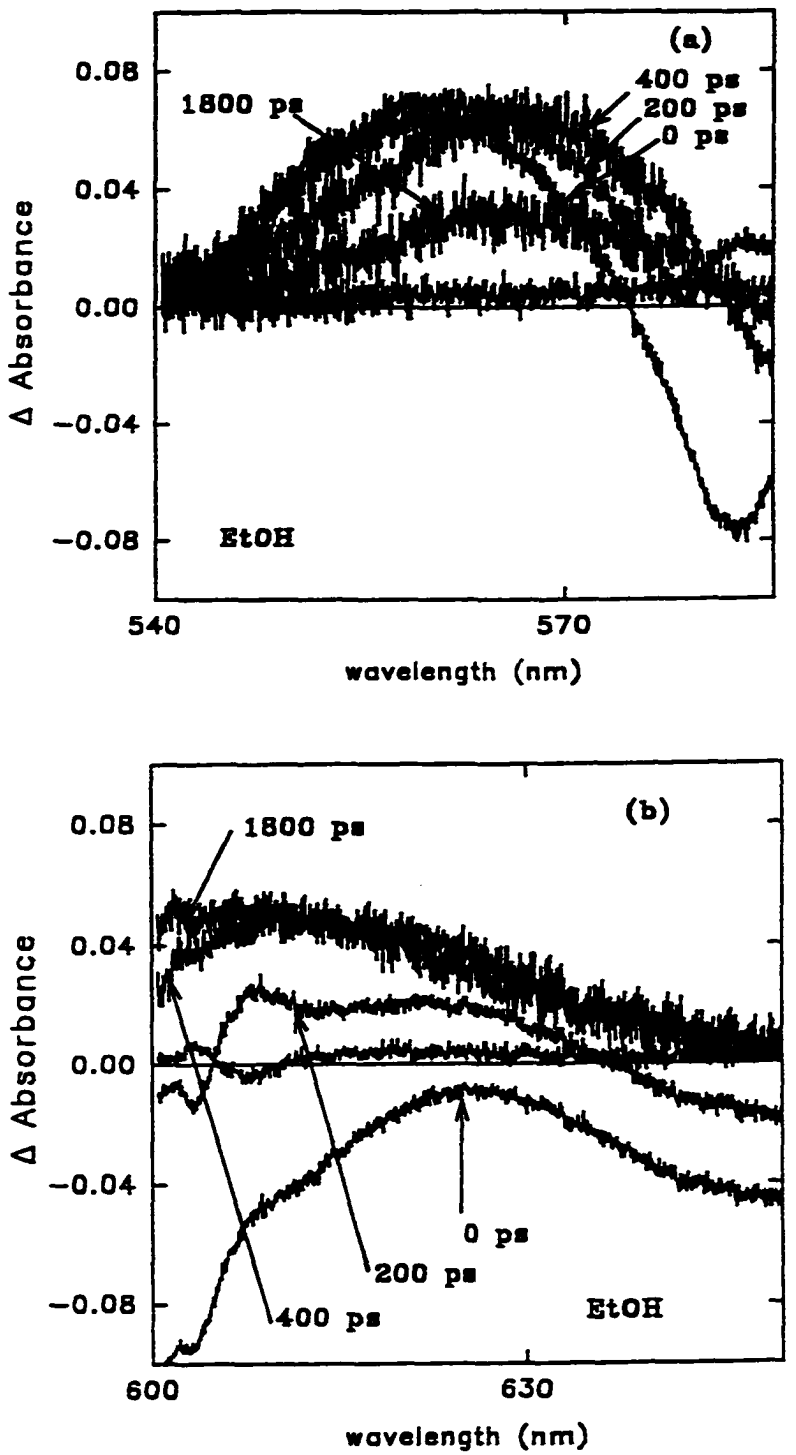

Figure 3.3 (a and b). Time-resolved spectra of hypocrellin in ethanol, λ_{pump} = 588 nm.

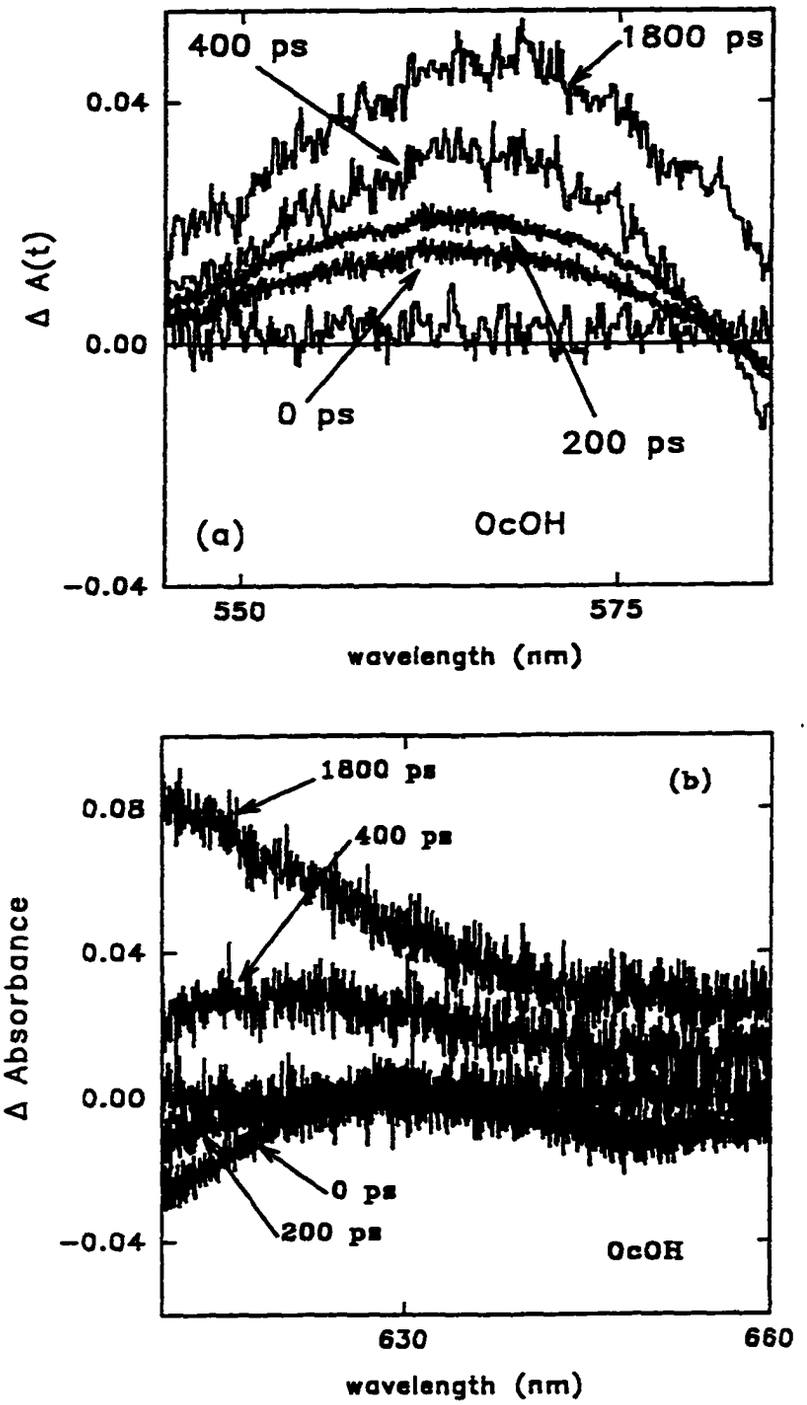

Figure 3.4 (a and b) Time-resolved spectra of hypocrellin in octanol, λ_{pump} = 588 nm. In panel (a) the data obtained at negative time delay (the flat line at zero), 400 ps, and 1800 ps have been smoothed to enhance the presentation.

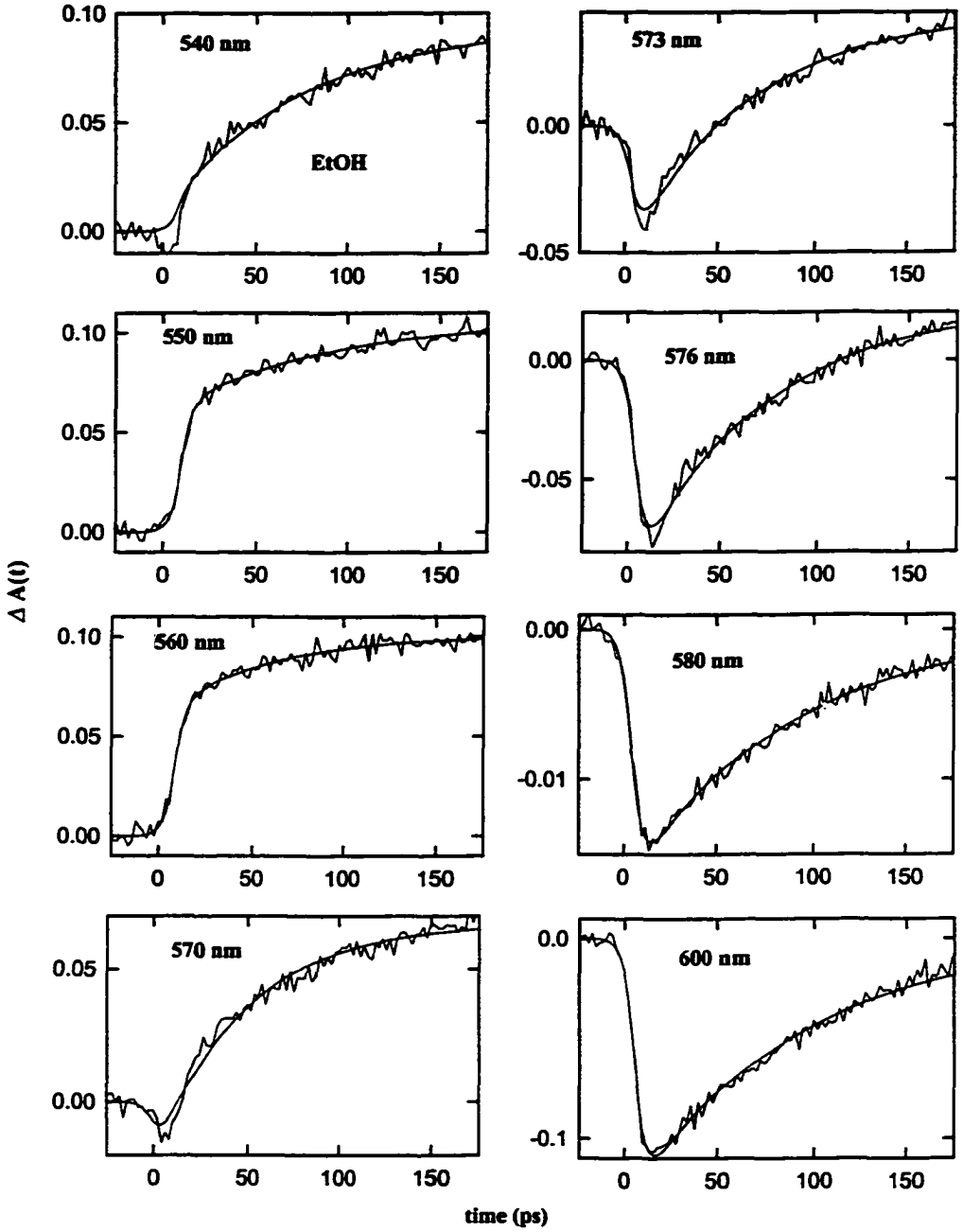

Figure 3.5 Kinetic traces of hypocrellin in ethanol at various probe wavelengths, λ_{pump} = 588 nm. The smooth lines passing through the data are the result of a global fit of the kinetic traces at all probe wavelengths.

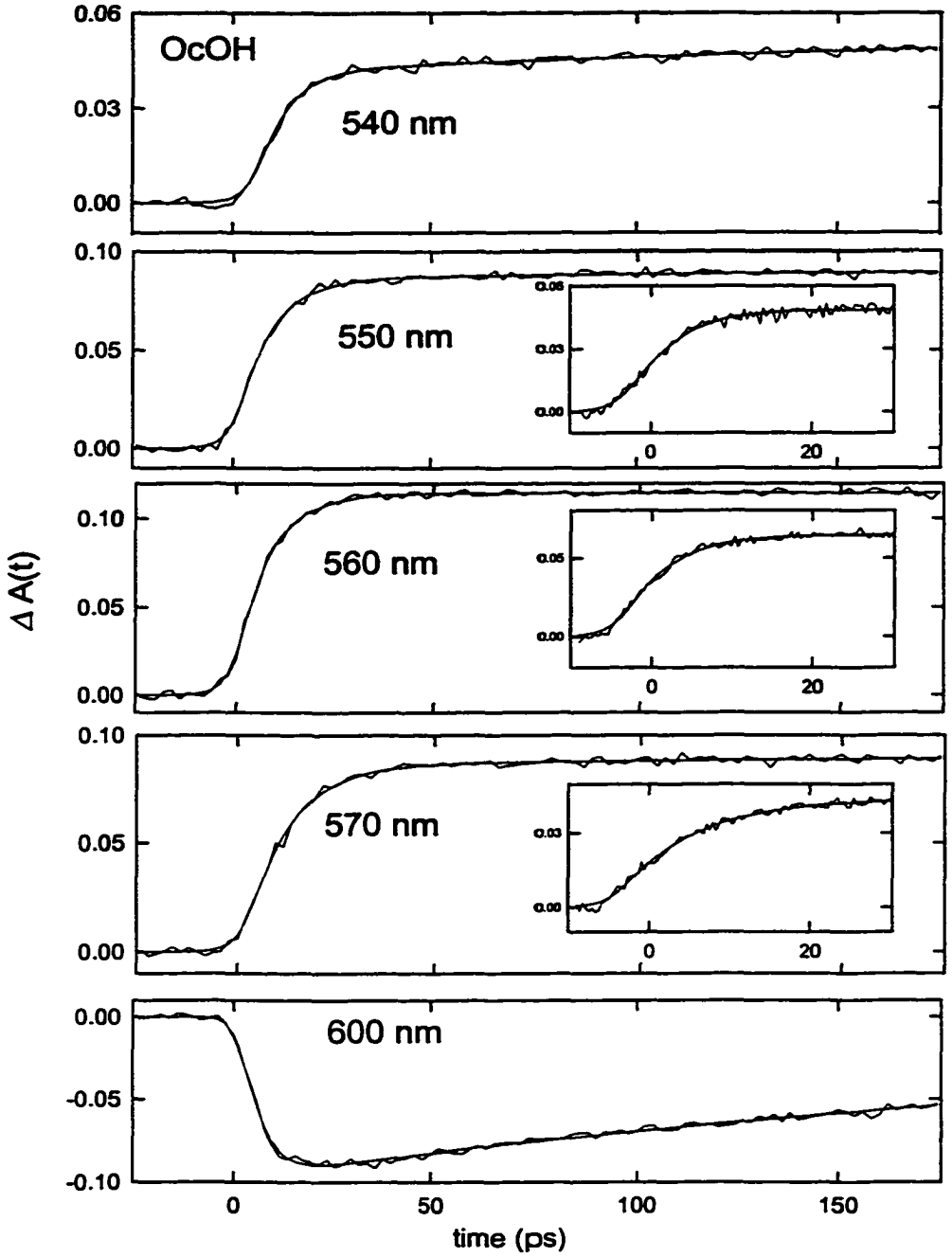

Figure 3.6 Kinetic traces of hypocrellin in octanol at various probe wavelengths, λ_{pump} = 588 nm. The smooth lines passing through the data are the result of a global fit of the kinetic traces at all probe wavelengths. Note that the traces presented as insets are on a 40-ps time scale. λ_{pump} = 588 nm. The smooth lines passing through the data are the result of a global fit of the kinetic traces at all probe wavelengths. Note that the traces presented as insets are on a 40-ps time scale.

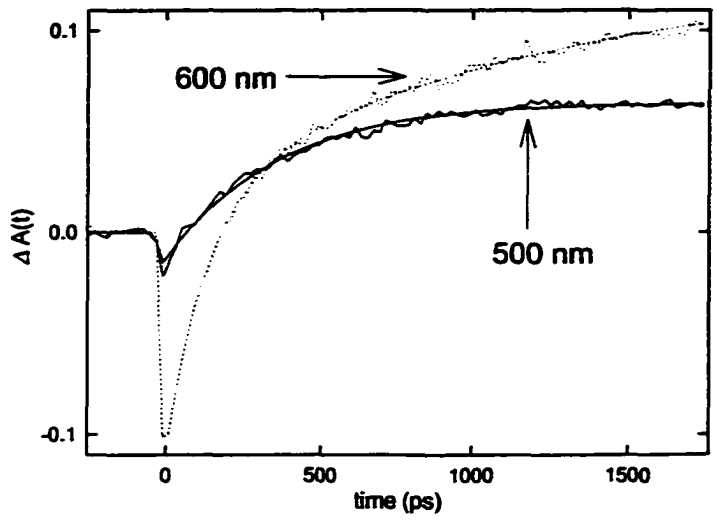

Figure 3.7 Kinetic traces on the nanosecond time scale of hypocrellin in ethanol at λ_{probe} = 500 nm and λ_{probe} = 600 nm; λ_{pump} = 588 nm.

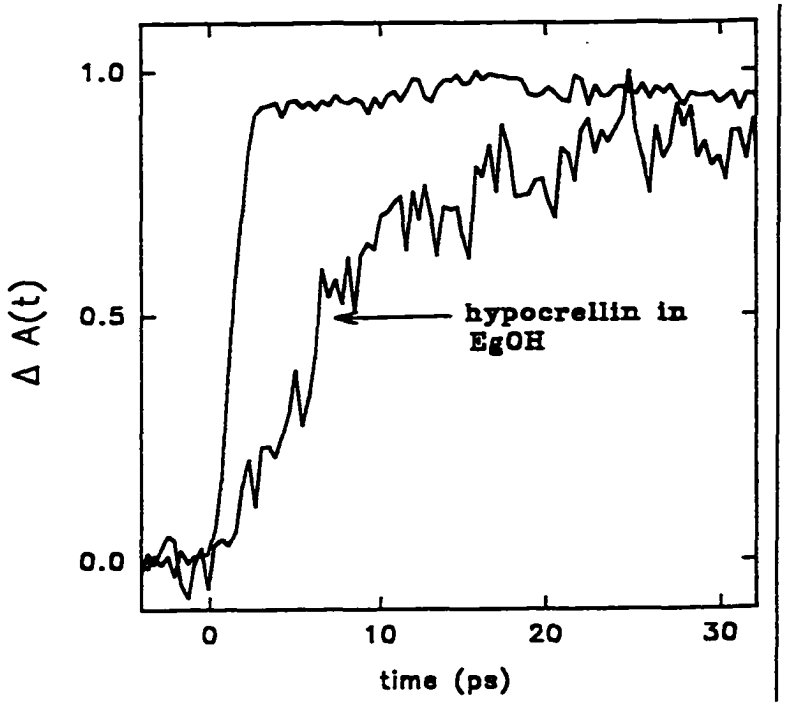

Figure 3.8 Transient absorption of hypocrellin in ethylene glycol, λ_{pump} = 588 nm. The ground-state bleach of the dye nile blue in ethanol is presented for comparison because it affords an instantaneous response. The rise time for the transient absorption of hypocrellin in ethylene glycol is ~10 ps.

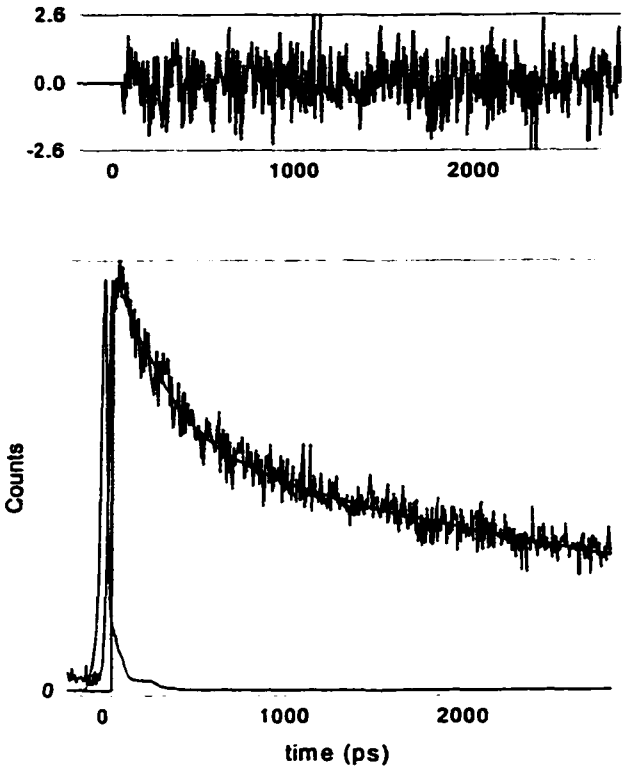

Figure 3.9 Fluorescence decay of hypocrellin in H_2SO_4. A fit to a double exponential yields $F(t) = 0.54 \exp(-t/230\ ps) + 0.46 \exp(-t/4200\ ps)$, $\chi^2 = 0.94$.

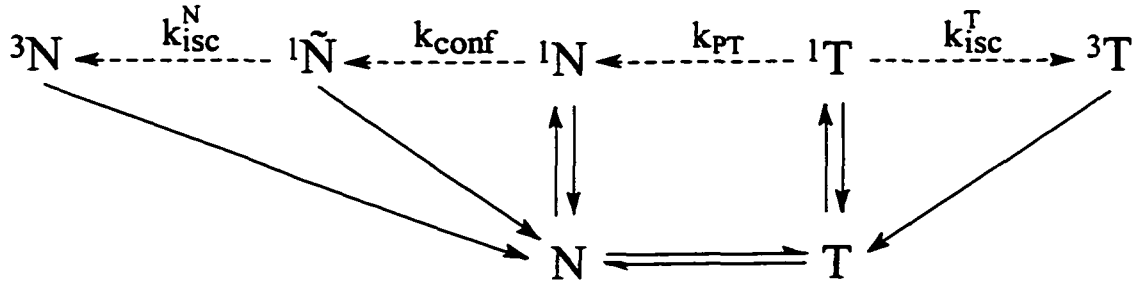

Figure 3.10 Kinetic scheme for the excited states of hypocrellin. k_{PT} is the back proton transfer rate; k_{conf} is the rate of conformational rearrangement suggested to be observed in octanol and ethylene glycol between states denoted as N and $\tilde{N}$. The intersystem crossing rates of the excited-state normal and tautomer forms are given by k^N_{isc} and k^T_{isc}, respectively

CHAPTER IV. PICOSECOND LINEAR DICHROISM AND ABSORPTION ANISOTROPY OF HYPOCRELLIN: TOWARDS A UNIFIED PICTURE OF THE PHOTOPHYSICS OF HYPERICIN AND HYPOCRELLIN

A paper published in the Journal of Physical Chemistry[1]

K. Das, A. V. Smirnov, M. D. Snyder, and J. W. Petrich[2]

ABSTRACT

The photophysics of hypocrellin are examined by means of transient absorption spectroscopy. On the shortest time scale investigated, an ~10-ps component is observed in the isotropic ("magic angle") transient absorption, $\Delta A(t)$, and in the anisotropy decay, r(t), for hypocrellin in viscous solvents such as octanol and ethylene glycol. Because the excited-state intramolecular proton transfer time of the related compound hypericin is ~10-ps, the observation of a transient of similar duration in hypocrellin is interpreted as evidence that the photophysics of hypericin and hypocrellin have common features. In particular, it is suggested that their ground- and excited-state potential energy surfaces are similar and that what distinguishes the observed kinetic behavior, which can differ

---

[2] To whom correspondence should be addressed.

significantly, is the ground-state heterogeneity, that is, the number and population of different forms of hypericin or hypocrellin, which may be tautomers, ions, or conformational isomers.

INTRODUCTION

The naturally occurring polycyclic quinones hypericin and hypocrellin (Figure 1) are of current interest because of their light-induced [1] antiviral (especially anti HIV) and antitumor activity [2-11]. In addition, hypericin has attracted attention for its antidepressant activity [12-15]. We have discussed elsewhere several aspects of the excited-state photophysics of hypocrellin and hypericin [16-25] and have proposed means of exploiting these properties [26,27]. These molecules have been the subject of several reviews [27-30].

It has been shown that the antiviral and antitumor activities of hypericin can be dependent on oxygen [9,10]. However, the mechanism of action of hypericin at the cellular level still remains unclear. Usually photosensitization processes involve molecules having a high triplet yield [31]. The triplet state of a photosensitizer, such as hypericin, may induce two different kinds of common and well known photoreactions. The first and perhaps most common is the so-called Type II, oxygen-dependent, mechanism. Singlet oxygen formation occurs via energy transfer from the triplet state of the photosensitizer to the ground triplet state of molecular oxygen. The second is the Type I radical mechanism. This complex mechanism involves the superoxide anion [32-37] and, when hypericin is the photosensitizer, perhaps the hypericinium ion.

In addition to the well known Type I and II mechanisms, alternative origins for the photoinduced biological activity of hypericin and hypocrellin have recently been proposed [38-42,71]. Comparative studies for nine perylenequinones, including hypocrellin and

hypericin, provide evidence that the quantum yield of singlet oxygen formation is not sufficient to explain the reported antiviral activities of these molecules and that other structural features of perylenequinones are involved [43]. In fact, the quantum yield of singlet oxygen from hypericin is much less than had initially been presumed. Recently, Jardon and coworkers have revised their earlier estimation of a singlet oxygen quantum yield of 0.73 [32], essentially equal to the triplet yield, to 0.35 in ethanol and less than 0.02 in water [44]. Based on this result, mechanisms involving oxygen clearly cannot explain all the activity of hypericin.

It has been our thesis from the very first that a significant nonradiative process in hypericin and its analogs is intramolecular proton (or atom) transfer [16-25]. The argument for such a process is the following. The hypericin analog lacking labile protons, *mesonaphthobianthrone* (Figure 1d), is significantly fluorescent and has optical spectra that resemble those of hypericin only when its carbonyl groups are protonated. In hypericin, the fluorescent state grows in on a time scale of several picoseconds, as measured by the rise time of stimulated emission. Therefore, the combined observations of the requirement of protonated carbonyls for strong hypericin-like fluorescence and the rise time of fluorescence in hypericin was taken as evidence for intramolecular excited-state proton transfer in hypericin.

Of special relevance to the role of labile protons for the light-induced biological activity of hypericin is the observation that hypericin acidifies its surroundings upon light absorption [39-42,71]. The role of photogenerated protons takes on significance in the context of the growing body of literature implicating pH decreases with pharmacologically important functions, such as virucidal activity (optimum pH values are important in the life cycles of many enveloped viruses) [45], antitumor activity [46,47], apoptosis (a form of cell death associated with DNA fragmentation and chromatin condensation) [48-50], and

the subcellular distribution of hexokinase [51]. In this light, current work on subcellular localization of hypericin [52] and the interaction of hypericin with DNA [53-55] and proteins [56-58] is of considerable interest.

The structural similarities of hypocrellin and hypericin, especially the hydroxyl groups *peri* to the keto groups, may initially give the impression that these two molecules exhibit very similar excited-state photophysics. This is not the case, and the photophysics of these molecules is compared and contrasted in Section A of the Discussion. Because of the different behavior manifested by the proton transfer reactions in hypericin and hypocrellin, these two molecules provide unique systems with which to clarify and to understand aspects of proton transfer reactions, which have been a subject of much experimental and theoretical study. An important goal, consequently, is to construct a *unified* and self-consistent model of the ground- and excited-state potential surfaces of hypericin and hypocrellin, with the aim of describing the proton or atom transfer in this class of polycyclic quinones. Such a model should necessarily include information on the number of ground-state species of hypocrellin and hypericin and which of them interconvert upon optical excitation. In order to address these topics, time-resolved experiments with polarized pump and probe pulses have been performed, from which anisotropy functions are constructed. If the excited-state tautomerization process is accompanied by a conformational or other change that induces a change in the transition dipole moment, this change should be detected in the polarized absorption data. Such effects are indeed observed in hypocrellin, as noted below. Measuring the time-dependent anisotropy thus permits a mapping out of the excited-state potential energy surface and a characterization of the species involved in the excited-state proton transfer.

EXPERIMENTAL

Hypocrellin A was obtained from Molecular Probes. Time-resolved linear dichroism experiments are performed with amplified dye laser pulses of ~1-3 ps duration at 30 Hz [21]. The time-resolved anisotropy of the hypocrellin transients was constructed for two solvents, ethanol and octanol, and was studied on time scales ranging from 40 ps to 2 ns (Tables 4.1 and 4.2). In these experiments the polarization of the probe was always kept constant, while the polarization of the pump (588 nm) was rotated. A photodiode was employed to integrate the pump energy in order to provide a shot-to-shot normalization of the intensities of the polarized kinetic traces.

The anisotropy was obtained as follows. All the parallel traces were globally fitted and the time constants and respective amplitudes were extracted. For the perpendicular traces, the transient at 595 nm is different from the other traces (570, 560 and 550 nm). Thus, the 595-nm trace was fit individually and the other three traces were fit globally, from which time constants and amplitudes were extracted. From those respective amplitudes and time constants deconvoluted decay curves for parallel and perpendicular polarization were constructed and finally the "magic angle" decay curves were constructed as follows:

$$\Delta A(t) = \Delta A_{\parallel}(t) + 2\Delta A_{\perp}(t)$$

The magic angle or isotropic transient absorption trace was also measured directly. This direct measurement is what is presented in Figures 3 to 7. And the anisotropy was found as usual:

$$r(t) = \frac{\Delta A_{\parallel}(t) - \Delta A_{\perp}(t)}{\Delta A_{\parallel}(t) + 2\Delta A_{\perp}(t)}$$

Because the anisotropy is discontinuous at 595 nm, only the other three probe wavelengths at 570, 560 and 550 nm could be employed in a global fitting procedure to

extract the amplitudes and the time constants. $\Delta A(t)$ and r(t) are fit to sums of two exponentials. Some data sets are presented for hypocrellin in the respective panels of Figures 3-7. In some cases (Table 4.2) the absolute magnitude of the limiting anisotropy is greater than the theoretical limit of 0.40. There is nothing contradictory in such a result since this limit corresponds to a single transition in the absence of coherence effects [59,60]. A limiting anisotropy whose absolute magnitude is in excess of 0.40 thus indicates that several different transitions are being probed simultaneously. Similar results have been obtained elsewhere [61,62].

RESULTS

Hypocrellin transients were typically investigated at four probe wavelengths: 595, 570, 560, and 550 nm. Time constants are extracted from these four wavelengths using a global fitting routine [21]. The main features of this study are the following. At 595 nm, there is *stimulated emission* for parallel pump and probe, whereas *induced absorbance* (whose signal is much weaker) is observed for perpendicular pump and probe. As a result the anisotropy is *discontinuous* (Figure 3). At the other three probe wavelengths (570, 560, 550 nm) induced absorbance is present for both parallel and perpendicular probe polarizations. However, the intensity for the perpendicular orientation is always *greater* than that of parallel, resulting in a negative anisotropy at these wavelengths. In viscous solvents (e.g., octanol) the parallel transients at 570, 560 and 550 also have a fast risetime (~7 ps) which is absent in the perpendicular traces.

DISCUSSION

A. *Intramolecular Proton Transfer*

We have provided the first detailed investigations that use both ≤ 1-ps time resolution and white-light continuum to examine and to unravel the excited-state *primary photoprocesses* of hypericin and hypocrellin and have argued that the excited-state transients we observe, coupled with data from model compounds, can be interpreted in terms of excited-state tautomerization [16-25]. The structural similarities of hypocrellin and hypericin, especially the hydroxyl groups *peri* to the keto groups, may initially give the impression that these two molecules exhibit very similar excited-state photophysics. We have made the following observations and conclusions:

1. The deshydroxy analog of hypericin, mesonaphthobianthrone (phenanthro[1,10,9,8,*o*,*p*,*q*,*r*,*a*]perylene-7-14-dione, (Figure 1d), is nonfluorescent except in strong acids [eg. sulfuric acid or triflic acid (CF_3SO_3H)] where it produces a fluorescence spectrum that has nearly the same shape as that of hypericin in DMSO (Figure 2). *These results demonstrate the importance of a protonated carbonyl group for producing hypericin-like fluorescence* [17,24].
2. The hypericin emission spectrum grows in on a 6-12-ps time scale in all solvents except in sulfuric acid where it is instantaneous. Based on the results for mesonaphthobianthrone (see above), *the rise time for the appearance of the hypericin emission is taken as evidence for an excited-state proton (atom) transfer* [17]. Confirming this interpretation are the fluorescence upconversion measurements [24] of hypericin and methylated hypericin analogs, which are incapable of executing intramolecular excited-state proton transfer reactions.
3. The transient absorbance [19,20] and upconversion [24] kinetics of hypericin differ with excitation wavelength and probe wavelength, respectively. These results are

strongly suggestive of ground-state heterogeneity. Also, the fluorescence properties of hypocrellin in sulfuric acid and the X-ray structure of hypocrellin suggest that it exists in the tautomerized form in the ground state (Figure 1g) [21-23,65].

4. The proton transfer rates of hypocrellin and hypericin differ almost by an order of magnitude. The X-ray and fluorescence data (above) consequently lead us to propose that hypocrellin exists at least partially in a tautomeric form that is similar to that which hypericin would assume in the ground state (Figure 8), if it were thermodynamically feasible. Given this assumption, the 50-230-ps transients in hypocrellin are interpreted in terms of "back transfer" reactions [64] with respect to the corresponding hypericin reaction.

5. The proton transfer reaction in hypericin is not dependent on viscosity and depends only very weakly on solvent [18]. This suggests that intramolecular vibrations control the proton transfer reaction in hypericin. However for hypocrellin the reaction is very strongly dependent on viscosity and polarity [21,22].

6. No deuterium isotope effect is observed for hypericin [17]; but a deuterium isotope effect of 1.4 is observed for hypocrellin [23]. *This isotope effect unambiguously identifies the excited-state process as a proton transfer event.*

7. For hypocrellin in viscous solvents such as octanol and ethylene glycol, a transient of ~10-ps duration is also detected [21]. *This is a crucial and unifying result for understanding the photophysics of these systems.*

8. The fluorescence lifetimes of hypericin and hypocrellin, measured with ~50 ps time resolution, are independent of excitation wavelength: identical results are obtained exciting at 300 or 570 nm [25]. Assuming that the ground-states of these species are heterogeneous, as noted above, this result suggests that the fluorescent species

(detected via methods with time resolution no better than 100 ps) for both hypocrellin and hypericin is an intermediate between (two) tautomeric or isomeric species.

9. The absorption transients of hypocrellin exhibit a strong polarization dependence (Figures 3 and 6) at a probe wavelength of 595 nm. While the traces obtained using the pump and probe polarized parallel to each other or at 54.7° (the "magic angle"), $\Delta A_{\parallel}(t)$ and $\Delta A(t)$, are essentially superimposable, the trace obtained using perpendicularly polarized pump and probe pulses, $\Delta A_{\perp}(t)$ is opposite to that of the parallel and magic angle traces at 595 nm. This result indicates the simultaneous probing of two species whose transition dipole moments are at large angles to each other.

Based on these results and conclusions, we are constructing a unified picture of the excited state proton transfer phenomena in these molecules.

B. Towards a Unified Picture of the Hypericin and Hypocrellin Photophysics

Structurally hypericin and hypocrellin are very similar. They both possess extended aromatic skeletons whose most important functional groups are the hydroxy and keto groups *peri* to each other. In this regard, the most significant structural difference between them is that hypocrellin possesses two fewer *peri* hydroxyl groups. (Another significant difference is that hypocrellin has a seven-membered ring in the "bay area.") The current picture that we have formed of the excited-state dynamics of hypericin and hypocrellin is that the different photophysical behavior that we have enumerated above of these two structurally very similar molecules arises because we are probing different regions of *very similar potential energy surfaces*. We suggest that at least one of the ground-state species excited in the hypocrellin experiments is very similar to the ground-state tautomer of

hypericin (Figure 1b), which we propose is thermodynamically inaccessible. These ideas are summarized schematically in Figure 8. A crucial result in forming this hypothesis is the observation that in viscous solvents such as octanol or ethylene glycol we resolve a time constant in the hypocrellin photophysics that is comparable to that observed in hypericin. *This ~10-ps component in hypocrellin unifies our picture of the photophysics of hypericin and hypocrellin if we can interpret it as an excited-state proton transfer arising from another tautomeric species and if we can relate it to the corresponding process in hypericin.*

The absence of a deuterium isotope effect on the excited state proton transfer in hypericin and the presence of a deuterium isotope effect on the excited-state proton transfer in hypocrellin can both be qualitatively understood in terms of a process that is adiabatic in the proton coordinate, in the sense of the theory developed by Borgis, Hynes, and coworkers [66-69]. We have considered the excited-state potential energy surfaces of hypericin and hypocrellin in terms of this theory [23,25].

The oxygen-oxygen distance between which the proton or hydrogen atom is transferred strongly modulates the magnitude of the matrix element that couples the reactant and product states and thus determines the size of the barrier separating them. When the O-O distance is < 2.6 Å, the *adiabatic limit* is obtained [68,69]. Here, because the vibrational energy levels of the proton stretch mode lie *above* a small barrier in the proton coordinate separating the reactant and product species, an isotope effect will not be observed as a result of proton transfer. We have argued that hypericin falls into the adiabatic limit [17,23] because its relevant oxygen-oxygen distance is ~2.5 Å [70]. In hypocrellin, this distance is comparable [65].

Staib et al. [69], however, suggest the intriguing possibility that deuterium substitution may lower the ground vibrational energy below the top of the barrier in the

proton coordinate. Such a lowering of the ground state energy level would induce an isotope effect because now the proton could tunnel through the barrier or effect an activated crossing of it. We propose that the isotope effect observed in hypocrellin has its origins in such an explanation. That the isotope effect is relatively small suggests that the vibrational ground state is not significantly lowered below the barrier and that the proton transfer is an activated process. Temperature studies will be useful to confirm this hypothesis.

C. Simulating the Excited-State Kinetics

Our picture of the excited-state kinetics of hypocrellin, and their relation to hypericin, has evolved significantly since our early work on hypocrellin [21]. Here we present the simulations for the excited state dynamics of hypocrellin A based upon the pump-probe transient absorbance data presented above. The unified model of the excited state photophysics for hypericin and hypocrellin is based upon the experimental observations cited above in Section A.

Based on the above results and conclusions, the simplest approach would be to assume that in the ground state there are two tautomers (N and T) in equilibrium. We also assume that the triplets and the excited singlets of the above mentioned tautomers were the only species responsible for the excited state photophysics:

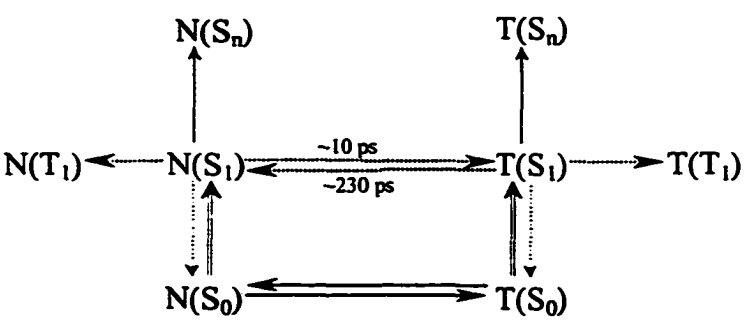

At best this model is capable of providing one rapidly rising or decaying component and one slowly decaying component (to the triplet or the ground state). Solvent relaxation processes can be viewed as negligible here since no Stokes shift was observed for the hypocrellin analog, hypericin, in fluorescence upconversion measurements with 100-fs time resolution [24]. The above model is not, therefore, consistent with our observation of at least three different transient components for hypocrellin on time scales from 40 to 2000 ps.

Consequently, it is necessary to introduce at least one more species into the kinetic scheme. In this new model the main feature is the intermediate tautomer (or conformational isomer) $I(S_1)$ that is produced from both $N(S_1)$ and $T(S_1)$.

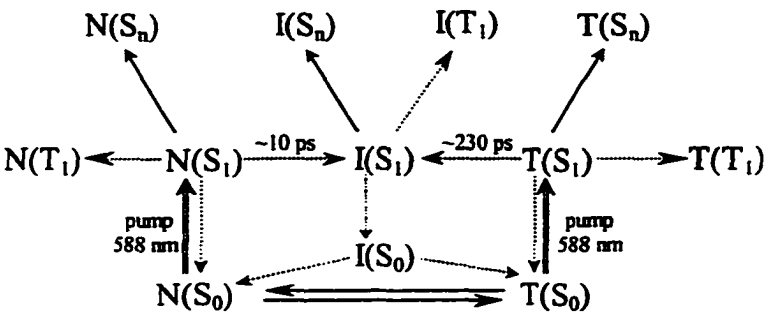

Other alternatives for the excited state kinetic scheme presented above include:

$$N(S_1) \xrightarrow{\sim 10\ ps} T(S_1) \xrightarrow{230\ ps} I(S_1)$$

$$N(S_1) \xrightarrow{\sim 10\ ps} I(S_1) \xrightarrow{230\ ps} T(S_1)$$

$$T(S_1) \xleftarrow{230\ ps} N(S_1) \xrightarrow{\sim 10\ ps} I(S_1)$$

These alternative schemes are readily eliminated if we assume that $N(S_1)$ and $T(S_1)$ have similar absorption and emission spectra, and if we interpret the experimental kinetic

traces as arising from an intermediate $I(S_1)$. If this is the case, no contribution to the 10- and/or 230-ps components should be observed when $N(S_1)$ and $T(S_1)$ interconvert into each other directly, or indirectly through $I(S_1)$. For example, in the first and third alternatives, if $N(S_1)$ decays into $T(S_1)$, equivalence of the excited-state spectra will render the transition undetectable. The second alternative is merely equivalent to an excited-state equilibrium of $N(S_1)$ with $I(S_1)$.

To evaluate the model, we performed computer simulations in an attempt to reproduce the main features of the data obtained for hypocrellin in ethylene glycol. First we solved the system of the first order ordinary differential equations as dictated by our kinetic scheme. Then we used the resulting time-dependent populations of the species involved to construct parallel and perpendicular transient absorbance traces. This required the use of different values of the extinction coefficients (for absorbance and stimulated emission) for different probe wavelengths. In order to allow for possibility of negative initial absorbance anisotropy for hypocrellin one has to assign in the first approximation orthogonality of transition dipole moments from the ground to the first excited and from the first excited to the second excited states. This can be also viewed as a consequence of the nearly C_{2v} symmetry of hypocrellin. In our model, each of the excited-state singlets is characterized by two orthogonal extinction coefficients, $\varepsilon_{||}$ and $\varepsilon_{\perp}$. More specifically, when probing at 595 nm, the parallel component ($\varepsilon_{||}$) is made negative to account for the dominating contribution of stimulated emission. On the other hand, the perpendicular component ($\varepsilon_{\perp}$) is made positive to account for the excited-state absorption that was present in all the data collected for perpendicular probe polarizations. It is assumed that all triplet states have very similar absorption spectra and that they do not contribute to the stimulated emission.

Depolarization owing to rotational diffusion of hypocrellin was taken into account

(τ_R~100-800 ps, depending on the solvent). Other mechanisms of depolarization were also taken into account: namely, conversion of one tautomer to another or intersystem crossing to the triplet state. In terms of our model this leads to the conclusion that the transition dipole for $I(S_0) \leftrightarrow I(S_1)$ is in fact at some angle relative to that for $N(S_0) \leftrightarrow N(S_1)$ and $T(S_0) \leftrightarrow T(S_1)$.

In order to model the rotational diffusion, we assumed hypocrellin to be a spherical rotor and used the general formalism developed by Chuang and Eisenthal [72] for an asymmetric rotor for fluorescence depolarization, which we extended in our case to the pump/probe experiments discussed here. For each species the corresponding contribution to the signal for the appropriate polarization is given by:

$$\Delta A_{i,\parallel}(t) = P_{i,\parallel}(t)\left(\tfrac{1}{9} + \tfrac{2}{45}(3\cos^2\theta_{i,\parallel} - 1)\cdot e^{-\frac{t}{\tau_r}}\right) + P_{i,\perp}(t)\left(\tfrac{1}{9} + \tfrac{2}{45}(3\cos^2\theta_{i,\perp} - 1)\cdot e^{-\frac{t}{\tau_r}}\right)$$

$$\Delta A_{i,\perp}(t) = P_{i,\parallel}(t)\left(\tfrac{1}{9} - \tfrac{1}{45}(3\cos^2\theta_{i,\parallel} - 1)\cdot e^{-\frac{t}{\tau_r}}\right) + P_{i,\perp}(t)\left(\tfrac{1}{9} - \tfrac{1}{45}(3\cos^2\theta_{i,\perp} - 1)\cdot e^{-\frac{t}{\tau_r}}\right)$$

$$P_{i,\parallel}(t) = \varepsilon_{i,\parallel} P_i(t) \quad P_{i,\perp}(t) = \varepsilon_{i,\perp} P_i(t)$$

where $P_i(t)$ is the probability for the species with transition dipoles oriented at angles $\theta_{i,\parallel}$ and $\theta_{i,\perp}$ relative to the ground-state absorption to survive by the time t.

In a program written for Maple V, we simulated both perpendicular and parallel transient absorption traces, from which the anisotropy decay was constructed. No convolution procedure was necessary for our purposes, given the time scale of the simulations. Semiquantitative values for the $\varepsilon_{||}$ and $\varepsilon_{\perp}$ are obtained by trial and error method. Time-dependent plots of intermediate populations are used as guidelines for this multiparametric search. Separate simulations with globally fixed temporal and orientational parameters for the transition dipoles were performed for each probing wavelength until a reasonable agreement with experimental data was achieved. *Figure 9*

describes the simulation results, the parameters are listed in Table 4.3 . It should be noted that though we were able to reproduce qualitatively the anisotropy and stimulated emission features, the absorbance features do not agree quantitatively with the experimental observations.

To summarize, the model proposed to rationalize hypocrellin transients absorbance traces proves to be self-consistent by providing reasonable parameters for the $\varepsilon_{\parallel}$ and $\varepsilon_{\perp}$. Although the real picture might be much more complicated from our point of view we found the simplest possible semiquantitative description of this remarkable photophysical system.

We stress that we have made no effort to *fit* the experimental kinetics, owing to the huge number of variable parameters, which we have noted above. We also note that the scheme provided is neither complete nor unique. It is our goal merely to reproduce qualitatively the salient features; and, indeed, the scheme presented is *consistent* with our emerging picture of the hypericin and hypocrellin photophysics.

CONCLUDING REMARKS

Over the past few years our efforts have been directed towards demonstrating that a fundamental *primary photoprocess* in hypericin and its analogs that possess hydroxyl groups *peri* to keto groups is excited state proton (or atom) transfer. This work addresses the excited-state proton transfer of hypericin and hypocrellin and attempts to incorporate their different behavior into a coherent picture. The link between the photophysics of hypericin and hypocrellin is established by the observation that under certain conditions a hypericin-like transient is observed in hypocrellin. We have proposed kinetic schemes and ground- and excited-state potential surfaces for these systems that are consistent with the experimental data.

We note that the excited-state proton transfer reaction observed in our experiments (ranging from 10-200 ps) is not detectable in steady-state fluorescence experiments or even in most time-correlated single-photon counting experiments. Consequently, it must be borne in mind that such experiments (e.g., fluorescence titrations [63,73-75]) can only yield information on the species that are formed as a result of these 10-200 ps proton transfer processes, that is, the long-lived nanosecond-duration fluorescent species that are detected in the steady-state measurements. While steady-state fluorescence titrations cannot report on the picosecond proton transfer events, they have been useful in demonstrating the acidity of the hydroxyls in the "bay region" of hypericin [63,73,74].

ACKNOWLEDGMENT

Mr. Tak Wee Kee provided technical assistance. We thank Dr. S. Savikhin for helpful discussions. This work was supported by NSF grant CHE-9613962 to J. W. P.

REFERENCES

1. Carpenter, S.; Kraus, G. A.; *Photochem. Photobiol* 1991, *53*:169-174.

2. Meruelo, D.; Lavie, G.; Lavie, D.; *Proc. Natl. Acad. Sci. USA.* 1988, *85*, 5230-5234.

3. Lavie, G.; Valentine, F.; Levin, B.; Mazur, Y.; Gallo, G.; Lavie, D.; Weiner, D.; Meruelo, D.; *Proc. Natl. Acad. Sci. USA*, 1989, *86*, 5963-5967.

4. Hudson, J. B.; Lopez-Bazzocchi, I.; Towers, G. H. N.; *Antiviral Research*, 1991, *15*, 101-112. b) Hudson, J. B.; Zhou, J.; Chen, J.; Harris, L.; Yip, L.; Towers, G. H. N.; *Photochem. Photobiol.* 1994, *60*, 253-255.

5. Lopez-Bazzocchi, I.; Hudson, J. B.; Towers, G. H. N; *Photochem. Photobiol.* 1991, *54*, 95-98.

6. Degar, S.; Prince, A. M.; Pascaul, D.; Lavie, G.; Levin, B.; Mazur, Y.; Lavie, D.; Ehrlich, L. S.; Carter, C.; Meruelo, D.; *AIDS Res. Hum. Retroviruses* **1992**, *8*, 1929-1936.

7. Meruelo, D.; Degar, S.; Amari, N.; Mazur, Y.; Lavie, D.; Levin, B.; Lavie, G. in Natural Products as Antiviral Agents (Chu, C. K. & Cutler, H. G., eds.), 1992, pp. 91-119, Plenum Press, New York.

8. Treating AIDS with Worts. *Science*, **1991**, *254*, 522.

9. Thomas, C.; Pardini, R. S.; *Photochem. Photobiol.* **1993**, *55*, 831-837.

10. Thomas, C.; MacGill, R. S.; Miller, G. C.; Pardini, R. S.; *Photochem. Photobiol.* **1992**, *55*, 47-53.

11. Lenard, J.; Rabson, A.; Vanderoef, R.; *Proc. Natl. Acad. Sci. USA* **1993**, *90*, 158-162.

12. Kreitmair, H.; *Pharmazie* **1950**, *5*, 556-557.

13. Linde, K.; Ramirez, G.; Mulrow, C. D.; Pauls, A.; Weidenhammer, W.; Melchart, D.; *Br. Med. J.* **1996**, *313*, 253-257.

14. Suzuki, O.; Katsumata, Y.; Oya, M.; Bladt, S.; Wagner, H.; *Planta Medica* **1984**, *50*, 272-274.

15. Anker, L.; Gopalakrishna, R.; Jones, K. D.; Law, R. E.; Couldwell, W. T.; *Drugs of the Future.* **1995**, *20*, 511-517.

16. Gai, F.; Fehr, M. J.; Petrich, J. W.; *J. Am. Chem. Soc.* **1993**, *115*, 3384-3385.

17. Gai, F.; Fehr, M. J.; Petrich, J. W.; *J. Phys. Chem.* **1994**, *98*, 5784-5795.

18. Gai, F.; Fehr, M. J.; Petrich, J. W.; *J. Phys. Chem.* **1994**, *98*, 8352-8358.

19. English, D. S.; Zhang, W.; Kraus, G. A.; Petrich, J. W.; *J. Am. Chem. Soc.* **1997**, *119*, 2980-2986.

20. English, D. S.; Das, K.; Zenner, J. M.; Zhang, W.; Kraus, G. A.; Larock, R. C.; Petrich, J. W.; *J. Phys. Chem.* **1997**, *101A*, 3235-3240.

21. Das, K.; English, D. S.; Fehr, M. J.; Smirnov, A. V.; Petrich, J. W.; *J. Phys. Chem.* **1996**, *100*, 18275-18281.

22. Das, K.; English, D. S.; Petrich, J. W.; *J. Am. Chem. Soc.* **1997**, *119*, 2763-2764.

23. Das, K.; English, D. S.; Petrich, J. W.; *J. Phys. Chem.* **1997**, *101A*, 3241-3245.

24. English, K. Das, K. D. Ashby, J. Park, J. W. Petrich, and E. W. Castner, Jr.; *J. Am. Chem. Soc.* **1997**, *119*, 11585-11590.

25. Das, K.; Dertz, E.; Paterson, J.; Zhang, W.; Kraus, G. A.; Petrich, J. W.; *J. Phys. Chem. B* **1998**, *102*, 1479-1484.

26. Carpenter, S.; Fehr, M. J.; Kraus, G. A.; Petrich, J. W.; *Proc. Natl. Acad. Sci. USA* **1994**, *91*, 12273-12277.

27. Kraus, G. A.; Zhang, W.; Fehr, M. J.; Petrich, J. W.; Wannemuehler, Y.; Carpenter, S.; *Chem. Rev.* **1996**, *96*, 523-535.

28. Duran, N.; Song, P.-S. *Photochem. Photobiol.* **1986**, *43*, 677-680.

29. Diwu, Z. *Photochem. Photobiol.* **1995**, *61*, 529-539.

30. Lown, J. W. *Can. J. Chem.* **1997**, *75*, 99-119.

31. Foote, C. S. in *Light-activated pesticides* (Heitz, J. R.; Downum, K. R., eds.), 1987, pp. 22, American Chemical Society, Washington, D.C.

32. Racinet, H.; Jardon, P.; Gautron, R.; *J. Chim. Phys.* **1988**, *85*, 971-977.

33. Hadjur, C., Richard, M. J., Parat, M. O., Favier, A., Jardon, P.; *J. Photochem. Photobiol. B Chem.* **1995**, *27*, 139-146.

34. Malkin, J.; Mazur, Y.; *Photochem. Photobiol.* **1993**, *57*, 929-933.

35. Weiner, L.; Mazur, Y; *J. Chem. Soc. Perkin Trans.* **1992**, 2, 1439-1442.

36. Diwu, Z.; Lowen, J. W.; *Free Rad. Biol. Med.* **1993**, *14*, 209-215.

37. Weiner, L.; Mazur, Y.; J. Chem. Soc. Perkin Trans. **1992**,

38. Fehr, M. J.; Carpenter, S. L.; Petrich, J. W.; *Biochem. Biophys. Res. Commun.* **1994**, *4*, 1339.

39. Fehr, M. J.; McCloskey, M. C.; Petrich, J. W.; *J. Am. Chem. Soc.* **1995**, *117*, 1833-1836.

40. Fehr, M. J.; Carpenter, S. L.; Wannemuehler, Y.; Petrich, J. W.; *Biochemistry*, **1995**, *34*, 15845-15848.

41. Sureau, F.; Miskovsky, P.; Chinsky, L.; Turpin, P. Y.; *J. Am. Chem. Soc.* **1996**, *118*, 9484-9487.

42. Chaloupka, R.; Sureau, F.; Kocisova, E.; Petrich, J. W.; *Biophys. J.*, submitted.

43. Hudson, J. B.; Imperial, V.; Haugland, R. P.; Diwu, Z.; *Photochem. Photobiol.* **1997**, *65*, 352-354.

44. Darmanyan, A. P.; Burel, L.; Eloy, D.; Jardon, P.; *J. Chim. Phys.* **1994**, *91*, 1774-1785.

45. Pinto, L. H.; Holsinger, L. J.; Lamb, R. A.; *Cell* **1992**, *69*, 517-528.

46. Newell, K. J.; Tannock, I. F.; *Cancer Res.* **1989**, *49*, 4447-4482.

47. Newell, K. J.; Wood, P.; Stratford, I.; Tannock, I.; *Br. J. Cancer* **1992**, *66*, 311-317.

48. Barry, M. A.; Reynold, J. E.; Eastman, A.; *Cancer Res.* **1993**, *53*, 2349-2357.

49. Li, J.; Eastman, A.; *J. Biol. Chem.* **1995**, *270*, 3203-3211.

50. Gottlieb, R. A.; Nordberg, J.; Skowronski, E.; Babior, B. M.; *Proc. Natl. Acad. Sci. USA* **1996**, *93*, 654-658.

51. Miccoli, L.; Oudard, S.; Sureau, F.; Poirson, F.; Dutrillaux, B.; Poupon, M. F.; *Biochem. J.* **1996**, *313*, 957-962.

52. Mikovsky, P.; Sureau, F.; Chinsky, L.; Turpin, P.-Y.; *Photochem. Photobiol.* **1995**, *62*, 546-549.

53. Sanchez-Cortes, S.; Miskovsky, P.; Jancura, D.; Bertoluzza, A.; *J. Phys. Chem.* **1996**, *100*, 1938-1944.

54. Sureau, F.; Moreau, F.; Millot, J.-M.; Manfait, M.; Allard, B.; Aubard, J.; Schwaller, M.-A.; *Biophys. J.* **1993**, *65*, 1767-1774.

55. Miskovsky, P.; Chinsky, L.; Wheeler, G. V.; Turpin, P.-Y.; *J. Biomol. Str. Dynamics* **1995**, *13*, 547-552.

56. Senthil, V., Longworth, J. W., Ghiron, C. A., Grossweiner, L. I.; *Biochim. Biophys. Acta*, **1992**, *1115*, 192-200.

57. Falk, H., Meyer, J.; *Monatsh. Chem.* **1994**, *125*, 753-762.

58. Miskovsky, P.; Sanchez-Cortes, S.; Jancura, D.; Kocisova, E.; Chinsky, L.; *Mol. Pharmacol.*, submitted.

59. Knox, R. S., Gulen, D.; *Photochem. Photobiol.* **1993**, *57*, 40-43.

60. Wynne, K., Hochstrasser, R. M., *Chem. Phys.*; **1993**, *171*, 179-188.

61. Song, Q., Harms, G. S., Wan, C., Johnson, C. K.; *Biochemistry*, **1994**, *33*, 14026-14033.

62. Savikhin, S., Tao, N., Song, P.-S., Struve, W. S.; *J. Phys. Chem.* **1993**, *97*, 12379-12386.

63. Freeman, D.; Frolow, F.; Kapinus, E.; Lavie, D.; Lavie, G.; Meruelo, D.; Mazur, Y.; *J. Chem. Soc. Commun.* **1994**, 891.

64. The designation of "back transfer" is based upon the assumption in the literature that the most stable form of hypocrellin is that illustrated in Figure 1g. The published X-ray structure indicates C(12)-O(12) and C(7)-O(7) bond lengths that are within experimental error greater than those of their C(1)-O(1) and C(6)-O(6) neighbors [65]. The coordinates available from the Cambridge Crystallographic Data Bank suggest that all four bond lengths are comparable. The former data set is consistent with Figure 1h, enol bonds being longer than keto bonds. The latter data set suggests a mixture of both the normal and the tautomer forms in the ground state.

65. Wei-shin, C.; Yuan-teng, C.; Xiang-yi, W.; Friedrichs, E.; Puff, H.; Breitmaier, E. *Liebigs Ann. Chem.* **1981**, 1880-1885.

66. Borgis, D.; Hynes, J. T. In *The Enzyme Catalysis Process*; Cooper, A.; Houben, J. L.; Chien, L. C., Eds.; NATO ASI Series, Plenum Press: NY, 1989; Vol. 178, p 293.

67. Borgis, D.; Hynes, J. T. *J. Chem. Phys.* 1991, *94*, 3619-3628.

68. Azzouz, H.; Borgis, D. *J. Chem. Phys.* 1993, *98*, 7361-7374.

69. Staib, A.; Borgis, D.; Hynes, J. T. *J. Phys. Chem.* 1995, *102*, 2487-2505.

70. Etzlstorfer, C.; Falk, H.; Müller, N.; Schmitzberger, W.; Wagner, U. G. *Monatsh. Chem.* 1993, *124*, 751-761. b) Falk, H., personal communication.

71. We had previously reported that hypericin does not require oxygen for its antiviral activity [24,27,38,40]. This conclusion was based on a previous inability to estimate accurately low oxygen levels in our virus samples. We consequently now believe that while antiviral pathways independent of oxygen may exist, the role of oxygen in this activity is significant. The ability of photogenerated protons to enhance the activity of activated oxygen species [42] is still considered to be of importance (J. Park, D. S. English, Y. Wannemuehler, S. Carpenter, and J. W. Petrich, *Photochem. Photobiol.* Submitted.)

72. Chuang, M. C.; Eisenthal, K. B.; *J. Chem. Phys.*, 1972, *57*, 5094-5097.

73. Eloy, D., Pellec, A. Le., Jardon, P.; *J. Chim. Phys.*, 1996, *93*, 442-457.

74. Altmann, R.; Falk, H. *Monatshefte für Chemie* 1997, *128*, 571-583.

75. Yamazaki, T.; Ohta, N.; Yamazaki, I.; Song, P.-S. *J. Phys. Chem.*, 1993, *97*, 7870-7875.

76. Zhang, M.-H.; Weng, M.; Chen, S.; Xia, W.-L.; Jiang, L.-J.; Chen, D.-W. *J. Photochem. Photobiol. A: Chem.* 1996, *96*, 57.

77. Redepenning, J.; Tao, N.; *Photochem. Photobiol.* 1993, *58*, 532-535.

78. Burel, L., Jardon, P., Lepretre, J. -C.; *New. J. Chem.*, 1997, *21*, 399-403.

79. Wells, T. A.; Losi, A.; Dai, R.; Scott, P.; Park, S.-U.; Golbeck, J.; Song, P.-S.; *J. Phys. Chem. A*, 1997, *101*, 366-372.

80. a) Turro, C.; Chang, C. K.; Leroi, G. E.; Cukier, R. I.; Nocera, D. G. *J. Am. Chem. Soc.* **1992**, *114*, 4013. b) O'Conner, D.; Shafirovich, V. Ya.; Geacintov, N. E. *J. Phys. Chem.* **1994**, *98*, 9831.

81. Diwu, Z.; Lown, J. W.; *J. Photochem. Photobiol. A: Chem.*, **1992**, *64*, 273-287.

Table 4.1 Magic angle decay parameters for hypocrellin[a].

solvent	time scale[c]	λ_{probe}(nm)	a_1	τ_1(ps)	a_2	τ_2(ps)[b]
ethanol	200 ps	595	-0.014±0.001	80±5	-0.001±0.0005	∞
		570	-0.06±0.02	80±5	0.01±0.005	∞
		560	-0.08±0.02	80±5	0.02±0.01	∞
		550	-0.08±0.01	80±5	0.02±0.004	∞
octanol	40 ps	570	-0.03±0.01	8±1	0.007±0.001	∞
		560	-0.05±0.02	8±1	0.005±0.0003	∞
		550	-0.03±0.01	8±1	0.001±0.0003	∞
	500 ps	595	-0.05±0.02	230±18	-0.001±0.0004	∞
		570	-0.09±0.03	230±18	0.02±0.003	∞
		560	-0.10±0.02	230±18	0.01±0.001	∞
		550	-0.05±0.01	230±18	0.01±0.001	∞

[a] λ_{pump} = 588 nm.

[b] Time constant for this second component is much greater than the time scale of the experiment, $\tau_2 = \infty$. The errors cited are the standard deviations of the average of several measurements, when more than one measurement was performed.

[c] On some timescales only two probe wavelengths are employed for the global fit.

Table 4.2 Anisotropy decay parameters for hypocrellin.[a]

solvent	Time scale[c]	λ_{probe}(nm)[d]	a_1	τ_1(ps)	a_2	τ_2(ps)[b]
ethanol	100 ps	570	-0.34	129	-0.22	∞
		560	-0.25	129	-0.1	∞
	200 ps	570	-0.18±0.05	118 ±6	-0.36±0.04	∞
		560	-0.20±0.02	118 ±6	0.001±0.001	∞
		550	-0.21±0.02	118 ±6	0.003±0.001	∞
	2000 ps	560	-0.12	176	-0.11	∞
		550	-0.09	176	-0.11	∞
octanol	40 ps	570	-0.20±0.1	6.3 ±0.3	-0.18±0.06	∞
		560	-0.35±0.01	6.3 ±0.3	-0.13±0.03	∞
		550	-0.24±0.06	6.3 ±0.3	-0.22±0.06	∞
	500 ps	570	-0.22	728	-0.08	∞
		560	-0.27	728	-0.04	∞
	2000 ps	570	-0.20	774	-0.09	∞
		560	-0.10	774	-0.17	∞
		550	-0.08	774	-0.22	∞

[a] λ_{pump} = 588 nm.

[b] Time constant for this second component is much greater than the time scale of the experiment, $\tau_2 = \infty$. The errors cited are the standard deviations of the average of several measurements, when more than one measurement was performed. On some timescales, only one measurement was performed.

[c] On some timescales only two probe wavelengths are employed for the global fit.

[d] Data for λ_{probe} = 595 nm could not be fit owing to the discontinuity incurred (see experimental section).

Table 4.3 Parameters and results for the simulations of hypocrellin photophysics.

Parameter type	Value
$N(S_1) \rightarrow I(S_1)$[a]	10 ps
$T(S_1) \rightarrow I(S_1)$[a]	230 ps
Rotational diffusion time[a]	800 ps
$S_1 \rightarrow S_0$ inverse radiative rate[b]	7000 ps
inverse intersystem crossing rate[b]	1000 ps
Transition dipole shift for $I(S_0) \leftrightarrow I(S_1)$	$\sim \pi/4$[c]

Extinction coefficient[d]	Probe wavelength		
	560 nm	570 nm	595 nm
$\varepsilon_{N(S_1),\parallel}$	0.82	0.30	-0.15
$\varepsilon_{N(S_1),\perp}$	0.95	1.90	0.92
$\varepsilon_{T(S_1),\parallel}$	0.82	0.30	-0.15
$\varepsilon_{T(S_1),\perp}$	0.95	1.90	0.92
$\varepsilon_{I(S_1),\parallel}$	0.95	0.70	-3.23
$\varepsilon_{I(S_1),\perp}$	0.95	1.80	3.68
$\varepsilon_{N(T_1)}$, $\varepsilon_{T(T_1)}$, $\varepsilon_{I(T_1)}$	1.82	2.00	2.81

[a] Experimental observations from our laboratory.

[b] Inverse of the radiative rate k_R of $N(S_1)$, $T(S_1)$, and $I(S_1)$ to the ground state. We assume k_R to be the same for all three of these species. Based on the reported [81] triplet yield of hypocrellin in benzene .

[c] Shift in angle relative to the ground-state absorption dipoles of N and T that was necessary to account for lower than theoretical initial fluorescence anisotropy value. In terms of our model this leads to the conclusion that the transition dipole for $I(S_0) \leftrightarrow I(S_1)$ is in fact at some angle relative to that for $N(S_0) \leftrightarrow N(S_1)$ and $T(S_0) \leftrightarrow T(S_1)$.

[d] Extinction coefficients relative to those of ground-state species, εN(S0), εT(S0), which are taken to be unity. All of these, except for εN(T1), εT(T1) and εI(T1), are determined to within ±0.05.

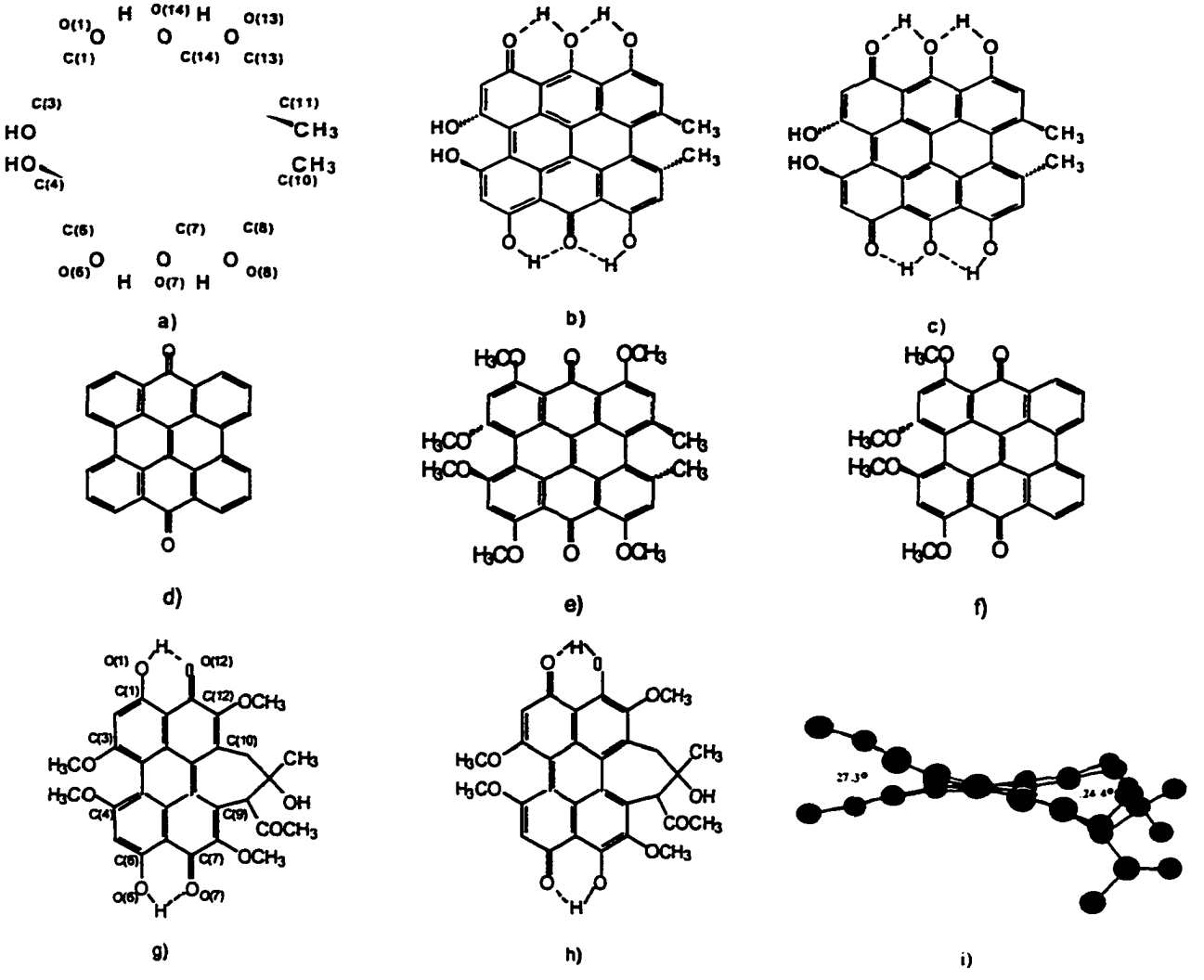

Figure 4.1 Two-dimensional structures of (a) "normal" form of hypericin, (b) one of the two possible hypericin mono tautomers , (c) one of the three possible hypericin double tautomers, (d) mesonaphthobianthrone (phenanthro[1,10,9,8,o,p,q,r,a]perylene-7-14-dione), (e) O-hexamethoxy hypericin (f) O-tetramethoxy hypericin. Two-dimensional structures of the "normal" form of hypocrellin (g) and the double tautomer of hypocrellin (h). The distortion of the hypocrellin skeleton due to the interactions of the side chain groups is indicated in (i). For hypocrellin, twist angles of 27.3° and 24.4° are measured with respect to C(3) and C(4) and C(9) and C(10), respectively. Comparable twist angles are observed in hypericin.

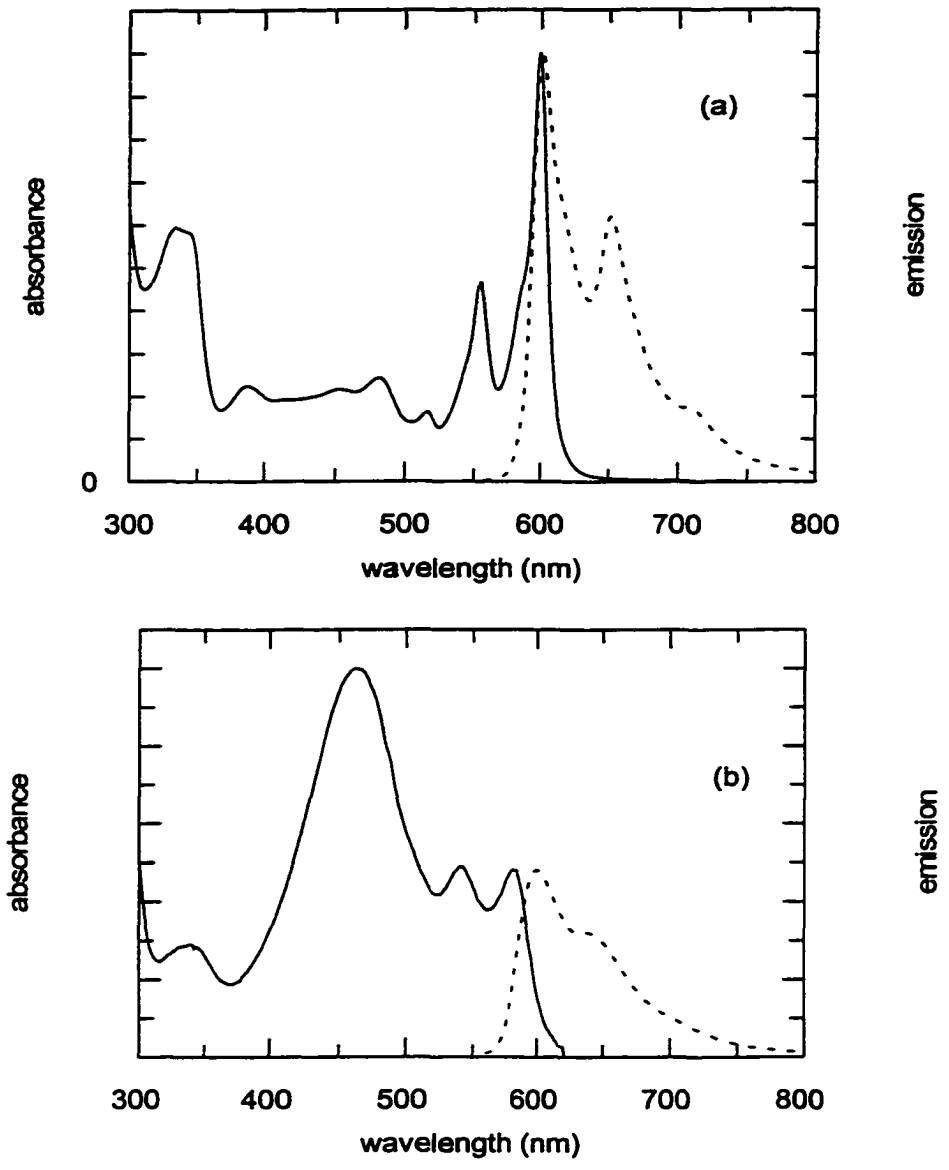

Figure 4.2 Normalized fluorescence spectra (dashed line) and absorption spectra (solid line) of hypericin (a) and hypocrellin (b) in DMSO. The spectra of hypocrellin and hypericin are relatively insensitive to solvent. The steady-state emission spectra bear a "mirror symmetry" relationship to the visible portion of the absorption spectrum. We attribute this symmetry to the presence of ground-state tautomers [17], ions or conformational isomers. Transient absorption measurements using two different excitation wavelengths are consistent with such heterogeneity [19,20]. Also consistent with this assignment is the observation that fluorescence upconversion measurements yield different kinetics at different emission wavelengths [24].

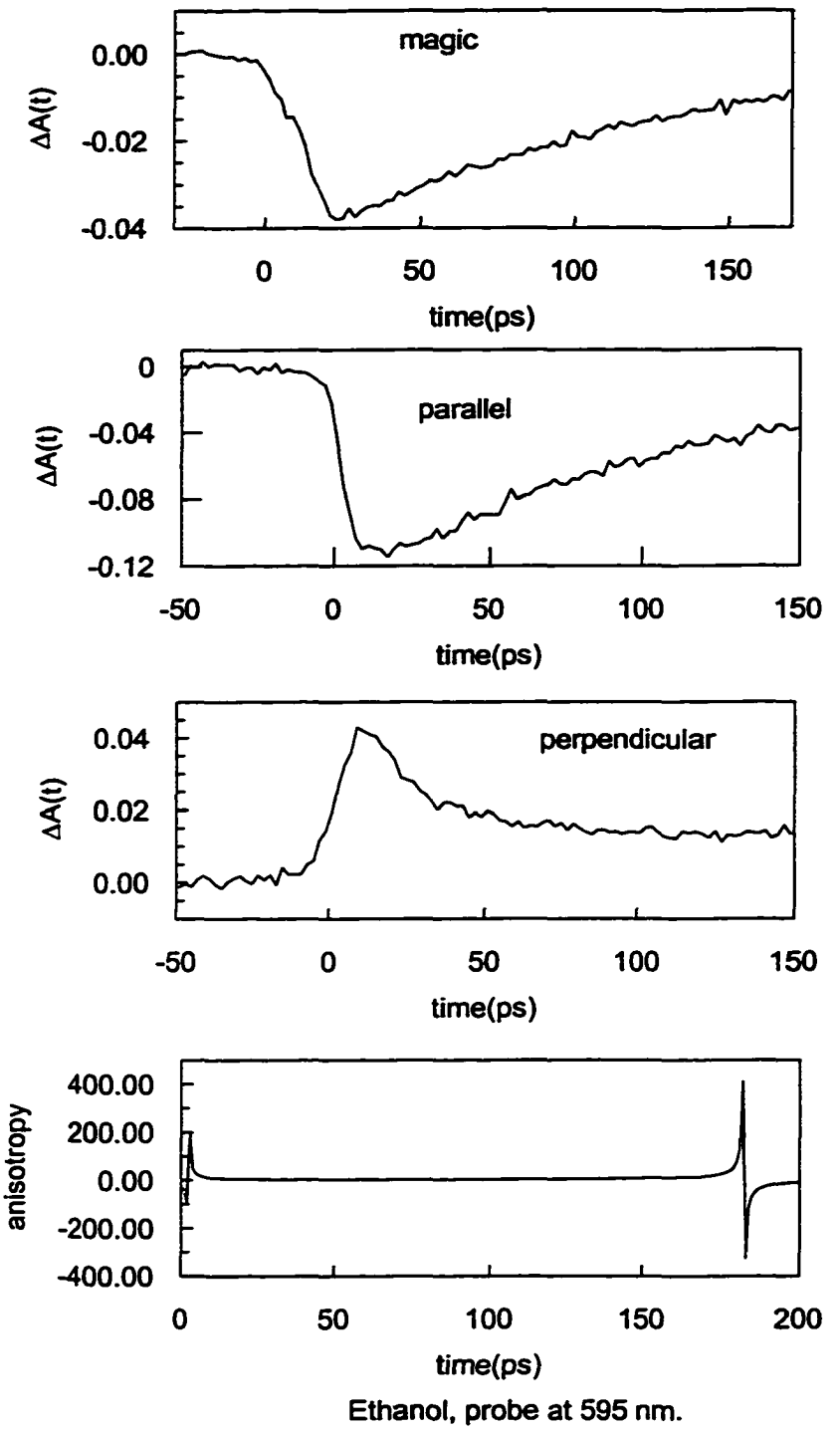

Figure 4.3 Transient absorption of hypocrellin in ethanol: λ_{pump} = 588 nm, λ_{probe} = 595 nm. Note that the sign of the perpendicular trace is opposite that of the parallel and magic angle traces.

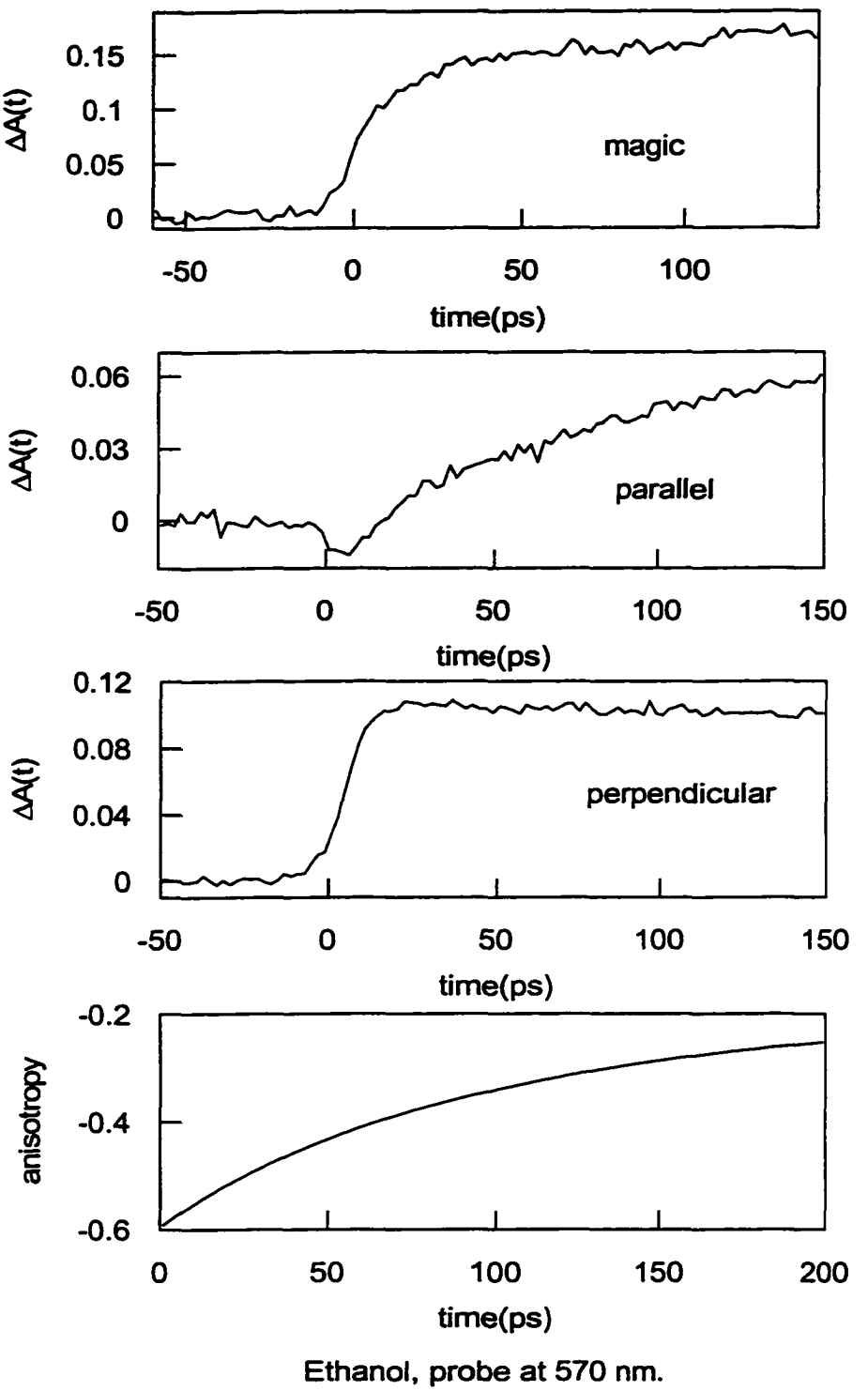

Figure 4.4 Transient absorption of hypocrellin in ethanol: λ_{pump} = 588 nm, λ_{probe} = 570 nm.

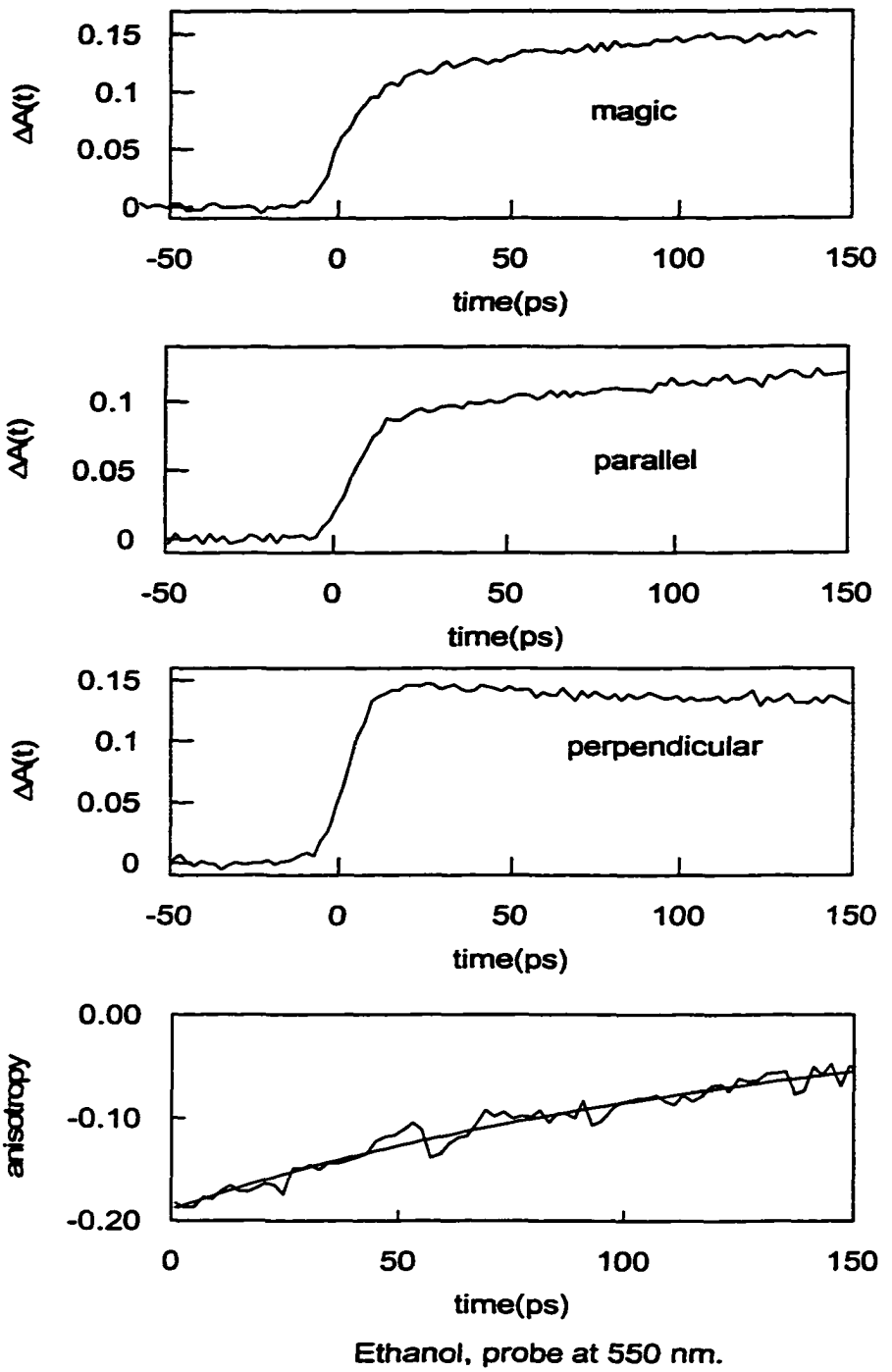

Figure 4.5 Transient absorption of hypocrellin in ethanol: λ_{pump} = 588 nm, λ_{probe} = 550 nm. The bottom panel compares the anisotropy calculated from the *fits* of the parallel and perpendicular traces (smooth line) with the anisotropy obtained directly from the experimental parallel and perpendicular traces (noisy line).

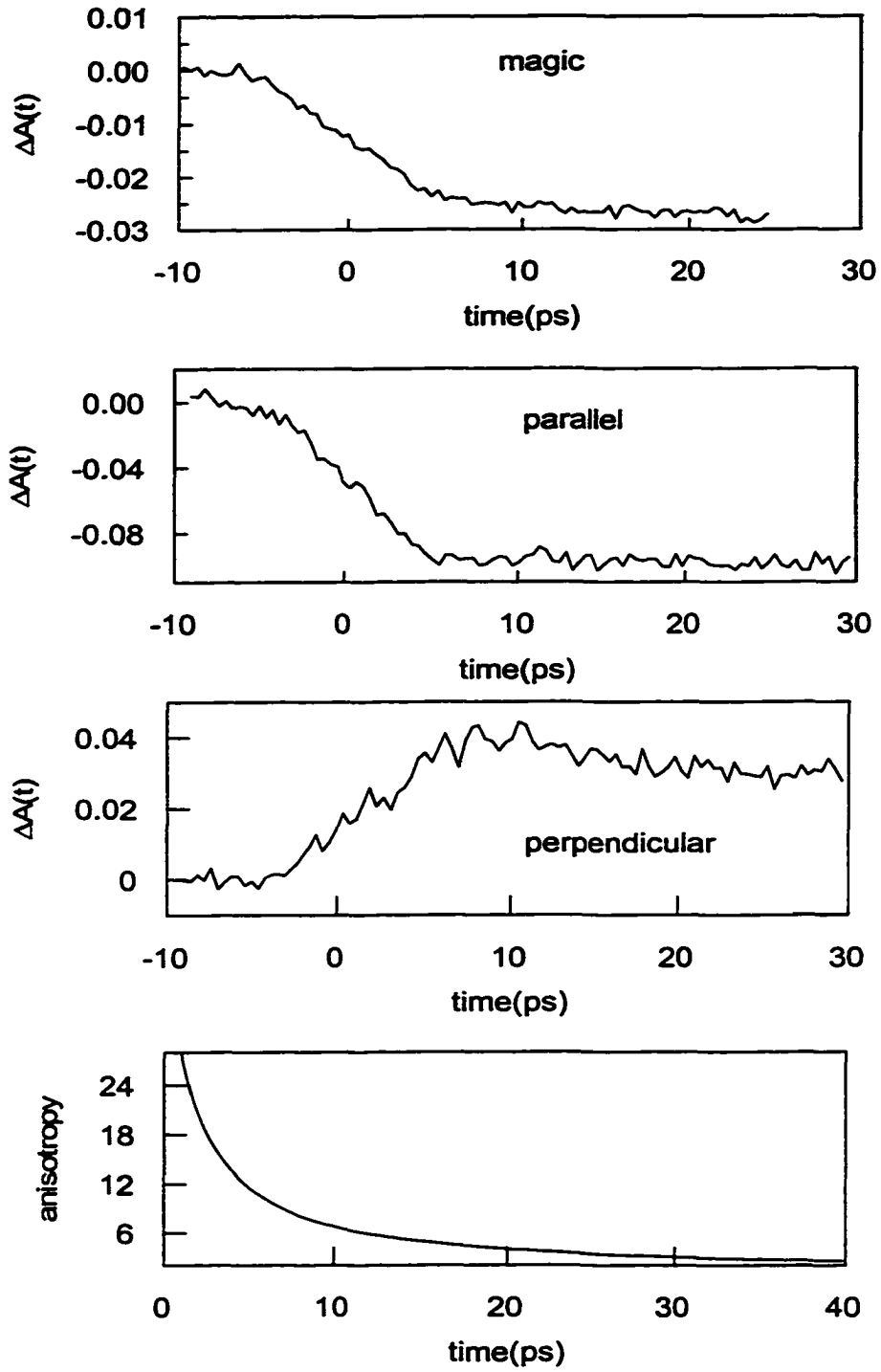

Figure 4.6 Transient absorption of hypocrellin in octanol: λ_{pump} = 588 nm, λ_{probe} = 595 nm. Note that the sign of the perpendicular trace is opposite that of the parallel and magic angle traces.

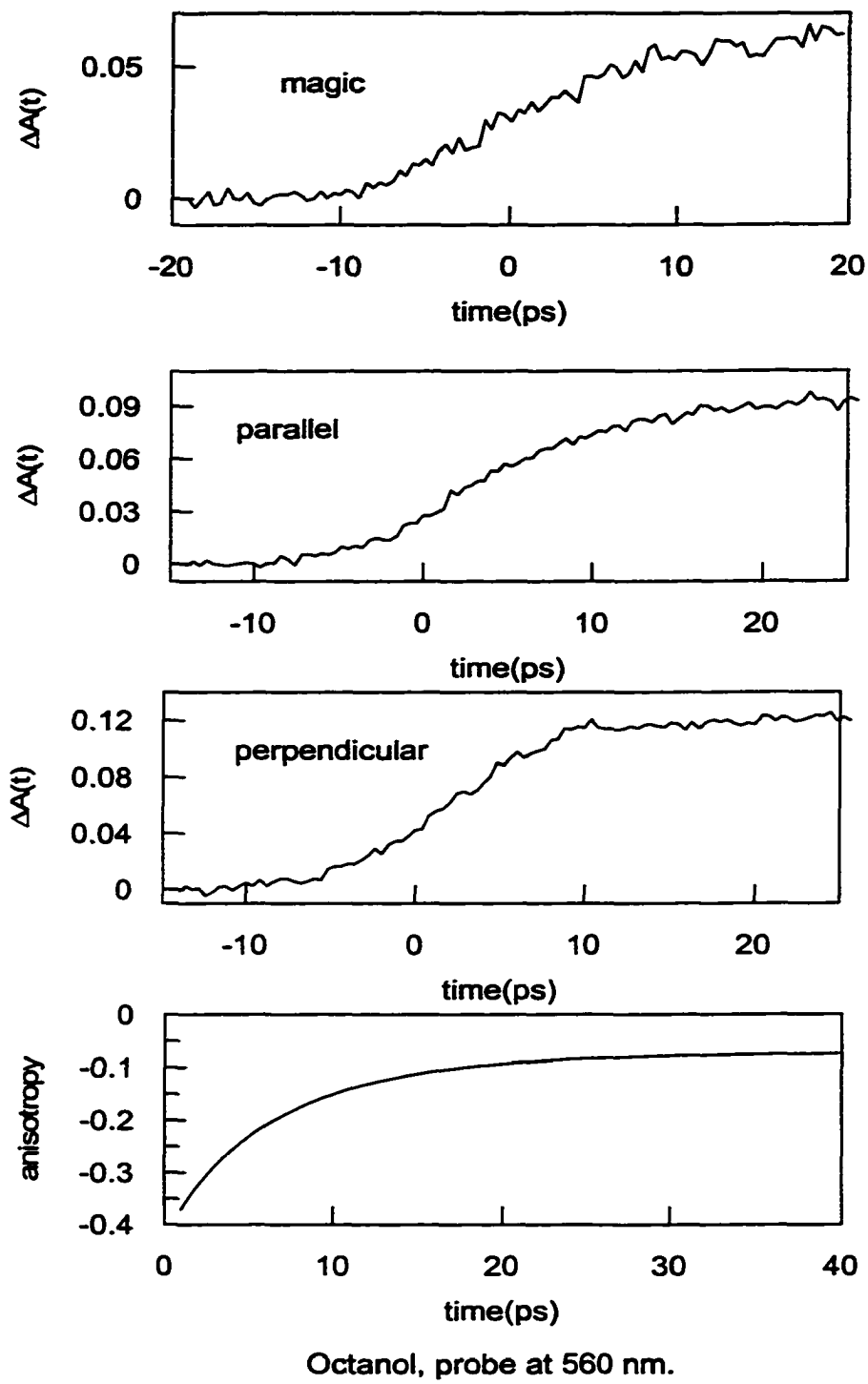

Figure 4.7 Transient absorption of hypocrellin in octanol: λ_{pump} = 588 nm, λ_{probe} = 560 nm.

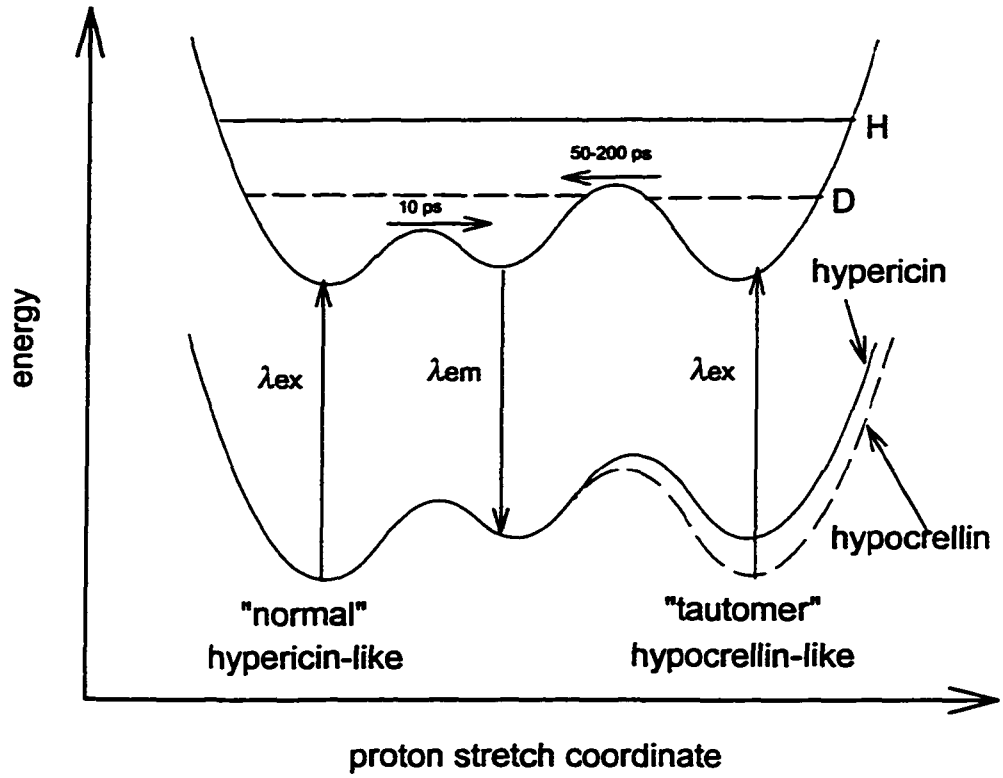

Figure 4.8 Unified picture depicting the ground- and excited-state potential energy surfaces for hypericin-like and hypocrellin-like molecules as a function of the proton stretch coordinate. The right-hand side of the ground-state potential energy surface depicts our proposal that the hypericin bi tautomer (Figure 1c) is not populated in the ground state, whereas the hypocrellin tautomer (Figure 1h) is populated. On the excited-state surface, the zero-point vibrational levels for an OH•••O or an OD•••O system are depicted [69]. The height of the zero-point level with respect to the barrier in the proton stretch coordinate determines whether an isotope effect will be observed. The third potential well, the middle of the Figure represents either another possible tautomeric form or some other intermediate between, for example, the normal and the fully or bi tautomer species of hypericin. The arrows in the diagram are meant to remind the reader of the time constants for the proton transfer processes in hypericin and hypocrellin. One should not identify the proton coordinate for the reaction coordinate in this system.

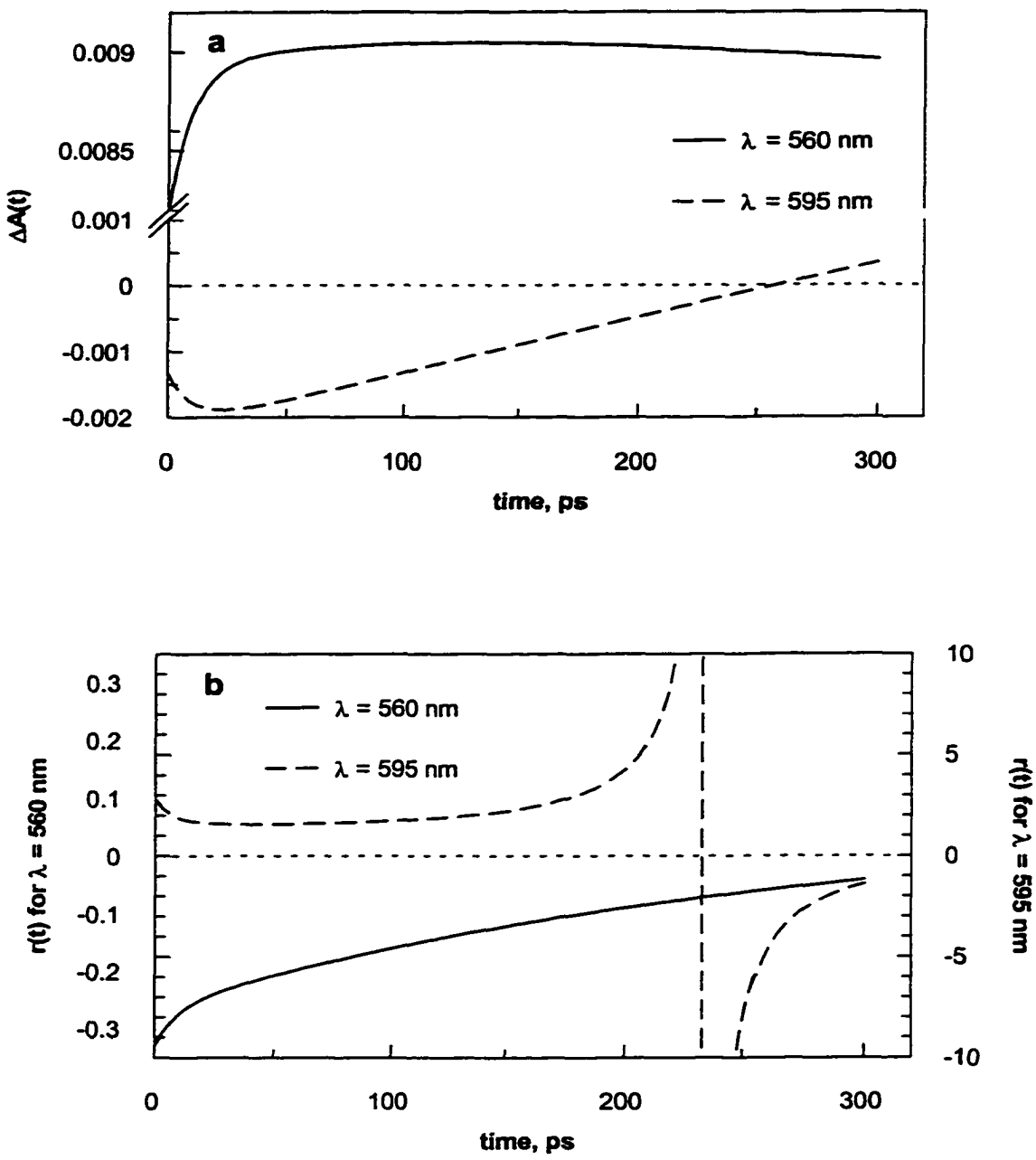

Figure 4.9 Results of simulations based on the kinetic scheme proposed in the text.

(a) Isotropic ("magic angle") transient absorption, ΔA(t), of hypocrellin in octanol at λ_{probe} = 560 and 595 nm.

(b) Anisotropy decay, r(t), of hypocrellin in octanol at λ_{probe} = 560 and 595 nm. Note the discontinuity for the 595 nm trace at around 230 ps.

These simulated traces when compared with their experimental counterparts (data not shown for octanol at longer time scales) shows that the salient features of the kinetics are qualitatively reproduced in all cases.

APPENDIX

Computer Implementation with "MAPLE V" Software: Solving System of Differential Equations

Below is a script written for Maple V that allows one to find solutions for each species population as a function of time. This information is necessary for the second part of simulations performed with MathCAD which also allows us to find the best model parameters that reproduce experimental data.

Script starts here (user commands start with ">"):

```
Kinetic model for hypocrellin A primary photoprocesses in alcohols.
```

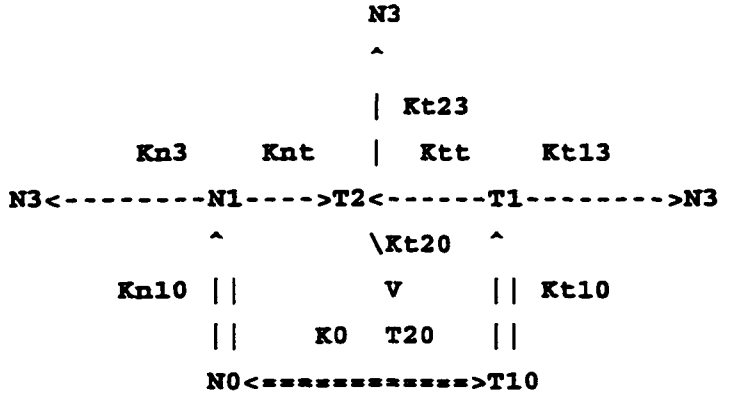


```
First lets define our differential equations:
> deN2:=diff(t1(t),t)=-(Kt13+Ktt+Kt10)*t1(t);
> deN3:=diff(t2(t),t)=-(Kt23+Kt20)*t2(t)+Ktt*t1(t)+Knt*n1(t);
> deN1:= diff(n1(t),t)=-(Kn3+Knt+Kn10)*n1(t);
```

$$deN2 := \frac{d}{dt} t1(t) = -(Kt13 + Ktt + Kt10)\ t1(t)$$

$$deN3 := \frac{d}{dt} t2(t) = -(Kt23 + Kt20)\ t2(t) + Ktt\ t1(t) + Knt\ n1(t)$$

$$deN1 := \frac{d}{dt} n1(t) = -(Kn3 + Knt + Kn10)\ n1(t)$$

```
> sys:= deN1, deN2,deN3 ; fns:= {n1(t), t1(t), t2(t)};
       d
sys := -- n1(t) = -(Kn3 + Knt + Kn10) n1(t),
       dt
    d
    -- t1(t) = -(Kt13 + Ktt + Kt10) t1(t),
    dt
    d
    -- t2(t) = -(Kt23 + Kt20) t2(t) + Ktt t1(t) + Knt n1(t)
    dt

                    fns := {n1(t), t1(t), t2(t)}
```

Next we find initial amounts of N1 and T1 just after the pump went through the sample and excited n*100 % of the ground-state population N0o. K0 is equil. konstant. This will define boundary conditions.

```
> N1o:=N0o*n/(1+K0): T1o:=N1o*K0:
>  solution:=simplify(dsolve({sys, n1(0)=N1o, t1(0)=T1o, t2(0)=0},
fns)):
```

Extract solution for T2 time-evolution:

```
> T2:=((rhs(op(select(has,solution,t2(t))))));
T2 := - N0o n (Ktt K0 Kt23 %1 + Ktt K0 Kt20 %1 - Ktt K0 Kn3 %1
     - Ktt K0 Knt %1 - Ktt K0 Kn10 %1 - Ktt K0 %3 Kt23
     - Ktt K0 %3 Kt20 + Ktt K0 Kn3 %3 + Ktt K0 Knt %3
     + Ktt K0 Kn10 %3 + Knt Kt13 %2 + Knt Ktt %2 + Knt Kt10 %2
     - Knt Kt23 %2 - Knt Kt20 %2 - Knt Kt13 %1 - Knt Ktt %1
     - Knt Kt10 %1 + Knt Kt23 %1 + Knt Kt20 %1)/(
    (Kt13 + Ktt + Kt10 - Kt23 - Kt20) (1 + K0)
    (-Kt23 - Kt20 + Kn3 + Knt + Kn10))
%1 := exp(-(Kt23 + Kt20) t)
%2 := exp(-(Kn3 + Knt + Kn10) t)
%3 := exp(-(Kt13 + Ktt + Kt10) t)
```

Extract solution for T1 time-evolution:

```
> T1:=rhs(op(select(has,solution,t1(t))));
                    exp(-(Kt13 + Ktt + Kt10) t) N0o n K0
              T1 := -----------------------------------
                                  1 + K0
```

Extract solution for N1 time-evolution:

```
> N1:= rhs(op(1,select(has,solution,n1(t))));
```

$$N1 := \frac{\exp(-(Kn3 + Knt + Kn10)\ t)\ N0o\ n}{1 + K0}$$

The three results above are very important as we use them in our MathCAD simulations.

Let N0o be conc. of normal species in ground state BEFORE n*100% molecules were excited up with the pulse;

Let No be conc. of normal species in ground state just AFTER the pulse, To -- same for tautomer

Here we assume that absorbance coeff. of normal species and tautomer are the same.

```
> No :=N0o*(1-n)/(1+K0);
N0:=simplify(rhs(dsolve({diff(n0(t),t)=Kn10*N1, n0(0)=No}, n0(t))));
```

$$No := \frac{N0o\ (1 - n)}{1 + K0}$$

```
N0 := - N0o (
    -Knt + n Knt - Kn3 + Kn10 exp(-(Kn3 + Knt + Kn10) t) n + n Kn3
     - Kn10)/(Kn3 + Kn3 K0 + Knt + Knt K0 + Kn10 + Kn10 K0)
> T1o:=No*K0; T10:=simplify(rhs(dsolve({diff(t10(t),t)=Kt10*T1,
t10(0)=T1o}, t10(t))));
```

$$T1o := \frac{N0o\ (1 - n)\ K0}{1 + K0}$$

```
T10 := - K0 N0o (-Ktt + n Ktt - Kt10 + n Kt13
     + Kt10 exp(-(Kt13 + Ktt + Kt10) t) n - Kt13)/(
    Kt13 + Kt13 K0 + Ktt + Ktt K0 + Kt10 + Kt10 K0)
```

Here is place where we can find explicit expression for ground state of T2 population:

```
> T2o:=0; T20:=simplify(rhs(dsolve({diff(t20(t),t)=Kt20*T2,
t20(0)=T2o}, t20(t)))):
```

(Output is not shown due to complexity)

Here we also assume that in the ground state the proton transfer rate is too small on our timescale.

```
Now we can start evaluating triplet (N3) dynamics:
> deN4:= diff(n3(t),t)=Kn3*N1+Kt13*T1+Kt23*T2;
        d           Kn3 %2 N0o n    Kt13 %3 N0o n K0
deN4 := -- n3(t) = ------------ + ---------------- - Kt23 N0o n (
        dt              1 + K0            1 + K0
    Ktt K0 Kt23 %1 + Ktt K0 Kt20 %1 - Ktt K0 Kn3 %1 - Ktt K0 Knt %1
     - Ktt K0 Kn10 %1 - Ktt K0 %3 Kt23 - Ktt K0 %3 Kt20
     + Ktt K0 Kn3 %3 + Ktt K0 Knt %3 + Ktt K0 Kn10 %3 + Knt Kt13 %2
     + Knt Ktt %2 + Knt Kt10 %2 - Knt Kt23 %2 - Knt Kt20 %2
     - Knt Kt13 %1 - Knt Ktt %1 - Knt Kt10 %1 + Knt Kt23 %1
     + Knt Kt20 %1)/((Kt13 + Ktt + Kt10 - Kt23 - Kt20) (1 + K0)
    (-Kt23 - Kt20 + Kn3 + Knt + Kn10))
%1 := exp(-(Kt23 + Kt20) t)
%2 := exp(-(Kn3 + Knt + Kn10) t)
%3 := exp(-(Kt13 + Ktt + Kt10) t)
Boundary condition is that no triplet present at time zero:
> N3:=(rhs(dsolve({deN4, n3(0)=0}, n3(t)))):
(Output is not shown due to complexity)
```

Computer Implementation with "MathCAD" Software: Transient Absorbance Signal Modeling and "Fitting" Procedure.

The symbolic expressions for the time-dependents populations of N*, T* and I*, obtained with Maple V in the previous section are now put to use in a procedure written for MathCAD 6.0. MathCAD interface is much more intuitive and also capable of formatted output of calculation results. The main advantage for using MathCAD is its ability to perform a multiparametric search for the best parameters provided function partial derivatives can be calculated. The whole procedure is composed of two steps: 1) find best parameters that describe isotropic system behavior and 2) use that information and experimental anisotropy decay to separate photobleach from excited-state absorbance and estimate angle between transition dipole moments.

A sample MathCAD protocol for this procedure is given below.

Fitting procedure for isotropic parameters of hypocrellin A excited-state kinetics in octanol. (with the the third tautomer in the ground state)

Initial conditions for excited state populations immediately after time-zero:

$$N_0 = K_t \cdot N0_o \cdot \frac{\eta}{K_t - 1} \qquad T1_0 = N0_o \cdot \frac{\eta}{K_t - 1}$$

$$T2_0 = T1_0 \qquad N3_0 = 0$$

where η is the fraction of population excited by the pump pulse. This additional parameter is needed later as a scaling factor when fitting experimental data.

For the ground state initial conditions will appear as (immediately after time-zero):

$$N0_0 = K_t \cdot N0_o \cdot \frac{1 - \eta}{K_t - 1} \qquad T10_0 = N0_o \cdot \frac{1 - \eta}{K_t - 1}$$

$$T20_0 = T10_0$$

$$solution = \left\{ t1(t) = \frac{\%3\, N0o\, n\, K0}{1 + K0},\ n1(t) = \frac{n\, N0o\, \%2}{1 + K0},\ t2(t) = (-K0\, Ktt\, \%3\, Kt20 - \%1\, Ktt\, Kn3\, K0 + K0\, Ktt\, \%3\, Knt + K0\, Ktt\, \%3\, Kn10 + K0\, Ktt\, \%3\, Kn3 + Kt23\, \%1\, Ktt\, K0 - \%1\, Ktt\, Kn10\, K0 - \%1\, Knt\, Ktt\, K0 + \%1\, Ktt\, Kt20\, K0 - Kt23\, K0\, Ktt\, \%3 + Knt\, \%2\, Kt13 - \%1\, Knt\, Kt13 - Kt23\, Knt\, \%2 - \%1\, Knt\, Kt10 + Kt23\, \%1\, Knt + \%1\, Knt\, Kt20 + Knt\, \%2\, Kt10 + Knt\, \%2\, Ktt - Knt\, \%2\, Kt20 - \%1\, Knt\, Ktt)\, n N0o / ((Kt13 + Kt13\, K0 + Ktt + Ktt\, K0 + Kt10 + Kt10\, K0 - Kt20 - Kt20\, K0 - Kt23 - Kt23\, K0)(Kt20 + Kt23 - Kn3 - Knt - Kn10)) \right\}$$

$$\%1 := e^{(-(Kt23 + Kt20)\, t)}$$

$$\%2 := e^{(-(Kn3 + Knt + Kn10)\, t)}$$

$$\%3 := e^{(-(Kt13 + Ktt + Kt10)\, t)}$$

Now we introduce results obtained with Maple V script (see picture above):

$$N(t) = N_0 \cdot e^{-t \cdot (k_{nt} - k_{nn3} + k_{nn0})} \qquad T1(t) = T1_0 \cdot e^{-t \cdot (k_{tt} + k_{tn3} + k_{t10})}$$

$$T2(t) = N0_o \cdot \eta \cdot \frac{\begin{aligned} & e^{-t \cdot (k_{tn3} + k_{t20})} \cdot \left[K_t \cdot k_{tt} \cdot (-k_{nn3} + k_{tn3} - k_{nn0} - k_{nt} - k_{t20}) \cdots \right. \\ & \left. + k_{nt} \cdot (-k_{tn3} - k_{t10} + k_{tn3} + k_{t20} - k_{tt}) \right] \cdots \\ & + e^{-t \cdot (k_{nt} - k_{nn3} + k_{nn0})} \cdot k_{nt} \cdot \left[k_{tn3} + k_{t10} - k_{tt} - (k_{tn3} + k_{t20}) \right] \cdots \\ & + e^{-t \cdot (k_{tt} + k_{tn3} + k_{t10})} \cdot K_t \cdot k_{tt} \cdot (k_{nn3} - k_{tn3} + k_{nn0} + k_{nt} - k_{t20}) \end{aligned}}{\left[k_{tn3} + k_{t20} - (k_{nt} - k_{nn3} - k_{nn0}) \right] \cdot (k_{tt} - k_{tn3} - k_{t10} - k_{t20} - k_{tn3}) \cdot (1 + K_t}$$

$T2(0) = 0$ as expected

N3(t) is better to evaluate numerically

$$N3(t) = \int_0^t k_{nn3}\cdot N(tt) - k_{tn3}\cdot(T1(tt) - T2(tt))\,dtt - N3_0 = \frac{7}{8}\cdot\eta\cdot\exp\left(\frac{-1}{875}\cdot t\right) - \frac{7}{8}\cdot\eta$$

$$N3(t) = \frac{-7}{8}\cdot\eta\cdot\exp\left(\frac{-1}{875}\cdot t\right) - \frac{7}{8}\cdot\eta$$

$$N0_{\Sigma}(t) = N(t) - T1(t) - T2(t) - N3(t)$$

Here we introduce anisotropic components:

$$P_{02.par}(t,\phi) = \frac{1}{9} - \frac{2}{45}\cdot\left(3\cdot\cos(\phi)^2 - 1\right)\cdot e^{-6\cdot D\cdot t}$$

$$P_{02.per}(t,\phi) = \frac{1}{9} - \frac{1}{45}\cdot\left(3\cdot\cos(\phi)^2 - 1\right)\cdot e^{-6\cdot D\cdot t}$$

$\varepsilon_{0.par}(t) = \varepsilon_0\cdot P_{02.par}(t,0)$ $\quad$ $\varepsilon_{0.per}(t) = \varepsilon_0\cdot P_{02.per}(t,0)$

$\varepsilon_{N.par}(t) = \varepsilon_{N.a}\cdot P_{02.par}(t,\phi_{N.a}) - \varepsilon_{N.e}\cdot P_{02.par}(t,0)$

$\varepsilon_{N.per}(t) = \varepsilon_{N.a}\cdot P_{02.per}(t,\phi_{N.a}) - \varepsilon_{N.e}\cdot P_{02.per}(t,0)$

$\varepsilon_{N.a}$ is for excited-state absorbance,
$\varepsilon_{N.e}$ is for stimulated emission

$\varepsilon_{T1.par}(t) = \varepsilon_{T1.a}\cdot P_{02.par}(t,\phi_{T1.a}) - \varepsilon_{T1.e}\cdot P_{02.par}(t,0)$

$\varepsilon_{T1.per}(t) = \varepsilon_{T1.a}\cdot P_{02.per}(t,\phi_{T1.a}) - \varepsilon_{T1.e}\cdot P_{02.per}(t,0)$

$\varepsilon_{T2.par}(t,\phi_{T2.a},\phi_{T2.e}) = \varepsilon_{T2.a}\cdot P_{02.par}(t,\phi_{T2.a}) - \varepsilon_{T2.e}\cdot P_{02.par}(t,\phi_{T2.e})$

$\varepsilon_{T2.per}(t,\phi_{T2.a},\phi_{T2.e}) = \varepsilon_{T2.a}\cdot P_{02.per}(t,\phi_{T2.a}) - \varepsilon_{T2.e}\cdot P_{02.per}(t,\phi_{T2.e})$

$\varepsilon_{N3.par}(t) = \varepsilon_{N3}\cdot P_{02.par}(t,\phi_{N3.a})$ $\quad$ $\varepsilon_{N3.per}(t) = \varepsilon_{N3}\cdot P_{02.per}(t,\phi_{N3.a})$ triplet only absorbs light

$$A_{par}(t,\phi_{T2.a},\phi_{T2.e}) = -\varepsilon_{0.par}(t)\cdot N0_{\Sigma}(t) - \varepsilon_{N.par}(t)\cdot N(t) + \varepsilon_{T1.par}(t)\cdot T1(t) \ldots + \varepsilon_{T2.par}(t,\phi_{T2.a},\phi_{T2.e})\cdot T2(t) + \varepsilon_{N3.par}(t)\cdot N3(t)$$

$$A_{per}(t,\phi_{T2.a},\phi_{T2.e}) = -\varepsilon_{0.per}(t)\cdot N0_{\Sigma}(t) - \varepsilon_{N.per}(t)\cdot N(t) + \varepsilon_{T1.per}(t)\cdot T1(t) \ldots + \varepsilon_{T2.per}(t,\phi_{T2.a},\phi_{T2.e})\cdot T2(t) + \varepsilon_{N3.per}(t)\cdot N3(t)$$

$$A_{mag}(t) := \frac{1}{3}\cdot A_{par}(t, \blacksquare, \blacksquare) - \frac{2}{3}\cdot A_{per}(t, \blacksquare, \blacksquare)$$

We can also verify, that the magic angle result is equvalent to using non-polarized light:

$$\varepsilon_N := \varepsilon_{N.a} - \varepsilon_{N.e} \qquad \varepsilon_{T1} := \varepsilon_{T1.a} - \varepsilon_{T1.e} \qquad \varepsilon_{T2} := \varepsilon_{T2.a} - \varepsilon_{T2.e}$$

$$A(t, \varepsilon_N, \varepsilon_{T1}, \varepsilon_{T2}, \varepsilon_{N3}, \eta) := \frac{1}{9}\cdot\left(\varepsilon_0\cdot N0\,\Sigma(t) - \varepsilon_N\cdot N(t) - \varepsilon_{T1}\cdot T1(t) \ldots + \varepsilon_{T2}\cdot T2(t) - \varepsilon_{N3}\cdot N3(t)\right)$$

Our goal is to fit this magic angle transient absorbasnce to experimental data
Now we see that we really need the values of $\varepsilon_N, \varepsilon_{T2}, \varepsilon_{N3}$ which are the sums of $\varepsilon_{.e}$ and $\varepsilon_{.a}$ components. The most straightforward way to get the is to consider the isotropic transient profile that we obtained earlier and fit it to the experimental data.

assume $\varepsilon_N, \varepsilon_{T2}, \varepsilon_{N3}$

$$A(t, \varepsilon_N, \varepsilon_{T1}, \varepsilon_{T2}, \varepsilon_{N3}, \eta) := -\frac{1}{18}\cdot\eta\cdot\exp\left(\frac{-177}{1750}\cdot t\right) - \frac{1}{18}\cdot\eta\cdot\exp\left(\frac{-221}{40250}\cdot t\right) - \frac{1}{9}\cdot\eta\cdot\exp\left(\frac{1}{875}\cdot t\right) - \frac{1}{2}\cdot\exp\left(\frac{-177}{1750}\cdot t\right)$$

when collenting on exponents simplifies to

$$AA(t, \varepsilon_N, \varepsilon_{T1}, \varepsilon_{T2}, \varepsilon_{N3}, \eta) := \left(\frac{1}{18}\cdot\varepsilon_{T1} - \frac{1}{18}\cdot\varepsilon_{T2}\right)\cdot\exp\left(\frac{-221}{40250}\cdot t\right) - \left(\frac{1}{9}\cdot\varepsilon_{T2} - \frac{1}{72} - \frac{7}{72}\cdot\varepsilon_{N3}\right)\cdot\exp\left(\frac{-1}{875}\cdot t\right) -$$

But in our model we postulate that

$$\varepsilon_{T1.a} := \varepsilon_{N.a} \qquad \varepsilon_{T1.e} := \varepsilon_{N.e}$$

Hence $\varepsilon_N := \varepsilon_{T1}$ After substitution we get:

$$A(t, \varepsilon_N, \varepsilon_{T2}, \varepsilon_{N3}, \eta) := AA(t, \varepsilon_N, \varepsilon_N, \varepsilon_{T2}, \varepsilon_{N3}, \eta)$$

$$A(t, \varepsilon_N, \varepsilon_{T2}, \varepsilon_{N3}, \eta) := \left(\frac{1}{18}\cdot\varepsilon_N - \frac{1}{18}\cdot\varepsilon_{T2}\right)\cdot\exp\left(\frac{-221}{40250}\cdot t\right) - \left(\frac{1}{9}\cdot\varepsilon_{T2} - \frac{1}{72} - \frac{7}{72}\cdot\varepsilon_{N3}\right)\cdot\exp\left(\frac{-1}{875}\cdot t\right) - \frac{1}{18}\cdot\varepsilon$$

Let's define fitting functional $F_A(t,p)$ as:

$$\begin{pmatrix} A(t,p1,p2,p3,p4) \\ \frac{d}{dp1}A(t,p1,p2,p3,p4) \\ \frac{d}{dp2}A(t,p1,p2,p3,p4) \\ \frac{d}{dp3}A(t,p1,p2,p3,p4) \\ \frac{d}{dp4}A(t,p1,p2,p3,p4) \end{pmatrix} \rightarrow$$

$$F_A(t,p) := \begin{bmatrix} \frac{1}{18}\cdot p_1 - \frac{1}{18}\cdot p_2\cdot \exp\left(\frac{-221}{40250}\cdot t\right) - \frac{1}{9}\cdot p_2 - \frac{1}{72} - \frac{7}{72}\cdot p_3\cdot \exp\left(\frac{-1}{875}\cdot t\right) - \frac{1}{18}\cdot p_1 - \frac{1}{18}\cdot p_2\cdot \exp\left(\frac{177}{1750}\cdot \right. \\ \left. \frac{1}{18}\cdot \exp\left(\frac{-221}{40250}\cdot t\right) - \frac{1}{18}\cdot \exp\left(\frac{-177}{1750}\cdot t\right)\cdot p_4 \right. \\ \left. \frac{-1}{18}\cdot \exp\left(\frac{-221}{40250}\cdot t\right) - \frac{1}{9}\cdot \exp\left(\frac{-1}{875}\cdot t\right) - \frac{1}{18}\cdot \exp\left(\frac{-177}{1750}\cdot t\right)\cdot p_4 \right. \\ \left. \frac{-7}{72}\cdot \exp\left(\frac{-1}{875}\cdot t\right) - \frac{7}{72}\cdot p_4 \right. \\ \left. \frac{1}{18}\cdot p_1 - \frac{1}{18}\cdot p_2\cdot \exp\left(\frac{-221}{40250}\cdot t\right) - \frac{1}{9}\cdot p_2 - \frac{1}{72} - \frac{7}{72}\cdot p_3\cdot \exp\left(\frac{-1}{875}\cdot t\right) - \frac{1}{18}\cdot p_1 - \frac{1}{18}\cdot p_2\cdot \exp\left(\frac{177}{175}\right. \end{bmatrix}$$

Some preparation for actual fitting is needed.

Define data to fit and the fitting points: The experiments were done in the time range of $t_{max} := 300$

$N := 20$ Number of points in fit

Maximum time

Select fit points

$parN := 4$ Number of parameters

$i := 1..N$ $\quad tt_i := \frac{(i-1)^3}{(N-1)^3}\cdot t_{max}$

Define experimental data to be fitted:

$A_{exp.par}(t) := -0.127\cdot \exp\left(\frac{-t}{230}\right)$ this is an example for 595 nm probe wavelength in octanol

$A_{exp.per}(t) := 0.025\cdot \exp\left(\frac{-t}{12}\right) - 0.05\cdot \exp\left(\frac{-t}{1159}\right) - 0.06\cdot \exp\left(\frac{-t}{50000}\right)$

$A_{exp_i} := A_{exp.par}(tt_i) - 2\cdot A_{exp.per}(tt_i) + 0.023$

Plot of experimental data for octanol

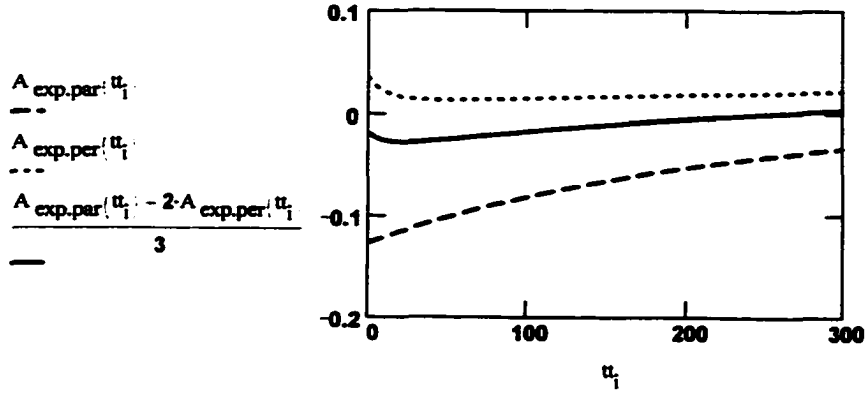

Define Vector of parameters to be fitted and initial guesses:

$$\begin{pmatrix} Ge_N \\ Ge_{T2} \\ Ge_{N3} \\ G\eta \end{pmatrix} = \begin{pmatrix} .85 \\ .3 \\ 3.8 \\ .1 \end{pmatrix} \qquad P_{guess} = \begin{pmatrix} Ge_N \\ Ge_{T2} \\ Ge_{N3} \\ G\eta \end{pmatrix}$$

Actual fit operator is here: $P = genfit(tt, A_{exp}, P_{guess}, F_A)$

Fit results:

$$P = \begin{pmatrix} 0.727 \\ 0.392 \\ 2.845 \\ 0.044 \end{pmatrix} \qquad A_{fit_i} = F_A(tt_i, P)_1$$

Plot before and after the Fit

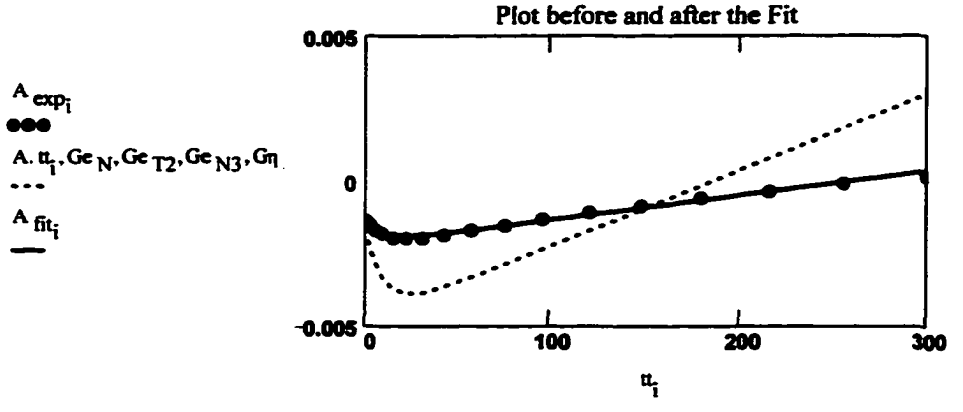

Plot of the Fit Residuals

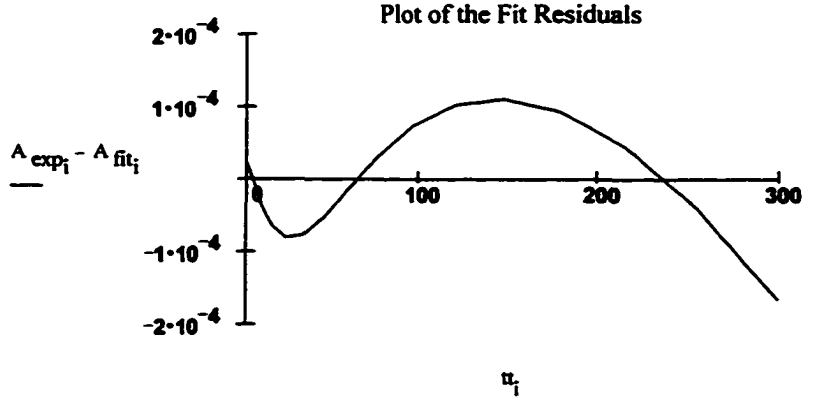

Fit quality:

$$Q = \frac{\sum_i \left| \frac{A_{exp_i} - A_{fit_i}}{A_{exp_i}} \right|}{N - parN}$$

$Q = 0.153$

Results

Finally, we obtain $\varepsilon_N = P_1$ $\varepsilon_{T2} = P_2$ $\varepsilon_{N3} = P_3$ $\eta = P_4$

$$\begin{pmatrix} \varepsilon_N \\ \varepsilon_{T2} \\ \varepsilon_{N3} \\ \eta \end{pmatrix} = \begin{pmatrix} 0.727 \\ 0.392 \\ 2.845 \\ 0.044 \end{pmatrix}$$

Output the fit results to data file:

$N' \equiv 100$ Number of points in fit The experiments were done in the time range of $t'_{max} \equiv 300$

$t'_{min} \equiv 0.0$

$ii \equiv 1 .. N'$ $tt_{ii} \equiv \frac{(ii - 1)}{(N' - 1)} \cdot (t'_{max} - t'_{min}) + t'_{min}$

$FIT_{ii} \equiv F_A(tt_{ii}, P)_1$ $RES \equiv augment(tt, FIT)$

$WRITEPRN(outfile) \equiv RES$

Summary of results: Wavelength $\lambda = 5.6 \cdot 10^{-7} \cdot m$

$\varepsilon_{N.a} = 0.8$ $\varepsilon_{T1.a} \equiv \varepsilon_{N.a}$

$\varepsilon_{N.e} \equiv \varepsilon_N - \varepsilon_{N.a}$ $\varepsilon_{N.e} = -0.073$ $\varepsilon_{T1.e} \equiv \varepsilon_{N.e}$

$\varepsilon_{T2.a} = 1.1$ [redacted] $= \cdot deg$

$\varepsilon_{T2.e} \equiv \varepsilon_{T2} - \varepsilon_{T2.a}$ $\varepsilon_{T2.e} = -0.708$ [redacted] $= \cdot deg$ These angle are yet to be found in the anisotropy part

$\varepsilon_{N3} = 2.845$

Global model parameters and some constants definitions:

$nm \equiv 10^{-9} \cdot m$

Observation(probe) wavelength: $\lambda \equiv 560 \cdot nm$

$K_t \equiv 1$ equllibrium constant. We postulate equivalence in energy from ground-state spectra data.

$N0_0 \equiv 1$ ground-state concentration. Really not important.

$\eta \equiv 0.1$ fraction of sample excited by the pump. Can be found from optical density, average power of the beam and sample thickness. In simulations it is used as a scaling factor to adjust for the observe signal intensity.

Rate constants in ps^{-1}:

$k_{nt} := \frac{1}{10}$ normat to tautomer

$k_{nn0} := \frac{1}{7000}$ normal to ground state

$k_{nn3} := \frac{1}{1000}$ normal to triplet

$k_{tt} := \frac{1}{230}$ tautomer to T2

$k_{t10} := \frac{1}{7000}$ tautomer to ground state

$k_{tn3} := \frac{1}{1000}$ tautomer or T2 to triplet

$k_{t20} := \frac{1}{7000}$ T2 to ground state

$D := \frac{1}{800} \cdot \frac{1}{6}$ rotational diffusion rate constatnt

The parameters that we are looking for are the absorption and extinction coefficients together with relative transition dipole angles.
These values are, in general, wavelength-dependant.

$\varepsilon_0 := 1$ ground-state absorption used as a reference value. We assume tautomers have similar absorption spectra.

For probe wavelength of $\lambda = 5.6 \cdot 10^{-7}$ m

Guesses for absorption coefficients

$\varepsilon_{N.a} := 0.8$

$\varepsilon_{N.e} := 1.4$

$\varepsilon_{N} := 2.2$

$\varepsilon_{T1.a} := 0.8$

$\varepsilon_{T1.e} := 1.4$

$\varepsilon_{T2.a} := 1.1$

$\varepsilon_{T2.e} := 1.3$

$\varepsilon_{T2} := 2.4$

$\varepsilon_{N3} := 2.10$

Angles for excited-state absorption dipoles relative to the ground-state transitions:

$\phi_{N.a} := \frac{\pi}{2}$ due to near C_{2v} symmetry

$\phi_{T1.a} := \frac{\pi}{2}$ due to near C_{2v} symmetry

$\phi_{T2.e} :=$ postulated to be different from N and T1

$\phi_{T2.a} := \frac{\pi}{2} - \phi_{T2.e}$ due to near C_{2v} symmetry

$\phi_{N3.a} := 0$

Fitting procedure for anisotropic parameters of hypocrellin A excited-state kinetics in octanol.

Initial conditions:

$$N_0 = K_t \cdot N0_o \cdot \frac{\eta}{K_t - 1} \qquad T1_0 = N0_o \cdot \frac{\eta}{K_t - 1}$$

$$T2_0 = 0 \qquad N3_0 = 0$$

where η is the fraction of population excited by the pump pulse.

For the ground state initial conditions will appear as:

$$N0_0 = K_t \cdot N0_o \cdot \frac{1 - \eta}{K_t - 1} \qquad T10_0 = N0_o \cdot \frac{1 - \eta}{K_t - 1}$$

$$T20_0 = 0$$

$$solution := \left\{ t1(t) = \frac{\%3\, N0o\, n\, K0}{1 + K0} \cdot n1(t) = \frac{n\, N0o\, \%2}{1 + K0} \cdot t2(t) = (-K0\, Kt\, \%3\, Kt20 - \%1\, Kt\, Kn3\, K0 + K0\, Kt\, \%3\, Knt + K0\, Kt\, \%3\, Kn10 + K0\, Kt\, \%3\, Kn3 + Kt23\, \%1\, Kt\, K0 - \%1\, Kt\, Kn10\, K0 - \%1\, Knt\, Kt\, K0 + \%1\, Kt\, Kt20\, K0 - Kt23\, K0\, Kt\, \%3 + Knt\, \%2\, Kt13 - \%1\, Knt\, Kt13 - Kt23\, Knt\, \%2 - \%1\, Knt\, Kt10 + Kt23\, \%1\, Knt + \%1\, Knt\, Kt20 + Knt\, \%2\, Kt10 + Knt\, \%2\, Kt - Knt\, \%2\, Kt20 - \%1\, Knt\, Kt)\, n\, N0o / ((Kt13 + Kt13\, K0 + Kt + Kt\, K0 + Kt10 + Kt10\, K0 - Kt20 - Kt20\, K0 - Kt23 - Kt23\, K0)(Kt20 + Kt23 - Kn3 - Knt - Kn10)) \right\}$$

$$\%1 := e^{(-(Kt23 + Kt20)\, t)}$$

$$\%2 := e^{(-(Kn3 + Knt + Kn10)\, t)}$$

$$\%3 := e^{(-(Kt13 + Kt + Kt10)\, t)}$$

$$N(t) = N_0 \cdot e^{-t \cdot (k_{nt} - k_{nn3} - k_{nn0})}$$

$$T1(t) = T1_0 \cdot e^{-t \cdot (k_{tt} - k_{tn3} + k_{t10})}$$

$$T2(t) = N0_o \cdot \eta \cdot \frac{\begin{aligned} & e^{-t \cdot (k_{tn3} - k_{t20})} \cdot \left[K_t \cdot k_{tt} \cdot (-k_{nn3} + k_{tn3} - k_{nn0} - k_{nt} - k_{t20}) \cdots \right. \\ & \left. + k_{nt} \cdot (-k_{tn3} - k_{t10} + k_{tn3} + k_{t20} - k_{tt}) \right] \cdots \\ & + e^{-t \cdot (k_{nt} - k_{nn3} - k_{nn0})} \cdot k_{nt} \cdot \left[k_{tn3} + k_{t10} + k_{tt} - (k_{tn3} + k_{t20}) \right] \cdots \\ & + e^{-t \cdot (k_{tt} + k_{tn3} - k_{t10})} \cdot K_t \cdot k_{tt} \cdot (k_{nn3} - k_{tn3} + k_{nn0} - k_{nt} - k_{t20}) \end{aligned}}{\left[k_{tn3} + k_{t20} - (k_{nt} - k_{nn3} + k_{nn0}) \right] \cdot (k_{tt} - k_{tn3} + k_{t10} - k_{t20} - k_{tn3}) \cdot (1 + K_t)}$$

$$N3(t) := \int_0^t \left(k_{nn3} \cdot N(tt) - k_{tn3} \cdot (T1(tt) - T2(tt)) \right) dtt - N3_0 = -\frac{7}{8} \cdot \eta \cdot \exp\left(\frac{-1}{875} \cdot t\right) - \frac{7}{8} \cdot \eta$$

$$N3(t) := \frac{-7}{8} \cdot \eta \cdot \exp\left(\frac{-1}{875} \cdot t\right) - \frac{7}{8} \cdot \eta$$

$$N0_{\Sigma}(t) := N(t) - T1(t) - T2(t) - N3(t)$$

$$P_{02.par}(t,\phi) := \frac{1}{9} - \frac{2}{45} \cdot \left(3 \cdot \cos(\phi)^2 - 1\right) \cdot e^{-6 \cdot D \cdot t}$$

$$P_{02.per}(t,\phi) := \frac{1}{9} - \frac{1}{45} \cdot \left(3 \cdot \cos(\phi)^2 - 1\right) \cdot e^{-6 \cdot D \cdot t}$$

$$\varepsilon_{0.par}(t) := \varepsilon_0 \cdot P_{02.par}(t,0) \qquad \varepsilon_{0.per}(t) := \varepsilon_0 \cdot P_{02.per}(t,0)$$

$$\varepsilon_{N.par}(t) := \varepsilon_{N.a} \cdot P_{02.par}(t,\phi_{N.a}) - \varepsilon_{N.e} \cdot P_{02.par}(t,0)$$

$$\varepsilon_{N.per}(t) := \varepsilon_{N.a} \cdot P_{02.per}(t,\phi_{N.a}) - \varepsilon_{N.e} \cdot P_{02.per}(t,0)$$

$$\varepsilon_{T1.par}(t) := \varepsilon_{T1.a} \cdot P_{02.par}(t,\phi_{T1.a}) - \varepsilon_{T1.e} \cdot P_{02.par}(t,0)$$

$$\varepsilon_{T1.per}(t) := \varepsilon_{T1.a} \cdot P_{02.per}(t,\phi_{T1.a}) + \varepsilon_{T1.e} \cdot P_{02.per}(t,0)$$

$$\varepsilon_{T2.par}(t,\phi_{T2.a},\phi_{T2.e}) := \varepsilon_{T2.a} \cdot P_{02.par}(t,\phi_{T2.a}) - \varepsilon_{T2.e} \cdot P_{02.par}(t,\phi_{T2.e})$$

$$\varepsilon_{T2.per}(t,\phi_{T2.a},\phi_{T2.e}) := \varepsilon_{T2.a} \cdot P_{02.per}(t,\phi_{T2.a}) - \varepsilon_{T2.e} \cdot P_{02.per}(t,\phi_{T2.e})$$

$$\varepsilon_{N3.par}(t) := \varepsilon_{N3} \cdot P_{02.par}\left(\frac{t}{S_{D.N3}},\phi_{N3.a}\right) \qquad \varepsilon_{N3.per}(t) := \varepsilon_{N3} \cdot P_{02.per}\left(\frac{t}{S_{D.N3}},\phi_{N3.a}\right)$$

$$A_{par}(t,\phi_{T2.a},\phi_{T2.e}) := -\varepsilon_{0.par}(t) \cdot N0_{\Sigma}(t) - \varepsilon_{N.par}(t) \cdot N(t) + \varepsilon_{T1.par}(t) \cdot T1(t) + \varepsilon_{T2.par}(t,\phi_{T2.a},\phi_{T2.e})$$

$$A_{per}(t,\phi_{T2.a},\phi_{T2.e}) := -\varepsilon_{0.per}(t)\cdot N0\,\Sigma(t) - \varepsilon_{N.per}(t)\cdot N(t) - \varepsilon_{T1.per}(t)\cdot T1(t) - \varepsilon_{T2.per}(t,\phi_{T2.a},\phi_{T2.e})$$

$$A_{mag}(t) := \frac{1}{3}\cdot A_{par}(t,\phi_{T2.a},\phi_{T2.e}) - \frac{2}{3}\cdot A_{per}(t,\phi_{T2.a},\phi_{T2.e})$$

We shall also verify, that the magic angle result is equvalent to using non-polarized light:

$$\varepsilon_N := \varepsilon_{N.a} - \varepsilon_{N.e} \qquad \varepsilon_{T1} := \varepsilon_{T1.a} - \varepsilon_{T1.e} \qquad \varepsilon_{T2} := \varepsilon_{T2.a} - \varepsilon_{T2.e}$$

$$A(t,\varepsilon_N,\varepsilon_{T1},\varepsilon_{T2},\varepsilon_{N3},\eta) := \frac{1}{9}\cdot(\varepsilon_0\cdot N0\,\Sigma(t) - \varepsilon_N\cdot N(t) - \varepsilon_{T1}\cdot T1(t) \ldots + \varepsilon_{T2}\cdot T2(t) - \varepsilon_{N3}\cdot N3(t))$$

Now construct anisotropy:

$$r(t,\phi_{T2.a},\phi_{T2.e}) := \frac{A_{par}(t,\phi_{T2.a},\phi_{T2.e}) - A_{per}(t,\phi_{T2.a},\phi_{T2.e})}{A_{par}(t,\phi_{T2.a},\phi_{T2.e}) + 2\cdot A_{per}(t,\phi_{T2.a},\phi_{T2.e})}$$

$$t,\varepsilon_{N.a},\varepsilon_{T1.a},\varepsilon_{T2.a},\varepsilon_{N.e},\varepsilon_{T1.e},\varepsilon_{T2.e},\varepsilon_{N3},\phi_{T2.a},\phi_{T2.e}$$

The results below are very long and truncated to fit page as their exact form is not of great importance.

Here we display reluts explicitly to obtain functional form for anisotropy

now we can define fitting function based on the result above

$$rr(t,\varepsilon_{N.a},\varepsilon_{T1.a},\varepsilon_{T2.a},\varepsilon_{N.e},\varepsilon_{T1.e},\varepsilon_{T2.e},\varepsilon_{N3},\phi_{T2.a},\phi_{T2.e}) := \frac{-2}{5}\cdot(-4\cdot\exp\left(\frac{-221}{40250}\cdot t\right)\cdot\varepsilon_{T1.e} - 2\cdot\exp\left(\frac{-2}{402}\right.$$

Next we approach fitting ***anisotropy data***. Constants $\varepsilon_N, \varepsilon_{T2}, \varepsilon_{N3}$ are obtained from the magic angle fit.

But in our model we postulate that

$\varepsilon_{T1.a} \equiv \varepsilon_{N.a}$ $\varepsilon_{T1.e} \equiv \varepsilon_{N.e}$ Hence $\varepsilon_N \equiv \varepsilon_{T1}$ So, do some substitutions:

$$rr(t, \varepsilon_{N.a}, \varepsilon_{T2.a}, \varepsilon_{N.e}, \varepsilon_{T2.e}, \phi_{T2.a}, \phi_{T2.e}) \equiv rr(t, \varepsilon_{N.a}, \varepsilon_{N.a}, \varepsilon_{T2.a}, \varepsilon_{N.e}, \varepsilon_{N.e}, \varepsilon_{T2.e}, \varepsilon_{N3}, \phi_{T2.a}, \phi_{T2})$$

$$rr(\alpha_i, \phi_{T2.a}, \phi_{T2.e}) - rr(\alpha_i, \varepsilon_{N.a}, \varepsilon_{T2.a}, \varepsilon_{N.e}, \varepsilon_{T2.e}, \phi_{T2.a}, \phi_{T2.e})$$

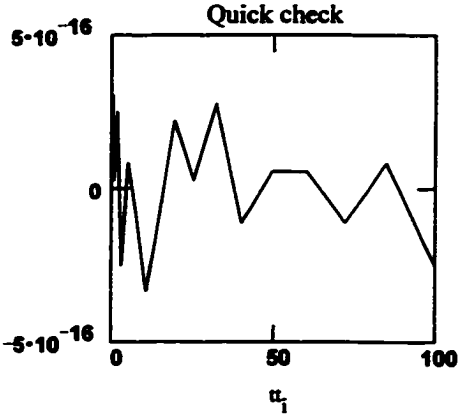

To minimize uncertainty in fitting space, it's time to use already familiar relations:

assume $\varepsilon_N, \varepsilon_{T2}, \varepsilon_{N.a}, \varepsilon_{T2.a}, \varepsilon_{N.e}, \varepsilon_{T2.e}$

given

$\varepsilon_N \equiv \varepsilon_{N.a} + \varepsilon_{N.e}$ $\varepsilon_{T2} \equiv \varepsilon_{T2.a} + \varepsilon_{T2.e}$

$$\text{find}(\varepsilon_{N.e}, \varepsilon_{T2.e}) \rightarrow \begin{pmatrix} 1.768 - \varepsilon_{N.a} \\ 1.908 - \varepsilon_{T2.a} \end{pmatrix}$$

ε_{N3} was already determined during the magic angle fit

Substitution of emission coefficients in $r(t,\varepsilon_{N.a},\varepsilon_{T2.a},\varepsilon_{N.e},\varepsilon_{T2.e},\phi_{T2.a},\phi_{T2.e})$ gives the final fitting function:

After substitutions: $\varepsilon_{N.e}$ by $\varepsilon_N - \varepsilon_{N.a}$

$\varepsilon_{T1.a}$ by $\varepsilon_{N.a}$

$\varepsilon_{T1.e}$ by $\varepsilon_N - \varepsilon_{N.a}$

$\cos(\phi_{T2e})$ by $\cos\phi_{T2e}$ use constant for faster procesing

and collecting on exponentials we define final fitting anisotropy function

$$r'(t,\varepsilon_{N.a},\varepsilon_{T2.a},\cos\phi_{T2e}) := \frac{2}{5}\cdot\exp\left(\frac{-1}{800}\cdot t\right)\cdot\left[-4\cdot\varepsilon_{T2} - 12\cdot\varepsilon_{T2.a} - 12\cdot\cos\phi_{T2e}^{2}\cdot\varepsilon_{T2.a} - 7\cdot\varepsilon_{N3} - 12\cdot\cos\phi_{T2}\right.$$

Here we evaluate fitting functional

$$\begin{bmatrix} r'(t,p1,p2,p3) \\ \frac{d}{dp1}r'(t,p1,p2,p3) \\ \frac{d}{dp2}r'(t,p1,p2,p3) \\ \frac{d}{dp3}r'(t,p1,p2,p3) \end{bmatrix} \rightarrow$$

$$r'(t,p1,p2,p3) \rightarrow \frac{2}{5}\cdot\exp\left(\frac{-1}{800}\cdot t\right)\cdot\left[-4\cdot\varepsilon_{T2} - 12\cdot p2 - 12\cdot p3^{2}\cdot p2 - 7\cdot\varepsilon_{N3} - 12\cdot p3^{2}\cdot(\varepsilon_{T2} - p2) - 1\right]\cdot\exp\left(\frac{-1}{875}\cdot t\right)$$

$$\left(-1 - 8\cdot\varepsilon_{T2}\right.$$

Using these results we define our fitting functional (it's exact form is not of interest):

$$p_1, p_2, p_3$$

$$F_r(t,p) = \frac{2}{5}\cdot\exp\left(\frac{-1}{800}\cdot t\right)\cdot\frac{-4\cdot\varepsilon_{T2} - 12\cdot p_2 - 12\cdot p_3^{\,2}\cdot p_2 - 7\cdot\varepsilon_{N3} - 12\cdot p_3^{\,2}\cdot\varepsilon_{T2} - p_2 - 1\cdot\exp\left(\frac{1}{875}\cdot t\right) - \frac{2}{5}\cdot\exp\left(\frac{-1}{800}\cdot t\right)\cdot\frac{}{-1 - 8\cdot\varepsilon_{T2}}}{-1 - 8\cdot\varepsilon_{T2}} \frac{2}{5}\cdot\exp\left(\frac{-1}{800}\cdot t\right)\cdot\frac{}{-1 - 8\cdot\varepsilon_{T2}} \frac{2}{5}\cdot\exp\left(\frac{-1}{800}\cdot t\right)\cdot\frac{-24\cdot p_3\cdot p_2 - 24\cdot p_3\cdot\varepsilon_{T2}}{-1 - 8\cdot\varepsilon_{T2}}$$

Define data to fit and the fitting points:

$N \equiv 20$ Number of points in fit The experiments were done in the time range of $t_{max} \equiv 100$

$parN = 3$ Number of parameters $t, \varepsilon_{N.a}, \varepsilon_{T2.a}, \cos\phi_{T2e.sq}$

Select fit points

$i \equiv 1..N$ $tt_i \equiv \frac{(i-1)^3}{(N-1)^3}\cdot t_{max}$ we need more points where fast change occurs

Define data to be fitted:

$$A_{exp.par}(t) := 0.035 \cdot \left(1 - \exp\left(\frac{-t}{10}\right)\right) + 0.012 \cdot \left(1 - \exp\left(\frac{-t}{230}\right)\right) + 0.036 \cdot \exp\left(\frac{-t}{50000}\right)$$

$$A_{exp.per}(t) := 0.02 \cdot \exp\left(\frac{-t}{1591}\right) + 0.14 \cdot \exp\left(\frac{-t}{50000}\right)$$

$$r_{exp_i} := \frac{A_{exp.par}(tt_i) - A_{exp.per}(tt_i)}{A_{exp.par}(tt_i) + 2 \cdot A_{exp.per}(tt_i)}$$

From the isotropic (magic angle) fit we obtain

$$P := \begin{pmatrix} 1.768 \\ 1.908 \\ 1.823 \\ 0.096 \end{pmatrix} \qquad \varepsilon_N := P_1 \qquad \varepsilon_{N3} := P_3 \qquad \varepsilon_{T2} := P_2 \qquad \eta := P_4$$

Initial guesses for the vector of parameters to be fitted:

$$\begin{pmatrix} \varepsilon_{N.a} \\ \varepsilon_{T2.a} \\ \cos\phi_{T2e} \end{pmatrix} := \begin{pmatrix} 0.945 \\ 0.952 \\ 0.703 \end{pmatrix} \qquad P_{guess} := \begin{pmatrix} \varepsilon_{N.a} \\ \varepsilon_{T2.a} \\ \cos\phi_{T2e} \end{pmatrix} \qquad P_{guess} = \begin{pmatrix} 0.945 \\ 0.952 \\ 0.703 \end{pmatrix} \qquad \begin{pmatrix} \varepsilon_N \\ \varepsilon_{T2} \\ \varepsilon_{N3} \\ \eta \end{pmatrix} = \begin{pmatrix} 1.768 \\ 1.908 \\ 1.823 \\ 0.096 \end{pmatrix}$$

Actual fit is here: $PP := genfit(tt, r_{exp}, P_{guess}, F_r)$

Fit results:

$$PP = \begin{pmatrix} 0.945 \\ 0.953 \\ 0.705 \end{pmatrix} \qquad r_{fit_i} := F_r(tt_i, PP)$$

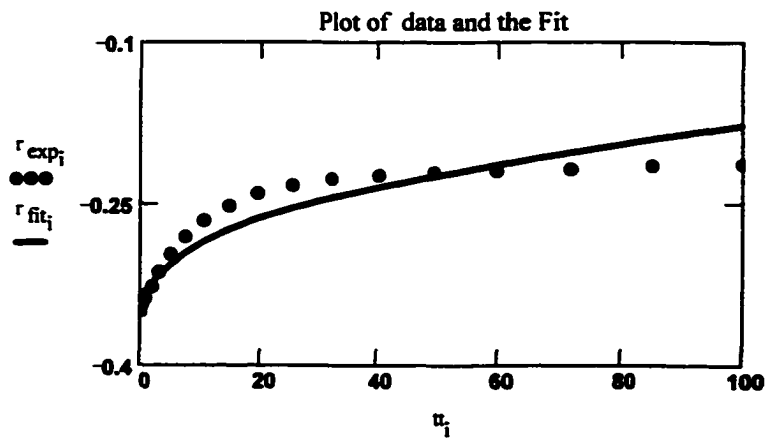

Finally, we obtain $\begin{pmatrix} \varepsilon_{N.a} \\ \varepsilon_{T2.a} \\ \cos\phi_{T2e} \end{pmatrix} = PP$ or $\begin{pmatrix} \varepsilon_{N.a} \\ \varepsilon_{T2.a} \\ \cos\phi_{T2e} \end{pmatrix} = \begin{matrix} 0.945 \\ 0.953 \\ 0.705 \end{matrix}$

$\phi_{T2.e} := \operatorname{acos}(PP_3)$

$\phi_{T2.e} = 45.185 \cdot deg$ $\quad \phi_{T2.a} := \frac{\pi}{2} - \phi_{T2.e}$ $\quad \phi_{T2.a} = 135.185 \cdot deg$

$\varepsilon_{N.e} := \varepsilon_N - \varepsilon_{N.a}$ $\quad \varepsilon_{T2.e} := \varepsilon_{T2.a} - \varepsilon_{T2}$ $\quad \varepsilon_{T2.a} = 0.953$ $\quad \varepsilon_{T2.e} = 0.955$

$\varepsilon_{T1.e} := \varepsilon_{N.e}$ $\quad \varepsilon_{T1.a} := \varepsilon_{N.a}$ $\quad \varepsilon_{T1} := \varepsilon_N$

Summary of results: Wavelength $\lambda = 5.6 \cdot 10^{-7} \cdot m$

$\varepsilon_{N.a} = 0.945$ $\quad \varepsilon_{T1.a} \equiv \varepsilon_{N.a}$ $\quad \varepsilon_{T1.a} = 0.945$ $\quad \varepsilon_{N3} = 1.823$

$\varepsilon_{N.e} = 0.823$ $\quad \varepsilon_{T1.e} \equiv \varepsilon_{N.e}$ $\quad \varepsilon_{T1.e} = 0.823$

$\phi_{T2.e} = 45.185 \cdot deg$

$\phi_{T2.a} = 135.185 \cdot deg$

Output the fit results to data file:

$N' \equiv 100$ Number of points in fit The experiments were done in the time range of $t'_{max} \equiv 300$

$ii \equiv 1 .. N'$ $\quad tt_{ii} := \frac{(ii - 1)}{(N' - 1)} \cdot (t'_{max} - t'_{min}) + t'_{min}$ $\quad t'_{min} \equiv 0.0$

$FIT_{ii} := F_T(tt_{ii}, PP_1)$ $\quad RES := \operatorname{augment}(tt, FIT)$

WRITEPRN(outfile) := RES

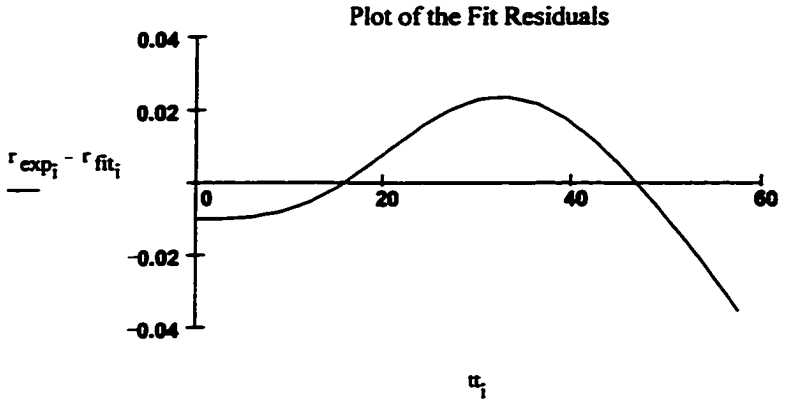

Fit quality:

$$Q = \frac{\sqrt{\sum_i \left| \frac{r_{exp_i} - r_{fit_i}}{r_{exp_i}} \right|}}{N - parN}$$

$Q = 0.065$

Global model parameters:

Observation(probe) wavelength: $\lambda \equiv 560 \cdot nm$ $\quad nm \equiv 10^{-9} \cdot m$

$K_t \equiv 1$ equllibrium constant. We postulate equivalence in energy from ground-state spectra data.

$N0_0 \equiv 1$ ground-state concentration. Really not important.

$\eta \equiv 0.1$ fraction of sample excited by the pump. Can be found from optical density, average power of the beam and sample thickness. In simulations it is used as a scaling factor to adjust for the observe signal intensity.

Rate constants in ps^{-1}:

$k_{nt} := \frac{1}{10}$ normat to tautomer

$k_{nn0} := \frac{1}{7000}$ normal to ground state

$k_{nn3} := \frac{1}{1000}$ normal to triplet

$k_{tt} := \frac{1}{230}$ tautomer to T2

$k_{t10} := \frac{1}{7000}$ tautomer to ground state

$k_{tn3} := \frac{1}{1000}$ tautomer or T2 to triplet

$k_{t20} := \frac{1}{7000}$ T2 to ground state

$D := \frac{1}{800} \cdot \frac{1}{6}$ rotational diffusion rate constatnt

The parameters that we are looking for are the absorption and extinction coefficients together with relative transition dipole angles. These values are in general wavelength-depenc

$\varepsilon_0 := 1$ ground-state absorption used as a reference value. We assume tautomers have similar ab spectra.

For probe wavelength of $\lambda = 5.6 \cdot 10^{-7} \cdot m$

$\varepsilon_{N.a} := 0.8$

$\varepsilon_{N.e} := \varepsilon_N - \varepsilon_{N.a}$ $\phi_{N.a} := \frac{\pi}{2}$ due to near C_{2v} symmetry

$\varepsilon_{T1.a} := \varepsilon_{N.a}$ $\phi_{T1.a} := \frac{\pi}{2}$ due to near C_{2v} symmetry

$\varepsilon_{T1.e} := \varepsilon_N - \varepsilon_{N.a}$

$\varepsilon_{T2.a} := 1.1$ $\phi_{T2.e} := \frac{\pi}{8}$ $\phi_{T2.a} := \frac{\pi}{2} - \phi_{T2.e}$ $S_{D.N3} := 1$

$\varepsilon_{T2.e} := \varepsilon_{T2} - \varepsilon_{T2.a}$ $\phi_{N3.a} := 0$ this value is just a guess. It shouldn't really influence the result

CHAPTER V. EXPLORING GROUND-STATE HETEROGENEITY OF HYPERICIN AND HYPOCRELLIN A AND B: DYNAMIC AND 2D ROESY NMR STUDY

A paper submitted to the Journal of American Chemical Society

A. V. Smirnov[1], D. B. Fulton[2], A. Andreotti[2], and J. W. Petrich[1]

ABSTRACT

A NMR study was conducted on the antiviral and antitumor agents, hypericin and hypocrellin A and B, whose activity is light induced. Elucidation of the conformational/tautomeric properties of these polycyclic quinones is important for interpreting their photophysical behavior in the excited state. Evidence for interconversion between ground-state tautomers or other conformational isomers was sought in temperature-dependent ^{1}H NMR and 2D-ROESY studies. For hypericin and hypocrellin B, only one ground-state species is observed. For hypocrellin A, however, three species are significantly populated in the ground state due to the higher flexibility of the carbon skeleton. In the latter case dynamic NMR simulation were performed to obtain kinetic and thermodynamic parameters for the sequential interconversion occurring between the three species. The implications of these results for the interpretation of the light-induced

---

[1] Department of Chemistry, Iowa State University

[2] Department of Biochemistry, Biophysics and Molecular Biology, Iowa State University

primary processes in these systems are discussed.

INTRODUCTION

The polycyclic quinones hypericin and hypocrellin (Figure 5.1) exhibit light-induced antitumor and antiviral activity [1-4]. Consequently, these compounds have been the subjects of numerous ultrafast and steady-state spectroscopic studies with the goal of elucidating the energetic and dynamic properties of their electronic excited states [5-24]. The corresponding properties of the electronic ground state, though important for interpreting the photophysical data, have, apart from some exceptions [27-31], received relatively little attention.

Each of the compounds has a twisted carbon skeleton resulting from the steric strain induced by substituents in the "bay" regions (positions 3, 4 and 10, 11 for hypericin, Figure 5.1a, and positions 6, 7 and 1, 12 for hypocrellin, Figure 5.1c) of the polycyclic ring systems. In addition, for hypocrellin A, the axial chirality arising from such twisting, combined with the chirality of the asymmetric carbon atoms, gives rise to diastereomerism. For some members of the perylenequinone family it has been possible to isolate both diastereomers and to observe their thermal interconversion [31]; but, until now, evidence for interconversion among the hypocrellin A conformers has not been observed.

Hypericin and the hypocrellins are capable of intramolecular hydrogen bond formation so that keto/enol tautomerism is possible. It can be shown through calculations [32,33] and by experimental observation [31] that only certain tautomers are sufficiently stable to be significantly populated at room temperature. For example, in a nonionizing environment hypericin in the ground state is thought to exist as only one tautomer, the so-called normal form [32] (Figure 5.1a). On the other hand, X-ray [34] and photophysical data [9, 15] suggest that hypocrellin A in the ground state exists in at least two tautomeric

forms (Figures 1c and 1d).

In this article we present an investigation of the ground-state tautomeric and conformational isomers of hypericin and hypocrellin and their temperature-dependent interconversion processes.

EXPERIMENTAL

Hypericin and hypocrellin A and B were purchased from Molecular Probes, Inc. and used without further purification. ^{1}H-NMR spectra were measured in anhydrous DMSO-d_6 and acetone-d_6 (Cambridge Isotope Laboratories) with a Bruker DRX-500 spectrometer. The concentrations were *ca.* 2 mg cm^{-3}. Chemical shifts are reported relative to 0.05% internal Me_4Si. Cross-peaks in 2D ROESY spectra as well as values reported in [31] were used in signal assignment.

1D ^{1}H NMR spectra of hypocrellin A and B were recorded at 293, 298, 308, and 318 K in DMSO and 240, 250, 260, 268, 273, 288, 298, and 313 K in acetone. The lineshapes of spectra below 268 K appeared to be in the slow exchange regime. Two-dimensional ROESY data were obtained at 268 K in acetone for two spectral regions: -2.0 to 18.0 ppm and 15.3 to 16.6 ppm.

For hypericin, 1D ^{1}H NMR spectra were recorded at 298, 313, 323, and 333 K in DMSO and 240, 268, 273, 298, and 313 K in acetone. 2D ROESY data were obtained at 298 K in acetone for the spectral range from -2.0 to 18.0 ppm. Hypericin samples were found to decompose upon prolonged exposure to ambient light and were kept in the dark as much as possible.

The 2D-ROESY spectra were acquired at 499.87 MHz with a continuous spin-lock during mixing (RF power 2.5 kHz, mixing time 300 ms) and the carrier frequency set at 8.0 ppm. Typically 340-512 complex FIDs of size 4096 were collected (10 kHz spectral width,

relaxation delay 2.0 s, 8 scans/FID) employing the States-TPPI method [38] for phase-sensitive detection in F1. The data were Fourier transformed, zero-filled, and apodized with a 90° shifted sine-bell squared function to yield 4096 x 512 real data points. The baseline of the 2D spectrum was corrected in both dimensions with a fifth degree polynomial fitting algorithm. In the second hypocrellin ROESY experiment (over a spectral range of 15.3 to 16.6 ppm)) offset and sweepwidth were adjusted to obtain a high-resolution spectrum of the down-field hydroxyl region. The spin-lock frequency was set up-field from the region of interest to avoid coherent (TOCSY-type) transfer artifacts [39].

Dynamic NMR simulations were performed with the program XNMR written by Uwe Seimet, Germany (available at ftp://acp5.chemie.uni-kl.de/pub/xnmr) and Mex written by Alex Bain, McMaster University (for information see http://www.chemistry.mcmaster.ca/faculty/bain). The two simulation programs produced identical results. The spectrum at 240 K was treated as having a zero interconversion rate for every pair of species. This was necessary to estimate chemical shifts and line widths at the slow exchange limit, which were fixed parameters in the simulations.

RESULTS AND DISCUSSION

A. Hypericin

The aromatic skeleton of hypericin adopts a nonplanar, twisted geometry due to the steric repulsion between the two methyl groups. This geometry retains a C_2 symmetry axis and magnetic equivalence of the corresponding protons in the upper and the lower part of the molecule (Figure 5.1a), resulting in a rather simple NMR spectrum. However, analysis of the NMR data was complicated by the presence of impurities in the commercially available material. The signals from impurities, water and the partially deuterated solvent

molecules were discriminated on the basis of their relative integrals and the expected values of their chemical shifts.

The ^{1}H NMR signals were assigned mostly based on the values of the chemical shifts (Table 5.1). We note that two methyl resonances were shifted considerably to the low field (2.75 ppm) as a consequence of anisotropic deshielding by the polyaromatic system in combination with the significant steric hindrance.

The primary goal of our NMR study of hypericin was to obtain experimental verification of the species populating the hypericin ground-state, which may consist of at least six non-ionized tautomeric species [32]: the normal form (Figure 5.1a); two monotautomers, arising from the transfer of one proton; and three double tautomers (e.g., Figure 5.1b), arising from the transfer of a proton at the "top" and the "bottom" of the molecule. One of these double tautomers, in which the proton is transferred from opposite sides of the molecule, does correspond to a minimum on the potential energy surface [32].

We collected ^{1}H-NMR spectra in the temperature range from 240 to 333 K in DMSO and acetone, solvents of different viscosity and polarity. Our attention was directed to the aromatic and very low-field (13-14 ppm) regions of the spectra where tautomerization processes are expected to be the most evident. In the aromatic region of the spectrum we observed two strong singlets at 6.6 and 7.4 ppm each flanked by a number of weaker satellites (Figure 5.2). In DMSO over the temperature range 298 to 333 K no lineshape coalescence typical of an exchanging system was observed. The temperature dependence of the satellite chemical shifts appeared to be either negligible or about an order of magnitude greater than that of the main components (from 6.63 ppm at 298 K to 6.40 ppm at 333 K). In addition, a small peak emerged from the shoulder of the aromatic hydrogen signal at 7.4 ppm, shifting to lower field as the temperature increased. By carefully overlaying and comparing the data obtained at various temperatures for this

spectral region we concluded that the observed changes in the NMR spectra were due to impurities and to the temperature dependence of the chemical shifts and linewidths of hypericin aromatic signals. We conclude that this line narrowing arises from the lower viscosity of DMSO at higher temperatures and not from an increased interconversion rate among possible tautomers. Consistent with this conclusion is that as the temperature is lowered to just above the freezing point of DMSO, and even lower (240 K) in acetone, no substantial increase in the line broadening of either aromatic or *peri*-hydroxyl signals was observed.

Hypericin possesses three pairs of non-equivalent phenolic hydroxyls in its most stable tautomeric form, the "normal" form (Figure 5.1a). In DMSO, the ^{1}H NMR signal of the bay hydroxyls was observed as a broad line in the expected region (8.1-8.3 ppm) that shifted slightly to higher field as the temperature increased. On the other hand, another pair of relatively narrow lines were observed at very low field (14.08 and 14.73 ppm at 298 K) and exhibited almost no chemical shift temperature dependence, attributes indicative of intramolecular hydrogen bonding [40]. These lines were assigned to the *peri*-hydroxyls (positions 1, 6, 8, 13 (Figure 5.1a)).

We conclude that the ground state of hypericin at temperatures as high as 333 K is represented by a single tautomer. Based on the x-ray data [36,37] and the results of *ab initio* quantum mechanical calculations [32], the structure of this tautomer is given by Figure 5.1a. As will be shown below, this is in contrast to what is observed for hypocrellin A.

To assist in the assignment of the low-field phenolic and aromatic signals of hypericin a 2D ROESY (rotating-frame Overhauser enhancement spectroscopy) NMR spectrum [39,41,42] was acquired in DMSO at 298K (Figure 5.3). The ROESY experiment has two advantages over NOESY [43] for this study: the magnitude of rotating-frame cross-

relaxation is favorable for molecules of this size, and ROE cross-peaks are readily distinguished from chemical exchange or *J*-correlated cross-peaks by their negative phase relative to the diagonal signals. Both positive- and negative-phase signals can be observed in the ROE experiment. In the absence of TOCSY and HOHAHA artifacts, positive-phase signals indicate a chemical or a conformational exchange process in which the proton changes its chemical shift (i.e., its environment). Negative-phase signals arise from the interactions of protons, in close proximity, within the molecule (i.e., the same conformational or tautomeric species).

The aromatic signal at 7.4 ppm (assigned to 9-H and 12-H) is correlated to the methyl singlet at 2.75 ppm *via* an intense negative ROE cross-peak, whereas its neighbor at 6.6 ppm (2-H and 5-H) has no cross-peaks at all (Figue 3). Due to their proximity to the bay hydroxyl groups, protons 9-H and 12-H are deshielded relative to protons 2-H and 5-H. This is because hydroxyl groups are much stronger π-donors than methyl groups.

It is more difficult to assign the nonequivalent intramolecular hydrogen-bonding hydroxyls (in the 14-15 ppm region) since neither of these signals has negative cross-peaks with the aromatic or methyl hydrogens

Although DMSO bears no labile hydrogens, significant hydrogen chemical exchange among all three types of hydroxyls was evident from positive cross-peaks in the ROESY spectrum. If we assume that this exchange, although perhaps mediated by traces of water in the solvent, is intramolecular, then it is reasonable to expect that the proton exchange rate among hydroxyls in close proximity will be greater than for those that are further apart. Hence, positive cross-peaks in the ROESY spectrum should a have higher volume for correlation between 1-OH and 3-OH (and, by symmetry 6-OH and 4-OH) as compared to 13-OH and 3-OH (and, by symmetry, 8-OH and 4-OH). Based on this consideration, the peak at 14.08 ppm can be assigned to 1-OH and 6-OH and that at 14.73

ppm to 8-OH and 13-OH.

B. Hypocrellin A

i. Ground-State Conformational Isomers

The room-temperature ^{1}H NMR spectrum of hypocrellin A in acetone is almost identical to that which has been previously reported [31]. However, we observe that lowering the temperature to 268 K results in significant changes and increased spectral complexity, especially in the low and medium-field spectral regions. Similar changes were observed at low temperature in DMSO but with considerably broader lines. As in the case of hypericin, the analysis was slightly complicated by the presence of impurities, the most abundant of which is hypocrellin B. By changing temperatures and by using 2D ROESY, most of these ambiguities were, however, successfully resolved.

The ^{1}H NMR spectrum of hypocrellin A is more complex than that of hypericin because of its lower symmetry and, as will be seen, the interconversion between conformational isomers and tautomeric forms. The presence of two asymmetric centers (C-16 and C-14) in combination with the helical topology of the aromatic ring system, permits hypocrellin to exist in two possible forms, denoted *gauche* and *anti* in Figure 5.4. The two conformers differ principally in the configuration of the invertible seven-membered ring fragment. The acetyl group attached to C-16 is expected to be sterically restricted in its rotation about the C(16)–C(17) σ-bond, especially at low temperature. If the interconversion among the conformers is slow on the NMR time-scale, peak broadening or even splitting will be observed due to differential anisotropic deshielding by the aromatic ring system and by the restricted acetyl's carbonyl group. In addition, each of the conformers can undergo keto-enol type tautomerization (Figures 1c and 1d). Tautomeric interconversion will affect the hydroxyl NMR signals directly, and may

indirectly perturb the chemical shifts of other protons *via* changes in the conjugation of the polycyclic ring system.

We observed nonequivalence of the aromatic and hydroxy protons despite the large distance to the acetyl group, which acts as the asymmetry-inducing moiety. Several peaks show additional splittings due to conformer/tautomer interconversion processes, as is evident in the temperature-dependent and ROESY data.

In spectra recorded in acetone at 268 K, we observe a group of six doublets in the aliphatic region each with an identical geminal coupling constant but with differing intensities (Figure 5.5). Among this group are three pairs of doublets, each of comparable intensity, that are correlated by negative ROESY cross-peaks (Figure 5.6). These pairs of doublets are attributed to the methylene group (13-H_a and 13-H_b, Figure 5.4) of the seven-membered ring appearing at different chemical shifts due to slow interconversion among multiple conformations. The relationship among these signals is revealed by exchange (positive) ROESY cross-peaks. The two strongest doublets (centered at 3.43 ppm and 2.65 ppm) of similar intensity have exchange correlations to two weaker ones (centered at 2.75 ppm and 3.65 ppm, respectively). In addition, the latter doublet has another pair of exchange correlations to doublets centered at 3.60 and 2.50 ppm, respectively, which are of intermediate intensity among the three pairs. *In the ground state, three significantly populated conformational species (A, B, C) are therefore involved in an interconversion process (A⇌B⇌C) in which there is no appreciable interconversion between species A and C.* At 300 K, the ground state population is 60.6% A, 29.4% B, and 10% C.

A similar three-site exchange pattern is observed involving singlets at 3.8 (A), 4.8 (B) and 5.8 (C) ppm, and is assigned to the methyne proton 16-H (Figure 5.7). Their relative intensities, however, only qualitatively follow the same pattern as for the 13-H doublets: accurate intensity measurements in this region of the spectrum were difficult due

to overlapping signals from impurities.

In a separate ROESY experiment with a spectral window covering the low-field (hydroxyl) part of the spectrum (Figures 8 and 9) we observed strong positive cross-peaks between pairs of singlets at 16.12, 16.20 ppm (A) and 16.48, 16.40 ppm (B), respectively as well as between the latter singlets and a pair at 16.13, 16.04 ppm (C, which partially overlaps peak A), again indicating an exchanging system of type A⇌B⇌C. The order of the labels A, B, and C relative to the 13-H methylenes was deduced from the relative intensities of the peaks.

As further evidence of interconversion between conformers, a multiplet at about 6.8 ppm (due to aromatic protons 2-H and 5-H) coalesces to the broadened singlet as the temperature is raised to 313 K. This multiplet has negative cross-peaks to another strong multiplet at 4.2 ppm due to the nearby methoxy protons. (Figure 5.7)

The 15-H methyl and 18-H (acetyl) methyl peaks also exhibit evidence of conformational exchange. Each methyl is observed at two chemical shifts (1.5 and 1.6 ppm for 15-H, and 1.9 and 1.3 ppm for 18-H) correlated by positive cross-peaks (Figure 5.10). In both cases, the downfield peak had much greater intensity. The observation of distinct conformational species for the acetyl methyl confirms that its position is sterically hindered.

Having a general picture of the dynamic equilibrium of this system, we now describe the specific conformers corresponding to species A, B, and C. The cross-peak pattern in the ROESY data shows that the chemical shift order of the 13-H_a and 13-H_b methylene doublets is reversed upon conversion from the A to the B species, and is again reversed on conversion to the C species (Figure 5.6). Inspection of Figure 5.4 shows that protons 13-H_a and 13-H_b interchange their lateral distance to the polycyclic ring system and to the acetyl group (denoted as Ar'Ac) on conversion between the *gauche* and *anti*

diastereomers. It is reasonable to expect that the component of the chemical shifts of the doublets due to anisotropic deshielding will also be reversed in the *gauche* and *anti* forms. Hence, we conclude that each step in the sequence A⇌B⇌C includes a *gauche-anti* conformational change. Next, we note that in the *gauche* form the methyl group attached to C-15 is in the *anti* position to 13-H_b whereas in the *anti* form it is equidistant to both 13-H_a and 13-H_b (Figure 5.4). A negative cross-peak to the methyl signal at 1.7 ppm is observed for only one of the doublets of species A (centered at 3.43 ppm) (see Figure 5.10). We conclude that species A and C are *gauche* conformers, B is an *anti* conformer, and the geminal doublets may be stereospecifically assigned as given in Table 5.2.

ii. Ground-State Tautomers

Referring now to the hydroxyl region of the spectrum, a change in chemical shift order was observed between species A and B but not between B and C (see Figure 5.9 and Table 5.2). Given the distance from the flexible portion of the seven-membered ring to the hydroxyls, it is unlikely that the *anti/gauche* diastereomerism is influencing these shifts. Rather, the dominating factor is expected to be hydrogen bond strength, *i.e.*, the tautomeric state. Therefore it is likely that during the first (but not the second) conversion step in the A⇌B⇌C system there is a change in tautomeric state accompanied by a change in the aromatic structure (conjugation) of the polycyclic system. This would explain the change in the order of chemical shifts of exchanging hydroxyls and the deshielding of methylene protons 13-$H_{a,b}$ and methyne proton 16-H in B as compared to A (Figure 5.8).

Based on the observation from x-ray crystallography [35] that the double tautomer of hypocrellin is the form isolated, we propose that the most populated form (A) of hypocrellin is the *gauche* diastereomer of the "double" tautomer. The *anti* diastereomer of

the "double" tautomer is apparently not sufficiently populated to be observed under our experimental conditions. This is plausible since such a species would be destabilized by the π-bond and acetyl oxygen lone pair interactions, and would undergo rapid double-proton transfer to the "normal" tautomer (B).

These conclusions are also consistent with the observation of only two exchanging species for the 15-H and 18-H methyls (Figure 5.10), since their shifts are not expected to be influenced by the tautomeric state, *i.e.*, states A and C (both in the *gauche* conformation) are indistinguishable with respect to the methyls.

iii. Simulating the Proposed Model for Hypocrellin A

To validate our model of interconverting tautomers/conformers we performed dynamic NMR simulations of hypocrellin A spectra in the temperature range from 268 to 300 K. In performing these simulations, we assumed that the NMR line widths (in the absence of exchange broadening), the enthalpy and entropy of reaction, and the activation enthalpy and entropy, all had negligible temperature dependence. A temperature-independent line width corresponding to an effective relaxation time T_2^* equal to 0.08 s was assumed for each type of proton. In addition, it was assumed that the interconversion rates at 240 K were negligible and the chemical shifts at this temperature were taken to be the slow exchange-limited values. In addition, our simulations did not account for the relative differences in temperature dependence of resonance frequencies for the protons involved. We believe this to be a reasonable assumption as the exchange processes studied occur among the hydrogen atoms of similar chemical environments. The relative population of species A, B and C at each temperature above 268 K had to be estimated because the spectra at these temperatures had intermediate-exchange lineshapes and could not be reliably integrated. This was done by extrapolation of the equilibrium constant to higher temperatures, once $\Delta H°$ and $\Delta S°$ for each process had been calculated by linear

regression analysis from the van't Hoff equation:

$$\ln K = -\Delta G^\circ / RT = -\Delta H^\circ / RT + \Delta S^\circ / R$$

The equilibrium constants K at temperatures 240, 250, 260, and 268 K were obtained from ratios of the integrals of methylene signals in the 2.45-2.90 ppm range, where interference with water and other impurities is minimal (Table 5.4).

While the relative population of A, B and C were held fixed at the calculated values, the interconversion rates from A to B and from B to C where allowed to vary until qualitative agreement between simulated and experimental line shape was achieved for each temperature (Figure 5.5). The same set of parameters was used to simulate data for the phenolic hydroxyl and methylene spectral regions (Figures 5 and 8). The activation enthalpy $\Delta H^\ddagger$ and entropy $\Delta S^\ddagger$ (Table 5.4) were recovered from the Eyring equation:

$$k = \kappa \, k_B T \exp(-\Delta G^\ddagger / RT) / h$$

or

$$\ln (k / T) = 23.76 - (\Delta H^\ddagger / RT) + (\Delta S^\ddagger / R)$$

where κ is the transmission coefficient, which is equal to unity if every transition state decays to product. The latter equation allowed for simple linear least-square analysis illustrated in Figure 5.13. (We use the Eyring equation because it allows extraction of activation parameters that are temperature independent. Fitting the data to a simple Arrhenius law with a temperature independent prefactor also produces a straight line within experimental error.)

Our model involves three species A, B and C, which sequentially interconvert among each other as represented by the following equation:

$$A \underset{k_{-1}}{\overset{k_1}{\rightleftharpoons}} B \underset{k_{-2}}{\overset{k_2}{\rightleftharpoons}} C$$

Forward and reverse rate constant are related to the reaction equilibrium constant as given by

$K_{AB} = [B] / [A] = k_1 / k_{-1}$

$K_{BC} = [C] / [B] = k_2 / k_{-2}$

where [A], [B] and [C] are populations of species A, B and C respectively. There is no interconversion between A and C in this model because we do not observe any positive cross-peaks for their signals in the 2D ROESY NMR spectra. Consistent with our assignments of states A, B and C is the observation that the activation enthalpy for the B→A process is greater than that for the B→C process. This is because B→A involves both tautomerization and a conformational transition of the carbon skeleton, whereas B→C only involves the *gauche-anti* transition.

C. Hypocrellin B

Hypocrellin B (Figure 5.1e) is very similar in structure to hypocrellin A and accompanies it in natural and commercial products [44,45]. Hypocrellin B is formed by the elimination of a water molecule at the C-14 and C-16 positions of hypocrellin A to form C-C double bond in the seven-membered ring. We anticipate that this double bond restricts rotation around the C(14)-C(16) bond and hence restricts interconversion between conformers, in contrast to hypocrellin A. The formation of the double bond also removes both chiral centers (at C-14 and C-16). However, the double bond does not render the molecule planar, and two conformational isomers differing in the sense of twist of the perylenequinone skeleton can still coexist. In contrast to hypocrellin A, however, the two atropoisomers constitute an enantiomeric pair and thus are energetically equivalent. This by no means implies that 13-H_a and 13-H_b are no longer diastereotopic, but suggests that they will interchange chemical shift should there be interconversion of conformers.

Hypocrellin B can exist in two stable tautomeric forms, analogous to the normal and double tautomers of hypocrellin A. There is a possible resonance interaction of the C(14)-C(16) double bond with the aromatic π-system despite the significant torsion angle relative to the molecular plane. Such an interaction should result in a significant difference in energy for the two tautomers, and we expect to observe only one dominating species in the ground-state population of hypocrellin B at room temperature and below.

As anticipated the ^{1}H-NMR spectrum of hypocrellin B in acetone is much simpler than that of hypocrellin A (Figure 5.11). Lowering the temperature from 313 to 240 K did not have a significant effect, except for the signals due to phenolic protons at 16.2-16.5 ppm. At low temperature, this region showed two pairs of singlets with significantly different relative intensities (Figure 5.12). Each pair was assigned to the nonequivalent aromatic hydrogens at the C-5 and C-7 positions. As the temperature is increased from 268 to 313K, the lines gradually broaden due to the proton-exchange processes and the weaker pair of singlets coalesces with the dominant one. (This is in contrast to the pair of nonequivalent aliphatic protons, which we referred to as 13-H_a and 13-H_b for hypocrellin A.) Having a typical geminal coupling constant of 11.6 Hz, their lineshapes are only slightly broadened at 313K (Figure 5.11). This indicates that, in contrast to hypocrellin A, interconversion between two possible atropoisomers of hypocrellin B is largely impeded at room temperature. A consequence of this latter observation should be the possibility of isolating (+) and (-) forms, which absorb circularly polarized light differently. However, the only report of which we are aware [44] states that the isolated natural product was not found optically active.

Consistent with the dynamic NMR experiments, the 2D ROESY spectrum of hypocrellin B exhibited only negative cross-peaks (Figure 5.12). The expected exchange cross-peaks among phenolic hydroxyls could not be observed due to the limited spectral

resolution, large difference in intensity and significant overlap of the singlet pairs. As in the case of hypocrellin A we observed significant ROE between aromatic (6.6 ppm) and methoxy (4.2 ppm), geminal H_a and H_b protons (4.1 and 3.3 ppm), and to a smaller extent between one of the geminal (4.1 ppm) and methyl (1.8 ppm) hydrogens. A negative cross-peak between acetyl (2.35 ppm) and a signal at about 4.1 ppm could not be resolved with confidence but most likely is due to the proximity of the methoxy group at the C-11 position.

Both 2D ROESY and 1D dynamic NMR data lead to the conclusion that due to the double bond in the seven member ring, hypocrellin B has higher structural rigidity than hypocrellin A. Consequently, only one tautomer of hypocrellin B is significantly populated in the ground state.

CONCLUSIONS

Based on the results of the present NMR study it appears that hypericin in DMSO or acetone exists as a single conformer/tautomer even at temperatures as high as 333 K (or at least that multiple conformers or tautomers cannot be detected by means of NMR spectroscopy). Its aromatic signals are now unambiguously assigned and interpreted. Proton exchange among all of the three pairs of hydroxyls was observed on the time scale of < 300 ms.

Hypocrellin A was shown to exist in an equilibrium involving three significantly populated species with an interconversion scheme that can be represented schematically as: $A \rightleftharpoons B \rightleftharpoons C$. Based on the detailed analysis of its 2D ROESY spectrum in acetone at 268 K it was deduced that the most populated species, A, is most likely the ***double*** tautomer in the *gauche* conformation; the least populated species, B, is the ***normal*** tautomer in the *anti* conformation; and C is the ***normal*** tautomer in the *gauche* form. Both interconversion

barriers are small enough to be frequently crossed on the time scale of the NMR experiment at temperatures of 298 K and above.

In contrast to hypocrellin A, its dehydrated form hypocrellin B exhibits less complex spectra of that are believed to arise from a single dominant species stabilized by the double bond in the 7-membered ring.

The results of this NMR study are important for understanding the photophysics of hypericin and hypocrellin. The assignment of the primary photoprocess in hypericin and hypocrellin has now been unambiguously attributed to excited-state intramolecular proton (or atom) transfer by means of transient absorption and fluorescence upconversion experiments and a careful comparison of the kinetics of methoxy analogs incapable of executing such processes. When this assignment was proposed in our early studies of hypericin, it was not, however, readily accepted in part because of the mirror image symmetry existing between the absorption and emission spectra. Such symmetry is typically taken as a signature of negligible structural changes between the absorbing and the emitting species. Intramolecular excited-state proton transfer usually generates a broad structureless emission spectrum that bears little resemblance to the absorbance spectrum. 3-Hydroxyflavone provides a good example [46-49].

There are at least two ways to respond to this objection. It is possible that the structural changes induced by proton transfer do not significantly affect the electronic structure of the tautomeric species in such a way as to destroy the mirror-image symmetry. We had also argued earlier [5,6,12], that the ground state of hypericin is already partially tautomerized or exists in equilibrium between various isomeric species and that this ground-state heterogeneity yields the observed mirror-image symmetry between absorption and emission spectra.

It is of considerable interest that recent *ab initio* calculations at the RMP2/6-

31G(d) level of theory [32] indicate that only the so-called normal form of hypericin is populated at room temperature. In recent transient absorption [7,8] and fluorescence upconversion studies [12] the excited-state kinetics of hypericin depended on the two different excitation wavelengths and the two different emission wavelengths employed. These results were used to confirm the assignment of ground-state heterogeneity in hypericin. Our assignment must be carefully reconsidered in the light of our *ab initio* calculations and the NMR results presented here. We are currently performing a more exhaustive investigation by measuring the excited-state kinetics with a tunable excitation source.

The ultrafast spectroscopic evidence for ground-state heterogeneity in hypocrellin A is much more convincing. We have noted that at first glance, the similarity of the structures (Figure 5.1) and the optical spectra [5-15] of hypericin and hypocrellin would lead one to believe that they should exhibit, at least superficially, similar excited-state photophysics. This is not the case. The time constant for excited-state proton transfer in hypericin is ~10 ps and essentially independent of solvent [6,15] whereas for hypocrellin it ranges from 50-250 ps in the solvents we have investigated [10,15]. In addition, the proton transfer reaction in hypericin exhibits no isotope effect [6,15], whereas in hypocrellin a small isotope effect of 1.4 is observed [11,15].

The current picture that we have formed of the excited-state dynamics of hypericin and hypocrellin is that the different photophysical behavior that we have enumerated above of these two structurally very similar molecules arises because we are probing different regions of very similar potential energy surfaces arising from the simultaneous optical excitation of at least two ground-state species [15]. A crucial result in forming this hypothesis is that we resolve a time constant in the hypocrellin photophysics that is comparable to that observed in hypericin. This ~10 ps component in hypocrellin, observed

in both transient absorption [15] and fluorescence upconversion measurements [50] unifies our picture of the photophysics of hypericin and hypocrellin if we can interpret it as an excited-state proton transfer arising from another tautomeric species and if we can relate it to the corresponding process in hypericin.

Finally, although it has been shown that the antiviral and antitumor activities of hypericin can be dependent on oxygen, comparative studies for nine perylenequinones, including hypocrellin and hypericin, provide evidence, however, that the quantum yield of singlet oxygen formation is not sufficient to explain the reported antiviral activities of these molecules, and that other structural features of perylenequinones are involved [54]. In fact, the quantum yield of singlet oxygen from hypericin is much less than had been presumed initially. Recently, Jardon and coworkers have revised their earlier estimation of a singlet oxygen quantum yield of 0.73 [23], essentially equal to the triplet yield, to 0.36 in ethanol and less than 0.02 in water [25]. Based on this result, mechanisms involving *only oxygen* clearly cannot explain all the activity of hypericin [51,53]. Of special relevance to the role of labile protons for this light-induced biological activity is the observation that hypericin and hypocrellin acidify their surroundings upon light absorption [14,52,53]. The role of photogenerated protons takes on significance in the context of the growing body of literature implicating pH decreases with pharmacologically important functions (see reference 53 and citations therein). A continuing theme of our research is to identify the light-induced photoprocesses responsible for the broad and potent biological activity of these naturally occurring chromophores and to determine their mechanism of action.

ACKNOWLEDGMENTS

This work was supported by NSF grant CHE-9613962 to J. W. P.

REFERENCES

1. Duran, N.; Song, P.-S. *Photochem. Photobiol.* **1986**, *43*, 677-680.

2. Diwu, Z. *Photochem. Photobiol.* **1995**, *61*, 529-539.

3. Lown, J. W. *Can. J. Chem.* **1997**, *75*, 99-119.

4. Kraus, G. A.; Zhang, W.; Fehr, M. J.; Petrich, J. W.; Wannemuehler, Y.; Carpenter, S. *Chem. Rev.* **1996**, *96*, 523-535.

5. Gai, F.; Fehr, M. J.; Petrich, J. W. *J. Phys. Chem.* **1994**, *98*, 5784-5795.

6. Gai, F.; Fehr, M. J.; Petrich, J. W. *J. Phys. Chem.* **1994**, *98*, 8352-8358.

7. English, D. S.; Zhang, W.; Kraus, G. A.; Petrich, J. W. *J. Am. Chem. Soc.* **1997**, *119*, 2980-2986.

8. English, D. S.; Das, K.; Zenner, J. M.; Zhang, W.; Kraus, G. A.; Larock, R. C.; Petrich, J. W. *J. Phys. Chem.* **1997**, *101A*, 3235-3240.

9. Das, K.; English, D. S.; Fehr, M. J.; Smirnov, A. V.; Petrich, J. W. *J. Phys. Chem.* **1996**, *100*, 18275-18281.

10. Das, K.; English, D. S.; Petrich, J. W. *J. Am. Chem. Soc.* **1997**, *119*, 2763-2764.

11. Das, K.; English, D. S.; Petrich, J. W. *J. Phys. Chem.* **1997**, *101A*, 3241-3245.

12. English, K. Das, K. D. Ashby, J. Park, J. W. Petrich, and E. W. Castner, Jr. *J. Am. Chem. Soc.* **1997**, *119*, 11585-11590.

13. Das, K.; Dertz, E.; Paterson, J.; Zhang, W.; Kraus, G. A.; Petrich, J. W. *J. Phys. Chem. B* **1998**, *102*, 1479-1484.

14. Fehr, M. J.; McCloskey, M. C.; Petrich, J. W. *J. Am. Chem. Soc.* **1995**, *117*, 1833-1836.

15. Das, K.; Smirnov, A. V.; Snyder, M. D.; Petrich, J. W. *J. Phys. Chem. B* **1998**, *102*, 6098.

16. Malkin, J.; Mazur, Y. *Photochem. Photobiol.* **1993**, *57*, 929-933.

17. Weiner, L.; Mazur, Y. *J. Chem. Soc. Perkin Trans.* **1992**, 2, 1439-1442.

18. Zhang, M.-H.; Weng, M.; Chen, S.; Xia, W.-L.; Jiang, L.-J.; Chen, D.-W. *J. Photochem. Photobiol. A: Chem.* **1996**, *96*, 57.

19. Wang, N.; Zhang, Z. *J. Photochem. Photobiol. B: Biol.* **1992**, *14*, 207-217.

20. Lu, Y.-Z.; An, J.-Y.; Qin, L.; Jiang, L.-J.; Chiang, L.-C. *J. Photochem. Photobiol. B: Biol.* **1994**, *78*, 247-251.

21. Yamazaki, T.; Ohta, N.; Yamazaki, I.; Song, P.-S. *J. Phys. Chem.*, **1993**, *97*, 7870-7875.

22. Wells, T. A.; Losi, A.; Dai, R.; Scott, P.; Park, S.-U.; Golbeck, J.; Song, P.-S. *J. Phys. Chem. A*, **1997**, *101*, 366-372.

23. Racinet, H.; Jardon, P.; Gautron, R. *J. Chim. Phys.* **1988**, *85*, 971-977.

24. Eloy, D., Pellec, A. Le., Jardon, P. *J. Chim. Phys.*, **1996**, *93*, 442-457.

25. Darmanyan, A. P.; Burel, L.; Eloy, D.; Jardon, P. *J. Chim. Phys.* **1994**, *91*, 1774-1785.

26. Angerhofer, A.; Falk, H.; Meyer, J.; Schopel, G. *J. Photochem. Photobiol. B: Biol.* **1993**, 20, 133-137.

27. Mikovsky, P.; Sureau, F.; Chinsky, L.; Turpin, P.-Y. *Photochem. Photobiol.* **1995**, *62*, 546-549.

28. Sanchez-Cortes, S.; Miskovsky, P.; Jancura, D.; Bertoluzza, A. *J. Phys. Chem.* **1996**, *100*, 1938-1944.

29. Miskovsky, P.; Chinsky, L.; Wheeler, G. V.; Turpin, P.-Y. *J. Biomol. Str. Dynamics* **1995**, *13*, 547-552.

30. Miskovsky, P.; Sanchez-Cortes, S.; Jancura, D.; Kocisova, E.; Chinsky, L. *J. Am. Chem. Soc.* **120**, 6374-6379.

31. Arnone, A.; Merlini, L.; Mondelli, R.; Nasini, G.; Ragg, E.; Scaglioni, L.; Weiss, U. *J. Chem. Soc. Perkin Trans. 2*, **1993**, 1447-1454.

32. Petrich, J. W.; Gordon, M. S.; Cagle, M. *J. Phys. Chem. A* **1998**, *102*, 1647-1651.

33. Etzlstorfer, C.; Falk, H. *Monatsh. Chem.* **1998**, *129*, 855-863.

34. There is a common assumption in the literature that the most stable form of hypocrellin is that illustrated in Figure 5.1c. The published X-ray structure indicates C(3)-O(3) and C(10)-O(10) bond lengths that are within experimental error greater than those of their C(4)-O(4) and C(9)-O(9) neighbors [35]. The coordinates available from the Cambridge Crystallographic Data Bank suggest, however, that all four bond lengths are comparable. The former data set is consistent with Figure 5.1d, enol bonds being longer than keto bonds. The latter data set suggests a mixture of both the normal and the tautomer forms in the ground state. Note that the numbering used in this article differs from that we have employed elsewhere [8,11].

35. Wei-shin, C.; Yuan-teng, C.; Xiang-yi, W.; Friedrichs, E.; Puff, H.; Breitmaier, E. *Liebigs Ann. Chem.* **1981**, 1880-1885.

36. Freeman, D.; Frolow, F.; Kapinus, E.; Lavie, D.; Lavie, G.; Meruelo, D.; Mazur, Y. *J. Chem. Soc. Commun.* **1994**, 891.

37. Etzlstorfer, C.; Falk, H.; Müller, N.; Schmitzberger, W.; Wagner, U. G. *Monatsh. Chem.* **1993**, *124*, 751-761. b) Falk, H. Personal communication.

38. Marion, D.; Ikura, M.; Tschudin, R.; Bax, A. *J. Magn. Reson.* **1989**, *85*, 393.

39. Bax, A.; Davis, D. G. *J. Magn. Reson.* **1985**, *63*, 207.

40. Schaefer, T. *J. Phys. Chem.* **1975**, *17*, 1888.

41. Bothner-By, A. A.; Stephens, R. L.; Lee, J. M.; Warren, C. D.; Jeanloz, R. W. *J. Am. Chem. Soc.* **1984**, *106*, 811.

42. Bax, A.; Grzesick, S. in *Encyclopedia of Nuclear Magnetic Resonance*, Eds., Grant, D. M.; Harris, R. K. (Wiley, New York, 1996). pp. 4157-4167.

43. Jeener, J.; Meier, B. H.; Bachman, P.; Ernst, R. R. *J. Chem. Phys.* **1979**, *71*, 4546.

44. Kishi, T.; Tahara, S.; Taniguchi, N.; Tsuda, M.; Tanaka, C.; Takahashi, S. *Planta Med.* **1991**, *57*, 376-379.

45. Wang, N.; Zhang, Z. *J. Photochem. Photobiol. B* **1992**, *14*, 207-217.

46. Schwartz, B. J.; Peteanu, L. A.; Harris, C. B. *J. Phys. Chem.* **1992**, *96*, 3591-3598.

47. Brucker, G. A.; Swinney, T. C.; Kelley, D. F. *J. Phys. Chem.* 1991, *95*, 3190-3195.

48. Strandjord, A. J. G.; Barbara, P. F. *J. Phys. Chem.* 1985, *89*, 2355-2361.

49. McMorrow, D.; Kasha, M. *J. Phys. Chem.* 1984, *88*, 2235-2243.

50. Smirnov, A. V.; Petrich, J. W. Unpublished results.

51. We had previously reported that hypericin does not require oxygen for its antiviral activity (e.g., references 4, 12, and citations therein). In these cases, however, we were not able to estimate accurately low oxygen levels in our virus samples. We consequently now believe that although the role of oxygen in this activity is significant, the ability of photogenerated protons to enhance or to complement the activity of activated oxygen species is still important (J. Park, D. S. English, Y. Wannemuehler, S. Carpenter, and J. W. Petrich, *Photochem. Photobiol.* 1998, *68*, 593-597.)

52. Sureau, F.; Miskovsky, P.; Chinsky, L.; Turpin, P. Y. *J. Am. Chem. Soc.* 1996, *118*, 9484.

53. Chaloupka, R.; Sureau, F.; Kocisova, E.; Petrich, J. W. *Photochem. Photobiol.* 1998, *68*,

54. Hudson, J. B.; Imperial, V.; Haugland, R. P.; Diwu, Z. *Photochem. Photobiol.* 1997, *65*, 352-354.

Table 5.1 ^1H Chemical shifts values (δ, ppm) for hypericin, hypocrellin A and B at 298K.

compound	hypericin acetone	hypericin DMSO	hypocrellin A acetone	hypocrellin B acetone
phenolic hydroxyls	14.82 (8,13-OH) 14.27 (1,6-OH)	14.74 (8,13-OH) 14.09 (1,6-OH)	16.05-16.45[a]	16.34, 16.37[c]
aromatic hydrogens	7.35 (9,12-H), 6.62 (2,5-H)	7.46 (9,12-H), 6.59 (2,5-H)	6.76 (b) (5,8-H)	16.58, 16.60[c] (5,8-H)
methoxy	-	-	4.07, 4.14, 4.21 (b)[c]	4.04, 4.16, 4.19, 4.20[c]
methylene	-	-	3.4-3.75; 2.4-2.8[b]	4.07 (d, 13-H_a) 4.34 (d, 13-H_b)
methyne	-	-	3.84, 4.79, 5.78 (all for H-16)	-
methyl	2.78	2.75	1.6-1.7 (15-H_3) 1.89 (18-H_3)	1.81 (18-H_3) 2.35 (15-H_3)

[a] see Table 5.3 for detailed assignment

[b] see Table 5.2 for detailed assignment

[c] detailed assignment was not possible or attempted.

Table 5.2 Chemical shift of hypocrellin A doublets in NMR spectrum and assignment of conformer type for species A, B and C.

species	Doublet center shift, ppm		methyne shift,	conformer
	H_a	H_b	ppm	type
A	3.43	2.65	3.8	*gauche*
B	2.75	3.65	4.8	*anti*
C	3.60	2.50	5.8	*gauche*

Table 5.3 Chemical shifts of hypocrellin A peri-hydroxyls in NMR spectrum and assignment of tautomer type for species A, B and C.

species	Hydroxyl shift, ppm		tautomer
	OH	OH'	type[a]
A	16.12	16.20	double
B	16.48	16.40	normal
C	16.13[b]	16.04	normal

[a] The exact assignment of structure for A (double or normal) and other species respectively still needs further evidence such as energy calculation in crystal and in solution or high-quality theoretical estimation of chemical shifts of *peri*-hydroxyls.

[b] This signal is assumed to overlap with the one originating from species A.

Table 5.4 Simulation results of hypocrellin A dynamic NMR spectra based on the model of three interconverting species A, B and C.

Process	Equilibrium constant at 300 K	$\Delta H°$, kJ/mol	$\Delta S°$, J/(mol K)	$\Delta G°$, kJ/mol
A→B	0.49	5.5 ± 0.3	12 ± 1	1.9
B→A	2.05	-5.5 ± 0.3	-12 ± 1	-1.9
B→C	0.34	-6.5 ± 0.5	-31 ± 2	2.7
C→B	2.95	6.5 ± 0.5	31 ± 2	-2.7
Process	Interconversion rate at 300 K, s^{-1}	$\Delta H^{\ddagger}$, kJ/mol	$\Delta S^{\ddagger}$, J/(mol K)	$\Delta G^{\ddagger}$, kJ/mol
A→B	45	67 ± 4	10 ± 12	64.0
B→A	93	62 ± 4	-3 ± 10	62.9
B→C	20	51 ± 2	-55 ± 7	67.4
C→B	43	57 ± 2	-26 ± 7	64.7

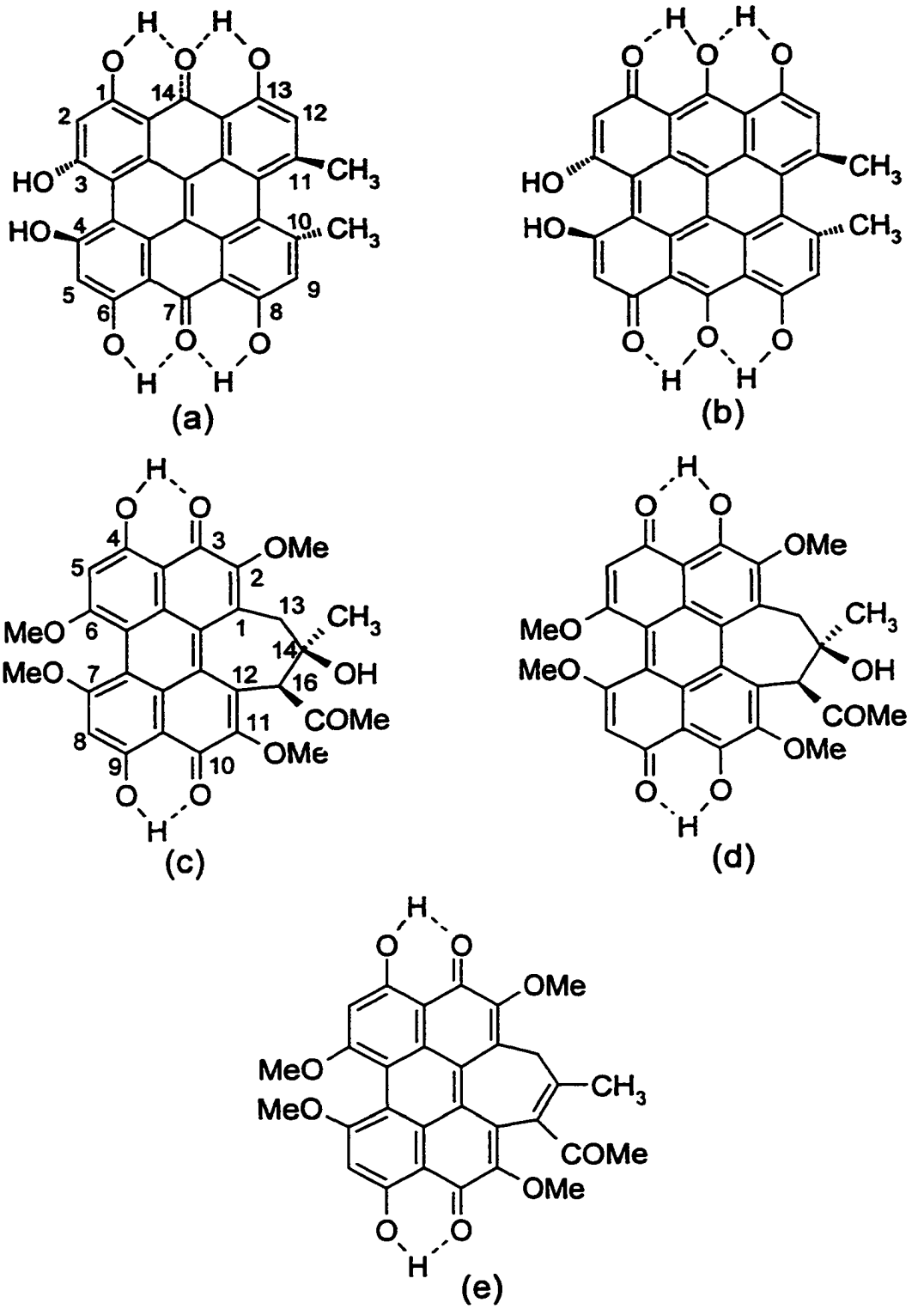

Figure 5.1 Structures of hypericin "normal" (a) and double tautomer (b) forms; hypocrellin A "normal" (c) and double tautomer (d) forms; and hypocrellin B (e).

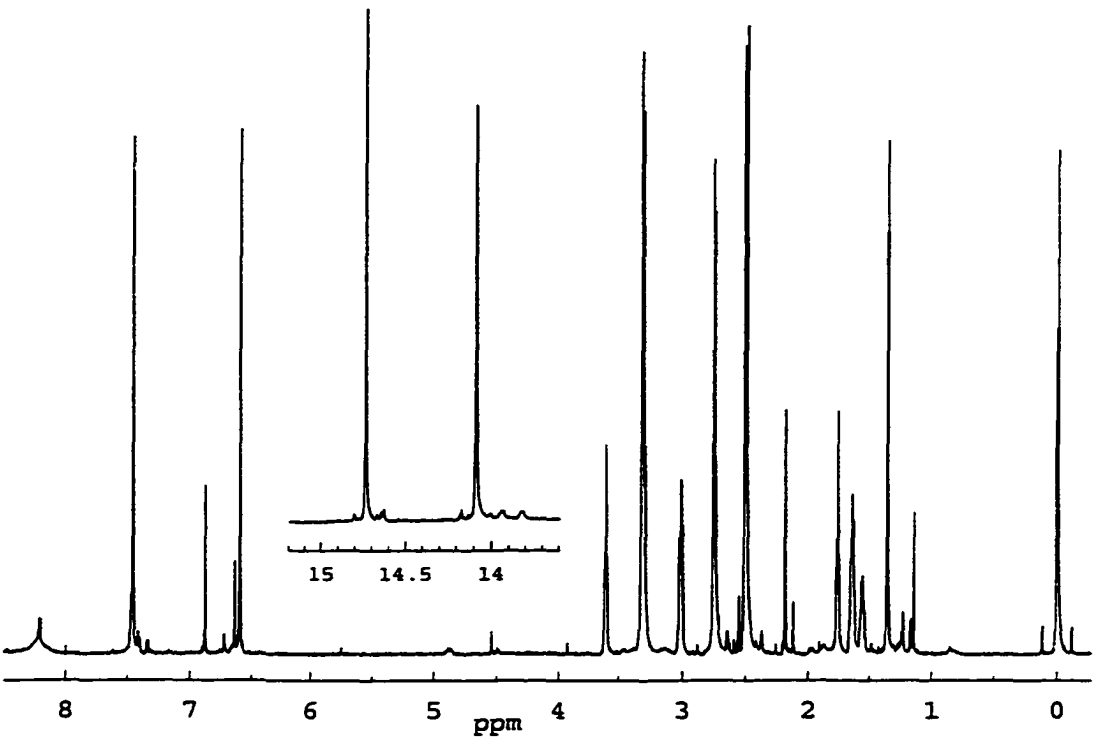

Figure 5.2 1D ^{1}H-NMR spectrum of hypericin in DMSO at 298 K. No lineshape coalescence typical of an exchanging system was observed but sample exhibited temperature-dependent line narrowing. As it is evident from the low-temperature data, this line narrowing clearly comes from lower viscosity of DMSO at higher temperatures and not due to the increased interconversion rate among possible tautomers. In the latter case, we would expect substantial signal broadening or even peak splitting at low temperatures.

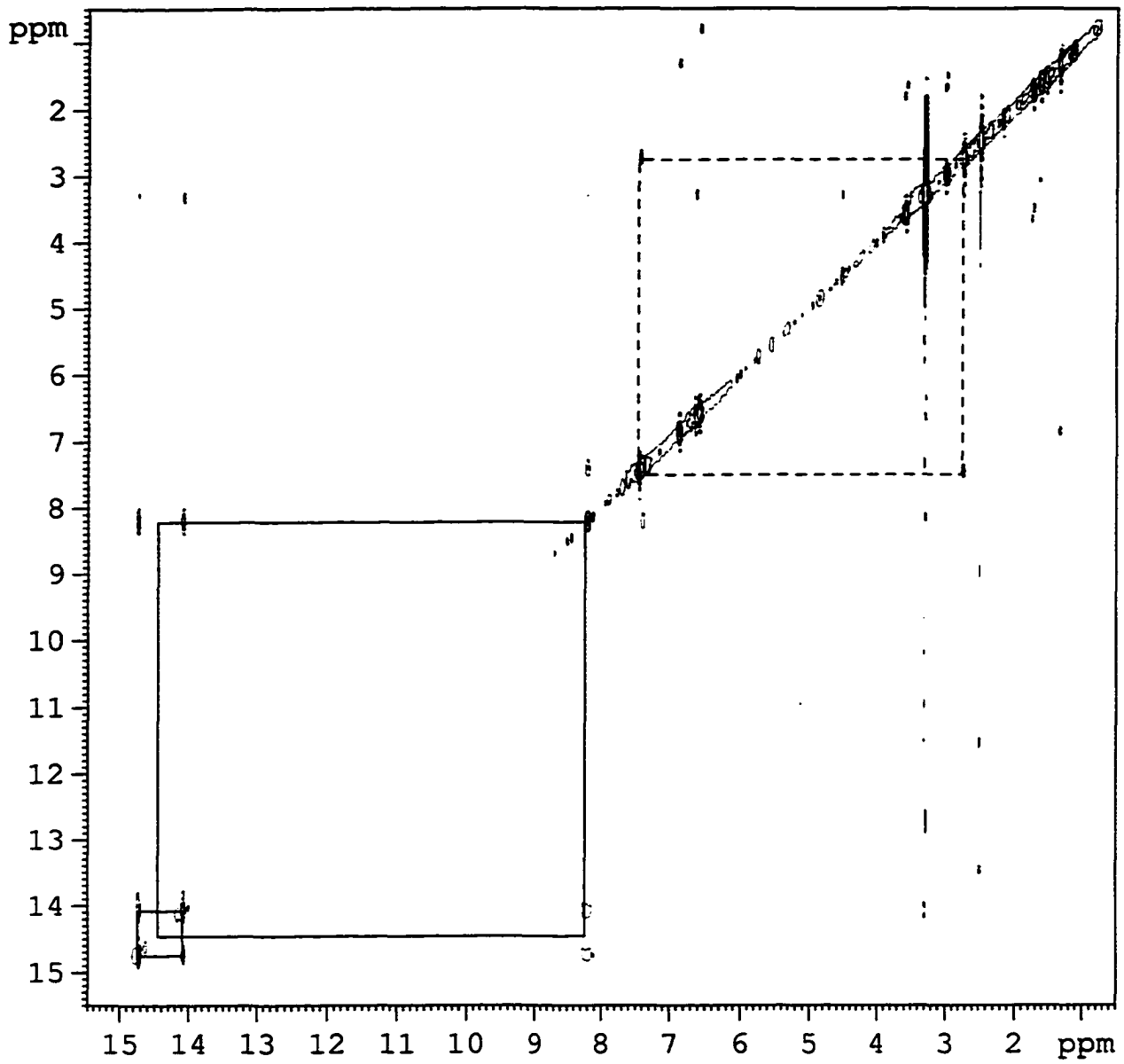

Figure 5.3 2D ROESY spectrum of hypericin in DMSO at 298 K. Solid lines denote positive contours; dashed lines denote negative contours.

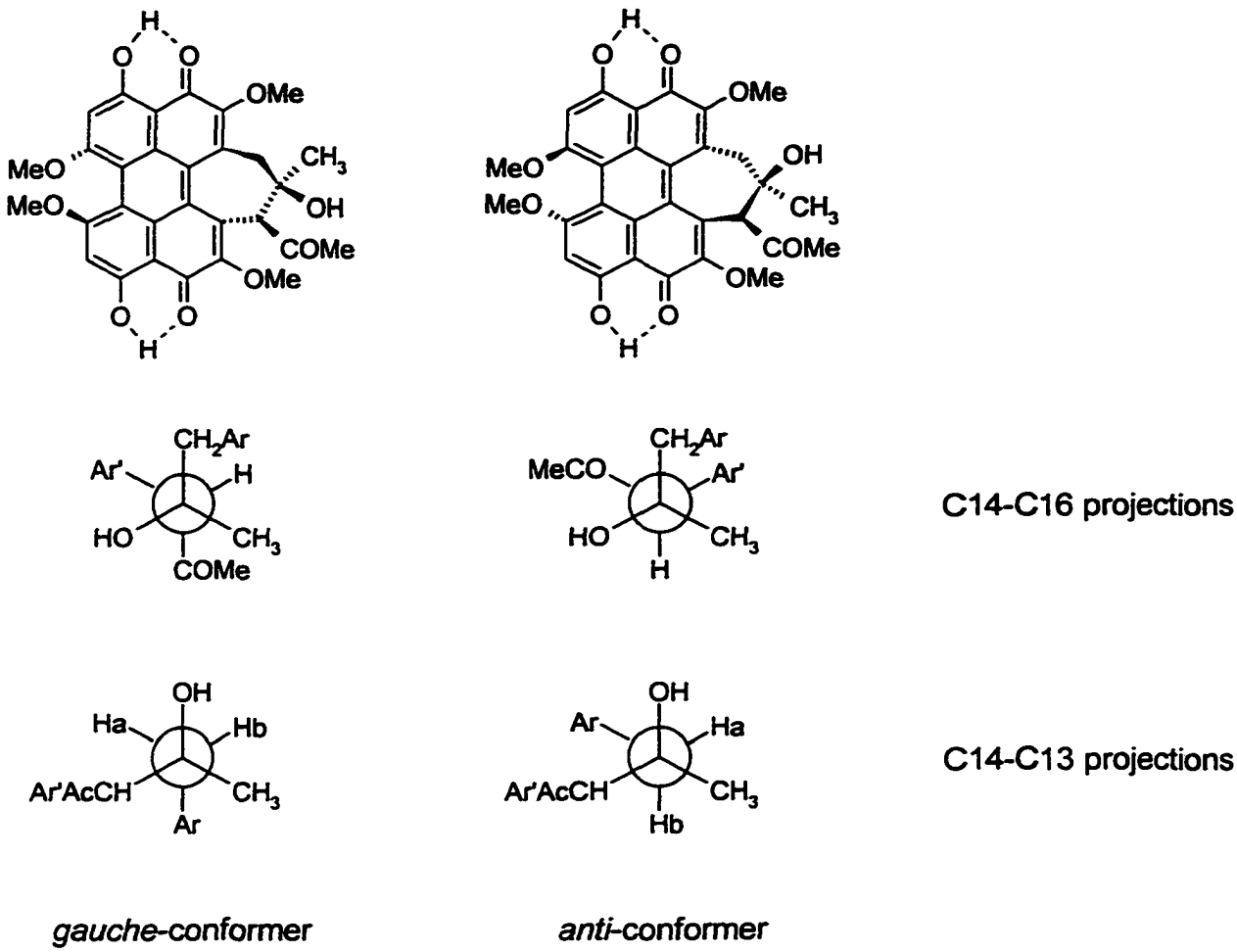

Figure 5.4 Two possible conformational forms of the hypocrellin A normal tautomer. The *anti/gauche* nomenclature is based on the relative position of the methyl and acetyl moieties as depicted by the C(14)-C(16) Newman projection.

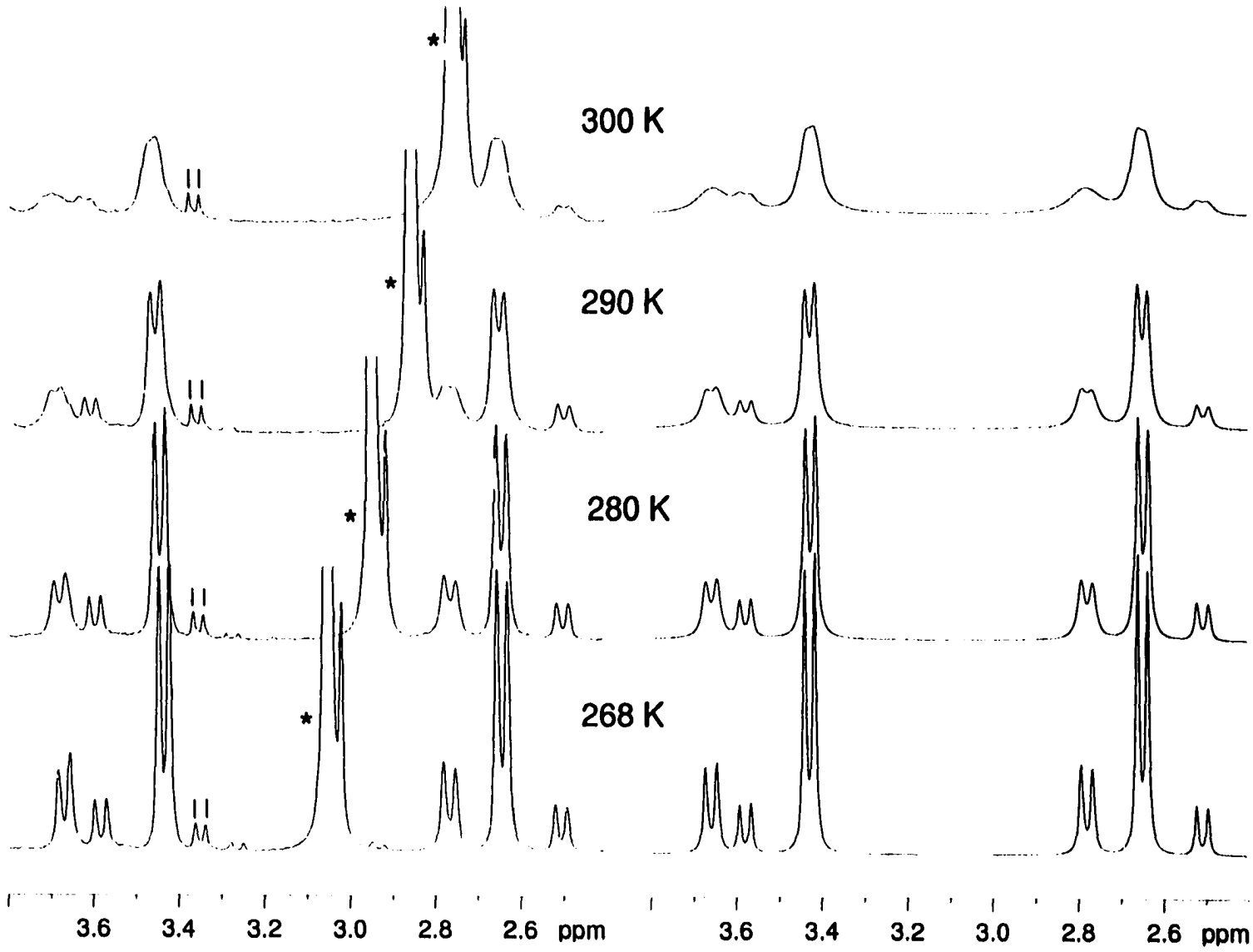

Figure 5.5 Dynamic NMR spectra of hypocrellin A doublets as a function of temperature. Experimental and simulated data are presented, respectively, on the left and right. Asterisks denote water signals, and small vertical dashes denote signals from hypocrellin B.

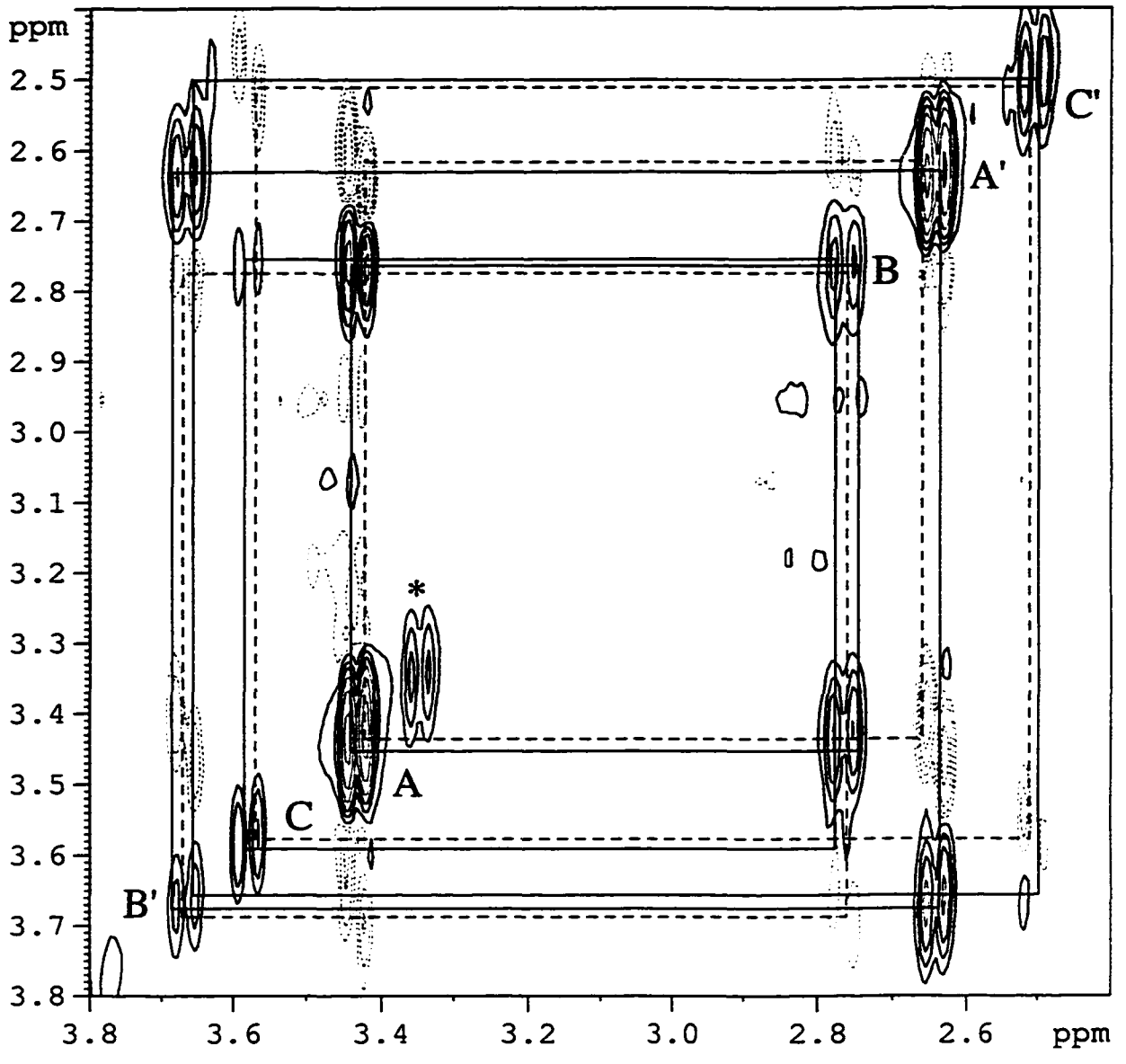

Figure 5.6 2D ROESY NMR spectrum of hypocrellin A methylene H_a (A, B, C) and H_b (A', B', C') protons at 268 K. Solid lines denote positive contours; dashed lines denote negative contours. An asterisk (*) denotes peaks due to the traces of hypocrellin B. Water peaks have been removed to clarify the spectrum.

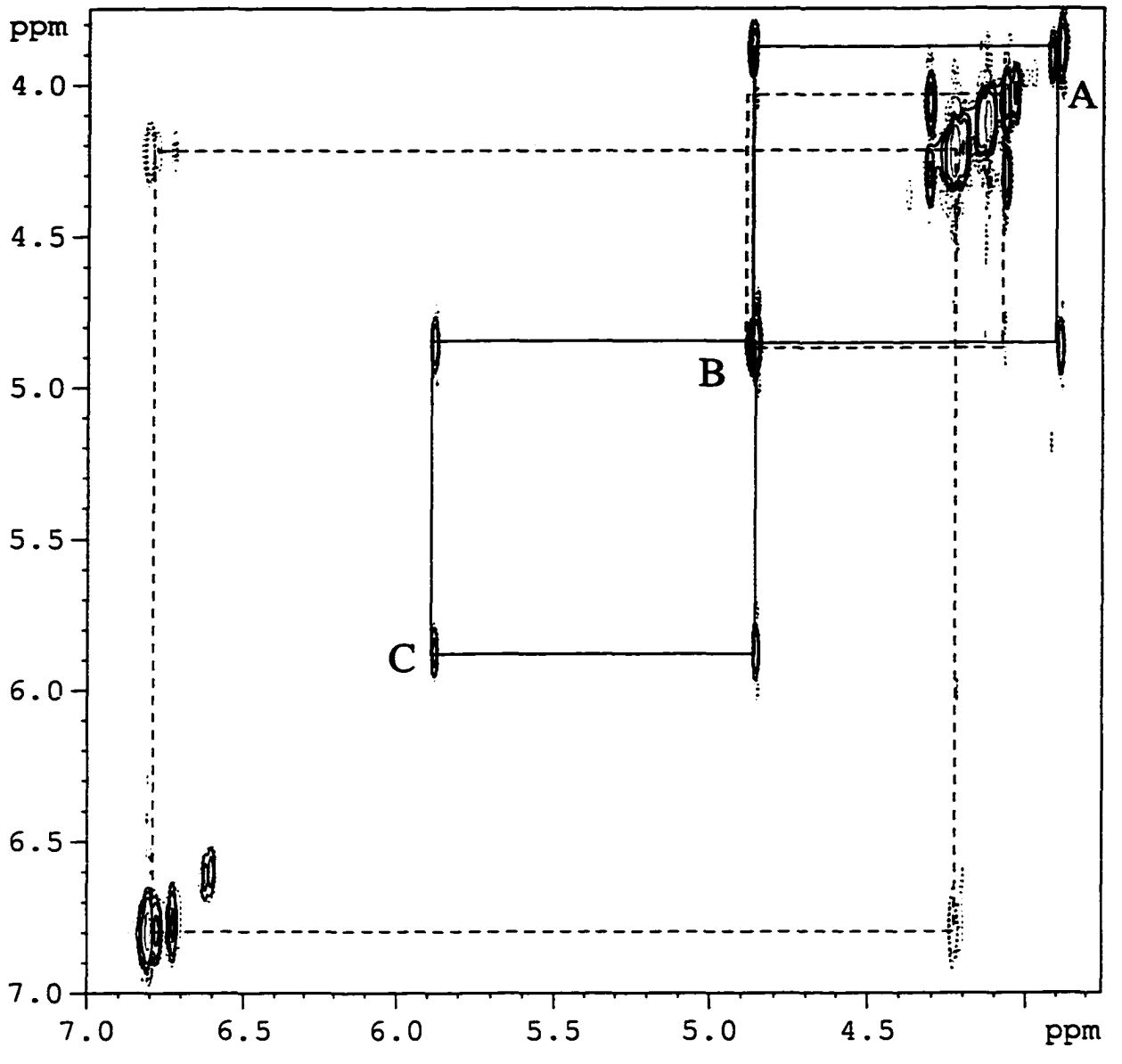

Figure 5.7 2D ROESY NMR spectrum of hypocrellin A aromatic and methyne protons. Solid lines denote positive contours; dashed lines denote negative contours. Water peaks have been removed to clarify the spectrum.

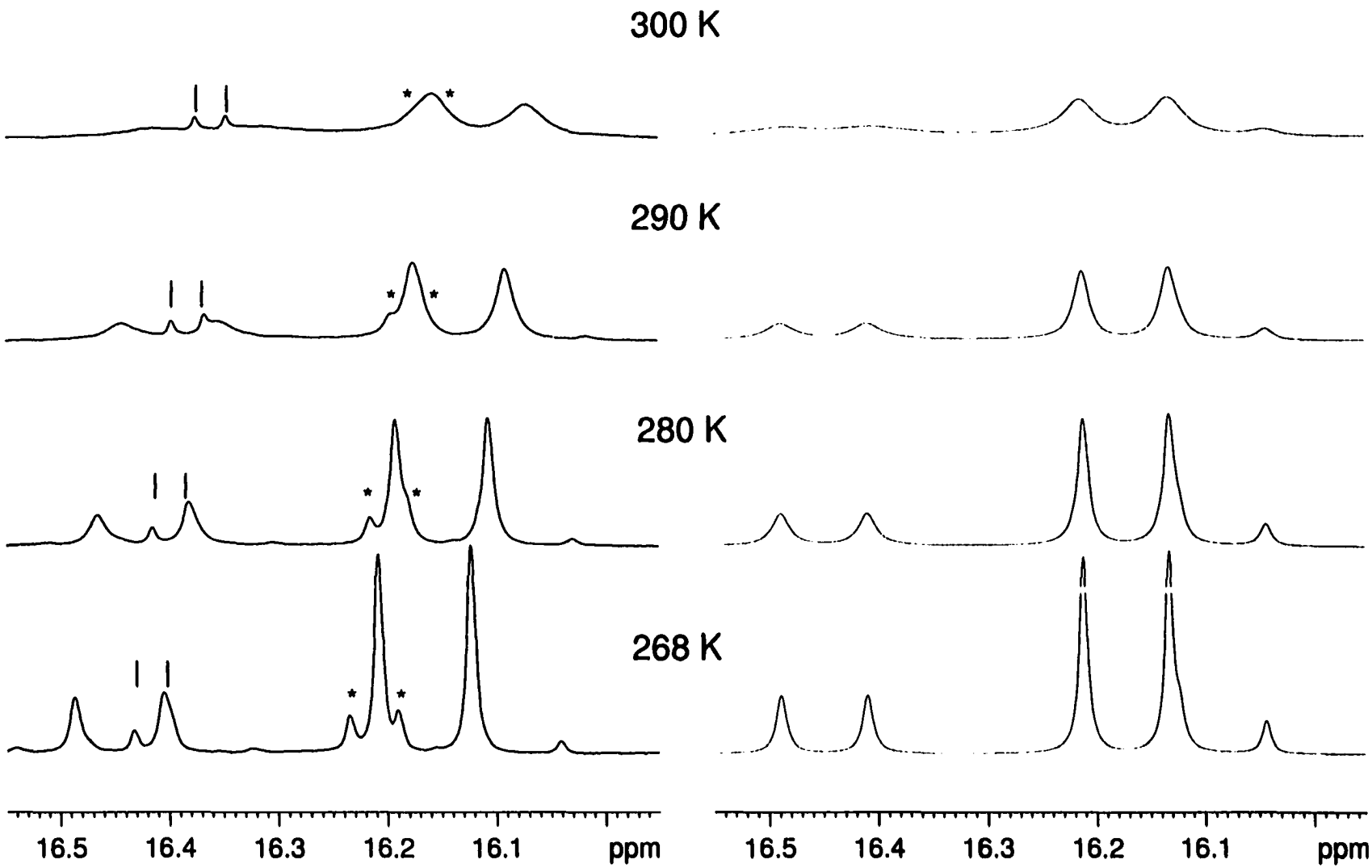

Figure 5.8 Dynamic NMR spectra hypocrellin A low field region as a function of temperature. Experimental and simulated data are presented, respectively, on the left and right. Asterisks denote impurities, and small vertical dashes denote signals from hypocrellin B. Due to the numerous factors that can affect line shapes of hydrogen-bonded protons it was only possible to achieve qualitative agreement with the experimental spectrum and be consistent with simulations for aliphatic region (see Figure 5). Asterisks denote impurities, and small vertical dashes denote hypocrellin B.

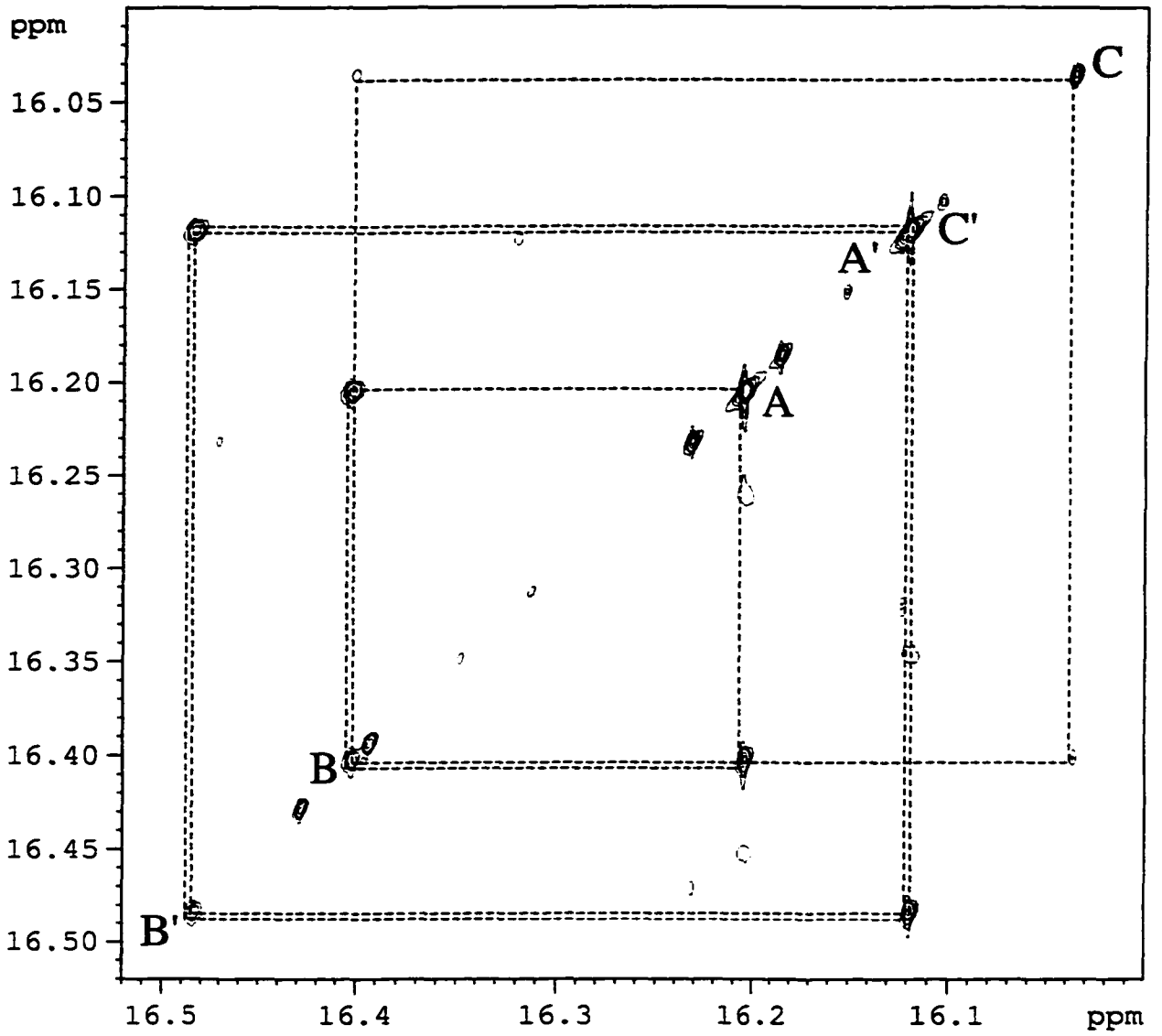

Figure 5.9 2D ROESY NMR spectrum of hypocrellin A in the low-field region at 268 K, showing signals from phenolic hydroxyls. Only positive-phase cross peaks (arising from tautomeric exchange) are evident in this region. Water peaks have been removed to clarify the spectrum.

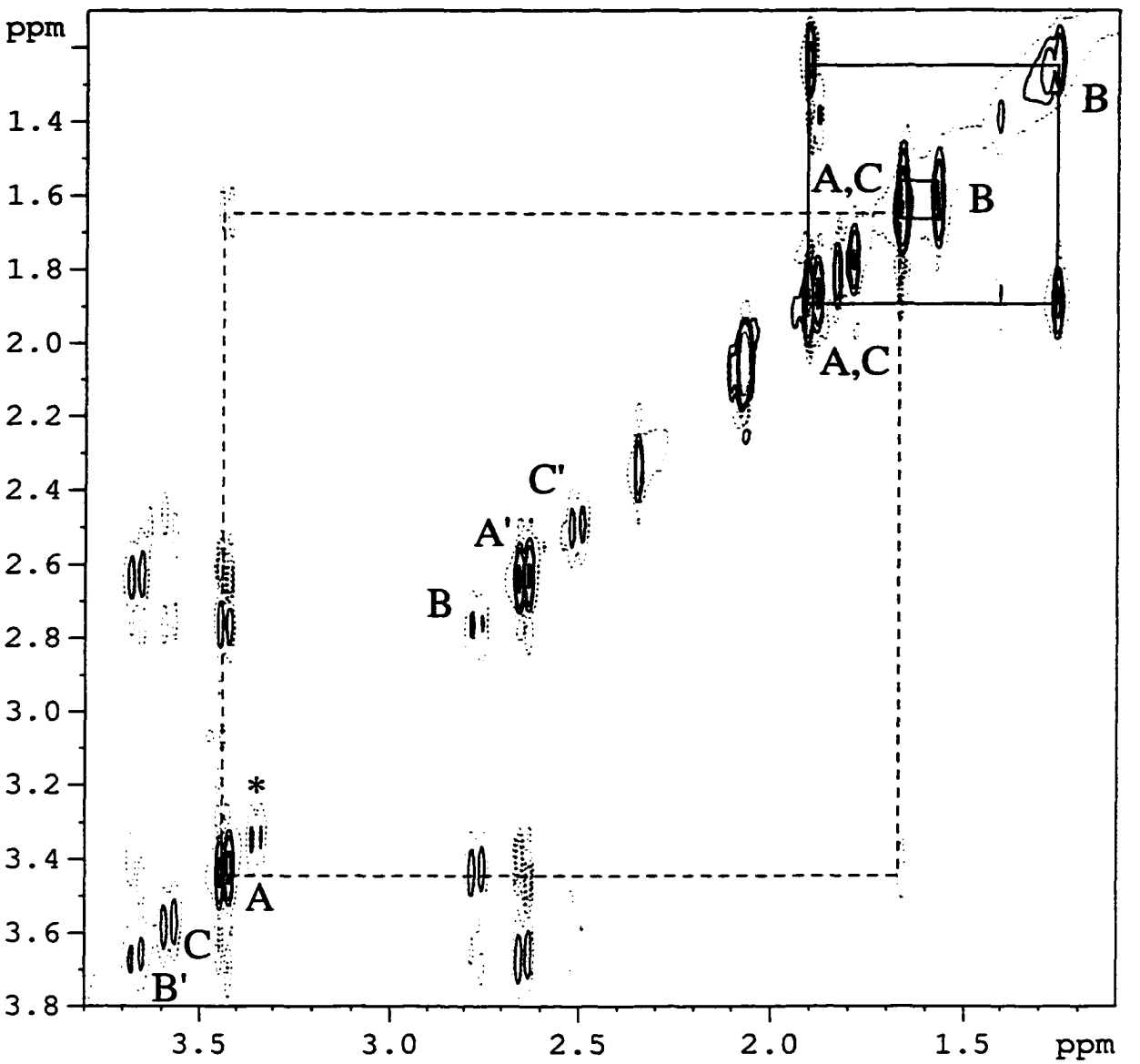

Figure 5.10 2D ROESY NMR spectrum of hypocrellin A in the high-field region at 268 K showing signals of 15-H and 18-H methyls. Solid lines denote positive contours; whereas dashed lines denote negative contours. Water peaks have been removed to clarify the spectrum.

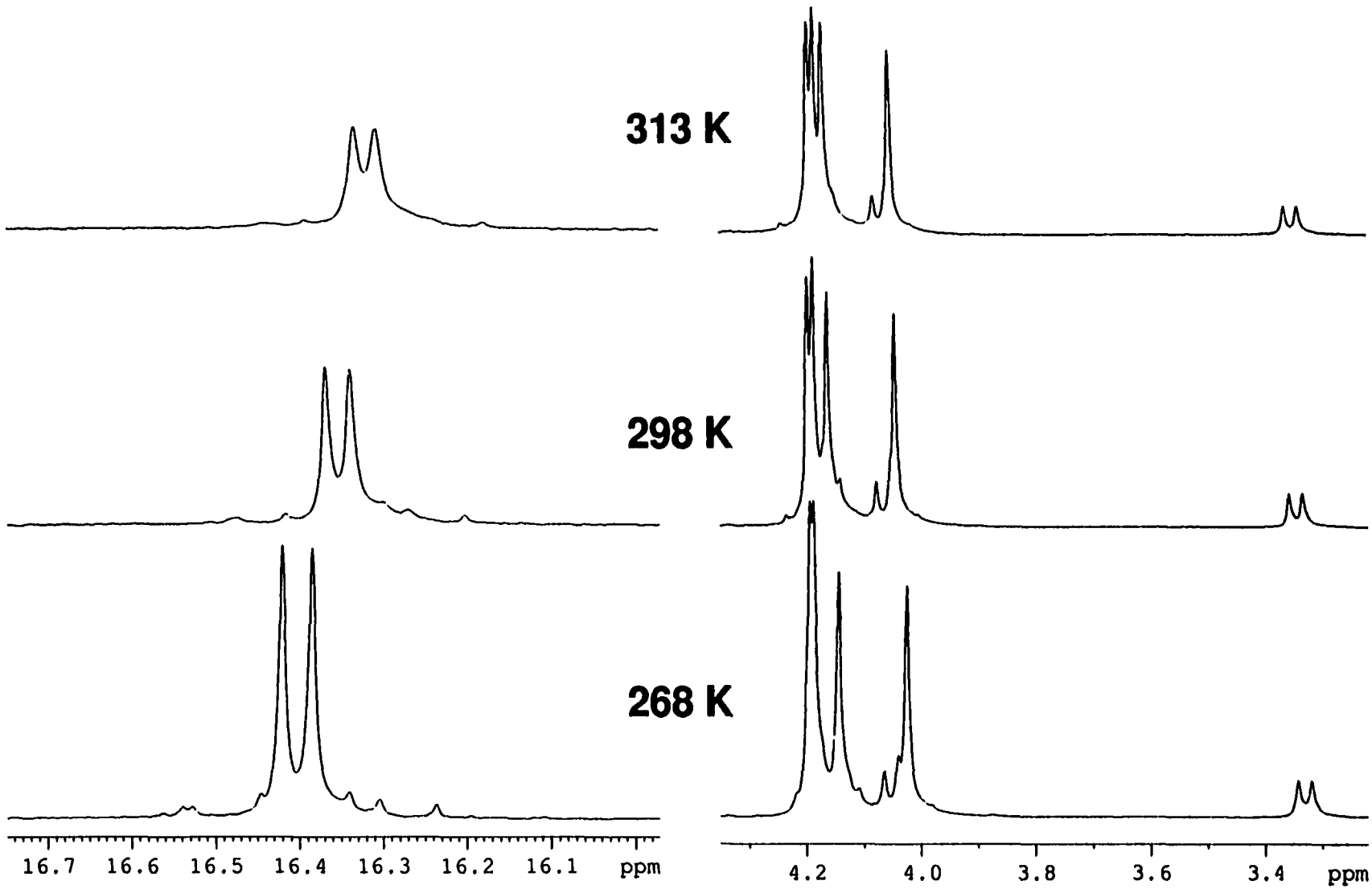

Figure 5.11 ^{1}H-NMR spectra of hypocrellin B doublets and low-field region of hypocrellin B NMR spectrum as a function of temperature. Line broadening is attributed to intermolecular proton exchange with trace amounts of water.

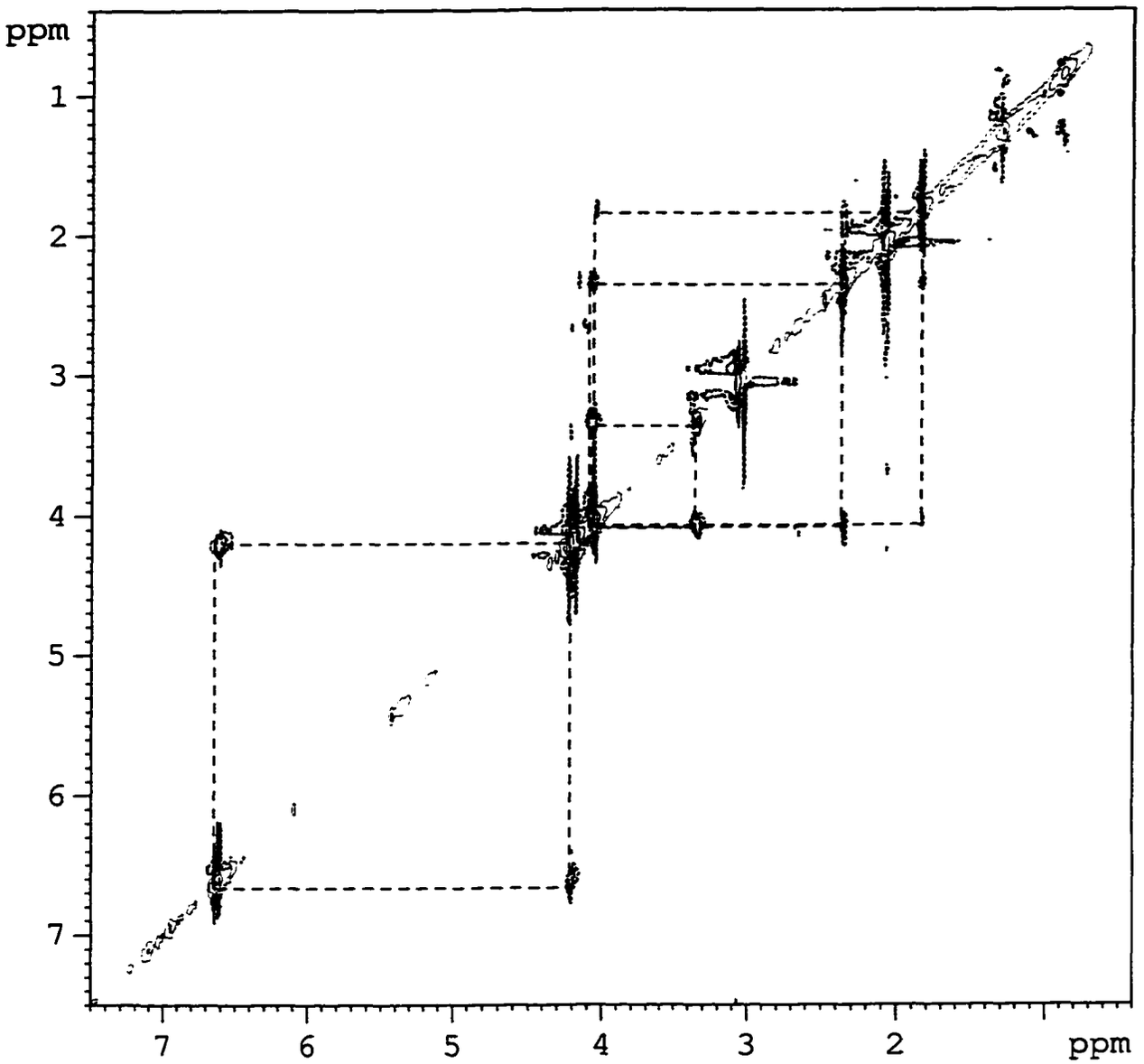

Figure 5.12 2D ROESY NMR spectrum of hypocrellin B at 268 K showing all signals except for phenolic hydroxyls. Dashed lines indicate negative contours.

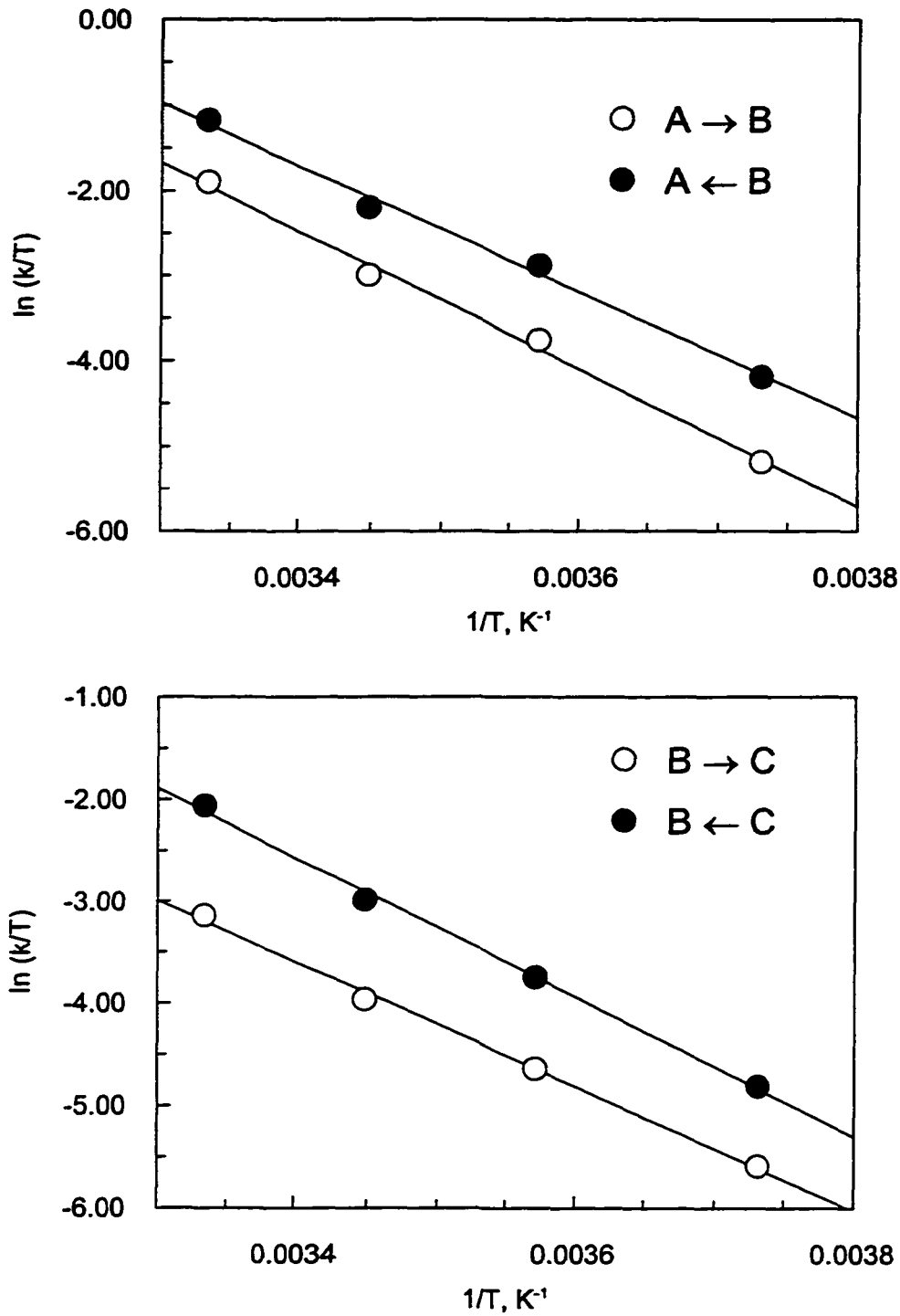

Figure 5.13 (top) Linear plot of rate constants *k* for A→B (open circles) and A←B (closed circles) processes *vs.* temperature according to Eyring equation. $r = -0.997$

(bottom) Linear plot of rate constants *k* for B→C (open circles) and B←C (closed circles) processes *vs.* temperature according to the Eyring equation. $r = -0.999$.

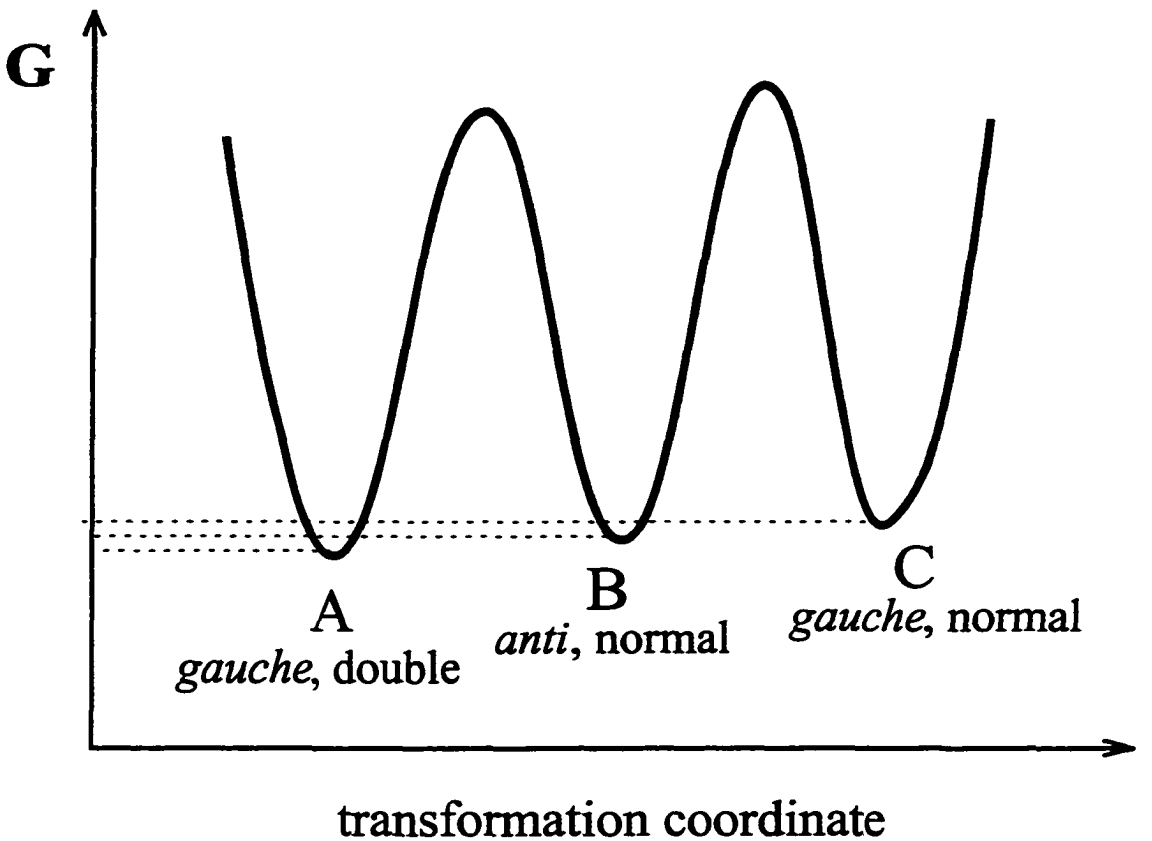

Figure 5.14 Ground-state energy surface for the three interconverting species A, B and C of hypocrellin A based on the results of dynamic NMR simulations.

CHAPTER VI. PHOTOPHYSICS OF HYPERICIN AND HYPOCRELLIN A IN COMPLEX WITH SUBCELLULAR COMPONENTS: INTERACTIONS WITH HUMAN SERUM ALBUMIN

A paper accepted by the Journal of Physical Chemistry

Kaustuv Das[1], Alexandre V. Smirnov[1], Jin Wen[1], Pavol Miskovsky[2] and Jacob W. Petrich[1,3]

Key words: hypericin, hypocrellin A, human serum albumin, transient absorption, fluorescence upconversion, excited-state proton transfer

Abbreviations: HSA, human serum albumin, HIV, human immunodeficiency virus, DMSO, dimethylsulfoxide, LBO, lithium triborate, BBO, β-barium borate, SNARF, carboxy-seminaphthorhodafluor-1, BCECF, 2′-7′-*bis*(carboxyethyl)5-carboxyfluorescein, Poly dG-dC, polydeoxyguanylic-deoxycytidylic acid, Brij-35, polyoxyethylene 23 lauryl ether, AOT dioctyl sulfosuccinate

---

[1] Department of Chemistry, Iowa State University, Ames, IA 50011-3111 USA

[2] Department of Biophysics, Safarik University, 041 54 Kosice, SLOVAKIA

[3] To whom correspondence should be addressed.

ABSTRACT

Time-resolved fluorescence and absorption measurements are performed on hypericin complexed with human serum albumin, HSA, (1:4, 1:1, and ~5:1 hypericin:HSA complexes). Detailed comparisons with hypocrellin A/HSA complexes (1:4 and 1:1) are made. Our results are consistent with the conclusions of previous studies indicating that hypericin binds to HSA by means of a specific hydrogen bonded interaction between its carbonyl oxygen and the N_1-H of the tryptophan residue in the II A subdomain of HSA. (They also indicate that some hypericin binds nonspecifically to the surface of the protein.) A single-exponential rotational diffusion time of 31 ns is measured for hypericin bound to HSA, indicating that it is very rigidly held. Energy transfer from the tryptophan residue of HSA to hypericin is very efficient and is characterized by a critical distance of 94 Å, from which we estimate a time constant for energy transfer of $\sim 3 \times 10^{-15}$ s. Although it is tightly bound to HSA, hypericin is still capable of executing excited-state intramolecular proton (or hydrogen atom) transfer in the ~5:1 complex, albeit to a lesser extent than when it is free in solution. It appears that the proton transfer process is completely impeded in the 1:1 complex. The implications of these results for hypericin (and hypocrellin A) are discussed in terms of the mechanism of intramolecular excited-state proton transfer, the mode of binding to HSA, and the light-induced antiviral and antitumor activity.

INTRODUCTION

Hypericin and hypocrellin A (Figure 6.1) are naturally occurring polycyclic quinones that have gained great interest recently owing to their light-induced biological activity (1-5). They display virucidal activity against several types of viruses, including the human immunodeficiency virus (HIV) (6-9), as well as antiproliferative and cytotoxic effects on tumor cells (10-12). Hypericin is also a potent antidepressant (13-15), exhibits

light-dependent inhibition of protein kinase C (PKC) (16,17), and is reported to possess numerous other types of biological behavior (19-23). Hypericin, like other anticancer drugs, also induces apoptosis (11,23,24).

Owing to this important biological activity, over the past few years we have been studying the photophysics of hypericin and hypocrellin (25-35). By means of H/D substitution, investigation of methoxy analogs, and complementary studies using both transient absorption and fluorescence upconversion spectroscopies, we have unambiguously demonstrated that the major primary photophysical process in hypericin and hypocrellin A in organic solvents is excited-state intramolecular proton or hydrogen atom transfer. Considerable effort was required to demonstrate this fact owing to the unusual mirror image symmetry between absorption and emission spectra, the lack of an H/D isotope effect on the proton transfer reaction in hypericin, and the occasional consideration of this ultrafast reaction in terms of equilibrium Förster-cycle type calculations (36).

We have suggested that the labile protons resulting from the intramolecular proton transfer reaction may be important for understanding the light-induced biological activity of hypericin and hypocrellin A. Notably, hypericin and hypocrellin A acidify their surroundings upon light absorption (37-39). The role of photogenerated protons takes on significance in the context of the growing body of literature implicating changes in pH with inhibition of virus replication (40), antitumor activity (41,42), and apoptosis (43,44,45). For example, comparative studies for nine perylenequinones, including hypericin, provide evidence that the quantum yield of singlet oxygen formation is not sufficient to explain the reported antiviral activities of these molecules and that other structural features of perylenequinones are involved (46). In fact, the quantum yield of singlet oxygen from hypericin is much less than had initially been presumed. Recently, Jardon and coworkers

have revised their earlier estimation of a singlet oxygen quantum yield of 0.73 (47,48), essentially equal to the triplet yield, to 0.35 in ethanol and less than 0.02 in water (49). Based on this result, mechanisms involving only oxygen clearly cannot explain all the activity of hypericin.

We had previously reported that hypericin does not require oxygen for its antiviral activity (5,18,34). This conclusion was based on an inability to estimate accurately low oxygen levels in our virus samples. Our most recent results indicate that while antiviral pathways independent of oxygen may exist, the role of oxygen in this activity is significant, although it seems to differ for hypericin and hypocrellin A. The ability of photogenerated protons to enhance the activity of activated oxygen species (39) is still considered to be of importance (50). De Witte and coworkers have also recently considered the relative role of oxygen in the phototoxicity of hypericin against A431 human skin carcinoma cells (51).

Although numerous studies dealing with the biological and photophysical properties of hypericin have been performed, the mechanism and site of action of hypericin at the cellular level is still unclear. Thus a better understanding of the interaction of hypericin with various possible cellular targets (membranes, proteins or nucleic acids) is essential for a determination of its function in biological systems. For human T47D mammary tumor cells, it has been shown that hypericin immediately associates with cell membrane and also localizes in the cytoplasm and nucleus after a long-time incubation (3 hr 30min) (52). And recently a study of hypericin in fetal rat neurons was performed, employing both fluorescence imaging and subnanosecond time resolution, that indicated localization in the membrane as well as in the nucleus (53).

Human serum albumin (HSA) is a transport protein in the blood plasma. It binds a wide variety of substances, such as metals, fatty acids, amino acid, hormones, and a large number of therapeutic drugs (54). Because of its clinical and pharmaceutical importance,

the interaction of HSA with a variety of ligands has been studied (55,56). HSA consists of six helical subdomains and its polypeptide back bone is formed by 585 amino acids. HSA has two major binding sites denoted IIA and IIIA according to the subdomains where they occur. The interaction of hypericin with HSA has been studied by various groups (57,58-60). Hypericin in aqueous physiological solution is aggregated (61), and binding with albumin helps to solubilize it in monomeric form, which is believed to be important for virucidal action (62). Burel and Jardon have also noted that the photodynamic properties of hypericin are greatly diminished when it is aggregated (63).

Previous studies have suggested that the binding site of hypericin was in the III A subdomain of the protein, where the hypericin is not completely shielded from the outer environment (59,60). Recent surface enhanced Raman (SERS) and resonance Raman (RR) studies, however, identify the binding site as the II A subdomain, where the binding occurs through an interaction between the carbonyl oxygen of hypericin and the N_1-H of the single tryptophan residue (W214) in the protein (57).

In this article we discuss the results of time-resolved fluorescence and absorption measurements of hypericin and hypocrellin A bound to HSA. An important problem that arises in the course of this investigation is understanding the nature of the complex that hypericin forms with subcellular components, in particular, HSA. Is this binding specific, that is, directed to a particular target site, or nonspecific? What nonradiative processes are induced upon binding? As will be seen, drastically different degrees of nonexponential fluorescence decay are observed for hypericin and hypocrellin A when they interact with HSA. In order to respond to these questions, hypericin was investigated in complex with other biological macromolecules whose binding interactions would be expected to present a considerable spectrum of variability with respect to that of HSA, namely poly dG-dC, Brij-35 micelles, and myoglobin.

MATERIALS AND METHODS

Hypericin, hypocrellin A, and the pH probes SNARF, and BCECF were purchased from Molecular Probes, and were used as received. Human serum albumin (99%, essentially fatty acid and globulin free), horse heart myoglobin (minimum 90%, lyophilized, essentially salt free), polydeoxyguanylic-deoxycytidylic acid (Poly dG-dC), Brij-35 (polyoxyethylene 23 lauryl ether), and AOT (dioctyl sulfosuccinate) were purchased from Sigma and were used as received.

Preparation of the hypericin-albumin and hypericin-myoglobin complexes. HSA and myoglobin solutions of 1.5×10^{-5} M concentration were prepared in 10-mM phosphate buffer (pH 7). A concentrated solution of hypericin in DMSO was added to the protein solution in microliter quantities so as to obtain a final DMSO concentration of ~ 0.8% and a final hypericin concentration of 4.0×10^{-6} M. The HSA/hypericin and myoglobin/hypericin complexes were equilibrated for 12 hours in the dark.

For steady-state spectra and time-resolved fluorescence studies we initially prepared a complex whose stoichiometry was 1:4 hypericin:HSA where the concentration of HSA was 1.5×10^{-5} M; and that of hypericin, 4.0×10^{-6} M. We also prepared 1:1 complexes where both the HSA and the hypericin concentrations were about 4.0×10^{-6} M. Both the 1:4 and the 1:1 hypericin:HSA complexes gave the same results in the fluorescence lifetime and anisotropy decay experiments..

For time-resolved absorption measurements, in order to obtain a measurable signal from the bound hypericin, it was necessary to increase the hypericin concentration to 7.0×10^{-5} M while keeping HSA at 1.5×10^{-5} M. This provided an ~5:1 hypericin:HSA complex. Attempts to make a 1:4 hypericin:HSA complex with [HSA] = 3.0×10^{-4} M and [hypericin] = 7.0×10^{-5} M resulted in aggregation of HSA. Furthermore, keeping [HSA] =

1.0×10^{-4} M in an attempt to make a 4:1 hypericin:HSA complex with [hypericin] = 4.0×10^{-4} M resulted in aggregation of hypericin. Finally a 1:1 hypericin:HSA complex was prepared where the concentration of each was 7×10^{-5} M. The association constant between hypericin and HSA has been given as $7.5 \times 10^{5}\ M^{-1}$ (58) and $1.3 \times 10^{7}\ M^{-1}$ (62).

Preparation of the hypericin-poly dG-dC complex. Ten units (one unit when dissolved in 1 mL buffer gives an absorbance of 1 at 260 nm in a 1 cm cell) of poly dG-dC was dissolved in 1 mL of 10 mM phosphate buffer (pH 7) by stirring for 24 hours. A concentrated solution of hypericin in DMSO was added in microliter amounts in order to obtain a final hypericin concentration of 3.0×10^{-6} M and a final DMSO concentration of 0.5%. The solution was stirred for 24 hours in the dark before performing experiments. Attempts to increase the concentration of hypericin for transient absorption experiments resulted in aggregation, so that pump-probe studies could not be performed.

Preparation of hypericin in micelles. To a concentrated (1.25×10^{-3} M) solution of Brij-35 in water a concentrated solution of hypericin in DMSO was added so as to have a final hypericin concentration of 2.0×10^{-6} M.

Time-resolved studies. Steady-state absorption spectra were obtained on a Perkin Elmer Lambda 18 double-beam UV-vis spectrophotometer with 1-nm resolution. Steady-state fluorescence spectra were obtained on a SPEX Fluoromax with a 4-nm bandpass, corrected for detector response. The apparatus for time-correlated single-photon counting and the 30-Hz pump-probe transient absorption spectrometer are described in detail elsewhere (25-27). Fluorescence decays are collected for a maximum of 10,000 counts in the peak channel. The polarized fluorescence traces used to obtain fluorescence anisotropy decay parameters were collected to a maximum of 20,000 counts in the peak channel.

Fluorescence upconversion. The fluorescence upconversion apparatus is based on a

homemade Ti:sapphire laser (64) producing pulses of less than 50 fs fwhm at a repetition rate as high as 90 MHz. The Ti:sapphire oscillator is pumped by an intracavity frequency-doubled Nd:YVO_4 continuous-wave laser (Millennia V, Spectra Physics) and produces tunable (750-850 nm) pulses which are precompensated for group velocity dispersion with a pair of glass prisms and a gold mirror. The fundamental beam is frequency doubled by a type-I, -mm LBO crystal from Super Optronics. These frequency-doubled excitation pulses, which typically were centered about 414 nm, are separated from the fundamental by a 400-nm dielectric mirror. To precompensate for group velocity dispersion a pair of quartz prisms oriented at Brewster's angle is used before focusing into the sample with 15 cm convex lens with anti-reflection coating for 400 nm. In order to reduce energy losses during precompensation a 400-nm zero-order quartz half-waveplate is used to minimize reflections at air-prism interfaces. The polarization orientation of the excitation light is then adjusted to the desired angle by another similar half-waveplate. For room temperature measurements, the sample was circulated in 1 mm flow cell by means of a dye laser pump with voltage-controlled rotation speed. The excitation light is removed from fluorescence by a 450-nm long-pass filter. The residual fundamental pulses are used as the gate to upconvert the fluorescence, which is collected with an LMH-10x microscope objective (OFR Precision Optical Products) coated for near infrared transmission. They are then focused by a 15-cm quartz lens onto a type-I 0.4-mm BBO crystal (cut at 31° and mounted by Quantum Technology, Inc.). The polarization of both excitation and gate beams is controlled with a set of zero-order half-wave plates coated for 400 and 800 nm respectively. The upconverted signal is sent directly into a H10 (8 nm/mm) monochromator (Jobin Yvon/Spex Instruments S.A. Group) coupled to a Hamamatsu R760 photomultiplier equipped with UG11 UV-pass filter and operated at maximum sensitivity. The photomultiplier output is amplified with two stages (total by a factor of 25) by a Stanford

Research Systems SR-445 DC-300 MHz amplifier with input terminated at 500 Ω and carefully calibrated after a long (1-2 hours) warm-up. Photon arrival events are registered with SR400 gated photon counter operated in CW mode with threshold level of 100-120 mV. At each delay step signal is obtained by averaging 3-5 samples collected for 1 s each. To reduce fluctuations due to laser flicker or sample instability (e.g. air bubbles in the flow cell) data are resampled if significant relative standard deviation or relative drift is detected. This approach also helps eliminate errors in data transmission lines. A translation stage (Klinger Scientific) with a resolution of 1 step/μm or 10 microsteps/μm is used to delay gate pulses and is controlled by a computer via an IEEE interface and Klinger Scientific CD-4 motor driver. The instrument response function is obtained by collecting a cross correlation function of the second harmonic and the fundamental (with the long-pass filter removed): The resulting third harmonic intensity is plotted against delay time. Cross correlation functions typically have a fwhm of 280-300 fs and for time scales greater 20 ps are assumed to be delta-function like. All curves were fit and deconvoluted from the instrument response function using an iterative convolute-and-compare nonlinear least-squares algorithm.

Average pump power was about 40-60 mW as measured at the second prism for precompensation. Spectral resolution was limited by the bandwidth of the upconversion crystal (BBO) and was estimated to be ±3 nm.

A sample of a total volume of ~10 ml was constantly pumped through a 1-mm quartz flow cell by a dye circulator. All experiments excluding sample preparation were performed in an unlit room.

An attempt was made to prepare a chromophore in buffer solution to serve as a reference sample for HSA complexes. Unfortunately, hypericin emission is efficiently quenched in the absence of the hydrophobic environment provided by the protein, and the

quantum yield was not sufficient to obtain a reasonable signal. Hypocrellin A was essentially *nonfluorescent both with and without* the protein, which is why no fluorescence upconversion results for hypocrellin A are reported here.

Attempts to observe light-induced acidification. Light induced pH drops by hypericin have been observed in different environments such as vesicles and 3T3 cells (37-39). We have employed the pH probes SNARF (Molecular Probes) to see if there is any light induced pH drops of hypericin bound to HSA. For the pH drop experiments, the solution was purged with argon for at least 30 minutes (argon was flowed gently over the top of the solution so as to prevent the formation of bubbles). The solutions are illuminated by the fluorimeter for 10 minutes at 550 nm (4-nm band pass). The hypericin/HSA complex was studied in pure water with and without buffer; but the SNARF spectra remained unchanged after illumination.

Consequently, a control experiment was performed to determine if there was any light induced pH drop of hypericin in a reverse micellar system in the absence of HSA. The system studied in this case was hypericin in n-heptane/AOT/water reverse micelles; and the pH probe used was SNARF. The concentration of AOT used was 0.5 M, and the amount of water added was 200 μL. The concentration of hypericin and SNARF were 2.2×10^{-6} M and 6.4×10^{-6} M. The solution was kept in the dark and purged with argon for one hour before illumination. The second harmonic of the Nd-YAG (532 nm) was used to illuminate the solution, and the power was a few microwatts. The composite fluorescence spectrum of hypericin and SNARF was recorded as soon as it was illuminated by the laser light and five minutes after. The two spectra showed no change in relative intensity, and consequently showed no indication of a light-induced pH change.

RESULTS

Steady-state Spectra

Figures 6.2a and 6.3 present the fluorescence excitation spectra of hypericin DMSO and in sulfuric acid (where the carbonyl groups are protonated). These differ in a number of ways. First, the sulfuric acid spectrum is red shifted with respect to that of DMSO. Secondly, the relative intensity of the 400-500 nm region of the sulfuric acid spectrum has increased considerably with respect to the DMSO spectrum. The emission spectrum in sulfuric acid is also red shifted compared to that in DMSO.

For purposes of comparison, Figs. 2a and 4 present the steady-state excitation and emission spectra of hypericin in complex with HSA and poly dG-dC, along with the spectrum in DMSO. In complex with HSA and with poly dG-dC, the excitation spectrum of hypericin is closer to that in sulfuric acid than in DMSO. The emission spectra are also red shifted, though not as much as in sulfuric acid.

The fluorescence quantum yield of hypericin/HSA (1:4) is 0.18, compared to 0.35 for hypericin in DMSO (32). The emission intensity of hypericin/poly dG-dC is very much weaker. The changes in the hypericin excitation spectra induced upon binding it to either HSA or poly dG-dC can be interpreted in terms of an interaction through its carbonyl oxygen if the above comparisons with the sulfuric acid spectra are justified. This interpretation is consistent with Raman studies which suggest that the carbonyl oxygen of hypericin interacts with the N_1-H of the single tryptophan residue present in II A subdomain of HSA (57). Raman studies also suggest that the hypericin interaction occurs via its carbonyl and *peri* hydroxyl groups with the N_7 nitrogen of the guanine residue in poly dG-dC (57,65-67). The reduction of the fluorescence quantum yield of hypericin/HSA with respect to that in DMSO may be due to the H-bonding interaction of

the carbonyl oxygen with the tryptophan residue, or a part of hypericin is projected outside of the protein, exposed to the solvent, or may be due to both. Similarly, in nucleic acid the very low emission can probably be accounted for greater interaction with the guanine residue, and/or greater exposure to the solvent. (It may be argued that the reduction of the fluorescence quantum yield of hypericin noted above is due to the formation of hypericin aggregates. At the micromolar concentrations used for the hypericin/HSA spectra, there was no evidence in the absorption spectra for aggregate formation. We did not, however, have enough nucleic acid to obtain a properly corrected absorption spectrum of the nucleic acid complex.)

Fluorescence Lifetime and Anisotropy Decay of Hypericin and Hypocrellin A in Complex with HSA

Tryptophan 214 of HSA. The fluorescence and fluorescence anisotropy decay parameters of the tryptophan of HSA are presented in Tables 6.1 and 6.2. In HSA, the tryptophan residue has a nonexponential fluorescence decay, which is best described by a sum of three exponentials. Its anisotropy decay is best characterized by a double exponential. These results are consistent with those obtained by other workers (68). The double exponential anisotropy decay of the tryptophan can thus be interpreted as arising from both rapid restricted local depolarizing motions and the overall rotational diffusion of the protein. The relative contributions of these two effects are related by the order parameter, S^2, from which can be calculated a hypothetical semi cone angle in which the tryptophan diffuses. For probes attached to globular proteins, the order parameter, S^2, is a model independent measure of the extent to which restricted motion can occur: $S^2 = [r(t)/r(0)] \exp(t/\tau_r) = r(0^+)/r_{eff}(0)$, where τ_r and $r(0^+)$ are determined by the fit of the long-time behavior of the anisotropy decay (the overall protein reorientation or tumbling) to a

single exponential and are equivalent to τ_2 and $r_2(0)$, respectively (69). $r_{eff}(0) = r_1(0) + r_2(0)$. For the tryptophan residue in HSA, $S^2 = 0.8 \pm 0.01$. The order parameter can be related to a hypothetical cone semiangle, θ_0, within which the transition dipole moment can diffuse: $S = (1/2)\cos\theta_0 (1 + \cos\theta_0)$. For the tryptophan residue in HSA, $\theta_0 = 30 \pm 1°$.

Hypericin. In comparison, hypericin has a single-exponential fluorescence decay of ~5.5 ns in all nonaqueous pure solvents. Bound to HSA (for both 1:4 and 1:1 complexes), however, its fluorescence decay is best described by a double exponential with a short component of ~2.5 ns (Figure 6.5 and Table 6.1). In order to understand what induces the nonexponential decay, hypericin was also studied in Brij-35 micelles and in complex with the protein myoglobin. In both cases, the resulting fluorescence decay is nonexponential. In the case of myoglobin, where hypericin can bind only to the surface of the protein, the decay is best described by a triple exponential (Table 6.1). Thus, in HSA the presence of this short component may arise from new nonradiative decay processes for a subset of hypericin molecules in the binding pocket, protruding into the solvent, or bound to the surface of the protein, or both.

The polarized fluorescence decay curves of hypericin bound to HSA are given in Figure 6.5. The limiting value for the anisotropy, r(0), for hypericin bound to the protein is 0.32 (Table 6.2). The anisotropy decay is single exponential and ~400-fold longer than that for the free molecule (31 ns in the protein as compared to ~80 ps in a 1:1 ethanol/methanol mixture (31)). This large rotational time constant is obviously a signature of the overall protein motion, thus indicating that hypericin is very rigidly bound to HSA. The anisotropy decay of hypericin bound to HSA must be considered carefully in light of the lifetime data discussed immediately above. Chromophores bound to proteins that exhibit no rapid restricted motion (with an apparatus providing ~50 ps time

resolution) are extremely rare. The example of the single tryptophan residue buried in the interior of *Pseudomonas aeruginosa* azurin is one example (70). The surfaces should be much less rigid and more disordered than the interiors. In addition, the surfaces are exposed to interactions with solvent. Consequently, the fluorescence anisotropy decay of the single surface exposed tryptophan residue in *Alcaligenes faecalis* azurin does exhibit rapid restricted motion, as is expected (70). We thus conclude that the single-exponential anisotropy decay of 31 ns for hypericin bound to HSA arises from hypericin molecules rigidly held in the binding pocket, but in sufficiently different conformations to experience different nonradiative interactions with neighboring amino acid residues. *If there are surface-bound hypericin molecules, the signal-to-noise ratio of our experiment is not sufficient to detect them in the anisotropy decay.*

Bound to poly dG-dC, the fluorescence intensity of hypericin was too low to permit time-resolved polarization studies. However, the time-resolved fluorescence (Figure 6.4c) shows a nonexponential decay, which can be best fit by a sum of three exponentials (Table 6.1).

Hypocrellin A. The effects of aqueous solvation and of binding to HSA on the fluorescence anisotropy decay and lifetime of hypocrellin A are illustrated in Figs. 6 and 7. There are considerable differences with respect to hypericin:

1. The fluorescence lifetime and anisotropy decays of the hypocrellin A/HSA complex depend on stoichiometry. Different kinetics are obtained for the 1:4 and the 1:1 complexes (Figure 6.6 and Tables 6.1 and 6.2). Most notable are the relative amplitudes of the shorter and 31-ns components of the anisotropy decays. Such an effect is not apparent for the hypericin/HSA complexes.

2. The steady-state absorption spectrum of hypocrellin A is much less sensitive to the presence of water than that of hypericin (compare Figs. 7a and 8a), as measured by the perturbation of the lowest energy transition upon addition of water.
3. The fluorescence lifetime of hypocrellin A is much less sensitive to the presence of water that that of hypericin (Figs. 7c and 8c).
4. The fluorescence decay of hypocrellin A bound to HSA is more similar to that of hypocrellin A in a 1% DMSO solution compared to hypericin bound to HSA (Figs. 7b and 8b).

Based on these fluorescence results, it is difficult to determine with any degree of certainty to what extent and in what manner hypocrellin binds to HSA. For example, the fluorescence lifetime data in mixed DMSO/water solutions clearly indicate that hypocrellin is much more hydrophilic than is hypericin. *We tentatively suggest that hypocrellin is aggregating nonspecifically at the surface of the protein.*

Investigating Ultrafast Excited-state Processes by Transient Pump-probe Absorption and Fluorescence Upconversion Techniques

Hypericin.

Transient absorption. In pump-probe transient absorption experiments, we have discovered that stimulated emission can be induced from the excited state of hypericin in the region of 600-660 nm (25-27). This stimulated emission grows with a time constant of 6-10 ps in all solvents, except sulfuric acid, where it appears within the duration of our laser pulses. We have argued that this transient is a signature of excited-state intramolecular proton (or hydrogen atom) transfer between the hydroxyl groups *peri* to the carbonyl. This interpretation has been confirmed in numerous experiments involving hypericin analogs (32,33) and by the fluorescence upconversion technique (34). Figure 6.9

presents the stimulated emission transients of hypericin in sulfuric acid, DMSO and in ~5:1 and 1:1 complexes with HSA.

The curves are distinctly different; and when the transients in DMSO and the protein are normalized and fit globally, the amplitude for the risetime of hypericin is smaller in HSA (0.36) than in DMSO (0.65) for the ~5:1 complex. It is thus possible to interpret these results as indicating that the excited-state proton or hydrogen atom transfer of hypericin is partially reduced, *but not stopped completely*, when it is complexed with HSA: i.e., that while one of the carbonyl groups is complexed to the N_1-H of the tryptophan residue, the other one is free to execute excited-state proton transfer. Because the ratio of hypericin to HSA in this experiment is approximately 5 to 1, the possibility that the observed kinetics are a superposition of intramolecular proton transfer reactions of surface-bound hypericin and pocket-bound hypericin cannot be unambiguously excluded For example, it may be argued that the transient in Figure 6.9c represents at least two different populations of hypericin molecules: those in which intramolecular proton transfer is *completely inhibited* because they are pocket bound and one of their carbonyls is coordinated to the N-H proton; and those that are bound to the surface and free to execute intramolecular proton transfer.

In order to investigate this possibility, the 1:1 complex of hypericin and HSA was investigated. *In the 1:1 complex, the rising component disappears, indicating that the intramolecular proton transfer process has been impeded.*

Fluorescence upconversion of the 1:1 complex. Because of the possibility that the rising component was obscured in the 1:1 complex by the presence of other absorbing species or because the signal-to-noise ratio was insufficient, we searched for the rising component with the fluorescence upconversion technique, which measures only emission. Figures 6.10 and 6.11 present fluorescence upconversion traces of the 1:1 hypericin/HSA

complex at two different emission wavelengths, 606 and 653 nm, corresponding to the first two maxima of the emission spectrum of the hypericin/HSA complex (Figure 6.2a). On the shortest time scales investigated (20 ps full scale) there was no evidence for a rising component in the fluorescence signal, confirming the conclusions obtained from the transient absorption measurements, that intramolecular proton transfer is impeded in the 1:1 hypericin/HSA complex.

Hypocrellin A. Because the fluorescence of hypocrellin A is so strongly quenched in the complex with HSA (Figures 6.6 and 6.7), it was impractical to obtain upconversion data. Transient absorption experiments with the 1:1 complex give no indication of excited-state proton transfer and only indicate a rapid decay of an excited state (~32 ps), consistent with the photon counting data (Figures 6.6 and 6.7).

Energy Transfer in the HSA Complexes

Between the tryptophan of HSA and hypericin . The emission spectrum of tryptophan overlaps the hypericin absorption spectrum, thus providing the possibility of energy transfer from tryptophan to hypericin. The total integrated emission intensity of the tryptophan residue in albumin is greater when there is no hypericin complexed to it. The ratio of the integrated emission intensity of tryptophan (after correcting for the inner filter effect due to hypericin absorption) without and with hypericin is 1.5, i.e. there is a 33% decrease in the integrated emission intensity. Figure 6.12 presents the corrected emission spectra of the tryptophan emission in the presence and in the absence of hypericin. The ratio of the integrated emission of hypericin at two wavelengths, 295 and 550 nm, was determined as follows (69):

$$\frac{\Phi_F(\lambda_1)}{\Phi_F(\lambda_2)} = \frac{1-10^{-A(\lambda_2)}}{1-10^{-A(\lambda_1)}} \frac{\int_0^\infty I_{em}(\lambda_1,\tilde{\nu})d\tilde{\nu}}{\int_0^\infty I_{em}(\lambda_2,\tilde{\nu})d\tilde{\nu}} \frac{c(\lambda_1)}{c(\lambda_2)}$$

where, $A(\lambda_i)$ is the absorbance (optical density) at the excitation wavelength, λ_i, $I_{em}(\lambda_i,\tilde{\nu})$ is the emission intensity at the excitation wavelength λ_i and $c(\lambda_i)$ is a correction factor taking into account fluctuations of the excitation intensity. The integrated emission (fluorescence quantum yield) of hypericin is 0.36 in DMSO and 0.53 when it is complexed with HSA (in this latter case, correction is made for the "inner filter effect" due to tryptophan absorption at 295 nm). Thus there is a 47% increase in the integrated emission of hypericin when excited at 295 nm, in the presence of albumin. This is in fair agreement with the percentage decrease of tryptophan emission. The fluorescence decay curves for tryptophan in the presence and in absence of hypericin are clearly different (Figure 6.12). The tryptophan residue in HSA has an emission maximum at 340 nm (compared to that of tryptophan in buffer at 352 nm) and the emission maximum has a slight red shift (342 nm) when complexed with hypericin. The quantum yield of tryptophan in HSA is 0.12 as compared to that of 0.18 for tryptophan in water at pH 7 (69,71). The average fluorescence lifetime of tryptophan in HSA decreases by 14% when hypericin is bound (data not shown). We were, however, unable to see any rise in the time resolved fluorescence of hypericin when exciting at 295 nm. This may be probably due to a very fast energy transfer that cannot be resolved with our instrument or whose amplitude is small compared to the prompt fluorescence arising from the direct excitation of the hypericin. Such a rapid energy transfer can explain our inability to observe a rise time in fluorescence emission of hypericin in our time-correlated single-photon-counting experiments.

In order to determine the efficiency of this energy transfer, we estimated the so-called critical distance. The efficiency of the nonradiative energy transfer in a Förster energy transfer mechanism is determined by, among other things, R_0, the critical distance at which the rate of energy transfer is equal to the inverse of the fluorescent lifetime of the donor.

$$k_{ET} = \frac{1}{\tau_F}\left(\frac{R_0}{R}\right)^6 \quad R_0^6 = \frac{9000(\ln 10)\Phi_D}{128\pi^5 n^4 N}\frac{2}{3}\int_0^\infty F_D(\tilde{\nu})\varepsilon_A(\tilde{\nu})\tilde{\nu}^{-4}d\tilde{\nu}$$

In the above equations k_{ET} is the rate of energy transfer, τ_F is the average lifetime of the tryptophan donor (3.4 ns), R is the distance of separation between the donor and acceptor, n is the index of refraction of the medium, N is Avogadro's number, Φ_D is the fluorescence quantum yield of the tryptophan donor (0.12), $F_D(\tilde{\nu})$ is the donor emission normalized to unit area on wavenumber scale, and $\varepsilon_A(\tilde{\nu})$ is the decadic molar extinction coefficient (in $L^{-1}mol^{-1}cm^{-1}$) on a wavenumber scale. R_0 calculated for the tryptophan-hypericin complex is 94 Å. This large value for R_0 is not surprising because there is a high degree of spectral overlap (Figure 6.13). Assuming the actual distance between these molecules to be 10 Å (center to center) the rate for energy transfer is 3.8×10^{14} s^{-1} (3×10^{-15} s). In order to resolve the energy transfer between tryptophan and hypericin, the two chromophores would need to be separated by 55 Å: such a separation, given the parameters of the calculation, yields an energy transfer time of 50 ps. We thus conclude that energy transfer between tryptophan and hypericin is too rapid to be observed with our apparatus. (We note that if the donor and acceptor are in physical contact, a Förster dipole-dipole mechanism may not be a quantitatively appropriate model for the energy transfer.)

If we assume that even in the 1:4 hypericin:HSA complex hypericin is nonspecifically bound to the surface of HSA (which is in agreement with the

nonexponential fluorescence decay of hypericin in this complex) as well as specifically coordinated to the tryptophan residue, a range of energy transfer times are expected. These can only be crudely estimated since even though a published structure for HSA exists (72,73), its coordinates have not been deposited in any data bank of which we are aware. The dimensions of HSA are approximately 30 × 80 × 80 Å. If we assume for a case of nonspecific binding that the tryptophan and hypericin lie on opposite extremes of the HSA the energy transfer time will be 0.4 ps at 30 Å and 790 ps at 80 Å. If all the hypericin molecules had a 10-Å center-to-center distance from tryptophan, it is expected that a negligible amount of tryptophan fluorescence be observed. Since this is not the case, we conclude that there is nonspecific binding of hypericin to HSA even in the 1:4 hypericin:HSA complex.

Between the tryptophan of HSA and hypocrellin A . We have no evidence for energy transfer from tryptophan to hypocrellin. In a 1:1 complex, the quantum yield of hypocrellin only increases 6%, which is negligible within the margin of error. In a 1:4 hypocrellin/HSA complex, the hypocrellin quantum yield decreases by 28%, which implies aggregation of hypocrellin. These results are again consistent with hypocrellin A binding to the surface of HSA in a nonspecific manner.

Discussion and Conclusions

A comparison of the steady-state spectra of hypericin in DMSO and sulfuric acid and in complex with HSA and poly dG-dC suggests that there is a strong interaction of the hypericin carbonyl group with the latter two macromolecules. Specific interactions of hypericin with DNA and its model compounds were studied by surface enhanced and resonance Raman spectroscopy (57,65-67). The results indicate that there is a site specific interaction between the terminal hydroxyl and carbonyl groups of hypericin and the

guanine residues in DNA probably through the N_7 atom. Raman studies also indicate that the carbonyl oxygen of hypericin interacts with the tryptophan residue in the II A sub domain of HSA. This interaction is suggested to occur via hydrogen bonding between the N_1-H of the tryptophan and the carbonyl oxygen of hypericin (57).

As indicated above, there are several important differences in the interactions of hypericin and hypocrellin A with HSA. It is reasonable to conclude from the 31-ns single-exponential fluorescence anisotropy decay of the HSA/hypericin complex and the fact that the form of this decay is independent of the stoichiometry of the complex (Figure 6.6), that the *majority* of hypericin binds rigidly and specifically in the IIA subdomain of HSA. On the other hand, not only is there a rapidly decaying component of ~150-250 ps in the anisotropy of the hypocrellin/HSA complex, but the form of the decay depends on the stoichiometry of the complex (Figure 6.6). The order parameters for the hypocrellin/HSA complex are ≤ 0.5 (as opposed to 1 for the hypericin/HSA complex) and indicate, along with the other data, that the majority of hypocrellin that binds to HSA binds to the more fluid-like exterior.

A comparison of the fluorescence properties of hypericin and hypocrellin in complex with HSA and in DMSO/water mixtures indicates that hypocrellin is more hydrophilic than hypericin, which is consistent with the above interpretation of the anisotropy data for hypocrellin binding largely to the HSA surface in a *nonspecific* manner. That there is no energy transfer from the HSA tryptophan to hypocrellin and that in the case of the 1:4 hypocrellin/HSA complex the fluorescence quantum yield of hypocrellin actually *decreases* when the tryptophan is excited strongly suggests that hypocrellin is aggregated at the surface of HSA.

In the 1:4 hypericin/HSA complex, it is very likely that some hypericin binds to the surface; but the fact that hypericin's lifetime in the complex is so much longer than that of

hypocrellin's (Figures 6.7b and 6.8b) indicates that these surface-bound molecules are not aggregated. Also, hypericin's ability to execute excited-state intramolecular proton transfer in *this* complex (Figure 6.9c) indicates that these surface-bound molecules are not aggregated—assuming aggregation most likely occurs end-to-end, so that the hydroxyl and carbonyl groups of neighboring hypericin molecules are mutually blocked (61). Note that there is no evidence for intramolecular excited state proton transfer for the hypocrellin/HSA complex in any stoichiometry. Study of the hypericin/HSA complex may also provide significant insight into the nature of the proton transfer reaction itself. If the specific binding interaction of hypericin to HSA is such as indicated in the Raman experiments (i.e., by coordinating one carbonyl group of hypericin and hence prohibiting it from accepting the neighboring hydroxyl proton), then the absence of intramolecular proton transfer in the 1:1 complex (Figures 6.9b, 6.10, 6.11) indicates that proton transfer cannot occur independently in the "top" or "bottom" of the molecule; and, consequently, *that the proton transfer is a concerted event involving both ends of hypericin.* It is also possible that the rigid binding of hypericin to HSA prohibits it from any intramolecular conformational change (74) that accompanies the proton transfer reaction and that this also is responsible for the absence of intramolecular proton transfer in the complex.

Finally, an important problem raised by this study is understanding the nature of the nonradiative processes induced upon binding hypericin to proteins, DNA, or micelles. In all the model systems to which hypericin is bound, nonexponential fluorescence decay is induced (Table 6.1). This question has been raised by Song and coworkers (75-76) in the context of another system that is very similar to that of hypericin, namely the stentorin chromophore (Figure 6.1). Stentorin serves as the primary photosensor in the single cell ciliate, *Stentor coeruleus.* Proton transfer has been suggested as a possible primary photoprocess in triggering the light signal transduction chain in *Stentor coeruleus.* The

stentorin chromophore is covalently linked to an ~50 kDa apoprotein. Bound to the protein, in water, this chromophore exhibits a very short-lived nonexponential fluorescence decay that is dominated (~95%) by an 8-ps component. Song and coworkers have shown that the long-lived hypericin fluorescence can be efficiently quenched by electron acceptors such as benzoquinone (77,78) and they have proposed that excited-state electron transfer of the stentorin chromophore to disulfide bonds in the protein result in photooxidation of the stentorin chromophore (HO—ST—OH) to oxystentorin (O = ST = O) and the loss of two protons by the following mechanism, which is reversible (75,78) :

$$HO—ST—OH + h\nu \rightarrow HO—ST—OH^{*} \rightarrow HO—ST—OH^{\bullet +} \rightarrow O = ST = O + 2H^{+}$$

Song and coworkers estimate the oxidation potential of excited-state hypericin to be ~1.2 V (77) and use the oxidation potential of dithiodiethanol (0.95 V) for that of a disulfide bridge. (There is considerable uncertainty in these numbers. For example, the oxidation potentials of cystine disulfide and oxidized β-mercaptoethanol are calculated to be 1.7 and 1.5 V, respectively (79)). It is quite possible that such electron transfer processes are occurring in HSA, which has 18 disulfide bridges (80). Excited-state electron transfer of hypericin bound to poly dG-dC is also feasible (the oxidation potentials of guanine and cytosine are 0.85 V and 1.2 V, respectively (81). It is also possible that the long-lived (~5.5 ns) excited state of hypericin is quenched by an excited-state *intermolecular* proton transfer process independent of any electron-transfer processes (for example, in myoglobin or micelles, where there are no disulfide bridges). Such excited-state proton transfer to an appropriate acceptor may explain our inability to observe a light-induced pH drop in micelles or bound to HSA (see Experimental Section).

The nonradiative rate processes that are introduced upon binding hypericin (or hypocrellin A) to protein, DNA, or micelles give rise to nonexponential fluorescence decay

in hypericin. In the context of what is known for the analogous stentorin chromophore, such nonradiative processes may involve excited-state electron transfer, excited-state proton transfer, or new processes introduced by the presence of surface-bound aggregates. Further work is required to understand the nature and the mechanisms of these pathways. To what extent they arise from specific or nonspecific binding, interior or surface binding, and aggregation of the chromophore is an important question that we hope to address by studying a more detailed series of target molecules than has been done in the present work where the nature of the chromophore-macromolecule interaction is known or can be predicted.

ACKNOWLEDGMENTS

This work was supported in part by NSF grant CHE-9613962 to J.W.P. P.M. was supported by grant 1/3258/96 of the Slovak Ministry of Education. We thank Professor Pierre Jardon and Dr. Anindya Dutta for their extremely careful reading of the manuscript and for their helpful comments.

REFERENCES

1. Duran, N. and P.-S. Song (1986) Hypericin and its photodynamic action. *Photochem. Photobiol.* **43**, 677-680.

2. Lown, J. W. (1997) Photochemistry and photobiology of perylenequinones. *Can. J. Chem.* 75, 99-119.

3. Diwu, Z. (1995) Novel therapeutic and diagnostic applications of hypocrellins and hypericins. *Photochem. Photobiol.* 61, 529-539.

4. Diwu, Z. and J. W. Lown (1990) Hypocrellins and their use in photosensitization. *Photochem. Photobiol.* 52, 609-616.

5. Kraus, G. A., W. Zhang, M. J. Fehr, J. W. Petrich, Y. Wannemuehler and S. Carpenter (1996) Research at the interface between chemistry and virology, development of a molecular flashlight. *Chem. Rev.* **96**, 523-535.

6. Meruelo, D., G. Lavie and D. Lavie (1988) Therapeutic agents with dramatic antiretroviral activity and little toxicity at effective doses: aromatic polycyclic diones hypericin and pseudohypericin. *Proc. Natl. Acad. Sci. USA.* **85**, 5230-5234.

7. Lenard, J., A. Rabson and R. Vanderoef (1993) Photodynamic inactivation of infectivity of human immunodeficiency virus and other enveloped viruses using hypericin and rose bengal: inhibition of fusion and syncytia formation. *Proc. Natl. Acad. Sci. USA* **90**, 158-162.

8. Hudson, J. B., J. Zhou, J. Chen, L. Harris, L. Yip and G. H. N. Towers (1994) Hypocrellin, from *Hypocrella bambuase*, is phototoxic to human immunodeficiency virus. *Photochem. Photobiol.* **60**, 253-255

9. Lopez-Bazzocchi, I., J. B. Hudson and G. H. N. Towers (1991) Antiviral activity of the photoactive plant pigment hypericin. *Photochem. Photobiol.* **54**, 95-98.

10. Couldwell, W. T., R. Gopalakrishna, D. R. Hinton, S. He, M. H. Weiss, R. E. Law and M. L. J. Apuzzo (1994) Hypericin a potential antiglioma therapy. *Neurosurgery.* **35**, 705-710.

11. Anker, L., R. Gopalakrishna, K. D. Jones, R. E. Law and W. T. Couldwell (1995) Hypericin in adjuvant brain tumor therapy. *Drugs of the Future* **20**, 511-517.

12. Thomas, C. and R. S. Pardini (1992) Oxygen dependence of hypericin-induced phototoxicity to EMT6 mouse mammary carcinoma cells. *Photochem. Photobiol.* **55**, 831-837.

13. Okpanyi, S. N. and M. L. Weischer (1987) Animal experiments on the psychotropic action of hypericum extract. *Arzneilmittel-Forschung* **37**, 10-13.

14. Linde, K., G. Ramirez, C. D. Mulrow, A. Pauls, W. Weidenhammer and D. Melchart (1996) St John's wort for depression—an overview and meta-analysis of randomised clinical trials. *Br. Med. J.* **313**, 253-258.

15. Suzuki, O., Y. Katsumata, M. Oya, S. Bladt and H. Wagner (1984) Inhibition of monoamine oxidase by hypericin. *Planta Medica* **50**, 272-274.

16. Takahashi, I., S. Nakanishi, E. Kobayashi, H. Nakano, K. Suziki and T. Tamaoki (1989) Hypericin and pseudohypericin specifically inhibit protein kinase C: Possible relation to their antiretroviral activity. *Biochem. Biophys. Res. Commun.* **165**, 1207-1212.

17. Utsumi, T., M. Okuma, T. Utsumi, T. Kanno, T. Yashuda, H. Kobuchi, A. A. Horton and K. Utsumi (1995) *Arch. Biochem. Biophys.* **316**, 493-497.

18. Fehr, M. J., S. L. Carpenter and J. W. Petrich (1994) The role of oxygen in the photoinduced antiviral activity of hypericin. *Bioorg. Med. Chem. Lett.* **4**, 1339-1344.

19. Andreoni, A., A. Colasanti, P. Colasanti, M. Mastrocinque, P. Riccio and G. Roberti (1994) Laser photosensitization of cells by hypericin. *Photochem. Photobiol.* **59**, 529-533.

20. Thomas, C., R. S. MacGill, G. C. Miller and R. S. Pardini (1992) Photoactivation of hypericin generates singlet oxygen in mitochondria and inhibits succinoxidase. *Photochem. Photobiol.* **55**, 47-53.

21. De Witte, P., P. Agostinis, P., J. Van Lint, W. Merlevede, J. R. Vandenheede (1993) Inhibition of epidermal growth factor receptor tyrosine kinase activity by hypericin. *Biochem. Pharmacol.* **46**, 1929-1936.

22. Miccoli, L., S. Oudard, F. Sureau, F. Poirson, B. Dutrillaux and M. F. Poupon. (1995) Intracellular pH governs the subcellular distribution of hexokinase in a glioma cell line. *Biochem. J.* **313**, 957-962.

23. Weller, M., M. Trepel, C. Grimmel, M. Schabet, D. Bremen, S. Krajewski and J. C. Reed (1997) Hypericin-induced apoptosis of human malignant glioma cells is light-dependent, independent of bcl-2 expression, and does not require wild-type p53. *Neurological Res.* **19**, 459-470.

24. Mirossay, L., A. Mirossay, E. Kocisova, I. Radvakova, P. Miskovsky and J. Mojzis (In press) Hypericin-induced apoptosis of human leukemic cell line HL-60 is potentiated by omeprazole, an inhibitor of H^+K^+-ATPase and 5'-(N,N-dimethyl)-amiloride, an inhibitor of Na^+/H^+ exchanger. *Physiological Research.*

25. Gai, F., M. J. Fehr and J. W. Petrich (1993) Ultrafast excited-state processes in the antiviral agent hypericin. *J. Am. Chem. Soc.* **115**, 3384-3385.

26. Gai, F., M. J. Fehr and J. W. Petrich (1994) Observation of excited-state tautomerization in the antiviral agent hypericin and identification of its fluorescent species. *J. Phys. Chem.* **98**, 5784-5795.

27. Gai, F., M. J. Fehr and J. W. Petrich (1994) Role of solvent in excited-state proton transfer in hypericin. *J. Phys. Chem.* **98**, 8352-8358.

28. Das, K., D. S. English, M. J. Fehr, A. V. Smirnov and J. W. Petrich (1996) Excited-state processes in polycyclic quinones, the light induced antiviral agent, hypocrellin, and comparison with hypericin. *J. Phys. Chem.* **100**, 18275-18281.

29. Das, K., D. S. English and J. W. Petrich (1997) Deuterium isotope effect on the excited-state photophysics of hypocrellin, evidence for proton or hydrogen atom transfer. *J. Phys. Chem. A.* **101**, 3241-3245.

30. Das, K., D. S. English and J. W. Petrich (1997) Solvent dependence on the intracellular excited-state proton or hydrogen atom transfer in hypocrellin. *J. Am. Chem. Soc.* **119**, 2763-2764.

31. Das, K., E. Dertz, J. Paterson, W. Zhang, G. A. Kraus and J. W. Petrich (1998) Hypericin, hypocrellin, and model compounds: steady-state and time-resolved fluorescence anisotropies. *J. Phys. Chem. B* **102**, 1479-1484.

32. English, D. S., W. Zhang, G. A. Kraus and J. W. Petrich (1997) Excited-state photophysics of hypericin and its hexamethoxy analog, intramolecular proton transfer as a nonradiative process in hypericin. *J. Am. Chem. Soc.* **119**, 2980-2986.

33. English, D. S., K. Das, J. M. Zenner, W. Zhang, G. A. Kraus, R. C. Larock and J. W. Petrich (1997) Hypericin, hypocrellin, and model compounds, primary photoprocesses of light-induced antiviral agent. *J. Phys. Chem. A.* **101**, 3235-3240.

34. English, D. S., K. Das, K. D. Ashby, J. Park, J. W. Petrich and E. W. Castner, Jr. (1997) Confirmation of excited-state proton transfer and ground-state heterogeneity in hypericin by fluorescence upconversion. *J. Am. Chem. Soc.* **119**, 11585-11590.

35. Das, K., A. V. Smirnov, M. D. Snyder and J. W. Petrich (1998) Picosecond linear dichroism and absorption anisotropy of hypocrellin: toward a unified picture of the photophysics of hypericin and hypocrellin. *J. Phys. Chem.* **102**, 6098-6106.

36. Falk, H., J. Meyer and M. Oberreiter (1992) Deprotonation and protonation of hydroxyphenanthroperylenes. *Monatsh. Chem.* **123**, 277-284.

37. Fehr, M. J., M. A. McCloskey and J. W. Petrich (1995) Light-induced acidification by the antiviral agent hypericin. *J. Am. Chem. Soc.* **117**, 1833-1836.

38. Sureau, F., P. Miskovsky, L. Chinsky and P. Y. Turpin (1996) Hypericin-induced cell photosensitization involves an intracellular pH decrease. *J. Am. Chem. Soc.* **118**, 9484-9487.

39. Chaloupka, R., F. Sureau, E. Kocisova and J. W. Petrich (1998) Hypocrellin A photosensitization involves an intracellular pH decrease in 3T3 cells. *Photochem. Photobiol.* **68**, 44-50.

40. Pinto, L. H., L. J. Holsinger and R. A. Lamb (1992) Influenza virus M_2 protein has ion channel activity. *Cell.* **69**, 517-528.

41. Newell, K. J. and I. F. Tannock (1989) Reduction of intracellular pH as a possible mechanism for killing cell in acidic region of solid tumor, effects of carbonylcyanine-3-chlorophenylhydrazone. *Cancer Res.* **49**, 4447-4482.

42. Newell, K. J., P. Wood, I. Stratford and I. Tannock (1992) Effect of agents which inhibit the regulation of intracellular pH on murine solid tumours. *Br. J. Cancer.* **66**, 311-317.

43. Barry, M. A., J. E. Reynold and A. Eastman (1993) Etoposide-induced apoptosis in human HL-60 cells is associated with intracellular acidification. *Cancer Res.* **53**, 2349-2357.

44. Gottlieb, R. A., J. Nordberg, E. Skowronski and B. M. Babior (1996) Apoptosis induced in Jurkat cells by several agents is preceded by intracellular acidification. *Proc. Natl. Acad. Sci. USA* **93**, 654-658.

45. Li, J. and A. Eastman (1995) Apoptosis in an interleukin-2-dependent cytotoxic lymphocyte cell line is associated with intracellular acidification. *J. Biol. Chem.* **270**, 3203-3211.

46. Hudson, J. B., V. Imperial, R. P. Haugland and Z. Diwu (1997) Antiviral activities of photoreactive perylenequinones. *Photochem. Photobiol.* **65**, 352-354.

47. Jardon, P., N. Lazortchak and R. Gautron (1987) Formation d'oxygène singulet $^1\Delta_g$ photosensibilisée par l'hypericine. Caractérisation et étude du mécanisme par spectroscopie laser. *J. Chim. Phys.* **84**, 1141-1145.

48. Racinet, H., P. Jardon and R. Gautron (1988) Formation d'oxygène singulet $^1\Delta_g$ photosensibilisée par l'hypericine étude cinétique en milieu micellaire non ionique. *J. Chim. Phys.* **85**, 971-977.

49. Darmanyan, A. P., L. Burel, D. Eloy and P. Jardon (1994) Singlet oxygen production by hypericin in various solvents. *J. Chim. Phys.* **91**, 1774-1785.

50. Park, J., D. S. English, S. Wannemuehler S. Carpenter and J. W. Petrich (1998) The role of oxygen in the antiviral activity of hypericin and hypocrellin. *Photochem. Photobiol.* **68**, 593-597.

51. Delaey, E. M., A. L. Vandenbogaerde, W. J. Merlevede and P. A. de Witte (1999) Photocytotoxicity of hypericin in normoxic and hypoxic conditions. *J Photochem. Photobiol. B.* (Submitted)

52. Miskovsky, P., F. Sureau, L. Chinsky and P.-Y. Turpin (1995) Subcellular distribution of hypericin in human cancer cells. *Photochem. Photobiol.* **62**, 546-549.

53. English, D. S., R. T. Doyle, J. W. Petrich and P. G. Haydon (In press) Subcellular distributions and excited-state processes of hypericin in neurons. *Photochem. Photobiol.*

54. Peters, T. (1985) Serum albumin. *Advances in Protein Chemistry* **37**, 161-245.

55. Fehske, K. J., W. E. Müller and U. Wollertt (1979) The lone tryptophan residue of human serum albumin as part of the specific warfarin binding site. *Mol. Pharmacology* 16, 778-789.

56. Davila, J. and A. Harriman (1990) Photochemical and radiolytic oxidation of a zinc porphyrin bound to human serum albumin. *J. Am. Chem. Soc.* 112, 2686-2690.

57. Miskovsky, P., D. Jancura, S. Sánchez-Cortés, E. Kocisova, D. Jancura and L. Chinsky (1998) Antiretrovirally active drug hypericin binds the IIA subdomain of human serum albumin: resonance Raman and surface-enhanced Raman spectroscopy study. *J. Am. Chem. Soc.* 120, 6374-6379.

58. Senthil, V., J. W. Longworth, C. A. Ghiron and L. I. Grossweiner (1992) Photosensitization of aqueous model systems by hypericin. *Biochem. Biophys. Acta* 1115, 192-200.

59. Köhler, M., J. Gafret, J. Friedrich, H. Falk and J. Meyer (1996) Hole-burning spectroscopy of proteins in external fields: human serum albumin complexed with the hypericinate ion. *J. Phys. Chem.* 100, 8567-8572.

60. Falk, H. and J. Meyer (1994) On the homo- and heteroassociation of hypericin. *Monatsh. Chem.* 125, 753-762.

61. Sevenants, M. R. (1965) Pigments of *Blepharisma undulans* compared with hypericin. *J. Protozool.* 12, 240-245.

62. Lavie, G., Y. Mazur, D. Lavie, A. M. Prince, D. Pascual, L. Liebes, B. Levin and D. Meruelo (1995) Hypericin as an inactivator of infectious viruses in blood components. *Transfusion* 35, 392-400.

63. Burel, L. and P. Jardon (1996) Homo-association de l'hypéricine dans l'eau et conséquences pour ses propriétés photodynamiques. *J. Chim. Phys.* 93, 300-316.

64. Huang, C. P., M. T. Asaki, S. Backus, H. Nathel, H. C. Kapteyn and M. M. Murnane (1993) 17-Fs pulses from a mode-locked Ti:sapphire laser. In *Ultrafast Phenomena VIII.* (Edited by J.-L. Martin, A. Migus, G. A. Mourou and A. H. Zewail), pp. 160-162. Springer, Berlin.

65. Jancura, D., S. Sánchez-Cortés, E. Kocisova, A. Tinti, P. Miskovsky and A. Bertoluzza (1995) Surface-enhanced resonance Raman spectroscopy of hypericin and emodin on silver colloids: SERRS and NIR FT SERS study. *Biospectroscopy* 1, 265-273.

66. Miskovsky, P., L. Chinsky, G. V. Wheeler and P.-Y. Turpin (1995) Hypericin site specific interactions within polynucleotides used as DNA model compounds. *J. Biomol. Str. Dyn.* 13, 547-552.

67. Sánchez-Cortés, S., P. Miskovsky, D. Jancura and A. Bertoluzza (1996) Specific interactions of antiretroviraly active drug hypericin with DNA as studied by surface enhanced Raman spectroscopy. *J. Phys. Chem.* 100, 1938-1944.

68. Munro, I., I. Pecht and L. Stryer (1979) Subnanosecond motions of tryptophan residues in proteins. *Proc. Natl. Acad. Sci. U.S.A.* 76, 56-60.

69. Rich, R. L., F. Gai, J. W. Lane, J. W. Petrich and A. W. Schwabacher (1995) Using 7-azatryptophan to probe small molecule–protein interactions on the picosecond time scale: the complex of avidin and biotinylated 7-azatryptophan. *J. Am. Chem. Soc.* 117, 733-739.

70. Petrich, J. W., J. W. Longworth and G. R. Fleming (1987) Internal motion and electron transfer in proteins: a picosecond fluorescence study of three homologous azurins. *Biochemistry* 26, 2711-2722.

71. Avouris, P., L. L. Yang and M. A. El-Bayoumi (1976) Excited state interactions of 7-azaindole with alcohol and water. *Photochem. Photobiol.* 24, 211-216.

72. Carter, D. C., X.-M. He and S. H. Munson (1989) Three-dimensional structure of human serum albumin. *Science* 244, 1195-1198.

73. Carter, D. C. (1992) Atomic structure and chemistry of human serum albumin. *Nature* 358, 209-215.

74. Das, K., K. D. Ashby, J. Wen, and J. W. Petrich (1999) The Temperature Dependence of the Excited-State Intramolecular Proton Transfer Reaction in Hypericin and Hypocrellin A. *J. Chem. Phys.* In press.

75. Dai, R., T. Yamazaki, I. Yamazaki and P.-S. Song (1995) Initial spectroscopic characterization of the ciliate photoreceptor stentorin. *Biochim. Biophys. Acta* **1231**, 58-68.

76. Tao, N., Orlando, M., Hyon, J.-S., Gross, M. and P.-S. Song (1993) A new photoreceptor molecule from *Stentor coeruleus*. *J. Am. Chem. Soc.* **115**, 2526-2528.

77. Wells, T. A., A. Losi, R. Dai, P. Scott, S.-M. Park, J. Golbeck and P.-S. Song (1997) Electron transfer quenching and photoinduced EPR of hypericin and the ciliate photoreceptor stentorin. *J. Phys. Chem. A* **101**, 366-372.

78. Angelini, N., Quaranta, A., Checucci, G., Song, P.-S., Lenci, F. (1998) Electron transfer fluorescence quenching of *Blepharisma japonicum* photoreceptor pigments. *Photochem. Photobiol.* **68**, 864-868.

79. Wardman, P. (1989) Reduction potentials of one-electron couples involving free radicals in aqueous solution. *J. Phys. Chem. Ref. Data* **18**, 1637-1657.

80. Rosenor, V. M., M. Oratz and M. A. Rothschild (1977) In *Albumin Structure, Function and Uses*, p 27. Pergamon Press.

81. Milazzo, G. (1976) In *Topics in Bioelectrochemistry and Bioenergetics* Vol. 1. p. 53. Wiley, London.

Table 6.1. Fluorescence lifetime parameters[a].

Sample	a_1	τ_1 (ps)	a_2	τ_2 (ps)	a_3	τ_3 (ps)
tryptophan in HSA[b]	0.29±0.01	363±30	0.23±0.02	2607±200	0.47±0.04	7787±500
tryptophan in hypericin/HSA complex[b]	0.32±0.03	296±45	0.29±0.01	2300±100	0.39±0.03	7720±470
hypericin in hypericin/HSA complex[c]	0.51±0.01	2850±350	0.49±0.01	5000±580		
hypocrellin A in hypocrellin/HSA complex[c]	0.4 (0.41)	89 (51)	0.25 (0.12)	540 (490)	0.35 (0.47)	1500 (1450)
hypericin in myoglobin[c]	0.33	180	0.27	1600	0.40	5800
hypericin in Brij-35 micelles[c]	0.05	1000	0.95	6500		
hypericin in poly dG-dC[c]	0.37	32	0.43	1300	0.20	3400

[a] Fluorescence lifetimes were fit to a sum of up to three exponentially decaying components and had the form: $F(t) = a_1 \exp(-t/\tau_1) + a_2 \exp(-t/\tau_2) + a_3 \exp(-t/\tau_3)$. The absence of values for a_3 and τ_3 implies that the lifetime was adequately described by a double exponential decay. $\chi^2 \leq 1.3$ for all data presented in the Table.

[b] For excitation and detection of the emission of the tryptophan residue of HSA, $\lambda_{ex} = 288$ nm, $\lambda_{em} = 300\text{-}400$ nm.

[c] For excitation and detection of hypericin and hypocrellin A, $\lambda_{ex} = 570$ nm, $\lambda_{em} \geq 610$ nm. Both 1:4 and 1:1 hypericin:HSA complexes gave identical results. Data shown here are for the 1:4 complex. For hypocrellin A, data for both 1:4 and 1:1 complexes are shown. The values in parentheses are those for the 1:1 complex.

Table 6.2. Fluorescence anisotropy parameters[a].

sample	r_1	τ_{r1} (ps)	r_2	τ_{r2} (ps)
tryptophan in HSA[b]	0.07±0.01	920±40	0.12±0.01	28000±3000
hypericin in HSA[c]	0.32±0.01	31000±4000		
hypocrellin A in HSA[c]	0.10 (0.14)	252 (165)	0.05 (0.12)	31000 (31000)
hypericin in Brij-35 micelles[c]	0.13	860	0.17	4700
hypericin in EtOH/MeOH(1:1)[c,d]	0.35±0.01	83±10		

[a] Fluorescence anisotropy decays were fit to a sum of up to two exponentially decaying components and had the form: $F(t) = r_2 \exp(-t/\tau_{r1}) + r_2 \exp(-t/\tau_{r2})$. The absence of values for r_2 and τ_{r2} implies that the lifetime was adequately described by a single exponential decay.

[b] For excitation and detection of the emission of the tryptophan residue of HSA, λ_{ex} = 288 nm, λ_{em} = 300 - 400 nm.

[c] For excitation and detection of hypericin and hypocrellin A, λ_{ex} = 570 nm, $\lambda_{em} \geq 610$ nm. Both 1:4 and 1:1 hypericin:HSA complex gave identical results. Data shown here are for the 1:4 complex. For hypocrellin A, data for both 1:4 and 1:1 complexes are shown. The values in parentheses are those for the 1:1 complex.

[d] Reference 31.

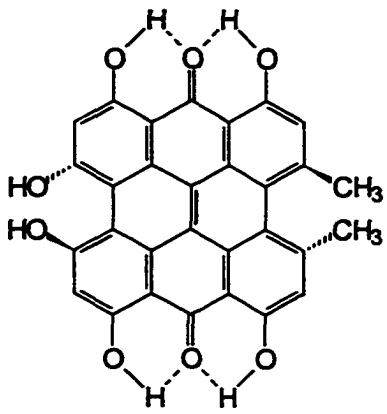

Hypericin

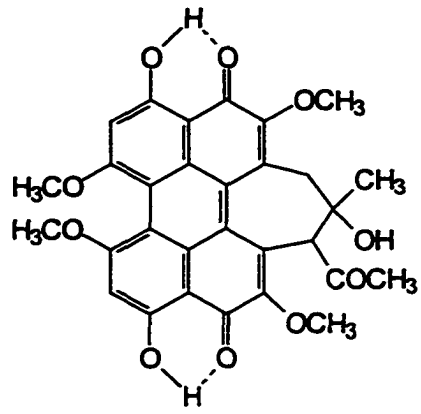

Hypocrellin A

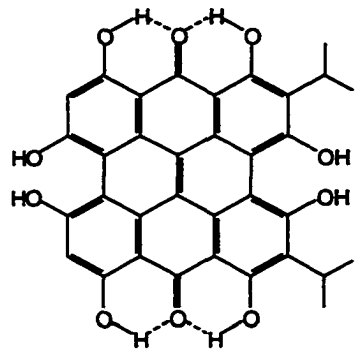

Stentorin chromophore

Figure 6.1 Two-dimensional structures of hypericin, hypocrellin A, and the stentorin chromophore.

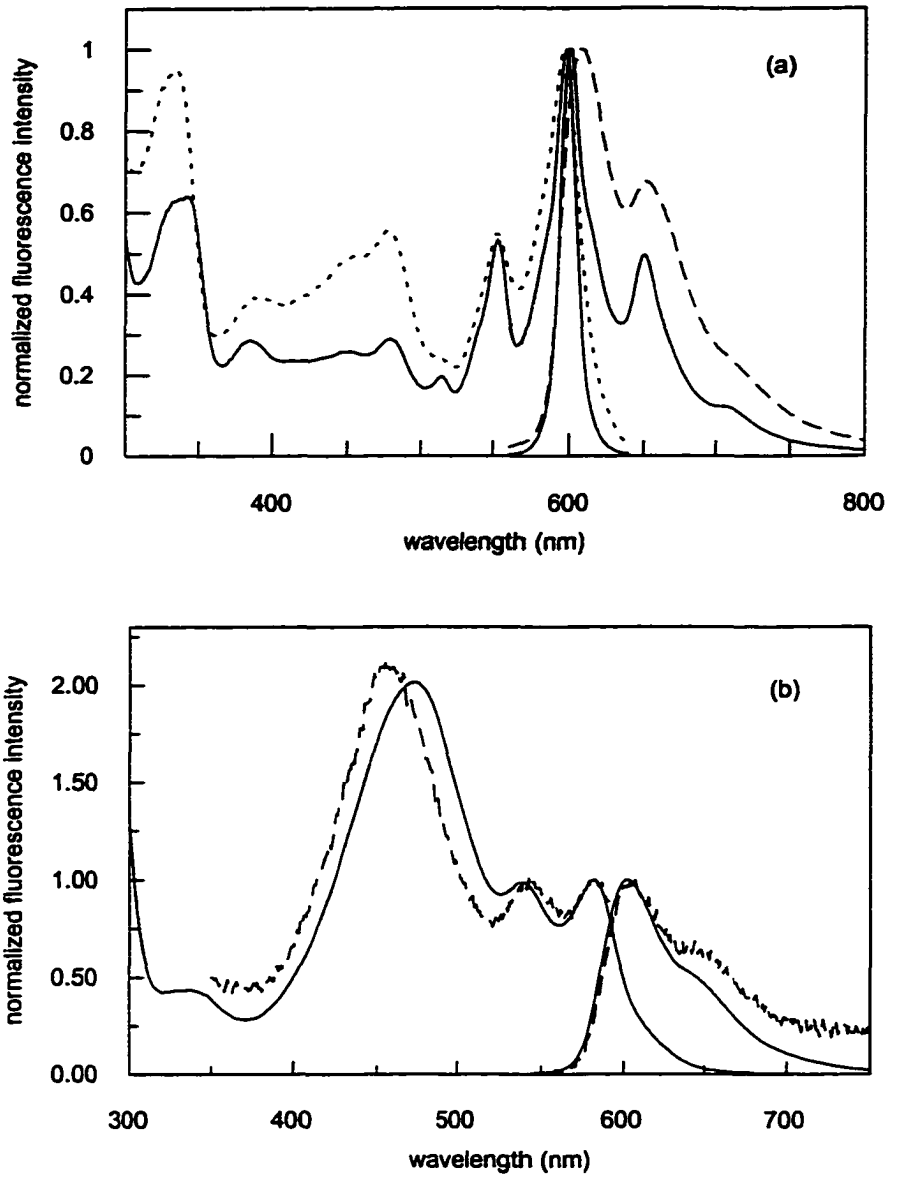

Figure 6.2(a) Fluorescence excitation (λ_{em} = 650 nm) and emission (λ_{ex} = 550 nm) spectra of hypericin in HSA (1:4 complex, [HSA] = 1.5×10^{-5} M and [hyp] = 7×10^{-6} M, dotted line) and in DMSO (solid line).

(b) Fluorescence excitation (λ_{em} = 650 nm for DMSO and 600 nm for HSA) and emission(λ_{ex} = 414 nm) spectra of hypocrellin A in HSA (1:1 complex, [HSA] = [hypocrellin] = 3.6×10^{-6} M, dotted line) and in DMSO (solid line). Greater noise in these data indicates considerably higher quenching efficiency as compared to hypericin/HSA complex.

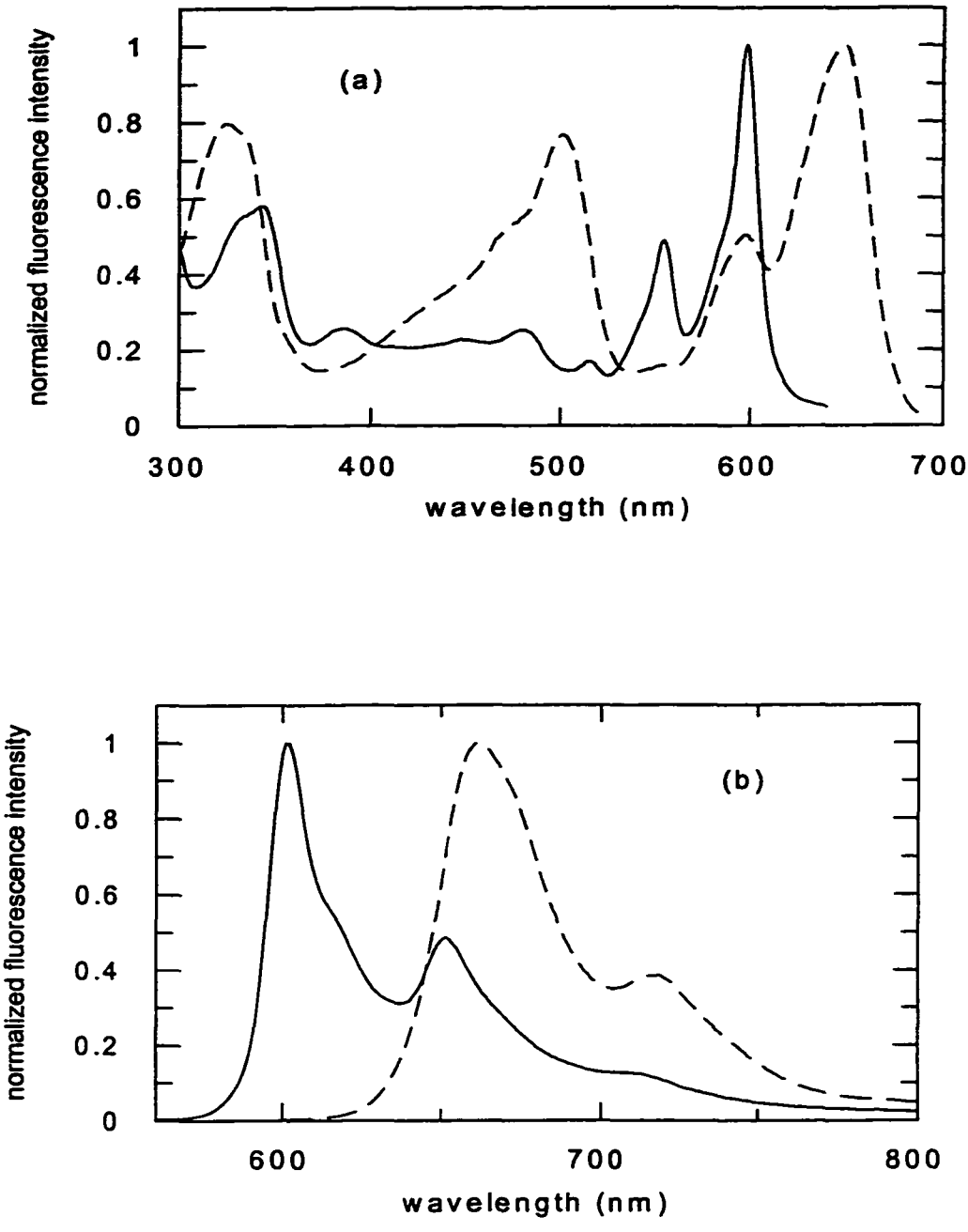

Figure 6.3 (a) Fluorescence excitation spectra of hypericin in sulfuric acid (λ_{em} = 750 nm, dotted line) and in DMSO (λ_{em} = 650 nm, solid line).

(b) Fluorescence emission spectra (λ_{ex} = 550 nm) of hypericin in sulfuric acid (dotted line) and in DMSO (solid line).

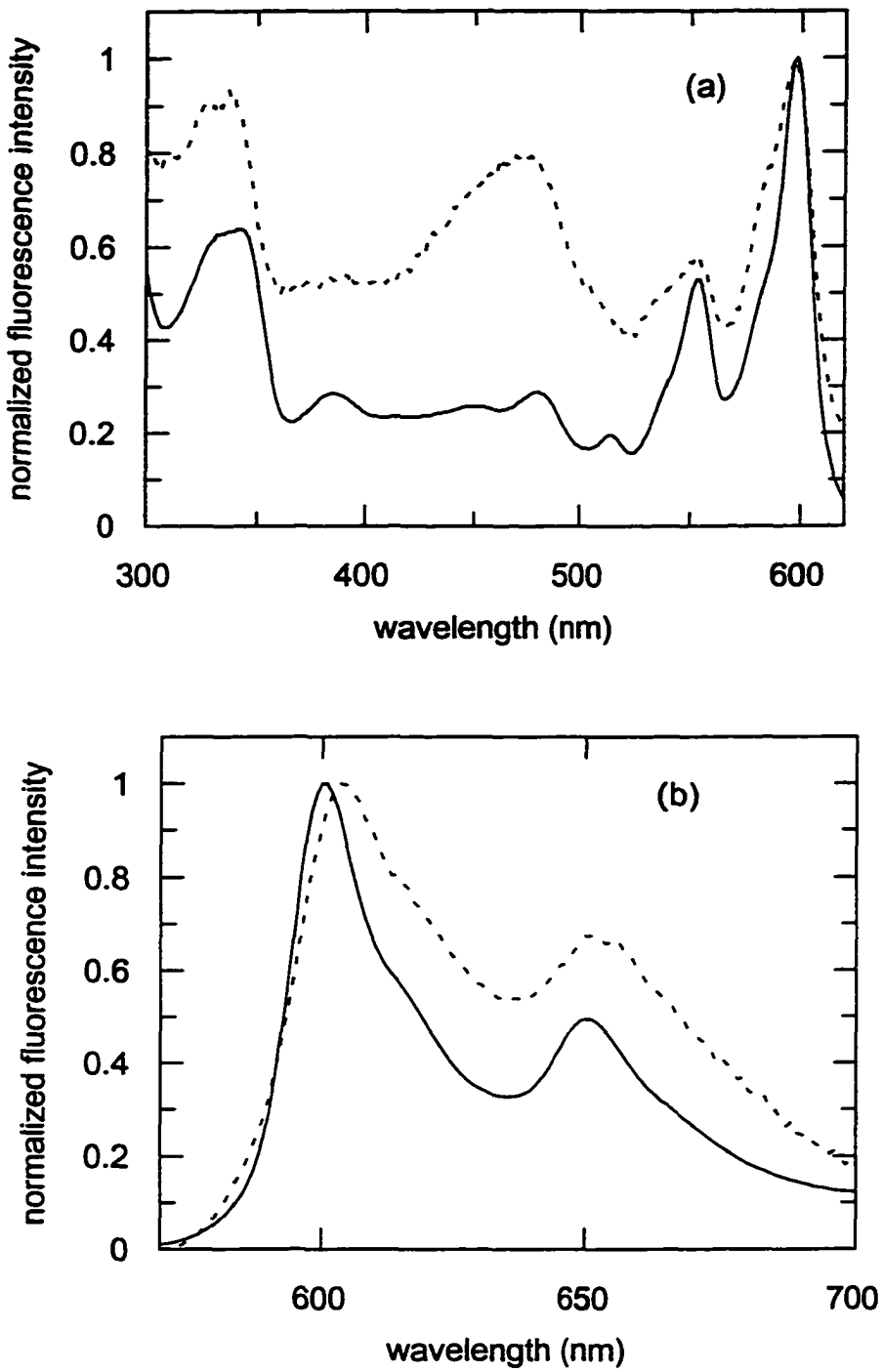

Figure 6.4 (a) Fluorescence excitation spectra (λ_{em} = 650 nm) of hypericin in poly dG-dC (dotted line) and in DMSO (solid line).

(b) Fluorescence emission spectra (λ_{ex} = 550 nm) of hypericin in poly dG-dC (dotted line) and in DMSO (solid line).

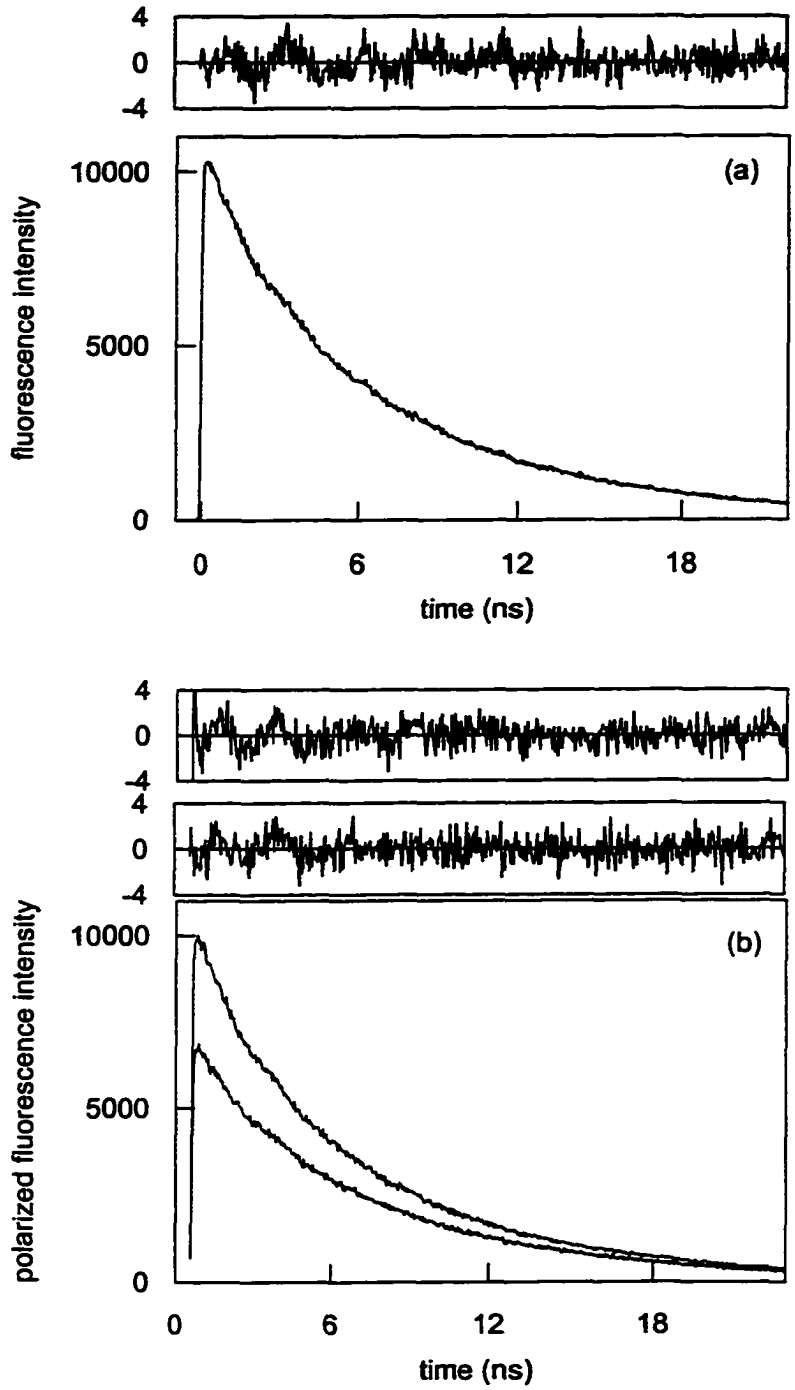

Figure 6.5 (a)Fluorescence decay of hypericin bound to HSA: λ_{ex} = 570 nm; $\lambda_{em} \geq 610$ nm, $\chi^2 = 1.10$.

(b) Fluorescence anisotropy decay of hypericin bound to HSA: λ_{ex} = 570 nm; $\lambda_{em} \geq 610$ nm, $\chi^2 = 1.12$. (*The anisotropy decay is independent of the stoichiometry of the complex.* Data not shown. See Table 6.2).

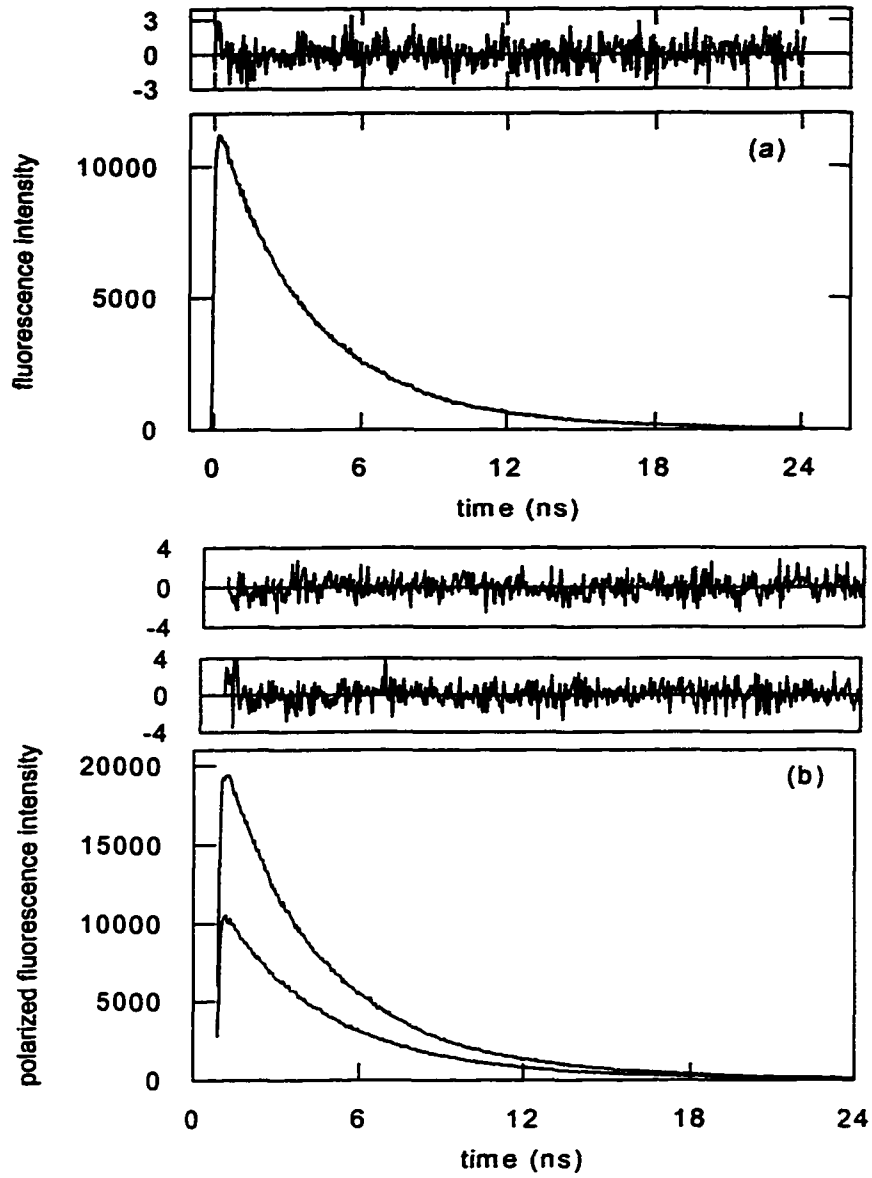

Figure 6.6 (a) Fluorescence anisotropy decay of hypocrellin A/HSA (1:4) in buffer. A fit to a double exponential yields r(t) = 0.10 exp(-t/0.25 ns) + 0.12 exp(-t/31 ns), χ^2 = 1.05. A fit of the lifetime to a triple exponential yields F(t) = 0.35 exp(-t/ 1.5ns) + 0.25 exp(-t/0.54 ns) + 0.40 exp(-t/0.09 ns), χ^2 = 1.0 (data not shown). The order parameter for this complex (1:4) is 0.54 and the half angle is 35.8°. See Table 6.2.

(b) Fluorescence anisotropy decay of hypocrellin A/HSA (1:1) in buffer. A fit to a double exponential yields r(t) = 0.14 exp(-t/0.17 ns) + 0.05 exp(-t/31 ns), χ^2 = 1.08. A fit of the lifetime to a triple exponential yields F(t) = 0.47 exp(-t/1.45ns) + 0.12 exp(-t/0.49 ns) + 0.41 exp(-t/0.05 ns), χ^2 = 1.15 (data not shown). The order parameter for this complex (1:1) is 0.28 and the half angle is 50.2°. See Table 6.2.

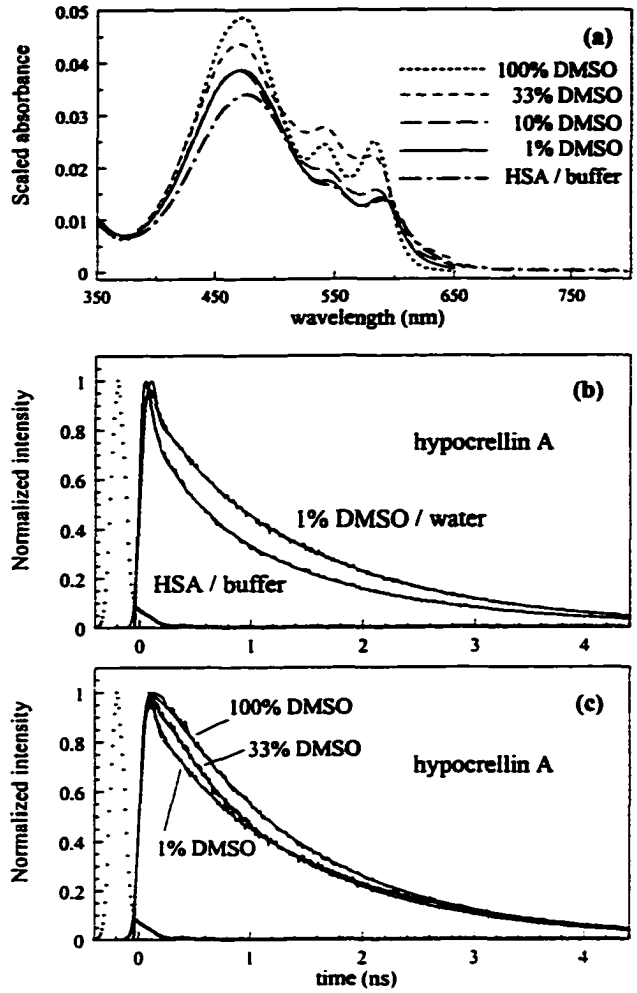

Figure 6.7(a) Absorbance spectra of hypocrellin A in 1:1 mixture with HSA in buffer (solid) and in DMSO/water mixtures of various proportions: 1% (dotted), 10% (long dashed), 33% (short dashed) and 100% DMSO (dash-dot). These spectra were scaled to compensate for slightly different chromophore concentration.

(b) Comparison of normalized lifetime decay traces in mixture with HSA (1:1 ratio) and in 1% DMSO/water solution. F(t) = 0.985exp(-t/4.2 ps)+0.002exp(-t/235 ps)+0.013exp(-t/1450 ps) for 1% DMSO. F(t) = 0.55exp(-t/63 ps)+0.19exp(-t/644 ps)+0.26exp(-t/1620 ps) for HSA/buffer solution.

(c) Normalized lifetime decay traces of hypocrellin A in DMSO/water mixtures of different proportions. F(t) = 0.97exp(-t/4.2 ps)+0.02exp(-t/235 ps)+0.01exp(-t/1450 ps) for 1% DMSO. F(t) = 0.83exp(-t/1.2 ps)+0.03exp(-t/363 ps)+0.13exp(-t/1335ps) for 33% DMSO. F(t) = 1.00 exp(-t/1310 ps) for 100% DMSO. The instrument response function is shown by the dotted line. It is also artificially shifted with respect to the fluorescence decays.

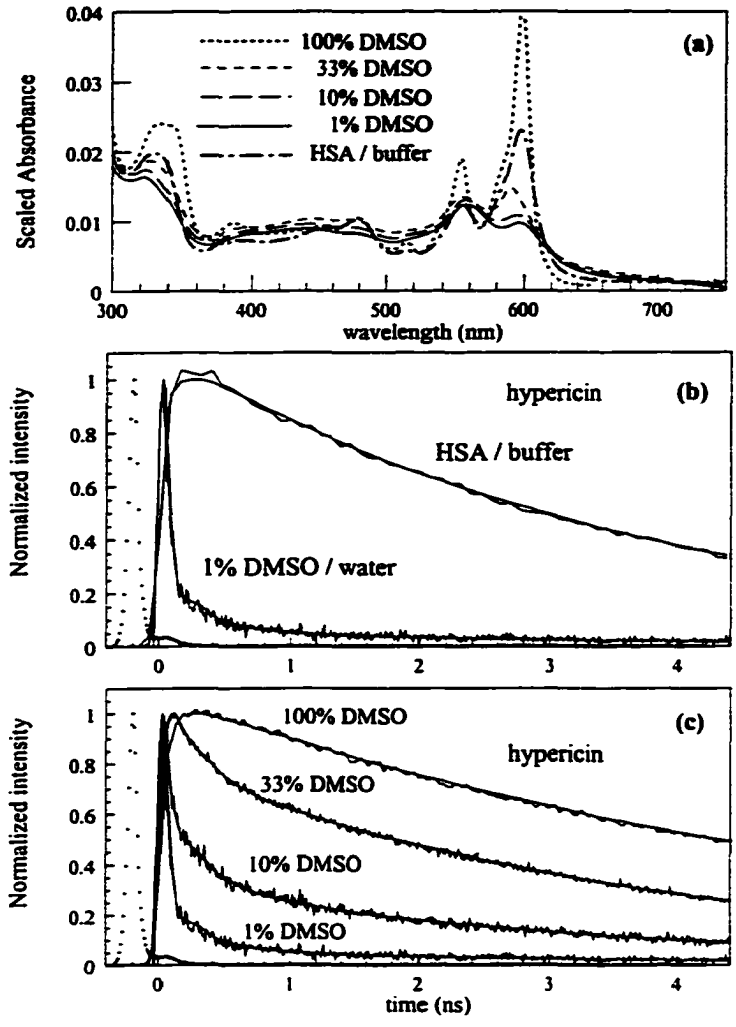

Figure 6.8(a) Absorbance spectra of hypericin in 1:1 mixture with HSA in buffer (dash-dotted) and in DMSO/water mixtures of various proportions: 1% (solid), 10% (long dashed), 33% (short dashed) and 100% DMSO (dotted). These spectra were scaled to compensate for slightly different chromophore concentration.

(b) Comparison of normalized lifetime decay traces of hypericin with HSA (1:1 ratio) and in 1% DMSO/water solution. F(t) = 0.96exp(-t/12 ps)+0.03exp(-t/304 ps)+0.01exp(-t/3680ps) for 1% DMSO. F(t) = 0.75exp(-t/3050 ps)+0.25exp(-t/5770 ps) for HSA/buffer solution.

(c) Normalized lifetime decay traces of hypericin in DMSO/water mixtures of different proportions. is shown in the insert. F(t) = 0.96exp(-t/12 ps)+0.03exp(-t/304 ps)+0.01exp(-t/3680ps) for 1% DMSO. F(t) = 0.91exp(-t/1.4 ps)+0.05exp(-t/264 ps)+0.04exp(-t/3380ps) for 10% DMSO. F(t) = 0.41exp(-t/190 ps)+0.59exp(-t/3870ps) for 33% DMSO. F(t) = 1.00 exp(-t/5580 ps) for 100% DMSO.

The instrument response function is shown by the dotted line. It is also artificially shifted with respect to the fluorescence decays.

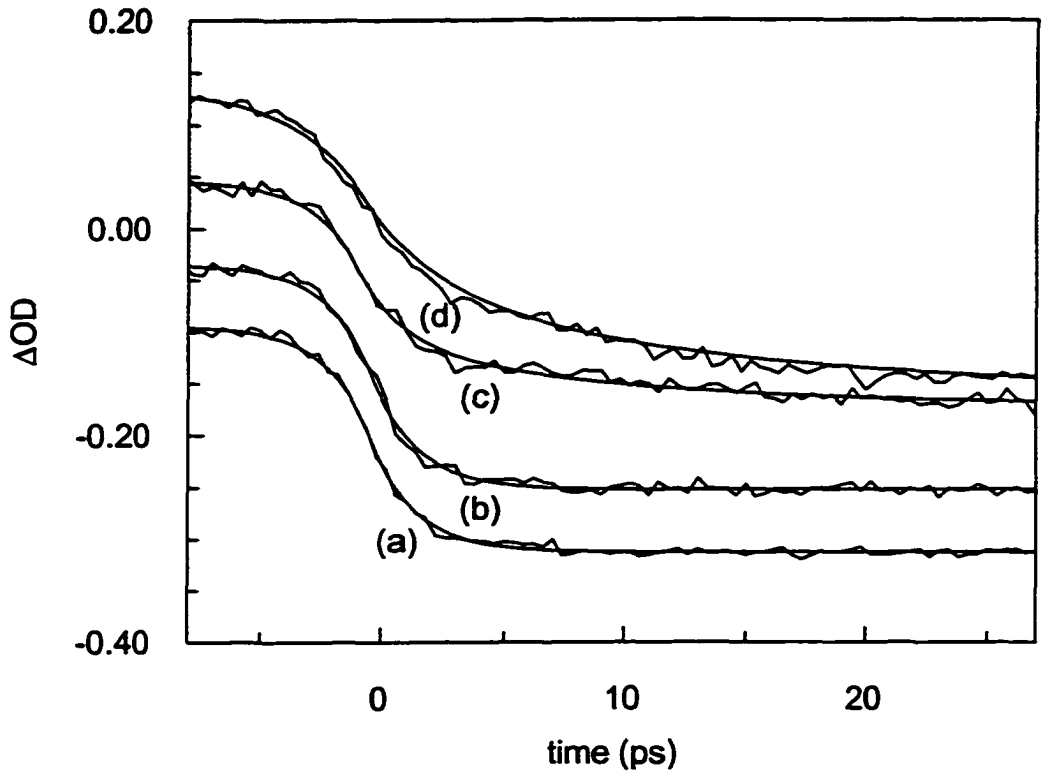

Figure 6.9Transient absorption traces of hypericin in different environments. The traces are normalized to the maximum absorption in the figure. λ_{pump} = 588 nm; λ_{probe} = 600 nm.

(a) Sulfuric acid: $\Delta A(t)/\Delta A_{max} = -1.0 \exp(-t/\infty)$.

(b) HSA: $\Delta A(t)/\Delta A_{max} = -1.0 \exp(-t/\infty)$; 1:1 complex, [HSA] = [hyp] = 7×10^{-5} M

(c) HSA: $\Delta A(t)/\Delta A_{max} = -0.36$ [exp(-t/6.0 ps) - 1] - 0.64; ~1:5 complex; [HSA] = 1.5×10^{-5} M; [hyp] = 7×10^{-5} M

(d) DMSO: $\Delta A(t)/\Delta A_{max} = -0.65$ [exp(-t/6.0 ps) - 1] - 0.35.

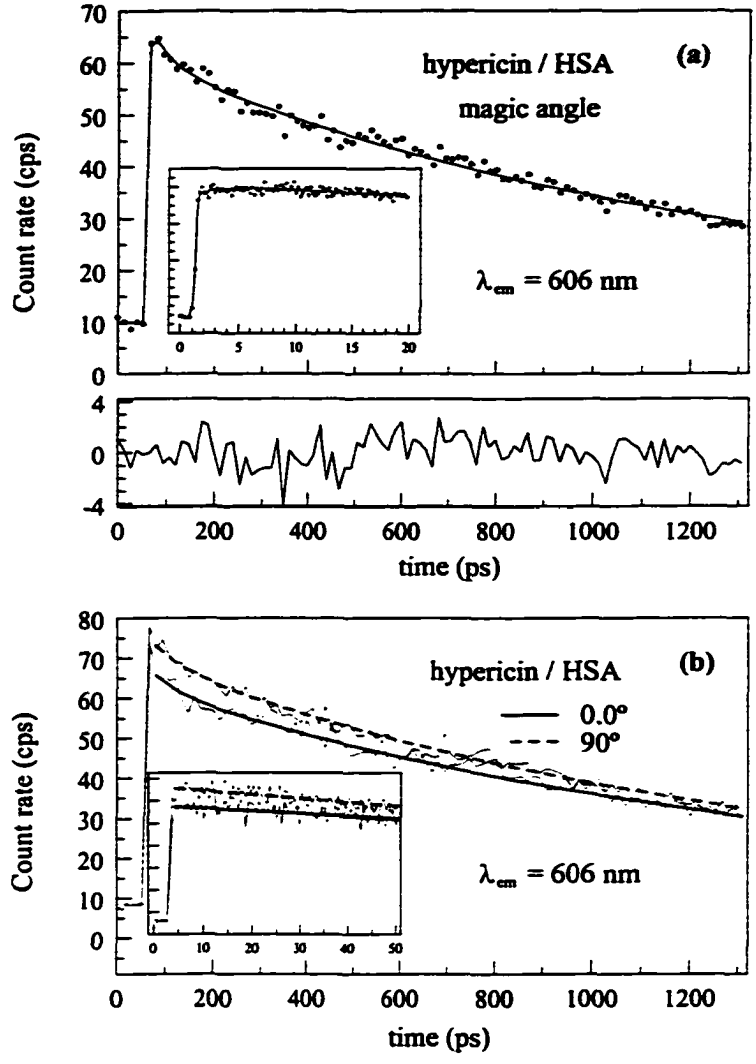

Figure 6.10 (a) Fluorescence upconversion at the "magic angle" of 1:1 hypericin:HSA complex, [HSA] = 1×10^{-4} M, λ_{ex} = 414 nm, λ_{em} = 606 nm. A fit to double exponential yields: F(t) = 0.12 exp(-t/50 ps) + 0.88 exp(-t/1320 ps). The 50-ps component is not observed with the limited resolution afforded by time correlated single photon counting measurements. The insert shows results obtained on a 20 ps time scale.

(b) Parallel and perpendicular fluorescence upconversion traces of the 1:1 hypericin:HSA complex, λ_{ex} = 414 nm, λ_{em} = 606 nm. Anisotropy decay fit with a single decaying component yields r(t) = -0.03 ± 0.01 exp(-t/2 ± 1 ns). The large relative error is due to the small value of limiting anisotropy at this excitation wavelength. The insert shows results obtained on a 20 ps time scale. That a value of ~2 ns instead of 31 ns (Table 6.2) is obtained is a result of collecting the data on a full scale of only 1.3 ns.

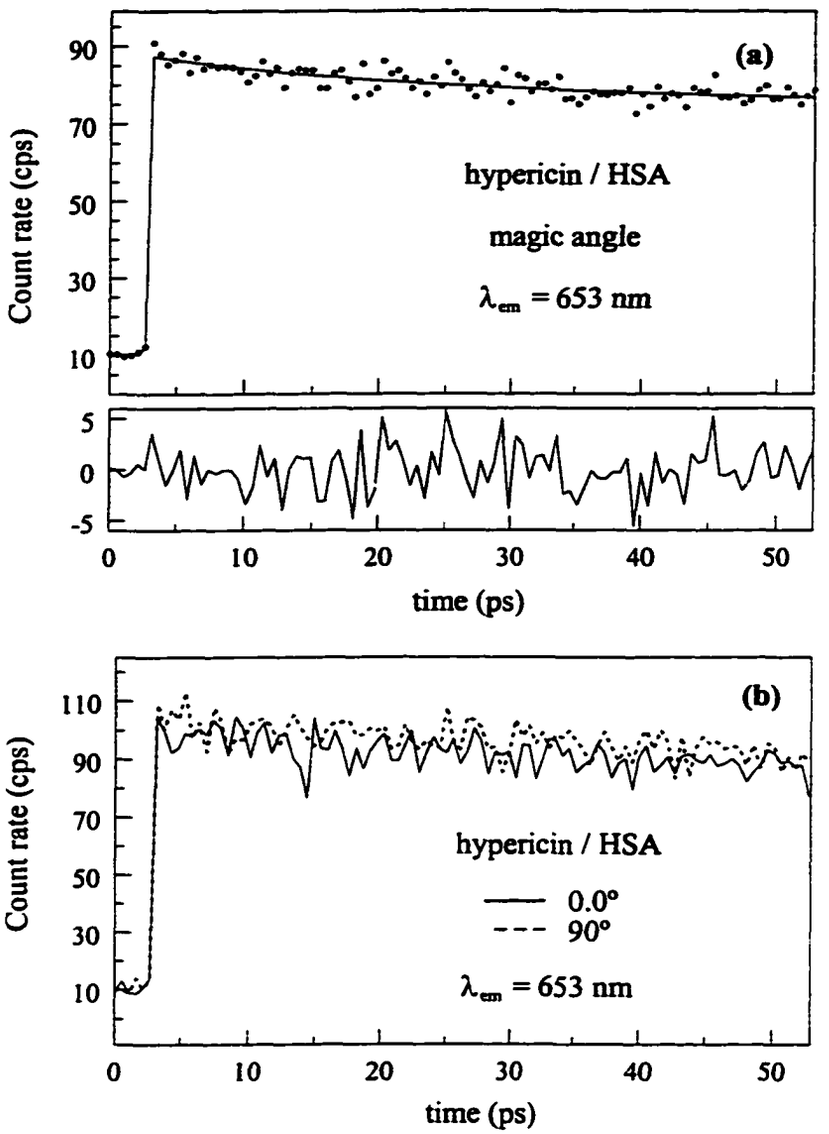

Figure 6.11 (a) Fluorescence upconversion at the "magic angle" of 1:1 hypericin:HSA complex, [HSA] = $1x10^{-4}$ M; λ_{ex} = 414 nm, λ_{em} = 653 nm.

(b) Parallel and perpendicular fluorescence upconversion traces of the 1:1 hypericin:HSA complex, λ_{ex} = 414 nm, λ_{em} = 653 nm.

These data were collected on the short timescale only.

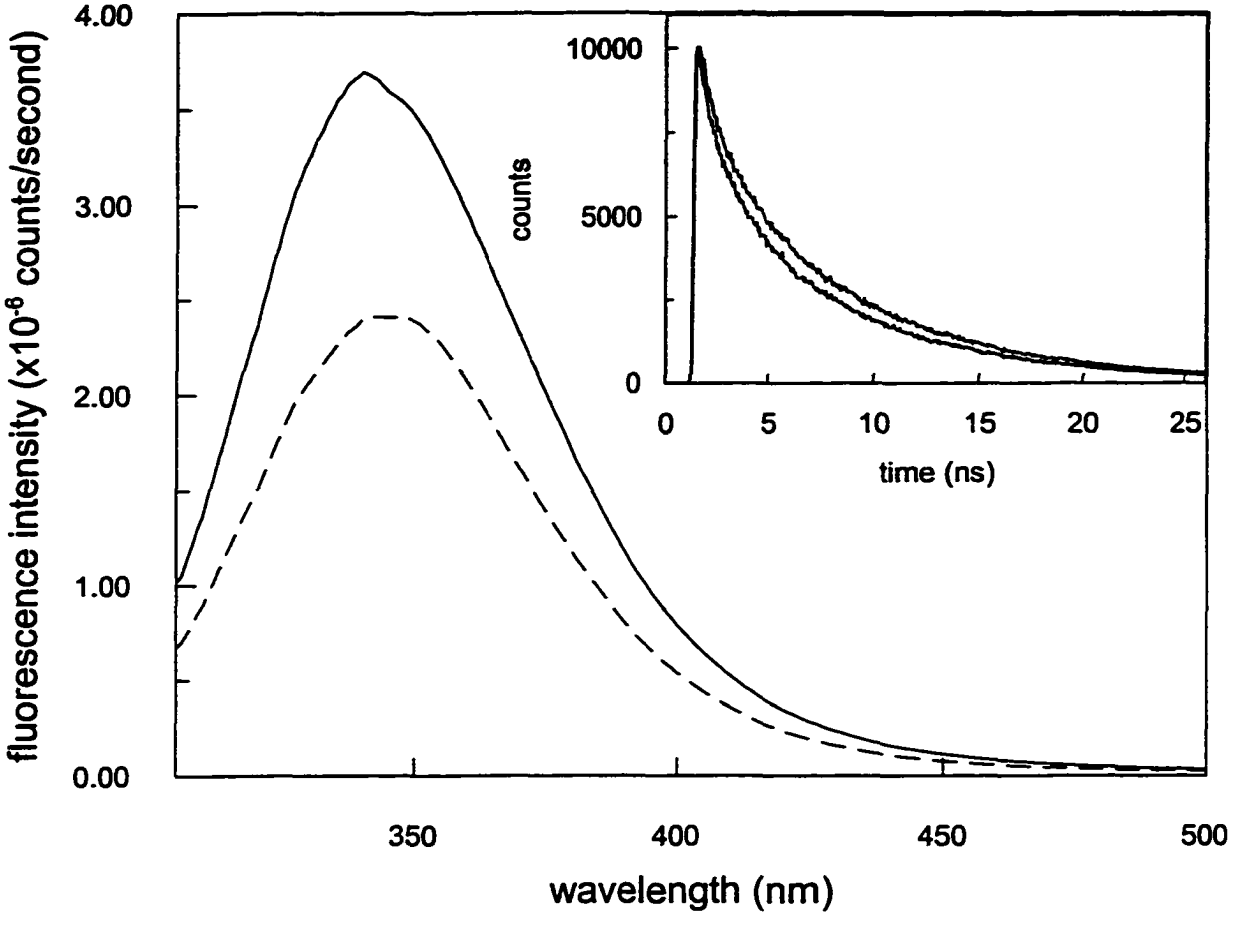

Figure 6.12 Corrected tryptophan emission of HSA in the presence (dashed line) and in the absence (solid line) of hypericin. Inset: Decay curve of the tryptophan residue of HSA in the absence (top) and in the presence (bottom) of hypericin. λ_{ex} = 288 nm; 300 ≤ λ_{em} ≤ 400 nm.

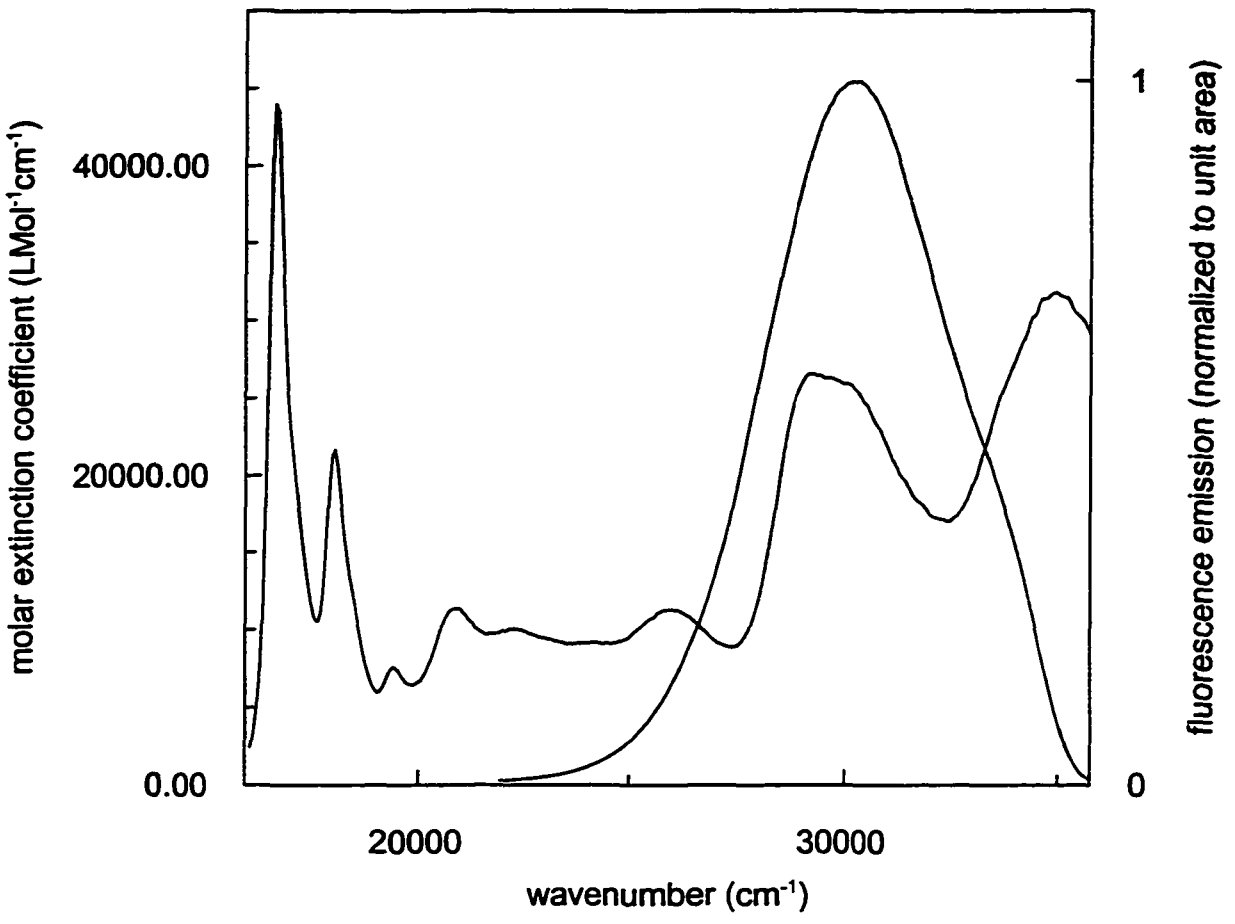

Figure 6.13 Spectral overlap between hypericin absorption and the tryptophan emission from HSA (in phosphate buffer at pH 7 and 22°C).

CHAPTER VII. EXCITED-STATE INTRAMOLECULAR H-ATOM TRANSFER OF HYPERICIN AND HYPOCRELLIN A INVESTIGATED BY FLUORESCENCE UPCONVERSION

A paper in preparation for submission to the Journal of Physical Chemistry

A. V. Smirnov, K. Das, D. S. English, Z. Wan, G. A. Kraus, and J. W. Petrich[1]

ABSTRACT

The excited-state intramolecular H-atom transfer reaction occurring in hypericin and hypocrellin is investigated by means of the fluorescence upconversion technique in a variety of solvents. Rising components of ~10 ps, attributable to intramolecular proton or H-atom transfer are clearly observed in the fluorescence upconversion traces of *both* hypericin and hypocrellin A. The amplitude of the rising component is emission wavelength dependent and occurs on the blue edge of the emission spectra. Neither in hypericin nor in hypocrellin A does this fluorescent component exhibit a deuterium isotope effect. This result identifies it with the ~10-ps component, also lacking a deuterium isotope effect, observed in hypericin in transient absorption measurements monitoring stimulated emission. The clear and complementary observation in fluorescence of the ~10-ps component in both hypericin and hypocrellin A is a crucial link in refining a unified model of the hypericin and hypocrellin photophysics that we first proposed in *J. Phys.*

---

[1] To whom correspondence should be addressed.

Chem. B 1998, *102*, 6098.

INTRODUCTION

The naturally occurring polycyclic quinones, hypericin and hypocrellin (Figure 7.1), have attained notoriety for their wide range of biological activities, many of which require light. These have been the subject of several reviews [1-3] and have been referred to in detail in our previous work [4-19]. One of the most interesting photophysical processes that these molecules execute is the excited-state proton (or H-atom) transfer, both intramolecular [4,6,13,20] and intermolecular [21,22]. We have suggested that the intermolecular proton transfer plays a role in certain aspects of the biological activity of hypericin and hypocrellin [8,21,23].

We have taken considerable pains to demonstrate that such H-atom transfer does occur in hypericin [4-6,9-12,17,24,25] and hypocrellin A [10,12-17,25]. One of the most convincing demonstrations was the observation of an ~10-ps rise time in the fluorescence upconversion signal of hypericin in DMSO [9]. One of the reasons for using the fluorescence upconversion technique is that often in transient absorption experiments it is difficult to distinguish stimulated emission from transient absorption. For example, if there are overlapping excited-state spectra, an apparent rise in induced absorption might in fact correspond to a decay of stimulated emission superimposed on an absorption transient that appears instantaneously and that does not decay on the time scale of the measurement. Thus, transient absorbance data can be subject to complications because they measure ground-state bleaching, absorption of all excited states present (both singlet and triplet), and stimulated emission. Because fluorescence upconversion monitors emission *only from the fluorescent singlet state*, it is not subject to these complications and hence provides complementary information not subject to the same ambiguities.

Our argument for intramolecular excited-state proton transfer in hypericin is as follows. The deshydroxy analog of hypericin, mesonaphthobianthrone (phenanthro-[1,10,9,8,*o,p,q,r,a*]perylene-7-14-dione, (Figure 7.1a), is non-fluorescent except in strong acids [6] (*e.g.* sulfuric acid or triflic acid (CF_3SO_3H)) where it produces a fluorescence spectrum that has nearly the same shape as that of hypericin in DMSO (Figure 7.2a). *These results demonstrate the importance of a protonated carbonyl group for producing hypericin-like fluorescence* [5,6]. The hypericin emission spectrum grows in on a 6-12-ps time scale in all solvents except in sulfuric acid where it is instantaneous. Based on the results for mesonaphthobianthrone (see above), *the rise time for the appearance of the hypericin emission is taken as evidence for an excited-state proton (H-atom) transfer* [6]. Confirming this interpretation are the fluorescence upconversion measurements [9] of hypericin and methylated hypericin analogs, which are incapable of executing intramolecular excited-state proton transfer reactions.

EXPERIMENTAL

Hypericin and *hypocrellin* A and B were obtained from Molecular Probes and were used as received. Anhydrous DMSO as well as HPLC grade methanol, ethanol and octanol from Aldrich were used (freshly opened) without further purification. Deuterated methanol (CH_3OD) and ethanol (CH_3CH_2OD) were 99.5+ grade and also came from Aldrich. To ensure thorough deuterium substitution solvent was repeatedly (3 times) added to the solid sample and evaporated under reduced pressure until dryness. The concentration of the sample was on the order of 10^{-4} M (0.05 mg/ml).

Steady-state absorbance spectra were obtained on a Perkin Elmer Lambda 18 double-beam UV-Vis spectrophotometer with 1-nm resolution. Steady state fluorescence spectra were obtained on a Spex Fluoromax with a 4-nm bandpass and corrected for lamp

spectral intensity and detector response.

The fluorescence upconversion apparatus is based on an amplified, homemade Ti:sapphire laser system producing pulses of less than 50 fs fwhm at a repetition rate as high as 90 MHz.. A Ti:sapphire oscillator pumped by intracavity doubled Nd:YVO_4 CW laser Millenia V (Spectra Physics) producing tunable (750-900 nm) pulses which are precompensated for group velocity dispersion with a pair of glass prisms and gold mirror. Frequency-doubled pulses are used to excite the sample. These pulses which typically were centered about 414 nm are also precompensated before focusing onto the sample with a pair of quartz prisms oriented at Brewster's angle. For room temperature measurements sample was circulated in 1 mm flow cell by means of dye laser pump with voltage-controlled rotation speed. Excitation light is removed from fluorescence by 450 nm long-pass filter. The residual fundamental wavelength is used as the gate pulse to upconvert the fluorescence, which is collected and focused into a 0.2-mm BBO crystal with an microscope objective coated for near-infrared region. Polarization of both excitation and gate beams is controlled with a set of zero-order quarter-wave plates coated for 400 and 800 nm respectively. The upconverted signal is sent directly into a H10 (8 nm/mm) monochromator from Jobin Yvon/Spex Instruments S.A. Group coupled to a Hamamatsu R760 photomultiplier equipped with UG11 UV-pass filter and operated at maximum sensitivity. PMT output is amplified with 2 stages (by a factor of 25) of Stanford Research Systems SR-445 DC-300 MHz amplifier terminated at 50 Ω and carefully calibrated after a long warm-up. Photon arrival events are registered with SR400 gated photon counter operated in CW mode with threshold level of 80-100 mV. At each delay step signal is obtained by averaging 3-5 samples collected for 1 s each. To reduce fluctuations due to laser flicker or sample instability (e.g. air bubbles in the flow cell) data are resampled if significant relative standard deviation or relative drift is detected. This approach also helps

eliminate errors due to data transmission. Translation stage from Microcontrole (France) with resolution of 1 step/μm or 10 microsteps/μm used to delay gate pulses is controlled by computer via IEEE interface and Klinger Scientific CD-4 motor driver. The instrument response function is obtained by collecting a cross correlation function of the second harmonic and the fundamental (with long-pass filter removed): the resulting third harmonic is plotted against delay time. Cross correlation functions typically have a fwhm of 280-300 fs and for time scales greater 20 ps are assumed to be delta-function like. All curves were fit and deconvoluted from the instrument function using an iterative convolute-and-compare nonlinear least-squares algorithm.

Methylation of hypocrellin A. One gram of potassium carbonate and 0.5 ml of MeI was added to 3 mg of hypocrellin A in 1 ml of acetone under nitrogen. This solution was boiled for 24 hrs with stirring. The solvent was removed, and residue was extracted with ethyl acetate. After ethyl acetate was removed under vacuum, the red crude product was purified by flash column chromatography (ethyl acetate:hexane / 4:1, then methanol:ethyl acetate / 1:1), giving 2.9 mg red solid. NMR showed that the phenol protons had disappeared. δ ppm ($CDCl_3$): 6.83-6.82 (2H); 4.05-4.21 (18H); 3.27-3.40 (2H); 2.51-2.56 (1H); 1.91-1.94 (3H); 1.62-1.69 (3H).

RESULTS

The steady-state absorption and emission spectra of hypericin, hypocrellin A and its methylated analog are presented in Figure 7.2c.

Fluorescence upconversion traces of hypericin and hypocrellin A are presented in Figures 7.3-7.8. The significant results are that: a ~10-ps rising component is observed on the blue edge of the emission spectra in all cases, except for hypocrellin A in DMSO; no long-lived (i.e. 50-230-ps) rising component is observed in the hypocrellin (or hypericin)

fluorescence upconversion traces; and no deuterium isotope effect is observed on the ~10-ps component for either hypericin or hypocrellin A.

Figure 7.7 presents the polarized fluorescence data of hypocrellin A in DMSO, ethanol, and octanol. The crucial result here is that no ~10-ps component is observed in the anisotropy decay, indicating that the origin of this component cannot be attributed to the relaxation of a higher lying excited state.

Figure 7.9 indicates the absence of the ~10-ps rising component in methylated analog of hypocrellin A (Figure 7.1b), further suggesting that its origin is intramolecular H-atom transfer.

DISCUSSION

A. Assignment of the ~10-ps Component to Intramolecular H-Atom Transfer

The original assignment of the ~10-ps component in hypericin to intramolecular H-atom transfer was based on the optical properties of the analog mesonaphthobianthrone in various solvents and the observation of a rise time in the stimulate emission of hypericin (see Introduction). Additional evidence was provided by the investigation of *O*-methoxy analogs [9-11,17] and the observation of the ~10-ps component in fluorescence upconversion [9]. The latter eliminates the possibility that the transient arises from spurious excited state absorbance decays that might overlap the stimulated emission spectrum. Also in complex with human serum albumin [19] this fast component was not observed which is accordance with resonance Raman measurements implicating aromatic hydroxyl engagement in interaction with host molecule (HSA).

The ~10-ps observed in the fluorescence upconversion signal for hypocrellin A in this work is also absent in the methylated analog (Figure 7.9), which lacks labile H atoms.

In addition, no component of this duration is observed in the fluorescence anisotropy decay of hypocrellin A. Hypocrellin A, like hypericin, has its $S_0 \rightarrow S_1$ transition polarized at large angles to its $S_0 \rightarrow S_2$ transition [17]. If a ~10-ps *fluorescence* anisotropy decay were observed, it could be attributed to excited-state relaxation from S_2 to S_1. On the other hand, a rapid relaxation was observed in the fluorescence anisotropy decay of 7-azaindole dimer [26], which also possesses transition dipole moments to closely lying excited-states at large angles to each other: in this case, the observation was used to argue quite convincingly that the proton transfer reaction in the 7-azaindole dimer in the condensed phase does not proceed by means of an intermediate—as has been argued to be the case in the gas phase [27].

Vibrational cooling effects may be eliminated since, again, the ~10-ps component is not observed in the *O*-methoxy analogs and also because in hypericin and hypocrellin, this component is observed using excitation wavelengths of 294, 415 and 588 nm [9-11,14]. Ultrafast (<5 ps) decay fluorescence component is registered for most of these analogs and is in great contrast to a slower rising feature of non-methylated compounds. With the current signal-to-noise ratio provided by upconversion technique it is almost impossible to reveal if same short decaying component is present in hypericin or hypocrellin. Lastly, no dynamic Stokes shifts have been observed [9-11] on this or any other time scale.

B. A Unified Picture of the Hypericin and Hypocrellin Photophysics

We had previously constructed a picture that unifies the photophysics of hypericin and hypocrellin A. The key points, subsequently refined and augmented, upon which this picture is based are the following:

1. Proton transfer rates of hypocrellin and hypericin can differ by more than an order of magnitude. X-ray and fluorescence data lead us to propose that hypocrellin

exists at least partially in a tautomeric form that is similar to that which hypericin would assume in the ground state (Figure 7.1b), if it were thermodynamically feasible. This conclusion has now been verified by NMR measurements [18]. Consequently, the 50-230-ps transients in hypocrellin A are interpreted in terms of "back transfer" reactions [13] with respect to the corresponding hypericin reaction.

2. The proton transfer reaction in hypericin is not dependent on viscosity and depends only very weakly on solvent [5]. This suggests that intramolecular vibrations control the proton transfer reaction in hypericin. However for hypocrellin, the "back-transfer" reaction rate is very strongly dependent on viscosity [12,13,15].

3. No deuterium isotope effect is observed for hypericin [6]; but a deuterium isotope effect of 1.4 is observed for hypocrellin [14]. *This isotope effect unambiguously identifies the excited-state process as a proton transfer event.*

4. For hypocrellin in viscous solvents such as octanol and ethylene glycol, a transient of ~10-ps duration is also detected in the transient absorption data [13]. The results presented here indicate that it is present as well in the fluorescence upconversion data. *This is a crucial and unifying result for understanding the photophysics of these systems.*

5. The excited-state intramolecular proton transfer reactions of hypericin and hypocrellin A are measured as a function of temperature in an ethanol/methanol mixture. The data yield activation energies of 0.044 ± 0.008 and 2.12 ± 0.070 kcal/mol for hypericin and hypocrellin A, respectively. The negligible activation energy of hypericin is consistent with previous suggestions that the proton-transfer reaction is adiabatic [14] and that a very low-amplitude displacement in at least one other coordinate be taken into account in order to describe the reaction dynamics. The proton transfer for hypocrellin is also considered to occur in the adiabatic

regime, but the significant activation energy suggests that a larger amplitude motion than that for the case of hypericin comprises part of the reaction coordinate. Much of the barrier cited above for hypocrellin A results from the temperature dependence of the viscosity of the solvent mixture. The *viscosity independent* part of the activation barrier, 0.41 ± 0.088 kcal/mol, is larger than that for hypericin but still quite small. The conformational changes that are coupled to the proton transfer reaction in hypericin and hypocrellin have yet to be identified and are currently under investigation.

6. The fluorescence lifetimes of hypericin and hypocrellin, measured with ~50 ps time resolution, are independent of excitation wavelength: identical results are obtained exciting at 300 or 570 nm [17]. Assuming that the ground-states of these species are heterogeneous, as noted above, this result suggests that the fluorescent species (detected via methods with time resolution no better than 100 ps) for both hypocrellin and hypericin is an intermediate between (two) tautomeric or isomeric species.

Structurally hypericin and hypocrellin are very similar. They both possess extended aromatic skeletons whose most important functionalities are the hydroxyls *peri* to the carbonyls. In this regard, the most significant structural difference between them is that hypocrellin possesses two fewer *peri* hydroxyls. *The current picture that we have formed of the excited-state dynamics of hypericin and hypocrellin is that the different photophysical behavior that we have enumerated above of these two structurally very similar molecules arises because we are probing different regions of very similar potential energy surfaces.* This picture is crudely illustrated in Figure 8 of reference [16] (or see Figure 4.8 in Chapter IV).

A crucial result in forming this hypothesis is the observation that under certain conditions we resolve a time constant in the hypocrellin photophysics in transient absorption measurements that is comparable to that observed in hypericin (point 4 above). This ~10 ps component in hypocrellin unifies our picture of the photophysics of hypericin and hypocrellin A if we can interpret it as an excited-state proton transfer arising from another tautomeric species and if we can relate it to the corresponding process in hypericin.

Three significantly populated species are observed for hypocrellin A [18]: two "normal" species differing in the orientation of the 7-membered ring (i.e., gauche or anti about the C14-C13 bond or the C14-C16 bond) and a double tautomer in the gauche conformation. This fits well in context of the proposed model mentioned above that postulates multiple closely separated minima on hypocrellin ground-state potential energy surface.

C. Construction of Potential Energy Surfaces and Simulations

Our inability to observe 50-230 ps component in hypocrellin emission can be explained by the similarity in structure of corresponding proton transfer educt and product. Indeed, if their fluorescence spectra and quantum yields are close enough it can be difficult to observe such a small change in fluorescence intensity on top of a dominant (~90%) slower decaying component. Presence of another faster growing component adds to the complexity of the issue. Our simulations of isotropic fluorescence decay profiles (Figure 7.10) are compared with the typical raw data and indicate that under these conditions up to 7% of 50 ps (observed in methanol [13]) and 15% of 230 ps (observed in octanol [13,16]) of hypocrellin A rising components are essentially indistinguishable among the other contributions, so their detection is limited by the uncertainty of the measurements afforded

by our instrument and the data analysis routines.

D. Outstanding Problems

i. Ground-State Heterogeneity

As we note in the Conclusions section, a recurring objection to our assignment of the excited-state reaction to H-atom transfer in these systems is the observation of mirror image symmetry between the absorption and emission spectra, which indicates minimal structural changes between the absorbing and emitting species — not usually the case for excited-state tautomerization.

Our first attempt to respond to this criticism was to suggest that the ground state was populated with at least one other species, for example, a mono tautomer [6]. This seemed to be reasonable, especially given the breadth of the visible absorption spectrum: there are no "gaps" of zero absorbance anywhere between the ultraviolet and ~600 nm. This suggestion also seemed to be supported by the observation that the transient absorbance [10,11] and upconversion [9] kinetics of hypericin differ with excitation wavelength and probe wavelength, respectively. On the other hand, *for hypericin*, evidence is emerging that the ground-state is much less heterogeneous than we had believed. Based on *ab initio* calculations, (RMP2/6-31G(d) level of theory, using geometries obtained with the 3-21G basis and Hartree-Fock wavefunctions) only one hypericin species, the "normal" form, is populated in the ground state for an unionized gas phase species [24]. Furthermore, on the NMR time scale, only one species of hypericin appears to be present in the ground state [18].

On the other hand, as noted above, three significantly populated species are observed for hypocrellin A [18]: two "normal" species differing in the orientation of the 7-membered ring (i.e., *gauche* or *anti* about the C14-C13 bond or the C14-C16 bond) and a

double tautomer in the *gauche* conformation.

ii. Reconciling the Kinetics

First we consider hypocrellin A. The excited-state dynamics modeled in Figure 7.11 and especially Figure 7.12 are an extension of the model presented in reference [16], enhanced by the knowledge that on the NMR time scale three ground-state species are present. As noted above (point 6 of section *B.*), it is an assumption of the model that only the "tautomer," not the "normal" species is significantly fluorescent. Consequently, in order to justify the absence of 50-230 ps rise times in the fluorescence upconversion kinetics, it was necessary to conclude that the concentration of the species giving rise to them is smaller than or comparable to that producing the ~10-ps component. This is consistent with our NMR data (obtained by integration of the resonance signals) in that one of the hypocrellin A forms among the heterogeneous ground-state population is found to be dominant (>70% at 268 K) over the other two with populations estimated to be about 10% and 20%.

Based on the enhanced version of the model, the instantaneous component of emission corresponds to the amount of double tautomer preexisting in the ground state. However, room temperature NMR results [28] tell us that this should be about 50%, not 80-90% as we see from the amplitude of the long-lived component in fluorescence upconversion measurements.It is tempting to rationalize this discrepancy by invoking a change in the population of ground-state species with concentration, since the NMR measurements were typically carried out at 4×10^{-3} M while the fluorescence measurements were performed at *ca.* 1×10^{-4} M. Such change due to aggregation is not likely as acetone is considered to be desegregating medium. Further, our experiments showed [unpublished data/] that no change in signal relative intensities or chemical shifts occur upon dilution down to about 10^{-5} M. The problem, however, is more acute for hypericin: only one

species is identified in the NMR and yet we observe an "instantaneous" rise in the upconversion signal with an amplitude of ~90%. It is possible that there are ground-state species interconverting faster than the NMR time scale of 300 ms. If this were the case, the "instantaneous" rise observed in hypericin and perhaps also in hypocrellin might be explained by an ultrafast (<300-fs) event that produces a ground-state double tautomer, which is subsequently excited. In fact, in our earlier investigations, an ~100-fs component was observed in the fluorescence rise time for hypericin, but it was also observed in the *O*-hexamethylated analog [9]. The resolution to this question clearly requires work using higher time resolution and a tunable excitation source.

CONCLUSIONS

The fluorescence upconversion measurements of hypericin and hypocrellin A presented here provide detailed and complementary information to the transient absorption data of reference [16] and permit a refinement of the model of the ground- and excited-state potential energy surfaces of this systems initially developed therein.

In concluding, we wish to address to two major objections that are still occasionally raised to our assignment of the excited state processes in hypericin and hypocrellin to excited-state H-atom transfer. These are the absence of a deuterium isotope effect in hypericin and the mirror image symmetry between the absorption and emission spectra in hypericin and hypocrellin.

We have treated the lack of a deuterium isotope effect in hypericin at length elsewhere. *Its absence is easily attributed to the reaction coordinate not being identified with the proton coordinate*, as we have depicted in Figure 7.11. There is precedent for this in other systems [29,30]. The ~10-ps component in neither hypericin nor hypocrellin A exhibits a deuterium isotope effect while the longer-lived transient in hypocrellin A,

assigned to a "back transfer," exhibits a deuterium isotope effect of 1.4 in methanol.

Requiring that a mirror image symmetry exist between the absorption and emission spectra assumes that the potential energy surface of the emitting species is significantly different from that of the absorbing species. Such a displacement in the coordinate of the emitting species is clearly evident in the most commonly studied proton transfer systems (Figure 7.13): methyl salicylate [30,31] (similar to 2-hydroxyacetophenone); 7-azaindole dimer [26,27,32-35]; 2-phenyl-benzotriazole [36]; and 3-hydroxyflavone [37-43]. It should be noted that one of the reasons that these systems have been so susceptible to investigation by optical spectroscopy is that there is such a marked difference between the emission and the absorption spectrum. This difference is clearly a result of the structural disparity between the normal species and the proton transferred species, which is indicated in Figure 7.13.

If, however, we consider systems in which the normal and tautomer species are symmetric, or nearly so, this disparity no longer exists or is significantly minimized. 5-Hydroxytropolone [44,45] presents an excellent example of such a case. And if a double H-atom transfer were to occur in naphthazarin [46] or the 4,9-dihydroxyperylene-3,10-quinone subunit of hypocrellin, a similar symmetric situation would arise Figure 7.13.

We argue that hypericin and hypocrellin A have similarly symmetric normal and tautomeric forms, although it may not be immediately apparent (see the emphasized bond systems in Figure 7.1a-b) . Even in case of mono-tautomerized species it is possible to draw resonance forms that upon superposition restore the aromatic character of the substructure involved in proton transfer reaction. Consequently, we conclude that the mirror image symmetry observed in hypericin and hypocrellin is not at all surprising. If, on the other hand, the excited-state reaction were a genuine *proton* transfer, then the resulting charge separated species would be expected to exhibit an emission spectrum significantly different

from that of the absorption spectrum, as in 3-hydroxyflavone; and the rate of reaction should be very sensitive to solvent *polarity*, which is not the case for hypericin or hypocrellin. In order to avoid any possible confusion in this matter, we now refer to the excited-state reactions in hypericin and hypocrellin as excited-state H-atom transfer.

ACKNOWLEDGMENT

This work was supported by NSF grant CHE-9613962 to J. W. P.

REFERENCES

1. Kraus, G. A.; Zhang, W.; Fehr, M. J.; Petrich, J. W.; Wannemuehler, Y.; Carpenter, S. *Chem. Rev.* **1996**, *96*, 523-535.

2. Diwu, Z. *Photochem. Photobiol.* **1995**, *61*, 529-539.

3. Diwu, Z.; Lown, J. W. *Photochem. Photobiol.* **1990**, *52*, 609-616.

4. Gai, F.; Fehr, M. J.; Petrich, J. W. *J. Am. Chem. Soc.* **1993**, *115*, 3384-3385.

5. Gai, F.; Fehr, M. J.; Petrich, J. W. *J. Phys. Chem.* **1994**, *98*, 8352-8358.

6. Gai, F.; Fehr, M. J.; Petrich, J. W. *J. Phys. Chem.* **1994**, *98*, 5784-5795.

7. Fehr, M. J.; Gai, F.; Petrich, J. W. *Springer Ser. Chem. Phys.* **1994**, *60*, 462-465.

8. Fehr, M. J.; Carpenter, S. L.; Petrich, J. W. *Bioorg. Med. Chem. Lett.* **1994**, *4*, 1339-1344.

9. English, D. S.; Das, K.; Ashby, K. D.; Park, J.; Petrich, J. W.; Castner, E. W. J. *J. Am. Chem. Soc.* **1997**, *119*, 11585-11590.

10. English, D. S.; Das, K.; Zenner, J. M.; Zhang, W.; Kraus, G. A.; Larock, R. C.; Petrich, J. W. *J. Phys. Chem. A* **1997**, *101*, 3235-3240.

11. English, D. S.; Zhang, W.; Kraus, G. A.; Petrich, J. W. *J. Am. Chem. Soc.* **1997**, *119*, 2980-2986.

12. Das, K.; Ashby, K.; Wen, J.; Petrich, J. W. *J. Phys. Chem.* , In press.

13. Das, K.; English, D. S.; Fehr, M. J.; Smirnov, A. V.; Petrich, J. W. *J. Phys. Chem.* 1996, *100*, 18275-18281.

14. Das, K.; English, D. S.; Petrich, J. W. *J. Phys. Chem. A* 1997, *101*, 3241-3245.

15. Das, K.; English, D. S.; Petrich, J. W. *J. Am. Chem. Soc.* 1997, *119*, 2763-2764.

16. Das, K.; Smirnov, A. V.; Snyder, M. D.; Petrich, J. W. *J. Phys. Chem. B* 1998, *102*, 6098-6106.

17. Das, K.; Dertz, E.; Paterson, J.; Zhang, W.; Kraus, G. A.; Petrich, J. W. *J. Phys. Chem. B* 1998, *102*, 1479-1484.

18. Smirnov, A. V.; Fulton, D. B.; Andreotti, A.; Petrich, J. W. *J. Am. Chem. Soc.* , Submitted for publication.

19. Das, K.; Smirnov, A. V.; Wen, J.; Miskovsky, P.; Petrich, J. W. *Biochemistry* , Submitted for publication.

20. Liu, J. *Kexue Tongbao (Foreign Lang. Ed.)* 1985, *30*, 1633-1637.

21. Fehr, M. J.; McCloskey, M. A.; Petrich, J. W. *J. Am. Chem. Soc.* 1995, *117*, 1833-1836.

22. Chaloupka, R.; Sureau, F.; Kocisova, E.; Petrich, J. W. *Photochem. Photobiol.* 1998, *68*, 44-50.

23. Park, J.; English, D. S.; Wannemuehler, Y.; Carpenter, S.; Petrich, J. W. *Photochem. Photobiol.* 1998, *68*, 593-597.

24. Petrich, J. W.; Gordon, M. S.; Cagle, M. *J. Phys. Chem. A* 1998, *102*, 1647-1651.

25. English, D. S.; Das, K.; Petrich, J. W. *Hypericin, hypocrellin and model compounds: Primary photoprocesses of light-induced antiviral agents.*; American Chemical Society, Washington, D, 1997, p. PHYS-405.

26. Takeuchi, S.; Tahara, T. *J. Phys. Chem. A* 1998, *102*, 7740-7753.

27. Douhal, A.; Kim, S. K.; Zewail, A. H. *Nature (London)* 1995, *378*, 260-263.

28. Arnone, A.; Merlini, L.; Mondelli, R.; Nasini, G.; Ragg, E.; Scaglioni, L.; Weiss, U. *J. Chem. Soc., Perkin Trans. 2* **1993**, 1447-1454.

29. Frey, W.; Laermer, F.; Elsaesser, T. *J.Phys.Chem.* **1991**, *95*, 10391-10395.

30. Herek, J. L.; Pedersen, S.; Banares, L.; Zewail, A. H. *J. Chem. Phys.* **1992**, *97*, 9046-9061.

31. Goodman, J.; Brus, L. E. *J. Am. Chem. Soc.* **1978**, *100*, 7472-7474.

32. Ingham, K. C.; Abu-Elgheit, M.; El-Bayoumi, M. A. *J. Amer. Chem. Soc.* **1971**, *93*, 5023-5025.

33. Suzuki, T.; Okuyama, U.; Ichimura, T. *J. Phys. Chem. A* **1997**, *101*, 7047-7052.

34. Takeuchi, S.; Tahara, T. *Chem. Phys. Lett.* **1997**, *277*, 340-346.

35. Teng, Q.; Feng, J.; Xu, W.; Li, Z. *Gaodeng Xuexiao Huaxue Xuebao* **1992**, *13*, 498-501.

36. Kim, Y. R.; Yardley, J. T.; Hochstrasser, R. M. *Chem. Phys.* **1989**, *136*, 311-319.

37. Swinney, T. C.; Kelley, D. F. *J. Phys. Chem.* **1991**, *95*, 10369-10373.

38. Strandjord, A. J. G.; Barbara, P. F. *J. Phys. Chem.* **1985**, *89*, 2355-2361.

39. Schwartz, B. J.; Peteanu, L. A.; Harris, C. B. *J. Phys. Chem.* **1992**, *96*, 3591-3598.

40. McMorrow, D.; Kasha, M. *Hydrogen-bonding solvent perturbations. J. Phys. Chem.* **1984**, *88*, 2235-2243.

41. Chattoraj, M.; King, B.; Boxer, S. G. *Investigating the solvent dependence of proton and deuterium transfer in 3-hydroxy flavone using femtosecond fluorescence upconversion.*; American Chemical Society: Chicago, IL, August 20-24, 1995, pp PHYS-108.

42. Brucker, G. A.; Swinney, T. C.; Kelley, D. F. *J. Phys. Chem.* **1991**, *95*, 3190-3195.

43. Brucker, G. A.; Kelley, D. F. *J. Phys. Chem.* **1987**, *91*, 2856-2861.

44. Ensminger, F. A.; Plassard, J.; Zwier, T. S.; Hardinger, S. *J. Chem. Phys.* **1993**, *99*, 8341-8344.

45. Ensminger, F. A.; Plassard, J.; Zwier, T. S.; Hardinger, S. *J. Chem. Phys.* **1995**, *102*, 5246-5259.

46. Mazzini, S.; Merlini, L.; Mondelli, R.; Nasini, G.; Ragg, E.; Scalioni, L. *J. Chem. Soc., Perkin Trans. 2* **1997**, 2013-2021.

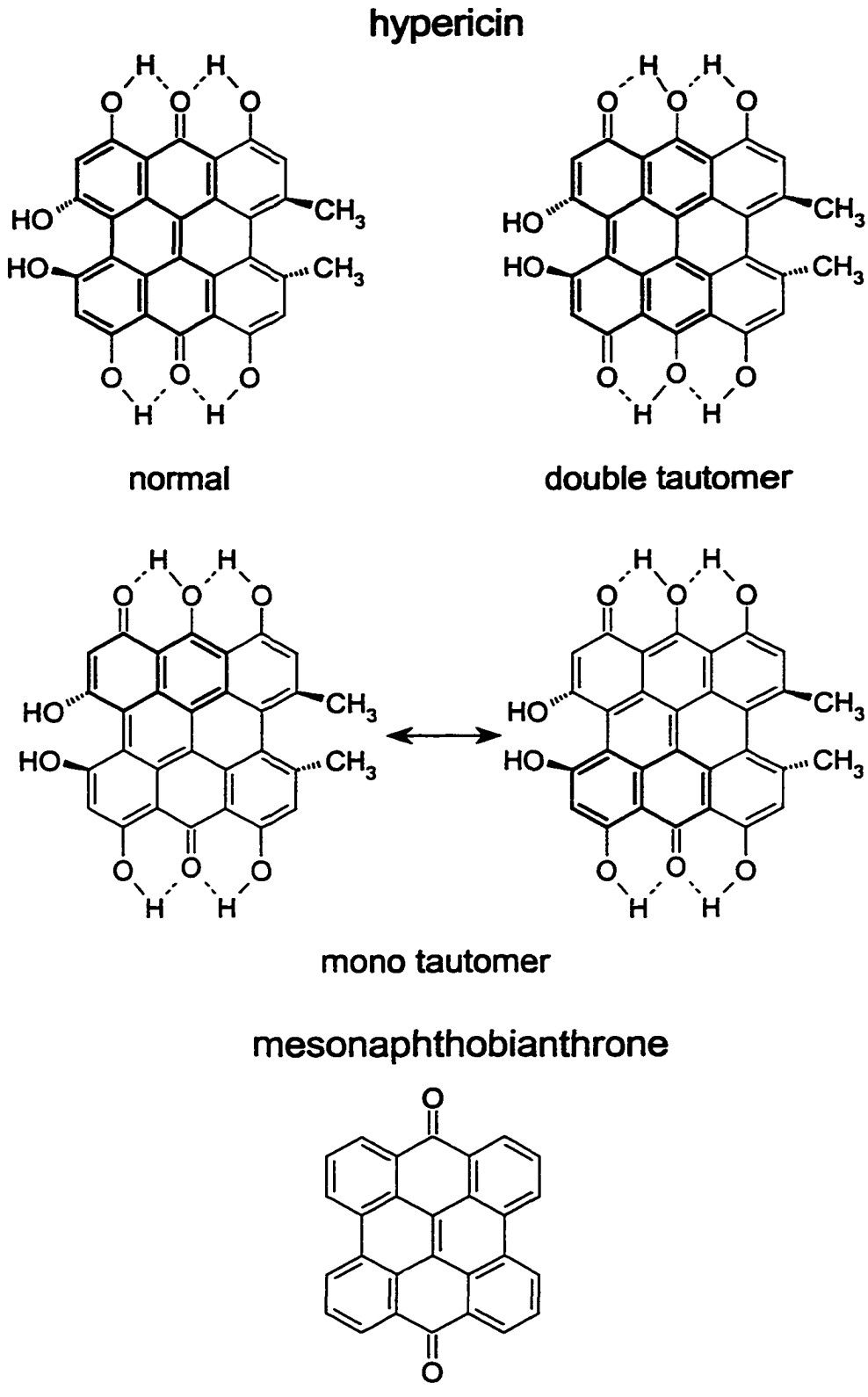

Figure 7.1 (a) Structures of hypericin tautomers and mesonaphthobianthrone.

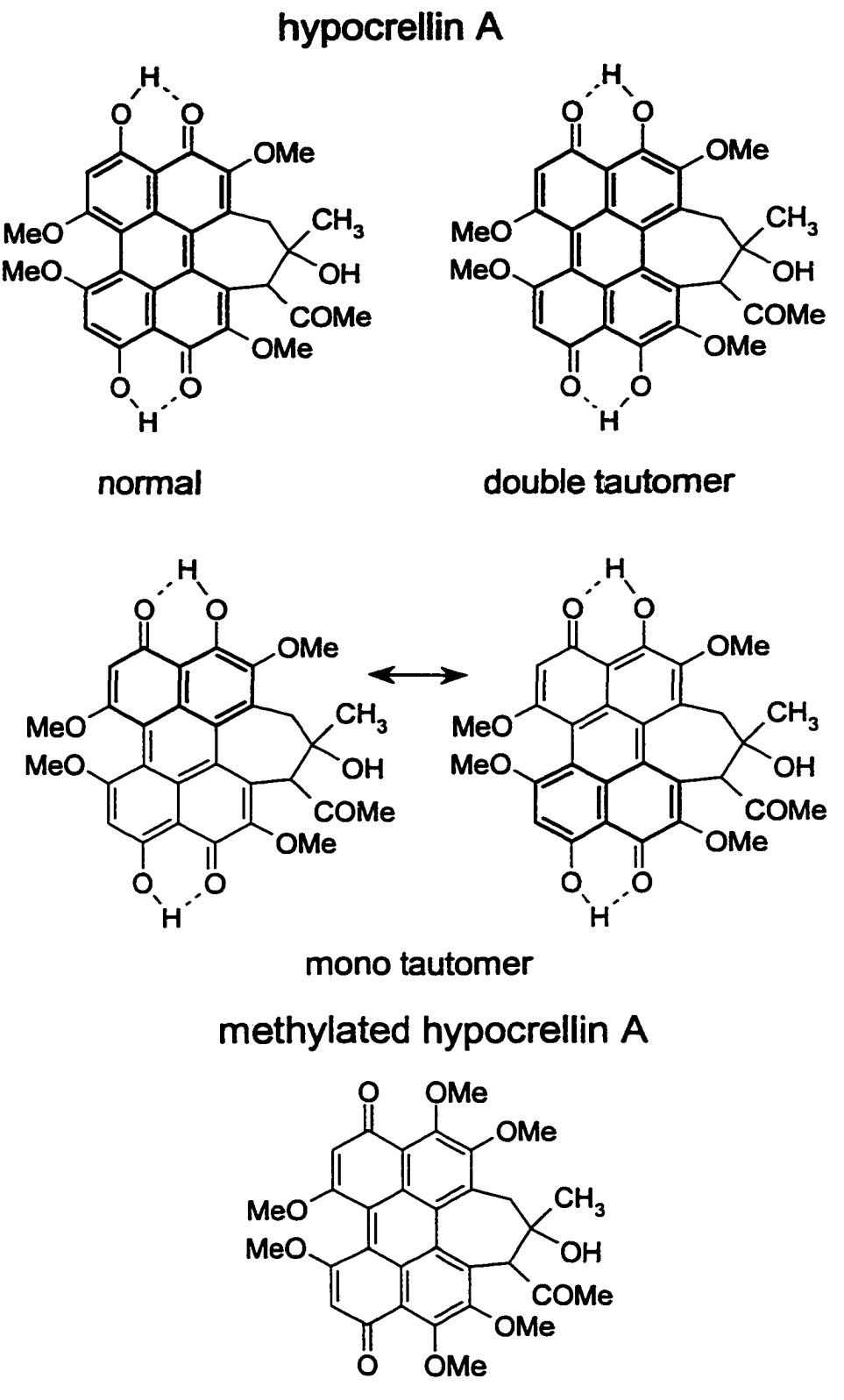

Figure 7.1 (continued, b) Structures of hypocrellin A tautomers and its methylated analog.

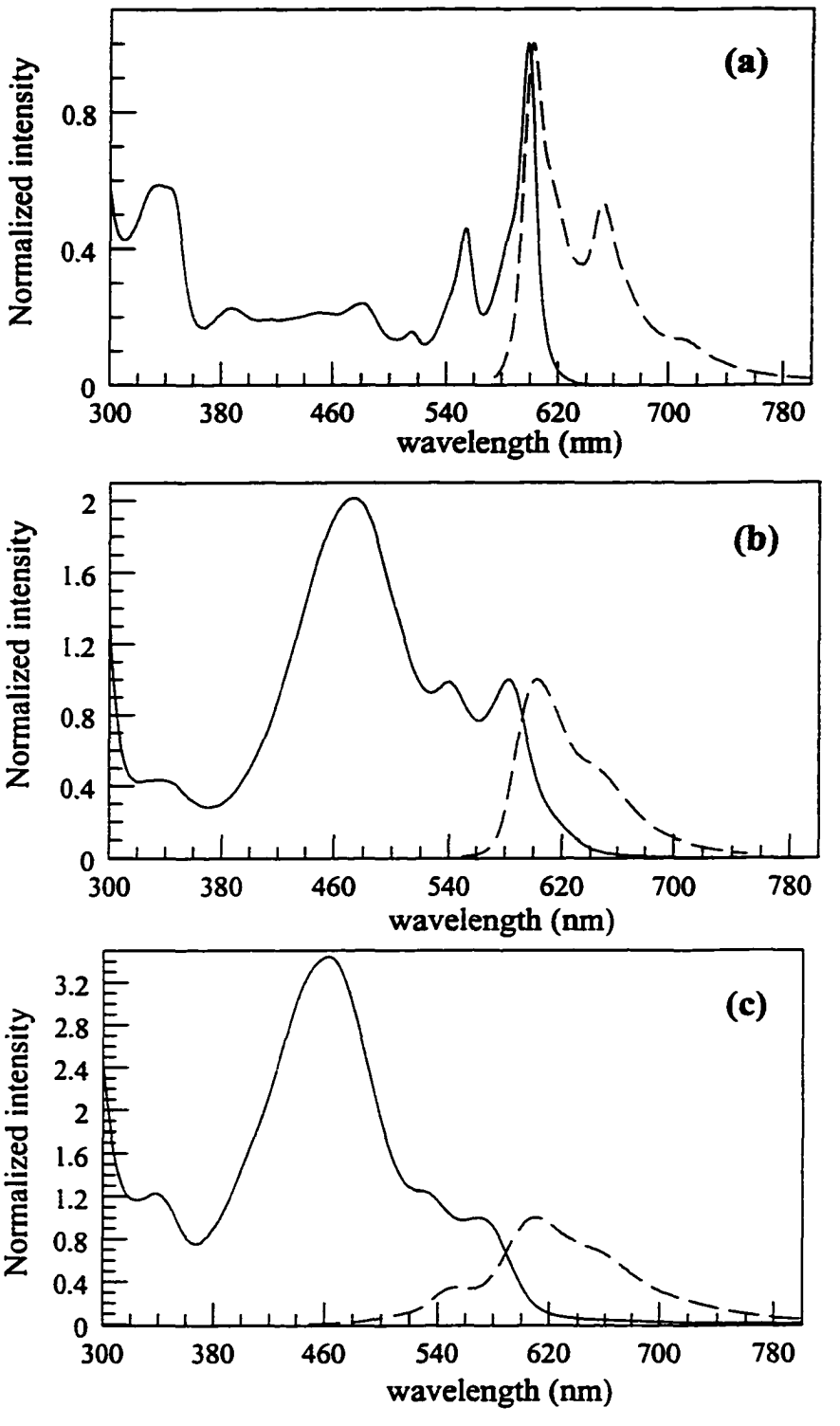

Figure 7.2 Absorbance and fluorescence emission spectra of hypericin (a), hypocrellin A (b) in DMSO and hypocrellin A methylated analog (c) in ethanol at room temperature. The emission spectra were obtained using excitation wavelength 414 nm (same as in the fluorescence upconversion experiment).

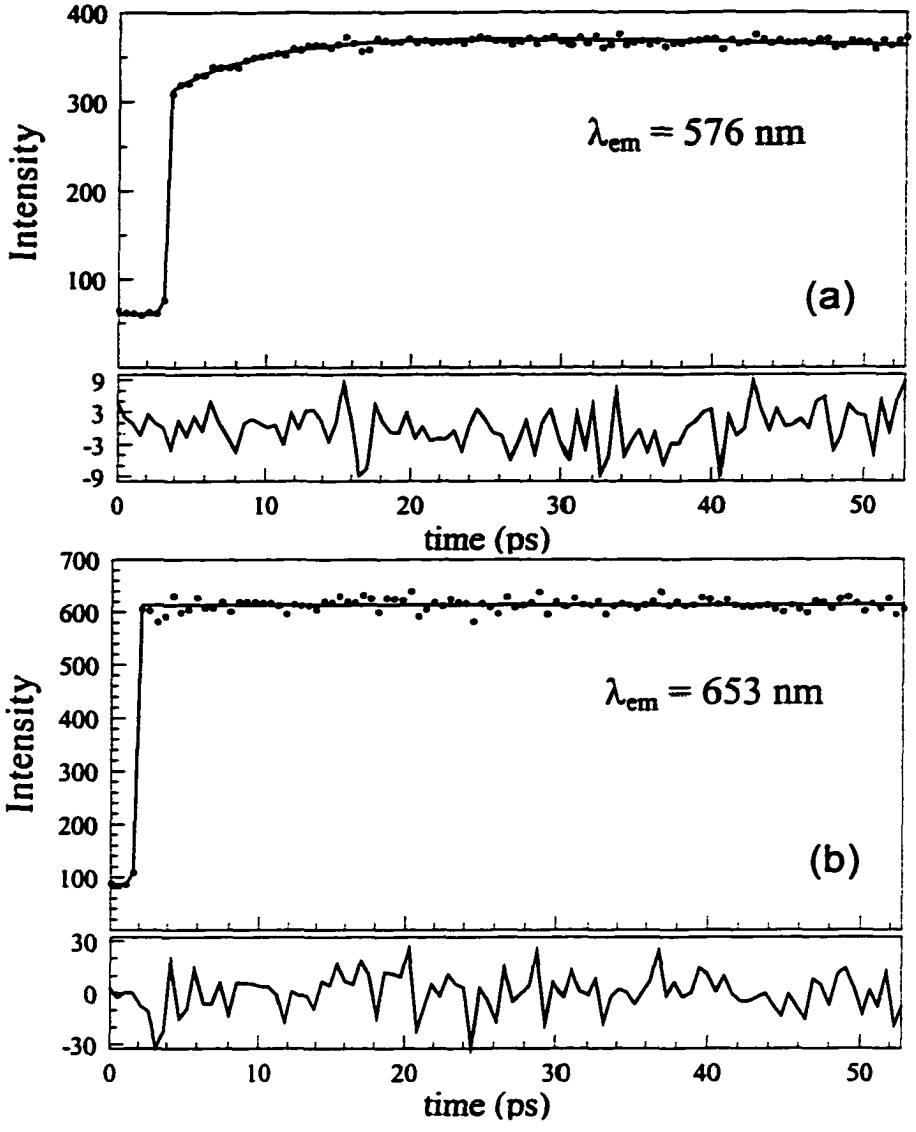

Figure 7.3 (a) Fluorescence upconversion transient for hypericin in DMSO at λ_{em} = 576 nm. The fit curve is described by the following equation (with background subtracted): $F(t)$= -0.21 exp(-t/6.5 ps) + 1.00 exp(-t /∞).

(b) Fluorescence upconversion transient for hypericin in DMSO at λ_{em} = 653 nm. The fit curve is described by the following equation (with background subtracted): $F(t)$ = 1.00 exp(-t/∞).

The excitation wavelength was the second harmonic of our unamplified Ti:sapphire oscillator, 414 nm.

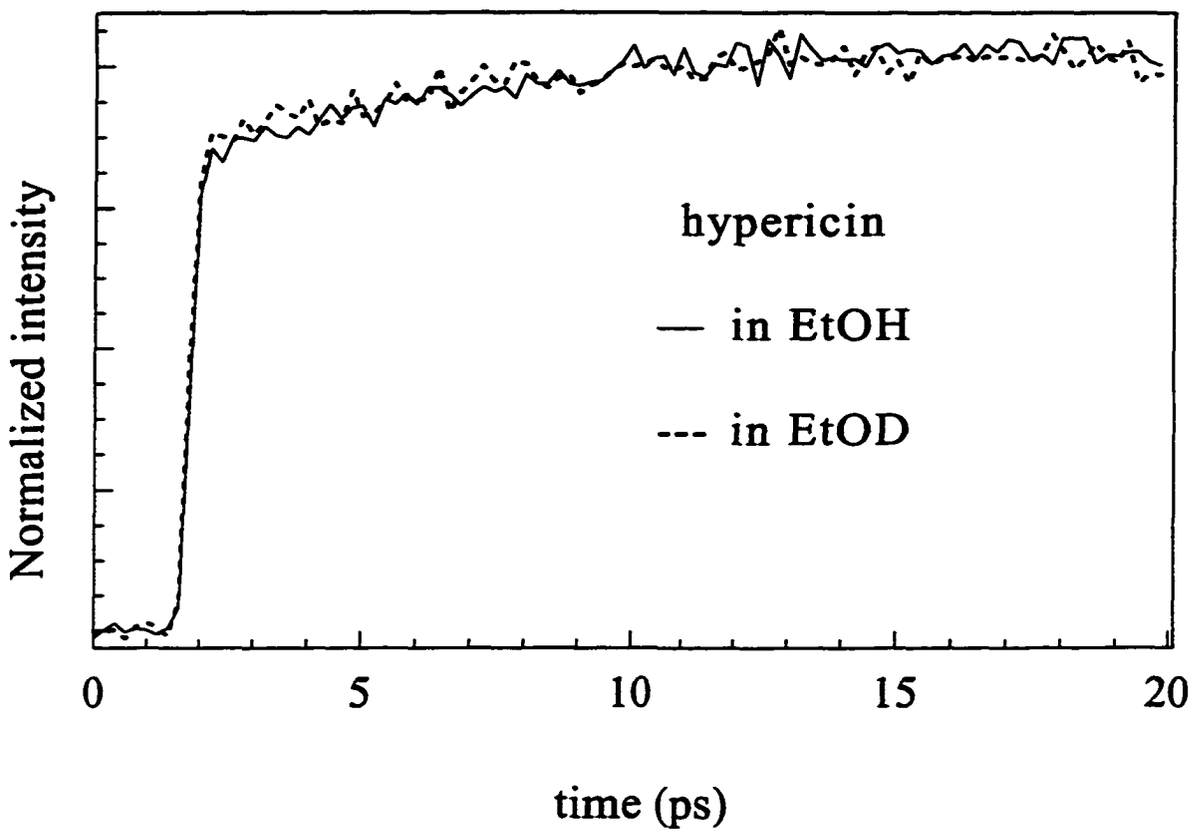

Figure 7.4 Lack of deuterium isotope effect in the hypericin excited-state proton transfer in ethanol demonstrated by fluorescence upconversion with λ_{ex}=415 nm and λ_{em}=576 nm.

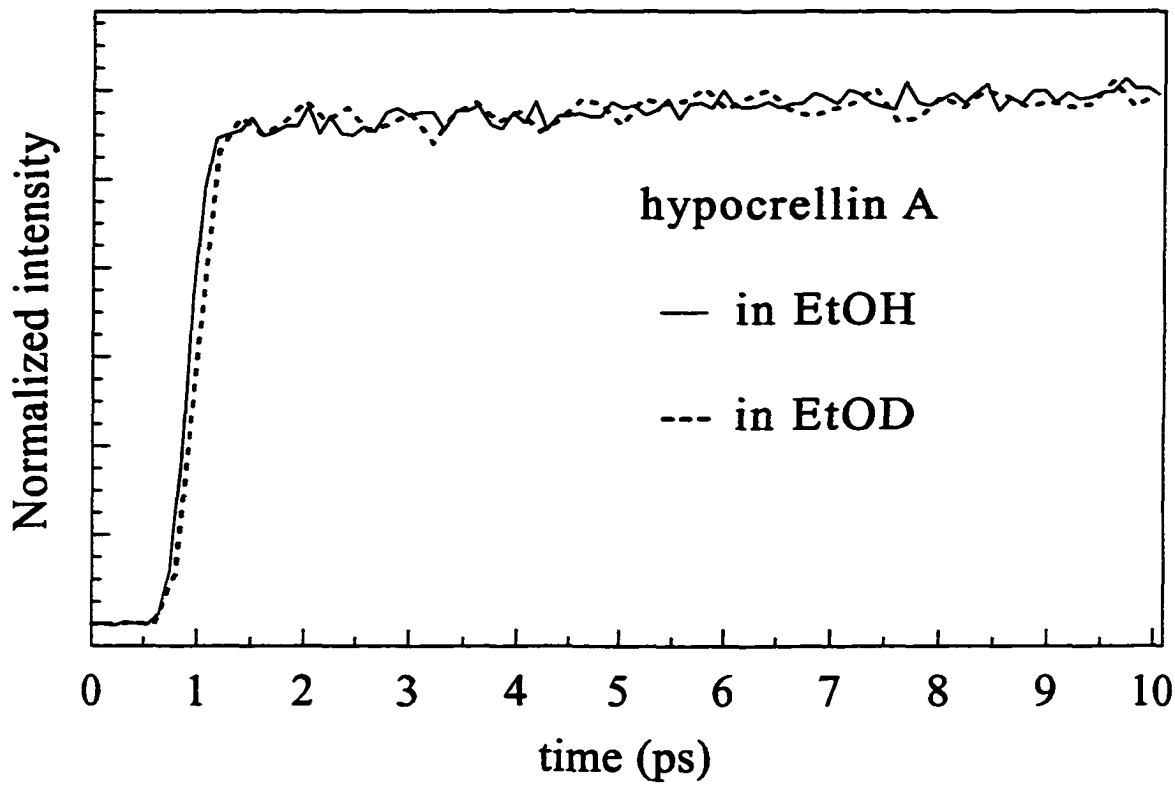

Figure 7.5 Lack of deuterium isotope effect in the hypocrellin A excited-state proton transfer in ethanol demonstrated by fluorescence upconversion with λ_{ex}=415 nm and λ_{em}=591 nm.

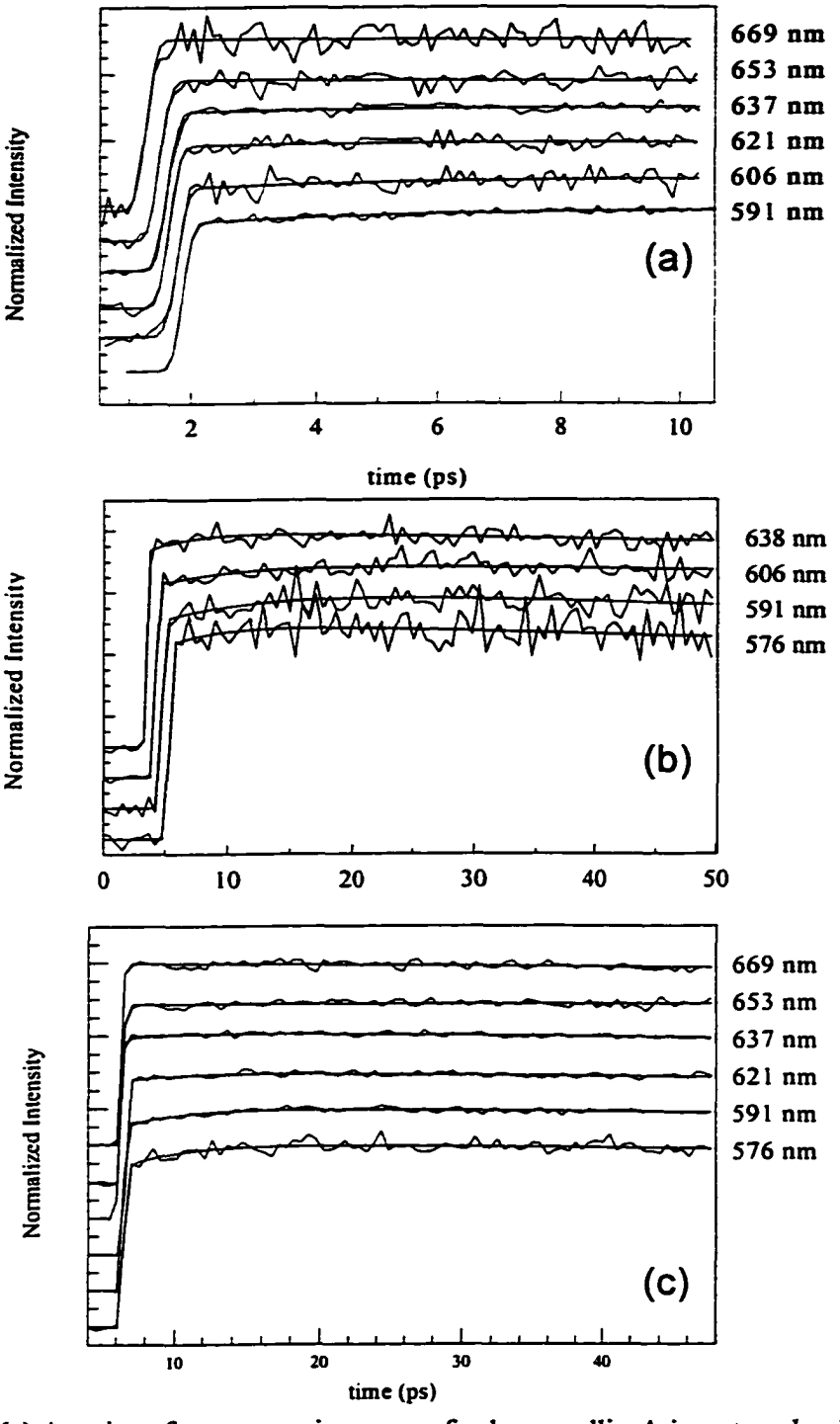

Figure 7.6 (a) A series of upconversion traces for hypocrellin A in octanol collected at different emission wavelengths.

(b) A series of upconversion traces for hypocrellin A in acetonitrile collected at different emission wavelengths.

(c) A series of upconversion traces for hypocrellin A in ethanol collected at different emission wavelengths.

Note the ~10 ps rise time of fluorescence at emission wavelengths ≤591 nm.

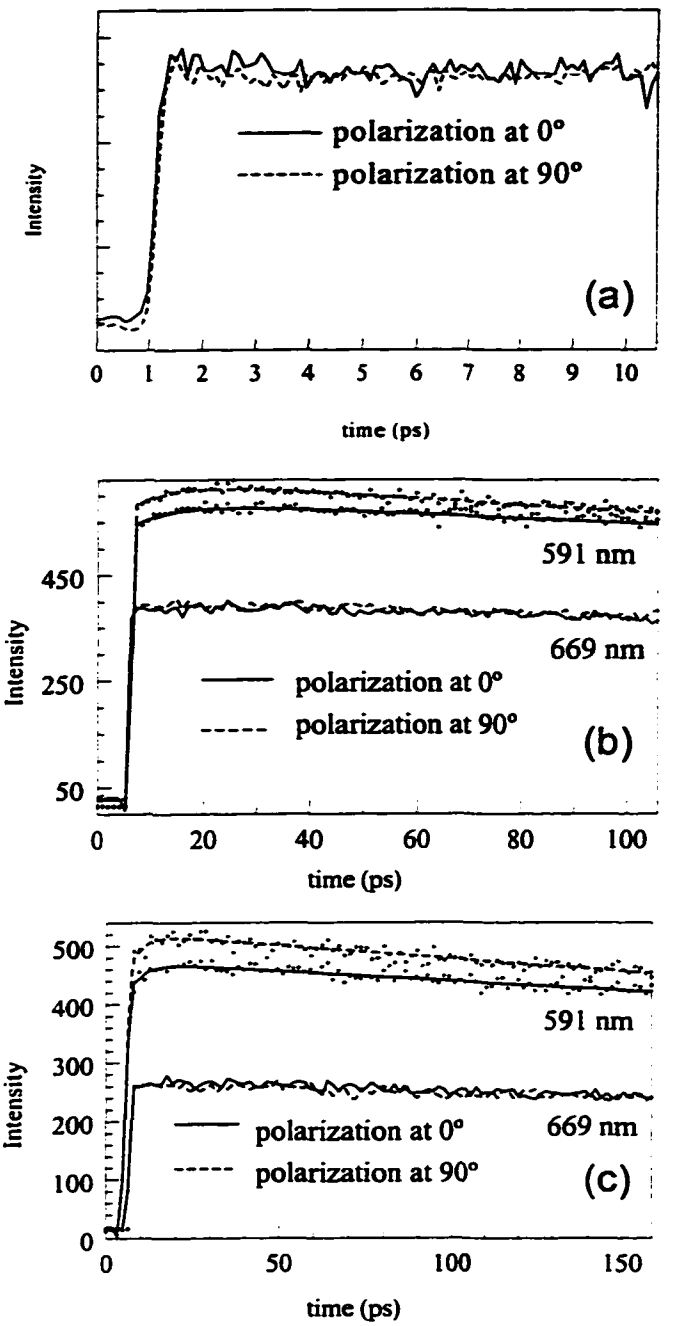

Figure 7.7 (a) Absence of fluorescence anisotropy decay of hypocrellin A in DMSO collected at 591 nm. Same was observed for other emission wavelengths up to 637 nm.

(b) Fluorescence anisotropy decay of hypocrellin A in ethanol collected at 591 nm and 669 nm. Fit results for 591 nm: $F(t) = 1.00 \exp(-t/1012 \text{ ps}) - 0.0785 \exp(-t/7.9 \text{ ps})$; $r(t) = -0.032 \exp(-t/282 \text{ ps})$.

(c) Fluorescence anisotropy decay of hypocrellin A in octanol collected at 591 nm and 669 nm. Fit results for 591 nm: $F(t) = 1.00 \exp(-t/1113 \text{ ps}) - 0.141 \exp(-t/3.65 \text{ ps})$; $r(t) = -0.034 \exp(-t/502 \text{ ps})$.

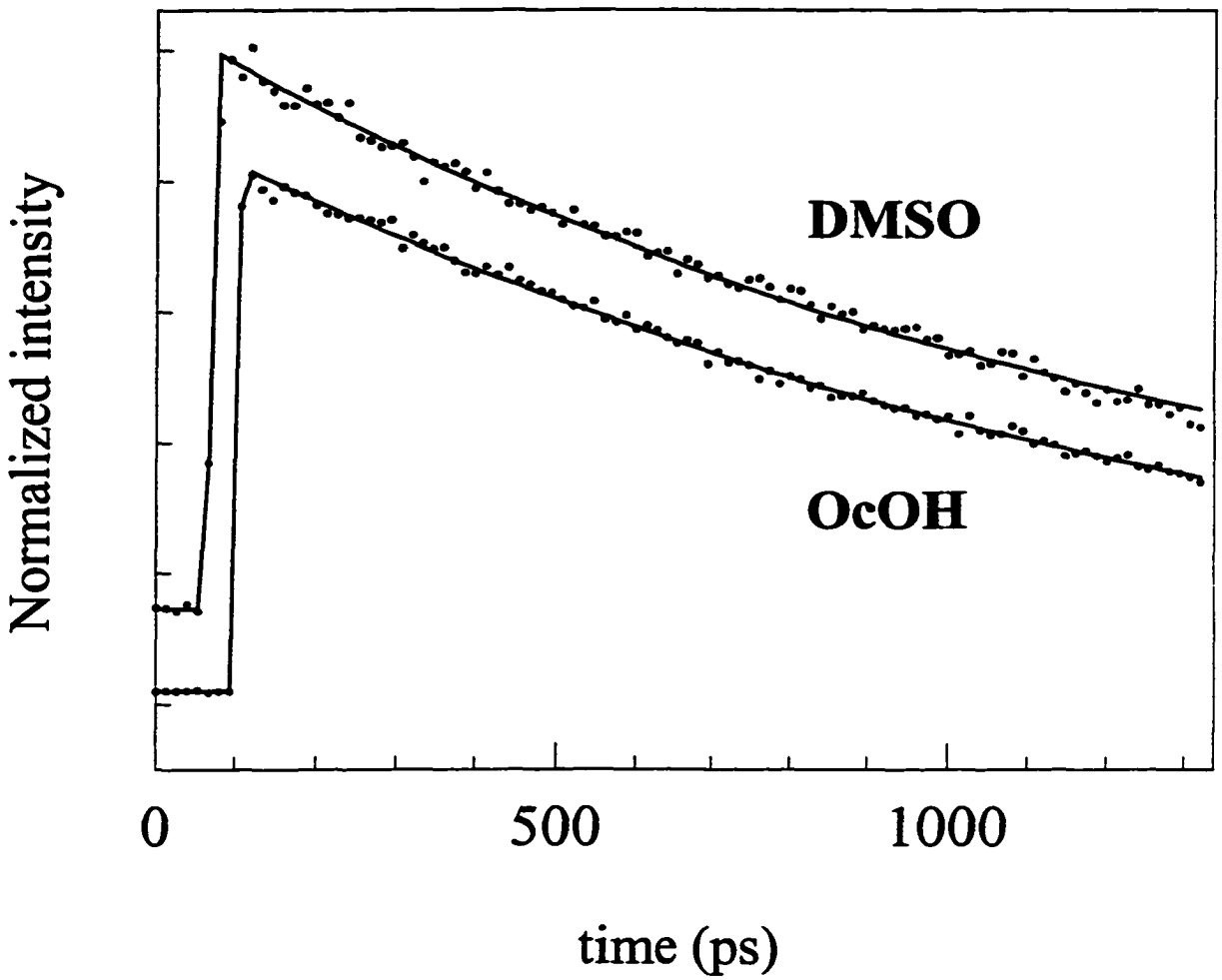

Figure 7.8 Fluorescence decay of hypocrellin A in octanol and DMSO on the longest available timescale. Fit results: $F(t) = 1.00 \exp(-t/ 1219 \text{ ps})$ for DMSO at 653 nm; $F(t) = 1.00 \exp(-t/ 1353 \text{ ps})$ for octanol at 621 nm.

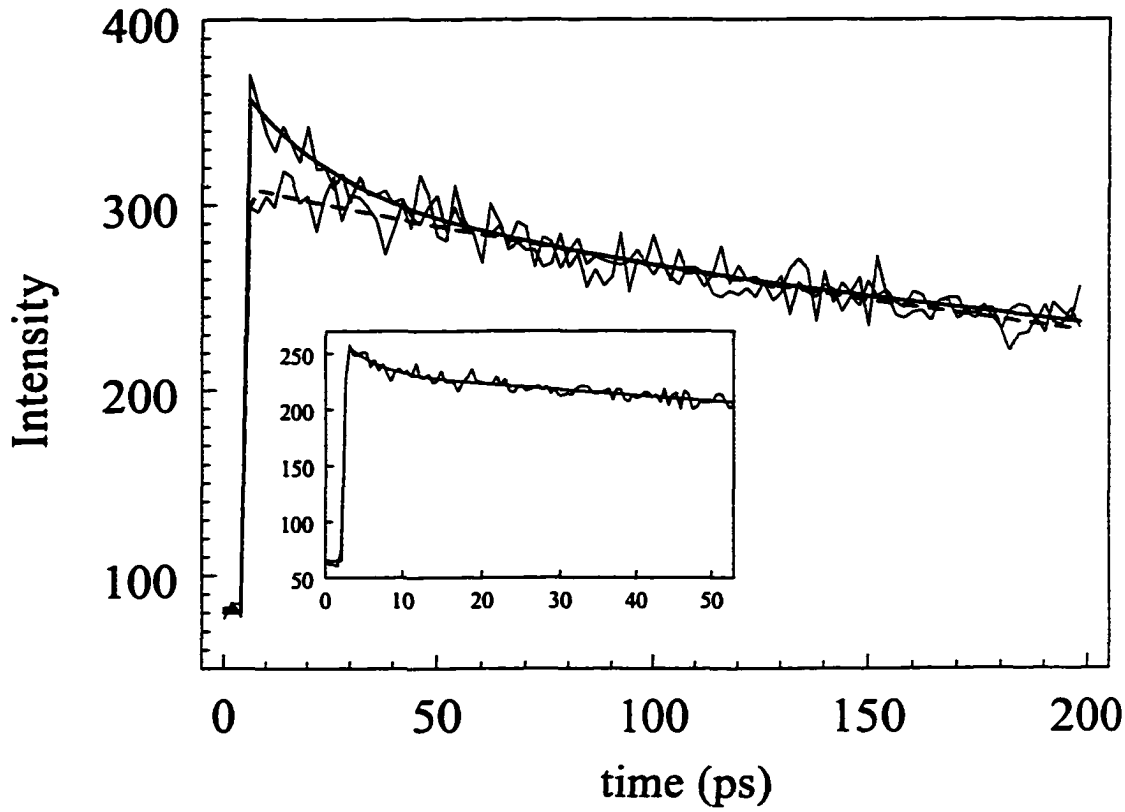

Figure 7.9 Fluorescence upconversion traces obtained at λ_{em}=576 nm (solid) and λ_{em}=653 nm (dashed) for hypocrellin A methylated analog in ethanol. Inset shows ultra-fast decay component on a smaller time scale at λ_{em}=560 nm where it appeared most evidently.
Fit results: $F(t) = 1.00 \exp(-t/\ 466\ \text{ps})$ for 653 nm;
$F(t) = 0.20 \exp(-t/\ 24\ \text{ps}) + 0.80 \exp(-t/\ 560\ \text{ps})$ for 576 nm and
$F(t) = 0.135 \exp(-t/\ 4.4\ \text{ps}) + 0.865 \exp(-t/\ 300\ \text{ps})$ for 560 nm.

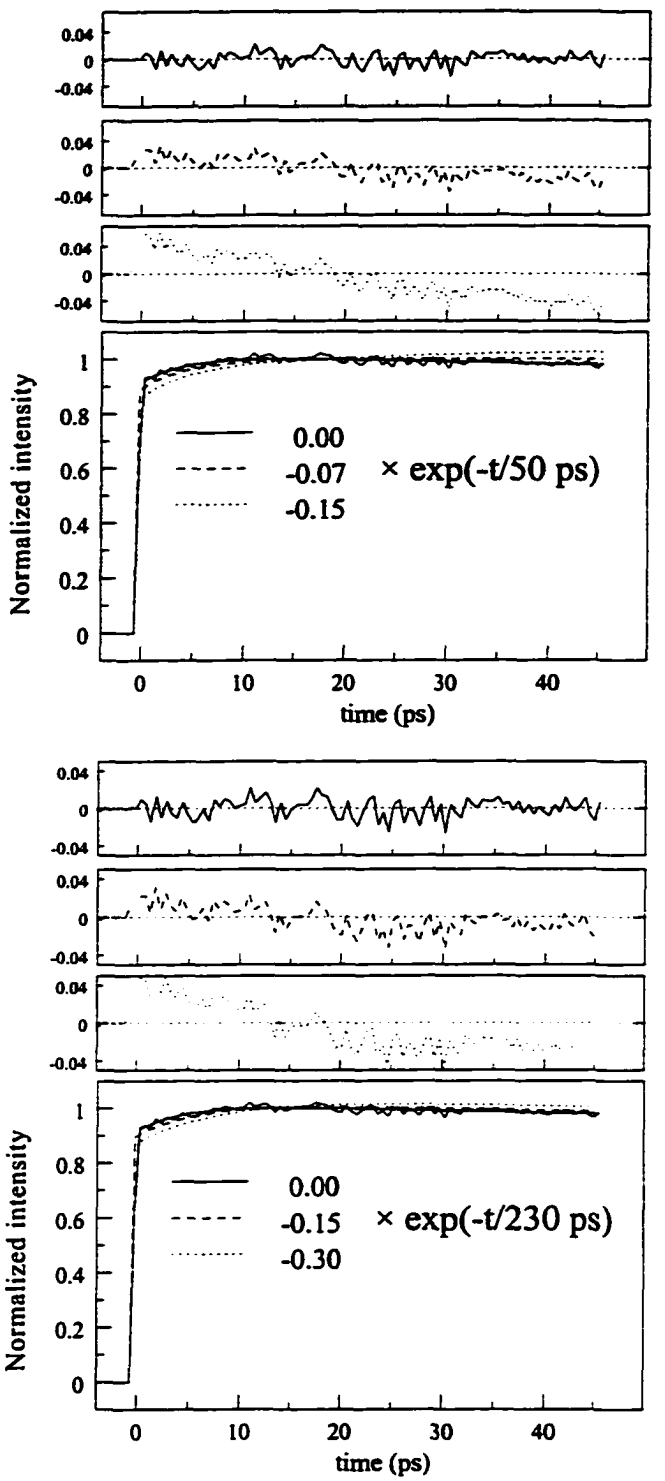

Figure 7.10 Simulated fluorescence upconversion traces with the increasing amplitudes of additional 50 ps (top) and 230 ps (bottom) rising components. The residuals show deviations from the data collected for hypocrellin A in octanol with λ_{em}=591 nm. These data afford the following fit results: $F(t)$ = -0.10 exp(-t/ 4.5 ps) + 1.0 exp(-t/ 1200 ps).

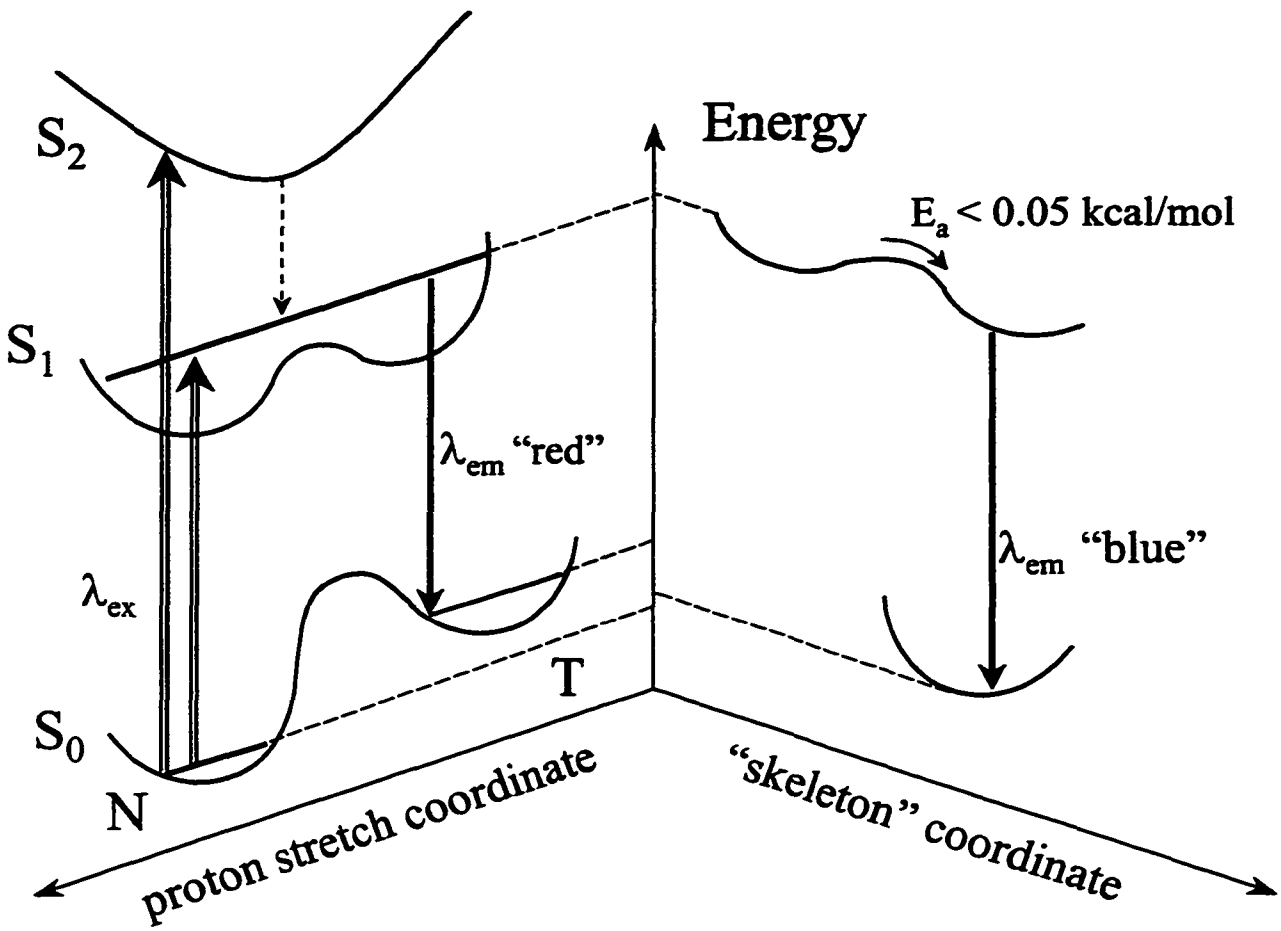

Figure 7.11 Potential energy surface for hypericin. This diagram illustrates how growing "blue" emission can be a result of excited-state tautomerization of the less fluorescent "normal" species (N). The adiabatic excited-state H-atom transfer is modulated along the "skeleton" coordinate. At the same time the instantaneous red-shifted fluorescence arises from the direct relaxation to the ground state which is likely to be one of the 6 hypericin relevant tautomers (T).

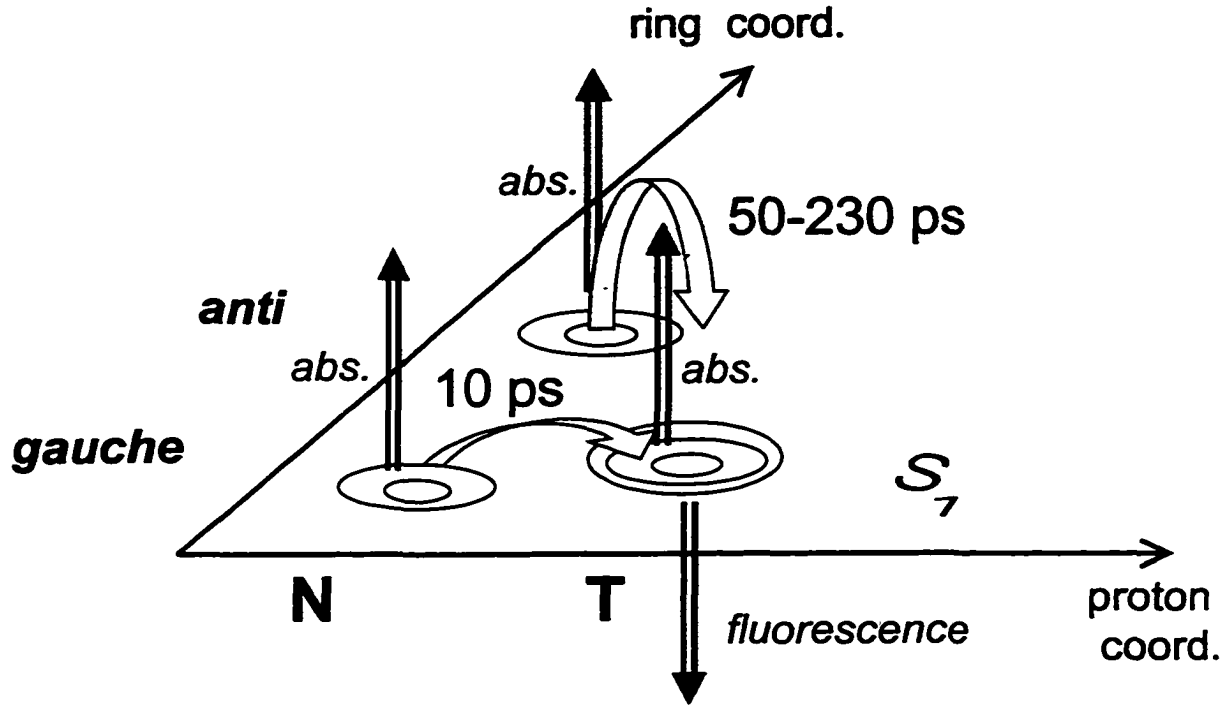

Figure 7.12 S_1 potential surface of hypocrellin A. Along with the hypericin-like proton and skeleton coordinates, this molecule exhibit additional degree of freedom associated with the twisting motion of the seven-membered ring (the "ring" coordinate). Just as it was found from NMR 2D ROESY data [18], such motion is also coupled to the H-atom transfer event in the excited state as it is illustrated on the diagram.

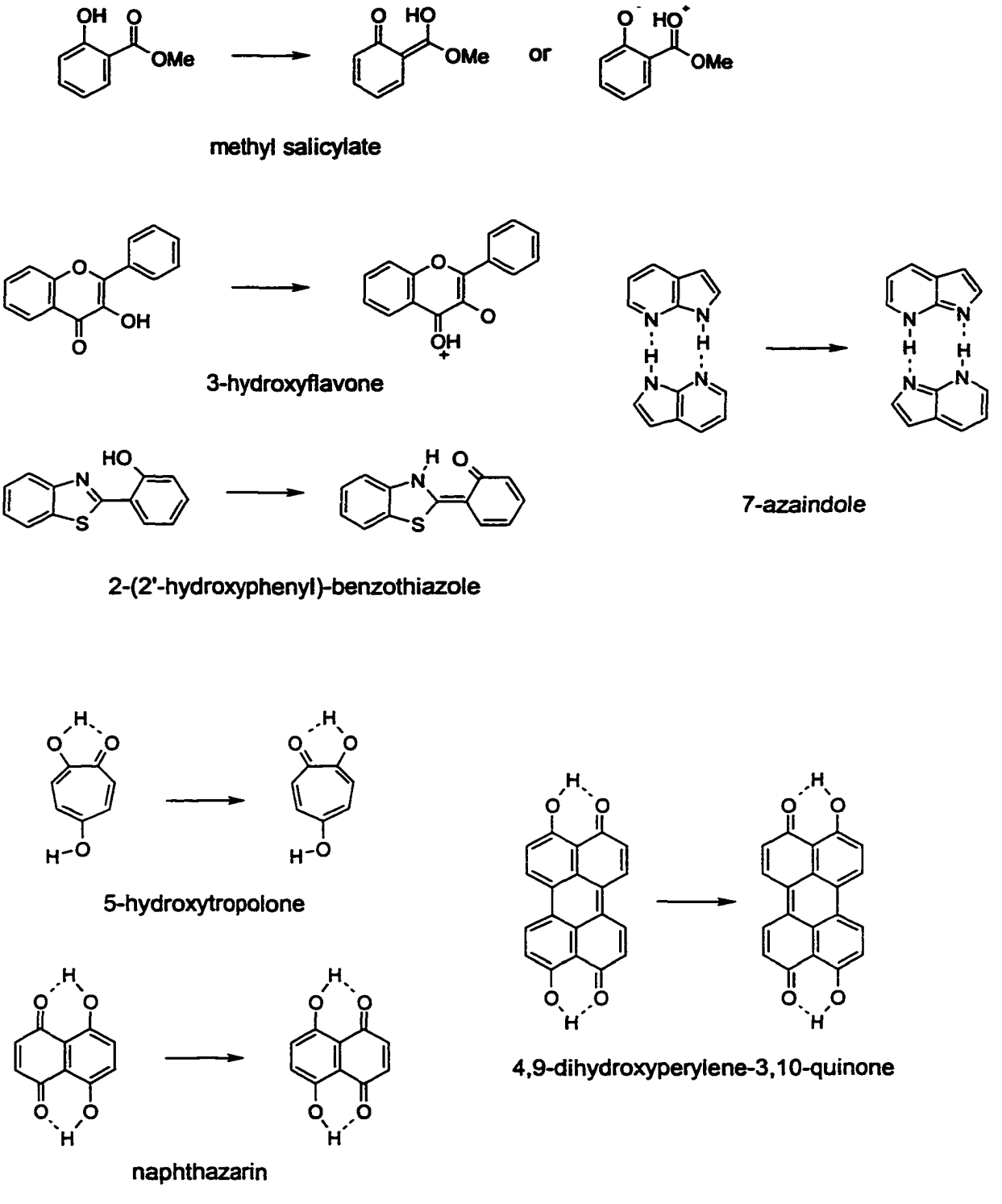

Figure 7.13 Proton transfer species. In the upper half of this figure the product of tautomerization is structurally and electronically different from educt. In contrast, H-atom transfer in 5-hydroxytropolone results in nearly identical species and double-tautomers of naphthazarin and 4,9-dihydroxyperylene-3,10-quinone are essentially the "mirror" images of "normal" structures.

CHAPTER VIII. GENERAL CONCLUSIONS AND FUTURE WORK

GENERAL CONCLUSIONS

By complementing the techniques of time-resolved absorption spectroscopy (Chapters III and IV) with those of fluorescence upconversion (Chapters VI and VII) and applying them to hypericin, hypocrellin A and B, and their methylated analogs that are unable to execute proton transfer, we have demonstrated unequivocally that intramolecular excited-state proton (or hydrogen atom) transfer is a dominant primary nonradiative process in hypericin and hypocrellins.

For hypocrellin A in viscous solvents such as octanol and ethylene glycol, an absorption transient of ~10-ps duration, similar to the hypericin transient, can also be detected (see Chapter IV). This transient is quite apparent in some solvents using the fluorescence upconversion technique (Chapter VII). Another transient component of hypocrellin A, most evident in pump/probe absorption spectroscopy, exhibits isotope effect [1] and a strong solvent bulk viscosity dependence (Chapter III, [2]). Such behavior is rationalized by postulating that excited-state tautomerization pathway, besides the proton stretch, involves at least one other reaction coordinate. This coordinate may involve molecule skeletal motion or even conformational change, e.g. flipping of seven-membered ring in hypocrellin A, and essentially modulates proton double-well potential. The lack or small magnitude of isotope effect is not surprising by itself and can be explained by invoking theory developed by Hynes, Bogis and coworkers [3-8] in which proton zero-level vibrational energy lies just above the reaction barrier. The only requirement is that O–O

distance for the relevant hydrogen bond must be <2.7 Å and X-ray data suggest that it is the case for the title polycyclic quinones [9-12].

Structurally hypericin and hypocrellin are very similar. They both possess extended aromatic skeletons whose most important functionalities are the hydroxyls peri to the carbonyls. In this regard, the most significant structural difference between them is that hypocrellin possesses two fewer peri hydroxyls but has flexible seven-membered ring giving rise to conformational lability. The current picture that we have formed of the excited-state dynamics of hypericin and hypocrellin is that the different photophysical behavior that we have enumerated above of these two structurally very similar molecules arises because we are probing different regions of very similar potential energy surfaces.

The ~10 ps component in hypocrellin A unifies our picture of the photophysics of hypericin and hypocrellin if we can interpret it as an excited-state proton transfer arising from another tautomeric species and if we can relate it to the corresponding process in hypericin. A thoroughly studied system that bears many similarities to this one is that of stilbene. The *trans*-to-*cis* photoisomerization of stilbene bears distinct differences from that of the *cis*-to-*trans* photoisomerization. For example, the former process has much stronger viscosity dependence and occurs on a longer time scale than the latter. The differences in behavior have been attributed to different reaction coordinates for the two isomerization processes [13-17].

The transient absorbance kinetics of hypericin differs with excitation and probe wavelengths [18]. This, along with "mirror-image" symmetry of absorbance and emission spectra leaded investigators to a preliminary conclusion that hypericin is heterogeneous in the ground state. In the light of a more detailed investigation, presented in the Chapter V, it was found that peculiar structural features of this molecule allow for different interpretation which is also consistent with *ab initio* calculations results [19].

Temperature-dependant ^{1}H NMR and 2D ROESY studies of hypericin and hypocrellins provide unambiguous proof that there is only one apparent conformational isomer/tautomer for hypericin in the ground state on the NMR time scale. On the other hand, these measurements indicate that three out of four possible ground-state species are significantly populated for hypocrellin A. These species where identified and their relative energies and interconversion barriers were determined through dynamic NMR simulations. Hypocrellin B, similar to hypericin, was found to be essentially homogeneous in the ground state which is attributed to the rigidity of its structure caused by the presence of double bond in its seven-membered ring.

In Chapter VI time-resolved fluorescence and absorption measurements of hypericin complexed with human serum albumin (HSA) indicate that hypericin very rigidly binds to HSA by means of a specific hydrogen bonded interaction between its carbonyl oxygen and the N_1-H of the tryptophan residue in the II A subdomain of HSA. (They also indicate that hypericin binds nonspecifically to the surface of the protein.) Energy transfer from the tryptophan residue of HSA to hypericin is very efficient and is characterized by a critical distance of 94 Å, from which we estimate a time constant for energy transfer of ~3 fs. It is remarkable that such a strong interaction does not cause hypericin to lose its biological activity [20].

Finally, the last chapter combines all the available to date information on the ground- and excited state dynamics of hypericin and hypocrellin and proposes a "stilbene-like" model to rationalize the whole complexity of the observed phenomena. It also effectively addresses the issue of "mirror-image" symmetry in these polycyclic quinones which was the key point of criticisms toward the very existence of excited-state proton transfer in the title compounds. Another challenge for our theory was associated with the presently discovered picosecond blue-shifted rising component in time-resolved

fluorescence. Careful analysis of the proposed model shows that its flexibility naturally permits for such unexpected behaviour and can not be attributed to a mere vibronic cooling processes [21].

FUTURE WORK

The amount of experimental data collected to date is limited to hypericin and its few methylated analogs, hypocrellin A, hypocrellin B and dimethyl derivative of hypocrellin A. We know that many other members of perylenequinone family also posses various degrees of light-induced antiviral and antitumor activity [22-24]. A lot more experiments need to be done if one hopes to establish clear relation between such activities and molecular structure. The nature of *inter*-molecular proton or hydrogen atom transfer that is a key step in the light-induced acidification by hypericin and hypocrellin A still wait to be addressed in the coming years.

Meanwhile, the list of our short term goals include:

— a more thorough photophysical characterization of hypocrellin B which at certain conditions is more potent in antiviral activity than A form, despite the lower $^1O_2$ quantum yield [22];

— expanding the flexibility of our transient absorbance spectrometer and fluorescence upconversion apparatus by constructing optical parametric amplifier (OPA). All our previous results were obtained at just two-three excitation wavelengths provided by laser fundamentals and their second harmonics. Simple wavelength tunability of OPA developed by Greenfield and Wasielewski [25,26] enables study of molecules excited-state dynamics over the whole visible range (450-750 nm) and with excellent time resolution (~100 fs). This additional information will bring deeper understanding and further enhancement of our model for polycyclic quinones primary photophysics. For

example, such issues as ground-state heterogeneity, vibrational cooling effects [21] and internal conversion among the closely separated excited states [27] can easily be investigated.

— another intriguing possibility is to study molecular vibrations with femtosecond time resolution. Application of conventional Raman spectroscopy is largely impeded by appreciable absorbance and fluorescence of the relevant chromophores among almost entire UV and visible spectrum. With the availability of self-mode locked Ti:sapphire oscillator producing ~10 fs pulses [28] it is now possible to coherently excite molecules into a certain vibrational state and then observe its evolution [29]. This impulsive Raman experiment is expected to provide information on molecule low-frequency vibrations/librations [30-32] which, in particular, are postulated to be involved in hypericin excited-state tautomerization. The goal is to determine which vibrational modes are coupled to the proton transfer by obtaining resonance Raman spectra via the Fourier transform of coherently excited vibrations, and by evaluating the hessian and mode-mode couplings along the reaction path. The intrinsic reaction path method will provide information about which coordinates are changing most rapidly as the H transfer proceeds.

— there is also a way to accomplish similar goals by means of time-resolved FT-IR spectroscopy [33-35]. After excitation molecular vibrational spectrum is determined with a certain delay by the interference of two IR pulses one of which travels through the sample. This experiment will make it possible to directly observe carbonyl group accepting proton or hydrogen atom in the course of excited-state tautomerization. Such an arrangement is more suitable for study of medium to high frequency vibrational modes.

— we expect continuation of our fruitful collaboration with a group of synthetic

chemists headed by Prof. G. Kraus [36-40]. They have proposed a variety of interesting hypocrellin analogs (Figure 8.1) which should be easily available through standard techniques of modern organic synthesis. Two important questions related to the polycyclic quinones will be investigated: 1) what are the origins of the excited-state transients and how does the ground-state heterogeneity (distribution of conformational isomers and tautomers) affect the observed kinetics; 2) why does hypocrellin behave differently from hypericin, more precisely what is the role of steric strain and substituents such as the hypocrellin 7-membered ring on these effects ?

— recent accurate *ab initio* calculations of hypericin tautomers and interconversion barriers were a result of partnership with Prof. M. Gordon and co-workers [19]. Meanwhile, hypocrellin A was studied with methods no better than semi-empirical AM1 calculations [41-43]. Our future collaboration will include implementation of higher levels of theory, a more detailed study of H/D transfer, energies of lowest excited states and development of a sophisticated model for treating solvent effects [44-47]. Continuing development of electronic structure code [48] that permit us to take advantage of state-of-the-art parallel computer hardware along with the exciting new developments in methods for treating excited electronic states [49] will the the keystones of the project success.

— to expand our studies of polycyclic quinones in complexes with subcellular components [50] we proposed a series of single-molecule spectroscopy experiments. The major question that we must address is whether diffusion of hypericin in the cell will complicate our measurements. In this respect, it will be important to perform FRAP (fluorescence recovery after photobleaching) experiments [51-53] to measure the rate of diffusion of hypericin in the cell and to determine if there is a fraction that is immobile on the time scale of the experiments. Another important problem that can be

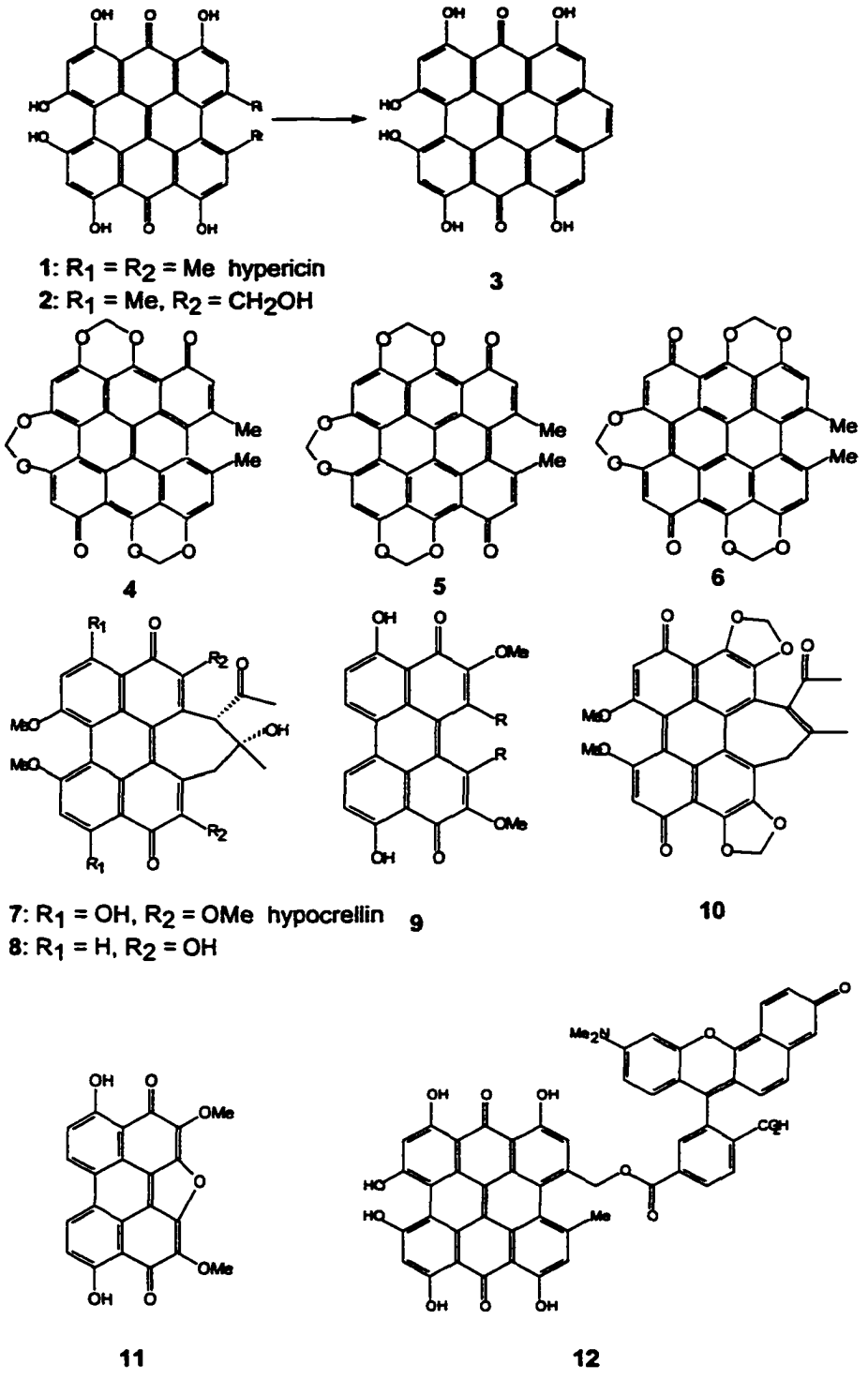

Figure 8.1 The proposed proton transfer analogs of hypericin, hypocrellin A and hypocrellin B.

addressed by this study is understanding the nature of the nonradiative processes induced upon binding hypericin and hypocrellin to cell membranes, proteins and nucleic acids. Such phenomena as conformational transitions of single molecules can also be studied [54].

REFERENCES

1. Das, K.; English, D. S.; Petrich, J. W. *J. Phys. Chem. A* 1997, *101*, 3241-3245.
2. Das, K.; Ashby, K.; Wen, J.; Petrich, J. W. *J. Phys. Chem.* , In press.
3. Borgis, D.; Hynes, J. T. *J. Chem. Phys.* 1991, *94*, 3619-3628.
4. Borgis, D.; Hynes, J. T. *J. Chem. Phys.* 1996, *100*, 1118-1128.
5. Borgis, D.; Tarjus, G.; Azzouz, H. *J. Phys. Chem.* 1992, *96*, 3188-3191.
6. Staib, A.; Borgis, D.; Hynes, J. T. *J. Phys. Chem.* 1995, *102*, 2487-2505.
7. Azzouz, H.; Borgis, D. *J. Chem. Phys.* 1993, *98*, 7361-7374.
8. Ando, K.; Hynes, J. T. *Ionization of acids in water*; Cramer, C. J. and Truhlar, D. G., Ed.; American Chemical Society: Washington D. C., 1994, pp 143-153.
9. Etzlstorfer, C.; Falk, H.; Mueller, N.; Schmitzberger, W.; Wagner, U. G. *Monatsh. Chem.* 1993, *124*, 751-61.
10. Freeman, D.; Frolow, F.; Kapinus, E.; Lavie, D.; Lavie, G.; Meruelo, D.; Mazur, Y. *J. Chem. Chem. Soc., Chem. Commun.* 1994, 891-892.
11. Chen, W. S.; Chen, Y. T.; Wan, X. Y.; Friedrichs, E.; Puff, H.; Breitmaier, E. *Liebigs Ann. Chem.* 1981, 1880-5.
12. Liang, L. N.; Zhu, N. J.; Zhang, M. H. *Kexue Tongbao (Foreign Lang. Ed.)* 1987, *32*, 56.
13. Waldeck, D. H. *Chem. Rev.* 1991, *91*, 415-436.

14. Todd, D. C.; Jean, J. M.; Rosenthal, S. J.; Ruggiero, A. J.; Yang, D.; Fleming, G. R. *J. Chem. Phys.* **1990**, *93*, 8658-68.

15. Abrash, S.; Repinec, S.; Hochstrasser, R. M. *J. Chem. Phys.* **1990**, *93*, 1041.

16. Fleming, G. R. *Chapter 6.*; Oxford University Press: London, 1986.

17. Repinec, S. T.; Sension, R. J.; Szarka, A. Z.; Hochstrasser, R. M. J. *J. Phys.Chem.* **1991**, *95*, 10380-10385.

18. English, D. S.; Das, K.; Ashby, K. D.; Park, J.; Petrich, J. W.; Castner, E. W. J. *J. Am. Chem. Soc.* **1997**, *119*, 11585-11590.

19. Petrich, J. W.; Gordon, M. S.; Cagle, M. *J. Phys. Chem. A* **1998**, *102*, 1647-1651.

20. Mazur, Y.; Lavie, G.; Prince, A. M.; Pascual, D.; Liebes, L.; Levin, B.; Meruelo, D. *Transfusion* **1995**, *35*, 392-400.

21. Sarkar, N.; Takeuchi, S.; Tahara, T. *in preparation.* **1999**.

22. Hudson, J. B.; Imperial, V.; Haugland, R. P.; Diwu, Z. *Photochem. Photobiol.* **1997**, *65*, 352-354.

23. Cohen, P. A.; Hudson, J. B.; Toweres, G. H. N. *Experientia* **1996**, *52*, 180-3.

24. Hudson, J. B.; Towers, G. H. N. *Photochem. Photobiol.* **1988**, *48*, 289.

25. Greenfield, S. R.; Wasielewski, M. R. *Appl* **1995**, *34*, 2688-2691.

26. Greenfield, S. R.; Wasielewski, M. R. *Opt. Lett.* **1995**, *20*, 1394-6.

27. Ruggiero, A. J.; Todd, D. C.; Fleming, G. R. *J. Am. Chem. Soc.* **1990**, *112*, 1003-14.

28. Asaki, M. T.; Huang, C. P.; Garvey, D.; Zhou, J.; Kapteyn, H. C.; Murnane, M. M. *Opt. Lett.* **1993**, *18*, 977-9.

29. Nelson, K. A.; Ippen, E. P. *Adv. Chem. Phys.* **1989**, *75*, 1-35.

30. Zhu, L.; Zhong, G.; Unno, M.; Sligar, S. G.; Champion, P. M. *Biospectroscopy* **1996**, *2*, 301-309.

31. Banin, U.; Kosloff, R.; Ruhman, S. *Transient resonance impulsive stimulated Raman-scattering study of nascent diiodide ions: experiment and simulation*; Springer: Berlin, 1994.

32. Dexheimer, S. L.; Wang, Q.; Peteanu, L. A.; Pollard, W. T.; Mathies, R. A.; Shank, C. V. *Chem. Phys. Lett.* **1992**, *188*, 61-66.

33. Bonvalet, A.; Joffre, M.; Migus, A.; Martin, J.-L. *Springer Ser. Chem. Phys.* **1996**, *62*, 71-72.

34. Joffre, M.; Bonvalet, A.; Martin, J.-L.; Migus, A. *Springer Ser. Chem. Phys.* **1996**, *62*, 42-43.

35. Joffre, M.; Bonvalet, A.; Migus, A.; Martin, J.-L. *Opt. Lett.* **1996**, *21*, 964-966.

36. Das, K.; Dertz, E.; Paterson, J.; Zhang, W.; Kraus, G. A.; Petrich, J. W. *J. Phys. Chem. B* **1998**, *102*, 1479-1484.

37. English, D. S.; Das, K.; Zenner, J. M.; Zhang, W.; Kraus, G. A.; Larock, R. C.; Petrich, J. W. *J. Phys. Chem. A* **1997**, *101*, 3235-3240.

38. English, D. S.; Zhang, W.; Kraus, G. A.; Petrich, J. W. *J. Am. Chem. Soc.* **1997**, *119*, 2980-2986.

39. Kraus, G. A.; Zhang, W.; Fehr, M. J.; Petrich, J. W.; Wannemuehler, Y.; Carpenter, S. *Chem. Rev. (Washington, D. C.)* **1996**, *96*, 523-35.

40. Carpenter, S.; Fehr, M. J.; Kraus, G. A.; Petrich, J. W. *Proc. Natl. Acad. Sci. U. S. A.* **1994**, *91*, 12273-7.

41. Zhang, H.; Zhang, Z. *Sci. China, Ser. B: Chem.* **1998**, *41*, 85-90.

42. Zhang, H.-Y. *Shengwu Huaxue Yu Shengwu Wuli Xuebao* **1998**, *30*, 272-276.

43. Zhang, H.; Zhang, Z. *Sci. China, Ser. B: Chem.* **1997**, *40*, 428-433.

44. Merrill, G. N.; Gordon, M. S. *J. Phys. Chem.* **1998**, *102*, 2650.

45. Chen, W.; Gordon, M. S. *J. Chem. Phys.* **1996**, *105*, 11081.

46. Day, P. N.; Jensen, J. H.; Gordon, M. S.; Webb, S. P.; Stevens, W. J.; Krauss, M.; Garmer, D.; Basch, H.; Cohen, D. *J. Chem. Phys.* **1996**, *105*, 1968.

47. Jensen, J. H.; Gordon, M. S. *J. Chem. Phys.* **1998**, *108*, 4772.

48. Fletcher, G. D. S., M. W.; Gordon, M. S. *Adv. Chem. Phys.* , In press.

49. Chaban, G. M.; Gordon, M. S. *J. Phys. Chem.* , Submitted for publication.

50. English, D. S.; Doyle, R. T.; Petrich, J. W.; Haydon, P. G. *Photochem. Photobiol.* , In press.

51. Xie, X. S. *Acc. Chem. Res* **1997**, *29*, 598-606.

52. Nie, S.; Chiu, D. T.; Zare, R. N. *Science* **1994**, *266*, 1018.

53. Vanden Bout, D. A. Y., W.-T.; Hu, D.; Fu, D.-K.; Swager, T. M.; Barbara, P. F. *Science* **1997**, *277*, 1074.

54. Edman, L.; Mets, Ü.; Rigler, R. *Proc. Natl. Acad. Sci. USA* **1996**, *93*, 6710-6715.

ACKNOWLEDGMENTS

I would like to express deep appreciation and gratitude to my research advisor, Dr. Jacob W. Petrich, for his vision, support and guidance. His enthusiasm and broad knowledge served as motivation and inspiration to me as a scientist.

I would also like to thank the members of Dr. Petrich's group, particularly Rebecca Rich for teaching me the secrets of photon counting, Mike Fehr for his cheerful character, and Douglas English and Kaustuv Das for their friendship and sharing my life as a graduate student. Without sincere dedication and impartial support of these individuals this study would never have been possible.

Dr. Sergei Savikhin is greatly appreciated for his insightful discussions and friendly technical advice along the many steps of this project. In addition, he is the author of unprecedent program SpectraSolve™ that saved me and other fellow members of our group many hours of spectra and data processing time. I would also like to mention Dr. Bruce Fulton whose enthusiam and expertise determined the success of our NMR experiments.

My heartfelt thanks directed to my dear wife Elise Luong and to my parents for their affectionate unconditional love, care, patience, and support.

I am also grateful to Chemistry Department faculty and stuff for all their efforts and dedication to make graduate study at ISU such an invaluable experience. I will never forget my Instructors and Teachers in every field whose humane qualities and level of expertise and dedication served as an example and inspiration for my own personal growth.

IMAGE EVALUATION
TEST TARGET (QA-3)

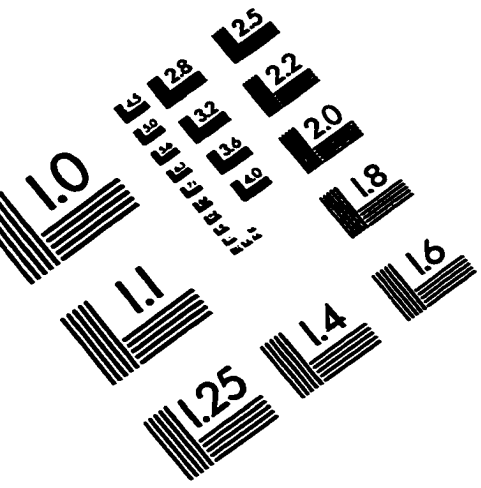

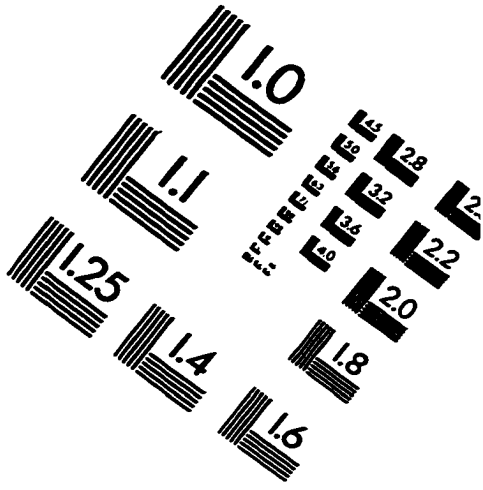

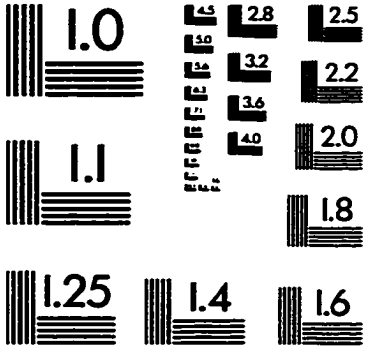

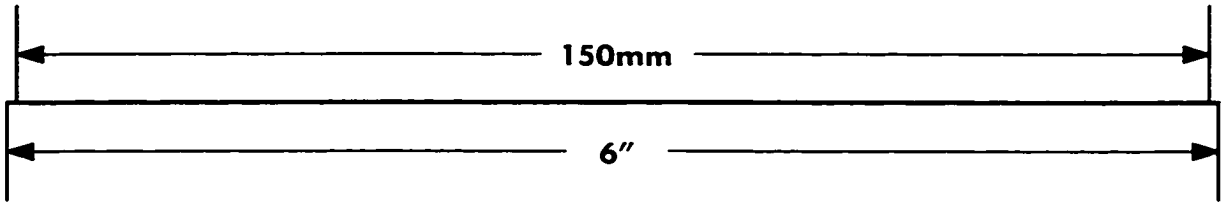

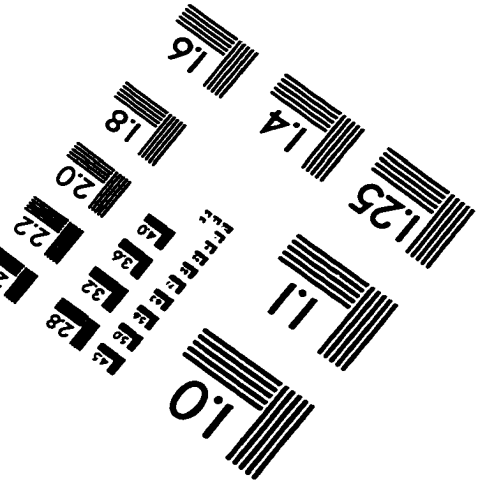

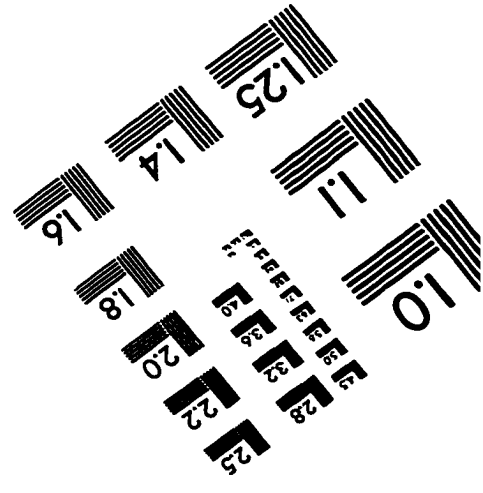

APPLIED IMAGE, Inc
1653 East Main Street
Rochester, NY 14609 USA
Phone: 716/482-0300
Fax: 716/288-5989